Contrails

DEVELOPMENTS IN DISCRETE ELEMENT FINITE DEFLECTION STRUCTURAL ANALYSIS BY FUNCTION MINIMIZATION

DIVISION OF SOLID MECHANICS, STRUCTURES AND MECHANICAL DESIGN

School of Engineering

CASE WESTERN RESERVE UNIVERSITY

This document has been approved for public release and sale. Its distribution is unlimited.

Approved for Public Release

Contrails

FOREWORD

This report was prepared by the Division of Solid Mechanics, Structures and Mechanical Design, School of Engineering, Case Western Reserve University, Cleveland, Ohio under United States Air Force Contract No. AF 33(615)-3432.

This research was sponsored and administered by the Air Force Flight Dynamics Laboratory, Air Force Systems Command, Wright-Patterson Air Force Base, Ohio. The work was initiated under Project No. 1467, "Structural Analysis Methods", Task No. 146701, "Stress-Strain Analysis Methods for Structures Exposed to Creep Environments", Mr. Laszlo Berke (FDTR) was the project engineer.

The analytical portion of this research effort was under the supervision of Professor Lucien A. Schmit, Jr. and the experimental portion of the program was under the supervision of Professor George G. Goble. Professor Richard L. Fox served as a faculty associate on the analytical work and made several important contributions to this research effort.

As principal investigator Professor Schmit had overall editorial responsibility for this report. Several members of the staff of the Division of Solid Mechanics, Structures and Mechanical Design contributed to its preparation. Sections 1, 2, 3 and 8 were written by Professor Schmit, Section 4 by Mr. E. L. Stanton, Sections 5 and 6 by Mr. W. Gibson, and Section 7 by Dr. G. G. Goble with assistance from Mr. J. D. Swarts and Mr. F. S. Campbell. Dr. R. L. Fox, in addition to his technical contributions, assisted Professor Schmit with the editing.

This report covers research carried out between December 1965 and May 1968. The report was submitted in August 1968.

This technical report has been reviewed and is approved.

FRANCIS J. JANIK, JR.
Chief, Theoretical Mechanics Branch
Structures Division

Approved for Public Release

Contrails

ABSTRACT

The discrete element energy search method of structural analysis is extended to predicting the geometrically nonlinear behavior of plate and shell type structures. Numerical results for example problems exhibiting nonlinear bending-membrane coupling and stable post-buckling behavior are presented. The results of a laboratory type experimental program, designed to provide data for comparison with analytical behavior predictions, are reported. It is shown that displacement patterns formed from products of one-dimensional interpolation functions can be used to generate a useful class of shell discrete elements, including geometric nonlinearity. These conforming elements can be joined together at arbitrary angles, although the current computer program is limited to tangential and right angle joining. While the major portion of this research program was based upon the principle of minimum potential energy, a rectangular plate discrete element exhibiting bending membrane coupling is developed within the Reissner energy framework. Energy search methods of structural analysis based on potential energy formulations and gradient minimization algorithms are found to be computationally competitive with conventional solution procedures. A variable scaling technique that has a strong effect on the convergence of the gradient minimization algorithms is presented. Using this variable scaling-technique it is found that the conjugate gradient algorithm often converges in substantially less than n cycles for over-discretized linear problems, where n is the number of independent degrees-of-freedom. A computer program that draws together most of the important separate contributions made within the potential energy framework during the course of this research program, is described. This computer program implements discrete element finite deflection analysis of a class of structures that can be modeled as assemblages of plate, cylindrical shell, and annular plate elements connected together tangentially or at right angles.

Approved for Public Release

Contrails

Approved for Public Release

Contrails

TABLE OF CONTENTS

Approved for Public Release

Contrails

TABLE OF CONTENTS (Continued)

Approved for Public Release

Contrails

TABLE OF CONTENTS (Continued)

Approved for Public Release

Contrails

LIST OF FIGURES

Approved for Public Release

Contrails

LIST OF FIGURES (Continued)

Approved for Public Release

Contrails

LIST OF FIGURES (Continued)

Approved for Public Release

Contrails

LIST OF FIGURES (Continued)

Approved for Public Release

Contrails

LIST OF FIGURES (Continued)

APPENDICES

Approved for Public Release

Contrails

LIST OF TABLES

Approved for Public Release

Contrails

LIST OF SYMBOLS

A,B,H	square matrices used in the variable metric algorithm (Fletcher-Powell)
a	x dimension of rectangular plate element
$\tilde{a}$	$\tilde{x}$ dimension of parallelogram plate element
b	y dimension of rectangular plate element
$\tilde{b}$	$\tilde{y}$ dimension of parallelogram plate element
C_N	conditioning number (see Equation 4.6)
C_b	bending contribution to the discrete element Reissner energy
C_c	bending-membrane coupling contribution to the discrete element Reissner energy
C_m	membrane contribution to the discrete element Reissner energy
C_0, C_1, C_2, C_3	constants
c	parameter in the step size generator
D	diagonal scaling matrix (see Equation 4.10)
$d = r_2 - r_1$	radial dimension of annular plate discrete element
E	modulus of elasticity
e = p,s,c,a	rectangular plate, parallelogram plate, cylindrical shell, annular sector
$\vec{F}_e$	vector of work equivalent loads for discrete element
F	vector of work equivalent loads for system
f(s)	function of s (see Equation 2.58)
g(θ)	function of θ (see Equation 2.52)
$\vec{g}(\vec{Z})$	a vector valued function
h	thickness
I	identity matrix
K_{2e}	discrete element ordinary stiffness matrix

Approved for Public Release

Contrails

K_{3e}	rectangular matrix associated with third degree contribution to discrete element strain energy
K_{4e}	square matrix associated with fourth degree contribution to discrete element strain energy
L	Lipschitz constant
ℓ	length of cylindrical shell element
M_e	discrete element consistent mass matrix
M_x, M_y, M_{xy}	bending force resultants
N	equivalent uniform load (see Equation 2.81)
$\vec{N}$	vector of discrete element membrane force unknowns (see Equation 3.15)
N_x, N_y, N_{xy}	membrane force resultants
n	number of variables
$\bar{n}$	number of cycles to convergence
$\vec{P}$	an energy search direction vector
p_z	transverse load distribution
Q_b	square matrix associated with bending contribution to discrete element Reissner energy (see Equation 3.12)
Q_c	rectangular matrix associated with the bending-membrane coupling contribution to discrete element Reissner energy (see Equation 3.14)
Q_m	square matrix associated with membrane contribution to discrete element Reissner energy (see Equation 3.10)
R	Gerschgorin circle radius
r	radius
r_1, r_2	inner, outer radius of annular plate discrete element
S_1	contribution to the discrete element Reissner energy of the force boundary conditions
S_2	contribution to the discrete element Reissner energy of the displacement boundary conditions
$\vec{S}, \vec{V}$	intermediate vectors in the variable metric algorithm (Fletcher-Powell)

Approved for Public Release

Contrails

t	linear search parameter
$\tilde{U}$	strain energy density
U_e	discrete element strain energy
U_{2e}	second degree discrete element strain energy
U_{3e}	third degree discrete element strain energy
U_{4e}	fourth degree discrete element strain energy
u,v,w	displacements
W_e	work done by loads applied to discrete element
$\vec{X}_b$	vector of discrete element bending unknowns (see Equation 3.13)
$\vec{X}_e$	vector of discrete element degrees of freedom
$\vec{X}_m$	vector of discrete element membrane unknowns (see Equation 3.11)
$\tilde{x},\tilde{y}$	oblique coordinates
x,y,z	Cartesian coordinates
$\vec{Y}$	vector of scaled system unknowns
$\vec{Y}_e$	vector containing 136 possible products of sixteen degrees of freedom in w taken in pairs of two
$\vec{Y}_r$	vector containing 136 possible products of sixteen degrees of freedom in w for Reissner energy discrete element
$\vec{Z}$	vector of system unknowns or degrees of freedom
$\|\|\vec{Z}\|\|$	a norm of $\vec{Z}$
$\|\|\vec{Z}\|\|_2$	Euclidean norm of $\vec{Z}$
$\|\|\vec{Z}\|\|_\infty$	infinity norm of $\vec{Z}$
β	skew angle (see Figure 4) or scalar used in the conjugate gradient algorithm (Fletcher-Reeves)
γ	shear strains
$\Delta\theta$	subtended angle of cylindrical shell element

Approved for Public Release

Contrails

δ	variational operator
δ_{ik}	Kronecker's delta
ϵ	normal strains
θ	angular coordinate
θ_1, θ_2	limits of θ for annular plate discrete element
$[\kappa_{ij}(\vec{Z})]$	matrix of second partial derivatives of $\Pi(\vec{Z})$, that is $[\frac{\partial^2 \Pi}{\partial z_i \partial z_j} (\vec{Z})]$
λ	eigenvalue
ν	Poisson's ratio
ξ, η	arc lengths in an orthogonal curvilinear coordinate system
$\xi=r, \eta=r\theta, z$	polar coordinates
$\xi=s, \eta=r\theta, z$	cylindrical coordinates
Π	total potential energy of an assemblage of discrete elements
Π_R	total Reissner energy of an assemblage of discrete elements
π_e	discrete element potential energy function
π_R	discrete element Reissner energy function
$\rho(K)$	spectral radius of K
$\rho = \frac{r}{d}$	normalized radial coordinate
σ	normal stresses
τ	shear stresses
ϕ	angle between two adjacent elements (see Figure 6)
∇	gradient operator
I,II	superscripts referring to elements I and II (see Figure 6)

Approved for Public Release

Contrails

Approved for Public Release

Contrails

SECTION 1

INTRODUCTION

The well known energy formulations of structural mechanics have until recently been used primarily as one means of deriving the equations governing static structural behavior. The energy search approach to structural analysis is based upon the application of mathematical programming methods to appropriate energy functions. Under Contract AF 33(615)-1022 an exploratory study of the energy search approach was carried out and the results of this research were reported in Refs. 1, 2 and 3.

Implementation of the energy search approach for three dimensional structures that can be represented by straight truss and frame members using a potential energy formulation is reported in detail in Ref. 4. Further study including solution of several interesting example problems and a users guide to the computer program are reported in Ref. 5. The results of this previously reported research were encouraging and this document reports on the results of a continuing research effort aimed at (a) extending the applicability of the energy search approach to nonlinear structural analysis of stiffened plates and shells, (b) carrying out a laboratory type experimental program to provide data for comparison with current and future analytical behavior predictions.

The static structural analysis problem, viewed in terms of a total potential energy formulation, is mathematically equivalent to finding a set of values for the generalized displacement variables such that the total potential energy is a minimum. Therefore algorithmic tools for seeking the unconstrained minimum of a function of many variables may be brought to bear on the structural analysis problem by using total potential energy formulations.

Approved for Public Release

Contrails

It should be noted that minimization algorithms can be used in conjunction with any one of several discretization procedures including finite difference, assumed mode and discrete element methods. It should also be mentioned in passing, that the structural analysis problem viewed in terms of a complementary energy formulation is mathematically equivalent to finding a set of values for the statically independent generalized force variables such that the complementary energy is a minimum (see Ref. 6). A major portion of the research effort reported herein deals with the generation of a capability for discrete element finite deflection analysis of plates and shells using unconstrained minimization algorithms to seek minimum total potential energy solutions numerically. The principal limitations on the total potential energy formulations presented are that the rotations of the deformed structure relative to the undeformed position of the structure must be small (i.e. $\sin\theta \simeq \theta$ and $\cos\theta \simeq 1$) and the material behavior is assumed to remain elastic. Extension of the work reported herein to any material behavior law that can be represented by a strain energy density type of potential function is relatively straight forward in principle but its implementation will require substantial effort.

Several significant developments generated in the course of this research program have already been documented in detail and these will only be summarized herein. Thus, for example, Section 2 summarizes the work on flat plate and cylindrical elements using a total potential energy formulation previously reported in Refs. 7, 8 and 9. The extension of the sixteen degree of freedom linear plate bending element to skew coordinates was reported in Refs. 10 and 11 and this contribution is also treated in summary fashion in Section 2.

Approved for Public Release

Contrails

The static structural analysis problem viewed in terms of the Reissner energy formulation is mathematically equivalent to finding a set of values for the generalized force and displacement variables such that the Reissner energy is stationary. An adequate algorithm for finding the stationary point of Reissner energy functions of many variables was not found in the course of this investigation. An alternative formulation based on seeking the minimum of a residual function was found to be inefficient and numerical solutions were obtained using the Newton-Raphson method. A rectangular plate element exhibiting bending-membrane coupling was developed. Linear membrane and linear bending elements, within the context of a mixed force-displacement formulation, are obtained as specializations. The mixed force-displacement discrete element developments documented in detail in Ref. 12 are presented in Section 3.

By and large this program has drawn on existing algorithmic tools for unconstrained minimization of a function of many variables. However, effort has been expended in adapting these tools to the class of problems at hand and in particular, scaling techniques have been generated, improvements in the one dimensional minimization scheme have been made, and termination criteria have been explored. A major portion of this aspect of the research program was reported in Ref. 13 and it is treated in summary fashion in Section 4.

Section 5 presents the development of an annular plate discrete element. This formulation is carried out in terms of the potential energy and these elements used in conjunction with the plate and cylindrical shell elements previously discussed will provide a capability for post-buckled elastic analysis of integrally stiffened cylindrical shell panels.

Approved for Public Release

Contrails

In Section 6 a computer program that draws together several of the important separate developments made in the course of this research program is discussed. The repertoire of discrete elements in this program includes linear and geometrically nonlinear 48 degree-of-freedom rectangular plate, cylindrical shell, and annular plate elements. Emphasis has been placed upon ease of data preparation and optimization of coding and storage allocation. Operational flexibility is provided by a variety of options including a selection of alternative solution methods.

The experimental program is reported in Section 7. The laboratory models, testing procedures, and experimental results are described. Efforts to correlate experimental and analytical results are also discussed. The data obtained from the tests is given in numerical form in Appendix C. Finally, conclusions and recommendations are set forth in Section 8.

Approved for Public Release

Contrails

SECTION 2

POTENTIAL ENERGY FORMULATION FOR PLATE AND SHELL DISCRETE ELEMENTS

2.1 Introduction

In this section potential energy formulations for various discrete elements are outlined. The potential energy for an assemblage of elements representing a structural system can be formed by simply summing up the energy contributions from each of the discrete elements. An approximate analysis of the structure can then be carried out using mathematical programming algorithms (unconstrained minimization methods) which seek the minimum of the total potential energy with respect to the independent degrees-of-freedom.

The development of a potential energy formulation for a discrete element begins with the selection of strain-displacement relations. This is followed by the adoption of a strain energy density potential function consistent with the stress-strain behavior to be represented. The potential energy for the discrete element is then obtained by integrating the strain energy density over the element volume and adding the potential of any external loads applied to the element. The true displacement functions for the element are in general unknown and selecting the assumed displacement patterns for the element is a crucial step. In selecting assumed displacement functions consideration should be given to geometric admissibility requirements, completeness, and rigid body displacement states (see pp. 17-28 Ref. 7). Substituting a particular set of assumed displacement functions into the potential energy expression for the element leads to the discretized form of the element potential energy.

Approved for Public Release

Contrails

It should be noted that for the special case of linear stress-strain and linear strain-displacement relations the discretized potential energy expression for an element is of the form

$$\pi_e = \frac{1}{2} \vec{X}_e^T K_{2e} \vec{X}_e - \vec{X}_e^T \vec{F}_e \tag{2.1}$$

where K_{2e} is the element stiffness matrix, $\vec{X}_e$ is the vector of element degrees of freedom and $\vec{F}_e$ is the work equivalent load vector. Thus it follows that development of discretized potential energy formulations yields element stiffness matrices and work equivalent load vectors as an ancillary result. Furthermore, the discretized kinetic energy maximum in harmonic motion is

$$T_e = \frac{\omega^2}{2} \vec{X}_e^T M_e \vec{X}_e \tag{2.2}$$

where M_e is the element mass matrix consistent with the assumed displacement patterns and ω is the frequency of the harmonic motion. While dynamic analysis was not an objective of this research effort, element mass matrices consistent with the element stiffness matrices for several linear cases have been generated.

2.2 Plate Elements

Several discrete element potential energy formulations have been generated in the course of this research program. Most of these are available as options within the computer program described in Section 6. The basic finite deflection strain displacement relations employed in the plate work are

Approved for Public Release

Contrails

$$\epsilon_x = \frac{\partial u}{\partial x} + \frac{1}{2}\left(\frac{\partial w}{\partial x}\right)^2 - z\frac{\partial^2 w}{\partial x^2} \tag{2.3a}$$

$$\epsilon_y = \frac{\partial v}{\partial y} + \frac{1}{2}\left(\frac{\partial w}{\partial y}\right)^2 - z\frac{\partial^2 w}{\partial y^2} \tag{2.3b}$$

$$\gamma_{xy} = \frac{\partial v}{\partial x} + \frac{\partial u}{\partial y} + \frac{\partial w}{\partial x}\frac{\partial w}{\partial y} - 2z\frac{\partial^2 w}{\partial x \partial y} \tag{2.3c}$$

The linear case is obtained by neglecting the terms $\frac{1}{2}\left(\frac{\partial w}{\partial x}\right)^2$, $\frac{1}{2}\left(\frac{\partial w}{\partial y}\right)^2$ and $\frac{\partial w}{\partial x}\frac{\partial w}{\partial y}$. Assuming a linear elastic isotropic material and plane stress behavior, the strain energy density ($\tilde{U}$) is given by

$$\tilde{U} = \frac{E}{2(1-\nu^2)}\left[\epsilon_x^2 + \epsilon_y^2 + 2\nu\,\epsilon_x\,\epsilon_y + \left(\frac{1-\nu}{2}\right)\gamma_{xy}^2\right] \tag{2.4}$$

which implies the following well known stress-strain relations

$$\frac{\partial \tilde{U}}{\partial \epsilon_x} = \sigma_x = \frac{E}{1-\nu^2}\left[\epsilon_x + \nu\,\epsilon_y\right] \tag{2.5a}$$

$$\frac{\partial \tilde{U}}{\partial \epsilon_y} = \sigma_y = \frac{E}{1-\nu^2}\left[\epsilon_y + \nu\,\epsilon_x\right] \tag{2.5b}$$

$$\frac{\partial \tilde{U}}{\partial \gamma_{xy}} = \tau_{xy} = \frac{E}{2(1+\nu)}\,\gamma_{xy} \tag{2.5c}$$

The potential energy for an isotropic elastic rectangular plate element of uniform thickness h (see Fig. 1) is given by

Approved for Public Release

Contrails

$$\pi_p = U_p - W_p \tag{2.6}$$

where the element strain energy U_p is

$$U_p = \int_0^a \int_0^b \int_{-\frac{h}{2}}^{+\frac{h}{2}} \frac{E}{1-\nu^2} \left[\varepsilon_x^2 + \varepsilon_y^2 + 2\nu\, \varepsilon_x\, \varepsilon_y + \left(\frac{1-\nu}{2}\right) \gamma_{xy}^2\right] dz\, dy\, dx \tag{2.7}$$

and W_p is the work done by external loads applied to the element.

2.2.1 Rectangular Bending-Membrane 48 Degree-of-Freedom Element

The most widely used rectangular plate element generated in the course of this research program has 48 degrees-of-freedom and is based upon assumed displacement patterns expressed in terms of products of first order Hermite interpolation polynomials and undetermined corner displacement parameters. The assumed displacement state for this plate element is of the form

$$w(x,y) = \sum_{i=1}^{2} \sum_{j=1}^{2} \left[H_{0i}^{(1)}(x)\, H_{0j}^{(1)}(y)\, w_{ij} + H_{1i}^{(1)}(x)\, H_{0j}^{(1)}(y)\, w_{xij} + H_{0i}^{(1)}(x)\, H_{1j}^{(1)}(y)\, w_{yij} + H_{1i}^{(1)}(x)\, H_{1j}^{(1)}(y)\, w_{xyij}\right] \tag{2.8}$$

with similar expressions for the u and v displacements. The w_{ij}, w_{xij}, w_{yij} and w_{xyij} denote 16 undetermined parameters, namely the displacement w and the derivatives $\frac{\partial w}{\partial x}$, $\frac{\partial w}{\partial y}$, and $\frac{\partial^2 w}{\partial x \partial y}$ of the displacement at the corners (see Fig. 1 for the corner identification numbering scheme).

Approved for Public Release

Contrails

The first-order Hermite interpolation polynomials are given by

$$H^{(1)}_{01}(x) = (2x^3 - 3a\,x^2 + a^3)/a^3 \tag{2.9a}$$

$$H^{(1)}_{02}(x) = -(2x^3 - 3a\,x^2)/a^3 \tag{2.9b}$$

$$H^{(1)}_{11}(x) = (x^3 - 2a\,x^2 + a^2x)/a^2 \tag{2.9c}$$

$$H^{(1)}_{12}(x) = (x^3 - a\,x^2)/a^2 \tag{2.9d}$$

and they are shown graphically in Fig. 2. Similar expressions for the y directions are obtained by replacing x by y and a by b. Every two point Hermite interpolation polynomial of order N, $H^{(N)}_{pi}(x)$, is uniquely determined by the following properties,

$$D^{\ell}\, H^{(N)}_{pi}(x_k) = \delta_{p\ell}\ \delta_{ik}\ ; \qquad i,k = 1,2 \qquad p,\ell = 0, 1, \ldots, N \tag{2.10a}$$

where

$$D^{\ell} \equiv \frac{d^{\ell}}{dx^{\ell}} \tag{2.10b}$$

The interpolation points, x_k, in Eqs. 2.9 are $x_1 = 0$ and $x_2 = a$ and the order, N = 1 gives the highest derivative interpolated. Because of these properties the assumed displacement states and their first derivatives along any particular edge depend only upon degrees of freedom associated with that edge and the satisfaction of interelement geometric admissibility conditions is facilitated.

Approved for Public Release

Contrails

Substituting these assumed displacements into the strain-displacement relation (Eqs. 2.3) and then substituting into Eqs. 2.6 and 2.7 leads to the following discretized form of the element potential energy

$$\pi_p = U_{2p} + U_{3p} + U_{4p} - W_p \tag{2.11}$$

where

$$U_{2p} = \frac{1}{2} \underset{1\times48}{\vec{X}_p^T} \underset{48\times48}{K_{2p}} \underset{48\times1}{\vec{X}_p} \tag{2.12a}$$

$$U_{3p} = \frac{1}{2} \underset{1\times48}{\vec{X}_p^T} \underset{48\times136}{K_{3p}} \underset{136\times1}{\vec{Y}_p} \tag{2.12b}$$

$$U_{4p} = \frac{1}{8} \underset{1\times136}{\vec{Y}_p^T} \underset{136\times136}{K_{4p}} \underset{136\times1}{\vec{Y}_p} \tag{2.12c}$$

and

$$W_p = \underset{1\times48}{\vec{X}_p^T} \underset{48\times1}{\vec{F}_p} \tag{2.12d}$$

The vector $\vec{X}_p$ contains the 48 corner degrees of freedom, 16 from each of the three displacements approximated [i.e. u(x,y), v(x,y) and w(x,y)]. The vector $\vec{Y}_p$ contains as its elements the 136 possible products of the 16 degrees of freedom in the w(x,y) assumed displacement function taken in pairs. The vector $\vec{F}_p$ contains the work equivalent loads associated with each of the 48 degrees of freedom. Explicit formulas for the elements of the work equivalent load vectors due to several of the more common types of loading are given in Ref. 7 (see p. 118, Table 4). The matrix K_{2p} is the ordinary

Approved for Public Release

Contrails

stiffness matrix associated with the quadratic strain energy of the linear formulation, K_{3p} is a rectangular matrix associated with the third degree contribution to the strain energy, and K_{4p} is a square matrix associated with the fourth degree contribution to the strain energy. A more detailed description of the discretized strain energy will be found in Appendix A of Ref. 7 or Appendix B of Ref. 9.

This 48 degree of freedom rectangular plate element is attractive in many applications because it provides a good approximation of the membrane stress state and because it makes the joining together of plate elements at any angle possible (see Section 2.4.1).

The ordinary stiffness matrix (K_{2p}) associated with the quadratic strain energy (U_{2p}) of the linear formulation may be written in partitioned form as follows

$$K_{2p} = \begin{bmatrix} K_{2p}^{(u)} & K_{2p}^{(vu)^T} & 0 \\ K_{2p}^{(vu)} & K_{2p}^{(v)} & 0 \\ 0 & 0 & K_{2p}^{(w)} \end{bmatrix} \qquad (2.13)$$

and explicit formulas for the elements of each submatrix are given in Ref. 7 (Pages 45 and 46). The zero submatrices in Eq. 2.13 reflect the fact that there is no coupling between membrane and bending behavior for a linear plate element. The ordinary stiffness matrix K_{2p} shown in partitioned form in Eq. 2.13 may be viewed as a thirty-two degree-of-freedom rectangular membrane plate element stiffness matrix and a sixteen degree-of-freedom rectangular bending plate element stiffness matrix.

Approved for Public Release

Contrails

The element mass matrix consistent with the assumed displacement states (see Eq. 2.8) used to derive the ordinary stiffness matrix K_{2p} (see Eq. 2.12a) may be written in partition form as follows

$$M_p = \begin{bmatrix} M^{(u)} & 0 & 0 \\ 0 & M^{(v)} & 0 \\ 0 & 0 & M^{(w)} \end{bmatrix} \tag{2.14}$$

where the elements of the submatrices are given explicitly by

$$M_{ij}^{(u)} = M_{ij}^{(v)} = \rho hab\, G_{ij}^{(5)}\, a^{L_{ij}}\, b^{M_{ij}} \tag{2.15a}$$

$$M_{ij}^{(w)} = \frac{\rho hab}{12}\left[12\, G_{ij}^{(5)} + \left(\frac{h}{a}\right)^2 G_{ij}^{(6)} + \left(\frac{h}{b}\right)^2 G_{ij}^{(7)}\right] a^{L_{ij}}\, b^{M_{ij}} \tag{2.15b}$$

and the numerical coefficients $G_{ij}^{(5)}$, $G_{ij}^{(6)}$, $G_{ij}^{(7)}$ as well as the exponents L_{ij}, M_{ij} are listed in Ref. 7 (see table 1, p. 114). Note that the second and third terms inside the square bracket in Eq. 2.15b represent rotary inertia terms which are very small for thin plates (i.e. $\frac{h}{2} << 1$ and $\frac{h}{b} << 1$).

2.2.2 Rectangular Stiffener Specialization

The plate element discussed in Section 2.2.1 may be used to represent integral stiffeners of rectangular cross section of the type shown schematically in Fig. 3. In situations characterized by high aspect ratio $\frac{b}{a} >> 1$, a long free edge, and no bending in the stiffener, it has been found that setting $\frac{\partial u}{\partial x} = 0$ over the entire element represents a useful simplification. The arguement in favor of this approximation proceeds as follows.

Approved for Public Release

Contrails

Consider a panel-stiffener system as shown in Fig. 3 with system coordinates $\bar{x}$, $\bar{y}$, and $\bar{z}$ aligned with stiffener coordinates y, z, and x, respectively. The system displacements $\bar{u}$, $\bar{v}$, and $\bar{w}$ correspond to the stiffener displacements v, w, and u, respectively. View this system as an equivalent shell which is thick enough so that transverse shear deformations must be accounted for, but not so thick as to allow the transverse displacement $\bar{w}$ to vary through the depth of the system, i.e.,

$$\frac{\partial \bar{w}}{\partial \bar{z}} = 0 \tag{2.16}$$

These assumptions are commonly employed in sandwich shell analysis. Transformed to the stiffener coordinate system, Eq. 2.16 becomes

$$\frac{\partial u}{\partial x} = 0 \tag{2.17}$$

The transverse shear strain which must be accounted for is that in the plane of the stiffener, namely

$$\bar{\gamma}_{xz} = \frac{\partial \bar{u}}{\partial \bar{z}} + \frac{\partial \bar{w}}{\partial \bar{x}} \tag{2.18}$$

Transforming the stiffener coordinates, this strain is

$$\gamma_{xy} = \frac{\partial v}{\partial x} + \frac{\partial u}{\partial y} \tag{2.19}$$

A rectangular plate element subject to the simplification expressed in Eq. 2.17 will thus fulfill the foregoing assumptions when used to model a straight stiffener, since the shear strain γ_{xy} is non-zero in such an element.

Having adopted the simplification that $\frac{\partial u}{\partial x} = 0$ over the entire element, the implementation of this condition is straight forward. Since the basic assumed displacement state for u(x,y) is given in terms of products of first-order Hermite interpolation polynomials it follows that:

Approved for Public Release

Contrails

$$\frac{\partial u}{\partial x}(x,y) = \sum_{i=1}^{2}\sum_{j=1}^{2}\left[\frac{\partial H_{0i}^{(1)}}{\partial x}(x)\ H_{0j}^{(1)}(y)\ u_{ij} + \frac{\partial H_{1i}^{(1)}}{\partial x}(x)\ H_{0j}^{(1)}(y)\ u_{xij}\right.$$

$$\left. + \frac{\partial H_{0i}^{(1)}}{\partial x}(x)\ H_{1j}^{(1)}(y)\ u_{yij} + \frac{\partial H_{1i}^{(1)}}{\partial x}(x)\ H_{1j}^{(1)}(y)\ u_{xyij}\right] \qquad (2.20)$$

Setting eight degrees of freedom to zero

$$u_{xij} = 0 \qquad \text{for} \quad i = 1,2; \quad j = 1,2 \qquad (2.21a)$$

$$u_{xyij} = 0 \qquad \text{for} \quad i = 1,2; \quad j = 1,2 \qquad (2.21b)$$

and linking four degrees of freedom

$$u_{11} = u_{21} \qquad (2.22a)$$

$$u_{12} = u_{22} \qquad (2.22b)$$

$$u_{y11} = u_{y21} \qquad (2.22c)$$

$$u_{y12} = u_{y22} \qquad (2.22d)$$

it follows that

Approved for Public Release

Contrails

$$\frac{\partial u}{\partial x}(x,y) = H^{(1)}_{01}(y)\left[\frac{\partial H^{(1)}_{01}}{\partial x}(x) + \frac{\partial H^{(1)}_{02}}{\partial x}(x)\right] u_{11}$$

$$+ H^{(1)}_{02}(y)\left[\frac{\partial H^{(1)}_{01}}{\partial x}(x) + \frac{\partial H^{(1)}_{02}}{\partial x}(x)\right] u_{12} \qquad (2.23)$$

$$+ H^{(1)}_{11}(y)\left[\frac{\partial H^{(1)}_{01}}{\partial x}(x) + \frac{\partial H^{(1)}_{02}}{\partial x}(x)\right] u_{y11}$$

$$+ H^{(1)}_{12}(y)\left[\frac{\partial H^{(1)}_{01}}{\partial x}(x) + \frac{\partial H^{(1)}_{02}}{\partial x}(x)\right] u_{y12} = 0$$

since it can be seen from Eqs. 2.9 a,b that

$$\frac{\partial H^{(1)}_{01}}{\partial x}(x) + \frac{\partial H^{(1)}_{02}}{\partial x}(x) = 0 \qquad (2.24)$$

For elements with high aspect ratio, a long free edge and negligible bending this stiffener element specialization reduces the number of unknowns from 48 to 36. It should also be noted that for elements with high aspect ratio the stiffener element specialization may help to improve the conditioning of the ordinary stiffness matrix by eliminating the u_{xyij} degrees of freedom.

2.2.3 Rectangular Bending-Membrane 24 Degree-of-Freedom Element

A rectangular plate element with only 24 degrees-of-freedom can be generated by using bilinear assumed displacement states for the inplane displacements u(x,y) and v(x,y) while retaining the bicubic sixteen degree-of-freedom assumed displacement statement given by Eq. 2.8 for w(x,y). The assumed u(x,y) and v(x,y) displacements expressed in terms of products of zeroth-order Hermite interpolation polynomials can be written in the following form

Approved for Public Release

Contrails

$$u(x,y) = \sum_{i=1}^{2} \sum_{j=1}^{2} H_{0i}^{(0)}(x)\, H_{0j}^{(0)}(y)\, u_{ij} \tag{2.25a}$$

$$v(x,y) = \sum_{i=1}^{2} \sum_{j=1}^{2} H_{0i}^{(0)}(x)\, H_{0j}^{(0)}(y)\, v_{ij} \tag{2.25b}$$

The zeroth order Hermite interpolation polynomials are given by

$$H_{01}^{(0)}(x) = -(x-a)/a \tag{2.26a}$$

$$H_{02}^{(0)}(x) = x/a \tag{2.26b}$$

and the corresponding functions for the y direction are obtained by replacing x by y and a by b. The displacements along an edge depend only upon degrees-of-freedom associated with that edge, the edges remain straight, and satisfaction of interelement geometric admissibility is easily achieved. The discretized total potential energy for this 24 degree-of-freedom rectangular bending-membrane element has exactly the same form as that given by Eqs. 2.11 and 2.12 except that the matrix dimension 48 in Eqs. 2.12 is replaced by the dimension 24.

This 24 degree-of-freedom rectangular element has been used to obtain solutions for various finite deflection plate problems with satisfactory deflection results. However, the assumed displacement states used for u(x,y) and v(x,y) yield a relatively coarse approximation of the membrane stress state. A more serious limitation of this 24 degree-of-freedom discrete element is that it does not lend itself to idealizations where

Approved for Public Release

Contrails

plate elements are joined together at an arbitrary angle.

The 24 x 24 ordinary stiffness matrix K_{2p} associated with the quadratic strain energy of the linear formulation may be viewed as an 8 degree-of-freedom rectangular membrane plate element stiffness matrix and a 16 degree-of-freedom rectangular plate bending element stiffness matrix. The 8 degree-of-freedom membrane stiffness matrix is given explicitly in Ref. 2 (see p. 421) and the 16 degree-of-freedom bending stiffness matrix is given explicitly in Ref. 2 (see p. 441) or in Ref. 7 (see p. 46). Note that this is the same 16 degree-of-freedom uncoupled bending stiffness matrix referred to in Section 2.2.1. The element mass matrix consistent with the 8 degree-of-freedom membrane stiffness matrix is given explicitly in Ref. 2 (see p. 422, Eq. A-2) and the elements of the mass matrix consistent with the 16 degree-of-freedom bending stiffness matrix are given by Eq. 2.15b of this report.

2.2.4 Rectangular Linear Bending 36 Degree-of-Freedom Element

The strain displacement relations of small deflection plate bending theory may be specialized from Eqs. 2.3 and they are

$$\varepsilon_x = - z \frac{\partial^2 w}{\partial x^2} \tag{2.27a}$$

$$\varepsilon_y = - z \frac{\partial^2 w}{\partial y^2} \tag{2.27b}$$

$$\gamma_{xy} = - 2z \frac{\partial^2 w}{\partial x \partial y} \tag{2.27c}$$

For linear elastic isotropic materials the potential energy for a rectangular plate element of constant thickness is given by Eqs. 2.6 and 2.7. This 36 degree-of-freedom rectangular plate bending element is based upon an assumed displacement state for w(x,y) which is formed from products of second

Approved for Public Release

Contrails

order Hermite interpolation polynomials and the undetermined corner displacement parameters. The assumed displacement state for this plate bending element is of the form

$$w(x,y) = \sum_{i=1}^{2}\sum_{j=1}^{2} [H^{(2)}_{01}(x)\, H^{(2)}_{0j}(y)\, w_{ij} + H^{(2)}_{1i}(x)\, H^{(2)}_{0j}(y)\, w_{xij}$$

$$+ H^{(2)}_{0i}(x)\, H^{(2)}_{1j}(y)\, w_{yij} + H^{(2)}_{1i}(x)\, H^{(2)}_{1j}(y)\, w_{xyij} + H^{(2)}_{2i}(x)\, H^{(2)}_{0j}(y)\, w_{xxij}$$

$$+ H^{(2)}_{0i}(x)\, H^{(2)}_{2j}(y)\, w_{yyij} + H^{(2)}_{2i}(x)\, H^{(2)}_{1j}(y)\, w_{xxyij}$$

$$+ H^{(2)}_{1i}(x)\, H^{(2)}_{2j}(y)\, w_{xyyij} + H^{(2)}_{2i}(x)\, H^{(2)}_{2j}(y)\, w_{xxyyij}\,] \qquad (2.28)$$

where the w_{ij}, w_{xij}, w_{yij}, w_{xyij}, w_{xxij}, w_{yyij}, w_{xxy0j}, w_{xyyij}, and w_{xxyyij} represent 36 undetermined nodal parameters, the subscripts x and y denote partial differentiation and the double index corner identification numbering scheme is shown in Fig. 1. The second order Hermite interpolation polynomials are given by

$$H^{(2)}_{01}(x) = \frac{1}{a^5}(a^5 - 10\,a^2x^3 + 15\,a\,x^4 - 6x^5) \qquad (2.29a)$$

$$H^{(2)}_{02}(x) = \frac{1}{a^5}(10\,a^2x^3 - 15\,a\,x^4 + 6x^5) \qquad (2.29b)$$

$$H^{(2)}_{11}(x) = \frac{1}{a^4}(a^4x - 6a^2x^3 + 8a\,x^4 - 3x^5) \qquad (2.29c)$$

Approved for Public Release

Contrails

$$H^{(2)}_{12}(x) = \frac{1}{a^4}(-4a^2x^3 + 7a\,x^4 - 3x^5) \qquad (2.29d)$$

$$H^{(2)}_{21}(x) = \frac{1}{2a^3}(a^3x^2 - 3a^2x^3 + 3a\,x^4 - x^5) \qquad (2.29e)$$

$$H^{(2)}_{22}(x) = \frac{1}{2a^3}(a^2x^3 - 2a\,x^4 + x^5) \qquad (2.29f)$$

and similar expressions for the y direction are obtained by replacing x by y and a by b. These interpolation polynomials have the basic Hermite properties given by Eqs. 2.10, that is

$$H^{(2)}_{0i}(x_k) = \delta_{ik}\ ; \qquad \frac{dH^{(2)}_{0i}}{dx}(x_k) = 0\ ; \qquad \frac{d^2H^{(2)}_{0i}}{dx^2}(x_k) = 0 \qquad (2.30a)$$

$$H^{(2)}_{1i}(x_k) = 0\ ; \qquad \frac{dH^{(2)}_{1i}}{dx}(x_k) = \delta_{ik}\ ; \qquad \frac{d^2H^{(2)}_{1i}}{dx^2}(x_k) = 0 \qquad (2.30b)$$

$$H^{(2)}_{2i}(x_k) = 0\ ; \qquad \frac{dH^{(2)}_{2i}}{dx}(x_k) = 0\ ; \qquad \frac{d^2H^{(2)}_{2i}}{dx^2}(x_k) = \delta_{ik} \qquad (2.30c)$$

for i = 1,2; k = 1,2 where it is understood that $x_1 = 0$ and $x_2 = a$. Because of these properties the assumed displacements, slopes, and curvatures ($\frac{\partial^2 w}{\partial x \partial y}$, $\frac{\partial^2 w}{\partial x^2}$, $\frac{\partial^2 w}{\partial y^2}$) along any particular edge depend only upon degrees of freedom associated with that edge. As a result of this, the satisfaction of interelement geometric admissibility conditions and the additional conditions of curvature continuity are easily satisfied by one to one variable linking. Substituting the assumed displacement (Eq. 2.28) into the linear strain-displacement relations (Eqs. 2.27) and then substituting into Eqs. 2.6

Approved for Public Release

Contrails

and 2.7 leads to a discretized total potential energy expression of the form

$$\pi_p = U_{2p} - W_p \tag{2.31}$$

where

$$U_{2p} = \frac{1}{2} \underset{1x36}{\vec{X}_p^T} \underset{36x36}{K_{2p}} \underset{36x1}{\vec{X}_p} \tag{2.32}$$

$$W_p = \underset{1x36}{\vec{X}_p^T} \underset{36x1}{\vec{F}_p} \tag{2.33}$$

The vector $\vec{X}_p$ contains the 36 corner degrees-of-freedom, 9 at each corner. The matrix K_{2p} is the ordinary stiffness matrix for this linear rectangular plate bending element based on the assumed displacement state given by Eq. 2.28 and an explicit formula for the elements of the stiffness matrix is given in Ref. 2 (p. 442, Eq. 64). The work equivalent load vector is represented by $\vec{F}_p$ and explicit formulas for the elements of this vector for several common loading conditions are given in Ref. 2 (Table 9). The element mass matrix M_p, consistent with the assumed displacement state (Eq. 2.28) used to derive the stiffness matrix, is given explicitly in Ref. 2(p. 442, Eq. 65), however the rotary inertia terms are omitted.

2.2.5 Parallelogram Plate Linear Bending 16 Degree-of-Freedom Element

The sixteen degree-of-freedom rectangular plate bending element originally set forth in Ref. 2 (see p. 441, Eq. 60) exhibits at least two important characteristics. First, the assumed displacement state is expressed in terms of products of first-order Hermite interpolation polynomials which facilitate the satisfaction of the geometric admissibility conditions. This assures monotonic convergence of the total energy as the

Approved for Public Release

Contrails

modeling is refined. Satisfaction of geometric admissibility assures monotonic convergence of the total potential energy, however it does not by itself insure convergence to the correct solution. Hence the second important characteristic of the assumed displacement state is that this set of functions can be shown to be complete (see Ref. 14, p. 119). Satisfaction of both geometric admissibility and completeness assure monotonic convergence of the total potential energy and convergence to the true displacement state as the modeling refinement is carried to the limit. The high accuracy and excellent convergence characteristics of the sixteen degree of freedom plate bending element has been illustrated by a variety of numerical examples (see Ref. 2, p. 443 and Ref. 15, p. 82).

In this section a sixteen degree-of-freedom total potential energy formulation for a parallelogram plate element, obtained by extending the work reported in Ref. 2, is discussed. This work was briefly reported in Ref. 10 and is documented in greater detail in Ref. 11. The total potential energy for the isotropic, elastic, constant thickness, parallelogram plate element shown in Fig. 4 is given by

$$\pi_s = U_s - W_s \tag{2.34}$$

where

$$U_s = \int_A \int_{-\frac{h}{2}}^{+\frac{h}{2}} \bar{U}\, dz\, dy\, dx \tag{2.35}$$

and W_s is the work done by external loads applied to the element. The strain energy density $\bar{U}$ is given by Eq. 2.4 and, assuming small deflection plate bending behavior, the strain-displacement relations are given by Eqs. 2.27. It is apparent from Fig. 4 that the coordinate transformation relations are

Approved for Public Release

Contrails

$$x = \tilde{x} - \tilde{y} \sin \beta \tag{2.36a}$$

$$y = \tilde{y} \cos \beta \tag{2.36b}$$

The strains ε_x, ε_y and γ_{xy} can be expressed as follows in the oblique coordinate system

$$\varepsilon_x = - z \frac{\partial^2 w}{\partial \tilde{x}^2} \tag{2.37a}$$

$$\varepsilon_y = - z[\frac{\partial^2 w}{\partial \tilde{x}^2} \tan^2\beta + 2 \frac{\partial^2 w}{\partial \tilde{x} \partial \tilde{y}} \sec \beta \tan \beta + \frac{\partial^2 w}{\partial \tilde{y}^2} \sec^2\beta] \tag{2.37b}$$

$$\gamma_{xy} = - 2z [\frac{\partial^2 w}{\partial \tilde{x}^2} \tan \beta + \frac{\partial^2 w}{\partial \tilde{x} \partial \tilde{y}} \sec \beta] \tag{2.37c}$$

Substituting Eqs. 2.37 into the strain energy density, $\tilde{U}$, then substituting the strain energy density into Eq. 2.35, replacing dy by $\cos \beta \, d\tilde{y}$, dx by $d\tilde{x}$ and integrating through the thickness yields the following results

$$U_s = \frac{D}{2 \cos^3\beta} \int_0^{\tilde{b}} \int_0^{\tilde{a}} \{\frac{\partial^2 w}{\partial \tilde{x}^2} + \frac{\partial^2 w}{\partial \tilde{y}^2} + 2(\sin^2\beta + \nu \cos^2\beta) \frac{\partial^2 w}{\partial \tilde{x}^2} \frac{\partial^2 w}{\partial \tilde{y}^2}$$

$$+ 4 \sin \beta (\frac{\partial^2 w}{\partial \tilde{x}^2} + \frac{\partial^2 w}{\partial \tilde{y}^2}) \frac{\partial^2 w}{\partial \tilde{x} \partial \tilde{y}} \tag{2.38}$$

$$+ [4 \sin^2\beta + 2(1-\nu) \cos^2\beta] [\frac{\partial^2 w}{\partial \tilde{x} \partial \tilde{y}}]^2 \} \, d\tilde{x} \, d\tilde{y}$$

where

$$D = \frac{E h^3}{12(1-\nu^2)} \tag{2.39}$$

Approved for Public Release

Contrails

The assumed displacement of the parallelogram plate element is expressed in terms of products of first-order Hermite interpolation polynomials in the oblique coordinate system. The assumed displacement function is therefore given by Eq. 2.8 with x replaced by $\tilde{x}$ and y replaced by $\tilde{y}$. Substituting the assumed displacement function into Eq. 2.38 and then substituting this expression for U_s into Eq. 2.34 yields the discretized form of the element potential energy

$$\pi_s = \frac{1}{2} \vec{X}_s^T K_{2s} \vec{X}_s - \vec{X}_s^T \vec{F}_s \tag{2.40}$$

The vector $\vec{X}_s$ contains the 16 corner degrees of freedom, $\vec{F}_s$ is the work equivalent load vector and K_{2s} represents the ordinary stiffness matrix. Explicit formulas for the elements of the stiffness matrix K_{2s} are given in Ref. 11 and the elements of the consistent mass matrix M_s are given by

$$M_{ij} = \frac{\rho hab \cos\beta}{1225} q_{ij}^{(7)} \tilde{a}^{\ell_{ij}} \tilde{b}^{n_{ij}} \tag{2.41}$$

where the coefficients $q_{ij}^{(7)}$ and the exponents ℓ_{ij}, n_{ij} are listed in Table 1 of Ref. 11.* The rotary inertia terms are omitted in Eq. 2.41. It is noteworthy that the explicit formula for equivalent load vectors given in Ref. 2 (p. 439 Table 9) for rectangular plates may be used for parallelogram plates provided a and b are understood to represent the plate edge lengths $\tilde{a}$ and $\tilde{b}$ parallel to the oblique coordinate system (see Fig. 4).

---

* Note that the factor $\cos\beta$, incorrectly omitted from Eqs. 14 of Ref. 11, is included in Eq. 2.41 of this report.

Approved for Public Release

Contrails

2.3 Cylindrical Shell Elements

Much of the research pertaining to the development of discrete elements for the analysis of shells has been focused on closed cylindrical or conical shell segments for modeling shells of revolution. Another approach that has been employed is to model a shell with flat plate elements. In Ref. 16 it was shown that the bending behavior of a curved arch is not adequately represented by flat bar elements and it was suggested that the development of reliable curved elements would be a significant contribution to the discrete element method of structural analysis. The use of plate elements to model shell structures introduces a modeling or idealization type of error. The consequences of this modeling error are likely to be particularly serious when buckling or post-buckling behavior is of interest, because the original shell is in effect replaced by a flat faceted shell.

In Ref. 7* a general theoretical development for constructing the discretized total potential energy for a rather general class of shell discrete elements was presented. The general development is given in terms of orthogonal curvilinear coordinates for any shell element bounded by lines of principal curvature. Finite displacements are included in the strain-displacement relations and the assumed displacement states for u, v and w are formed from products of first-order Hermite interpolation polynomials leading to 48 degree-of-freedom potential energy expressions.

2.3.1 Hermite Interpolation Polynomials - 48 Degrees-of-Freedom

The most widely used cylindrical shell element generated in the course of this research program has 48 degrees-of-freedom and is based upon assumed displacement patterns expressed in terms of products of first-order Hermite interpolation polynomials and undetermined corner displacement parameters.

---

* It should be noted that Ref. 7 represents an interim report on research carried out as a part of this program (i.e. Contract AF 33(615)-3432).

Approved for Public Release

Contrails

The development of the discretized total potential expression for this cylindrical element has been previously reported in Refs. 7 and 8, however a brief summary will be given herein for completeness. The strain displacement relations employed are

$$\varepsilon_s = \frac{\partial u}{\partial s} + \frac{1}{2}\left(\frac{\partial w}{\partial s}\right)^2 - z\frac{\partial^2 w}{\partial x^2} \tag{2.42a}$$

$$\varepsilon_\theta = \frac{1}{r}\frac{\partial v}{\partial \theta} + \frac{w}{r} + \frac{1}{2r^2}\left(\frac{\partial w}{\partial \theta}\right)^2 - \frac{z}{r^2}\left(\frac{\partial^2 w}{\partial \theta^2} - \frac{\partial v}{\partial \theta}\right) \tag{2.42b}$$

$$\gamma_{s\theta} = \frac{\partial v}{\partial s} + \frac{1}{r}\frac{\partial u}{\partial \theta} + \frac{1}{r}\frac{\partial w}{\partial s}\frac{\partial w}{\partial \theta} - \frac{2z}{r}\left(\frac{\partial^2 w}{\partial s \partial \theta} - \frac{\partial v}{\partial s}\right) \tag{2.42c}$$

Note that the corresponding linear case is obtained by neglecting $\frac{1}{2}\left(\frac{\partial w}{\partial s}\right)^2$, $\frac{1}{2r^2}\left(\frac{\partial w}{\partial \theta}\right)^2$ and $\frac{1}{r}\frac{\partial w}{\partial s}\frac{\partial w}{\partial \theta}$. Assuming a linear elastic isotropic material and plane stress behavior the total potential energy for the cylindrical shell element (see Fig. 5) is given by

$$\pi_c = U_c - W_c \tag{2.43}$$

where the element strain energy U_c is*

$$U_c = \int_0^{\ell}\int_0^{\Delta\theta}\int_{-\frac{h}{2}}^{+\frac{h}{2}} \frac{E}{2(1-\nu)^2}\left[\varepsilon_s^2 + \varepsilon_\theta^2 + 2\nu\,\varepsilon_s\,\varepsilon_\theta + \left(\frac{1-\nu}{2}\right)\gamma_{s\theta}^2\right] r\,dz\,d\theta\,ds \tag{2.44}$$

and W_c is the work done by external loads applied to the cylindrical element. The assumed displacement states are given by approximations similar to Eq. 2.8 by replacing x by s, a by ℓ, y by $\eta = r\theta$ and b by $r\Delta\theta$. That is

---

* Note that the subscript c refers to the cylindrical shell element and not to complementary energy.

Approved for Public Release

Contrails

$$w(s,\eta) = \sum_{i=1}^{2}\sum_{j=1}^{2} [H_{0i}^{(1)}(s)\, H_{0j}^{(1)}(\eta)\, w_{ij} + H_{1i}^{(1)}(s)\, H_{0j}^{(1)}(\eta)\, w_{sij} + H_{0i}^{(1)}(s)\, H_{1j}^{(1)}(\eta)\, w_{\eta ij} + H_{1i}^{(1)}(s)\, H_{1j}^{(1)}(\eta)\, w_{s\eta ij}] \qquad \text{where } \eta = r\theta, \tag{2.45}$$

with similar expressions for u and v. The degrees of freedom $w_{\eta ij}$ and $w_{s\eta ij}$ can also be expressed in the following alternate form

$$w_{\eta ij} = \frac{1}{r}\, w_{\theta ij} \tag{2.46a}$$

$$w_{s\eta ij} = \frac{1}{r}\, w_{s\theta ij} \tag{2.46b}$$

Furthermore, it is to be understood that w_{ij}, w_{sij}, $w_{\eta ij}$ and $w_{s\eta ij}$ represent 16 undetermined nodal parameters, the subscripts s, η, and θ denote partial differentiation and the double index corner identification scheme is shown in Fig. 5. Because of the special properties of the first order Hermite interpolation polynomials given by Eq. 2.10 the assumed displacement states and their derivatives along an edge depend only upon degrees of freedom associated with that edge and the satisfaction of geometric admissibility between elements is facilitated.

The discretized potential energy expression for the cylindrical shell discrete element is obtained by substituting the assumed displacement states into the strain-displacement relations Eq. 2.42 and then substituting these into Eqs. 2.43 and 2.44. This expression is similar to that for the plate element discussed in Section 2.2.1 and is given by Eqs. 2.11 and 2.12, with

Approved for Public Release

Contrails

p replaced by c. A more detailed description of the discretized strain energy will be found in Appendix A of Ref. 7 or Appendix B of Ref. 9. Work equivalent load vectors for several common loadings can be obtained by adapting the information in Table 4 of Ref. 7. The ordinary stiffness matrix K_{2c} associated with the quadratic strain energy of the linear formulation may be written in partitioned form as follows

$$K_{2c} = \begin{bmatrix} K_{2c}^{(u)} & K_{2c}^{(vu)^T} & K_{2c}^{(wu)^T} \\ K_{2c}^{(vu)} & K_{2c}^{(v)} & K_{2c}^{(vw)^T} \\ K_{2c}^{(wu)} & K_{2c}^{(wv)} & K_{2c}^{(w)} \end{bmatrix} \tag{2.47}$$

and explicit formulas for the elements of each submatrix are given by Eq. 12* of Ref. 8. There are no zero submatrices in Eq. 2.47, indicating that bending-membrane coupling exists even for the linear case in a cylindrical shell. The mass matrix consistent with the assumed displacement states used to derive the ordinary stiffness matrix (K_{2c}) may be written in partitioned form and explicit formulas for the elements the mass matrix are given by Eq. 18 of Ref. 8. It should be noted that Eqs. 18 of Ref. 8 includes rotary inertia terms that can usually be neglected for thin shells. Two other linear cylindrical shell discrete elements have recently been reported.

---

* The expression for $K_{ij}^{(wv)}$ in Eq. 12 of Ref. 8 should be corrected to read as follows:

$$K_{ij}^{(wv)} = \frac{D}{\ell r \Delta\theta}\left[\frac{12\ell^2\Delta\theta}{h^2}\, G_{ij}^{(11)} - \frac{\ell^2}{r^2\Delta\theta}\, G_{ij}^{(12)} - 2(1-\nu)\,\Delta\theta\, G_{ij}^{(13)} - \nu\,\Delta\theta\, G_{ij}^{(14)}\right] \ell^{L_{ij}} (r\Delta\theta)^{M_{ij}}$$

Approved for Public Release

Contrails

In Ref. 17 a twenty-four degree-of-freedom cylindrical shell element based upon bilinear assumed displacement states for u, v and a bicubic assumed displacement state for w is presented. An eigenvalue analysis of this twenty-four degree-of-freedom cylindrical shell element indicates that the assumed displacement patterns admit only four linearly independent displacement states (eigenvectors) that produce essentially zero strain energy relative to the elastic states.≠ Thus, the absence of an adequate approximation for two rigid-body modes limits the usefulness of the element reported in Ref. 17. In Ref. 18 a 24 degree-of-freedom cylindrical shell element is reported based upon assumed displacement patterns that can be shown to contain the six rigid-body modes exactly. Successful inclusion of the rigid-body modes was also confirmed by eigenvalue analyses as reported in Ref. 18.

The 48 degree-of-freedom cylindrical shell element discussed in this section has three noteworthy features. First, it is theoretically possible to join this element at any angle with other 48 degree-of-freedom plate or cylindrical shell elements and satisfy interelement geometric admissibility. Second, this element provides a good approximation of the middle surface stress state which can be particularly important when seeking to predict buckling and post buckling behavior. Third, for practical subtended angles (say $\Delta\theta < 30°$) it can be shown by eigenvalue analysis of the stiffness matrix that there exist six linearly independent displacement states which produce very little strain energy compared with the elastic deformation modes.

≠ The zero strain energy displacement states are often called the rigid-body modes. However, it should be understood that these rigid-body motions are approximations to the general rigid-body displacements of kinematics which take the form of a general orthogonal transformation and a translation.

Approved for Public Release

Contrails

2.3.2 Rigid Body Modes

In order for a discrete element to represent the behavior of a portion of a structural system it is necessary that the assumed displacement pattern be capable of approximating both rigid-body and deformation inducing displacements. In dealing with flat elements it has been common to approximate the displacements with polynomial expansions. Polynomials naturally contain the plate rigid-body modes and hence their representation has not presented a problem. However, polynomials can not in general be specialized to give the rigid-body modes when dealing with curved elements. As is pointed out in Ref. 19, it is not necessary that the element assumed displacement states represent the rigid-body displacement states exactly but rather the assumed displacement states must admit the six linearly independent rigid-body modes in the limit as the element size is reduced. On the other hand, for an element to be useful, the rigid-body modes (as well as the deformation behavior) must be adequately approximated for elements large enough to limit the system degrees-of-freedom to a practical number. The following remarks are intended to give some further explanation of why the 48 degree-of-freedom ordinary stiffness matrix K_{2c} discussed in Section 2.3.1 provides adequate, although not exact, representation of the rigid-body modes.

For a specific set of strain-displacement relations it will often be possible to determine the analytical form of six independent displacement states which produce zero-strain. For example, the linearized strain-displacement relations for a cylindrical shell given by Eqs. 2.42 omitting the terms $\frac{1}{2}\left(\frac{\partial w}{\partial s}\right)^2$, $\frac{1}{2r^2}\left(\frac{\partial w}{\partial \theta}\right)^2$ and $\frac{1}{r}\frac{\partial w}{\partial s}\frac{\partial w}{\partial \theta}$ imply the following zero-strain displacement states

Approved for Public Release

Contrails

$$u = C_1 \sin\theta + C_2 \cos\theta + C_6 \tag{2.48a}$$

$$v = \frac{s}{r}(-C_1 \cos\theta + C_2 \sin\theta) + C_3 \sin\theta + C_4 \cos\theta + C_5 \tag{2.48b}$$

$$w = \frac{s}{r}(-C_1 \sin\theta - C_2 \cos\theta) - C_3 \cos\theta + C_4 \sin\theta \tag{2.48c}$$

Sometimes the assumed displacement patterns are such that they can be specialized to represent the six zero-strain displacement states exactly (see for example the assumed displacement given by Eqs. 4 of Ref. 18 or those given by Eqs. 2.61 in Section 2.3.3 of this report). In such cases, it can be said that the rigid body displacement states are represented exactly by a specialization of the assumed displacement states. It may be of interest, however, to compare the zero strain states with the rigid-body displacement states for the element when subjected to a general orthogonal transformation and a translation. These should agree provided the basic simplifying assumptions made in the derivation of the strain-displacement relations are also invoked when comparing the general rigid-body displacement states with the zero strain states.

The linearized strain-displacement relations imply six linearly independent zero-strain displacement states (see Eqs. 2.48) and it is apparent that the displacement states used to generate the 48 degree-of-freedom cylindrical shell element described in Section 2.3.1 cannot be specialized to yield the rigid-body modes exactly. Nevertheless, eigenvalue analysis of the 48 x 48 stiffness matrix based on the polynomial interpolation functions indicates that for practical subtended angles there exist six linearly independent displacement states which produce "very little" strain energy compared with the other states.

Approved for Public Release

Contrails

Some qualitative insight into why the zero strain displacement states (Eqs. 2.48) are adequately approximated by the cubic interpolation is afforded by examining Taylor series expansions of sin θ and cos θ. If the angle θ is small enough so that sin θ may be replaced by $(\theta - \frac{\theta^3}{3!})$, and cos θ may be replaced by $(1 - \frac{\theta^2}{2!})$ then the zero-strain energy displacement states (Eqs. 2.48) may be expressed as follows

$$u \simeq C_1 \left(\theta - \frac{\theta^3}{3!}\right) + C_2 \left(1 - \frac{\theta^2}{2!}\right) + C_6 \tag{2.49a}$$

$$v \simeq \frac{s}{r}\left[-C_1\left(1 - \frac{\theta^2}{2!}\right) + C_2\left(\theta - \frac{\theta^3}{3!}\right)\right] + C_3\left(\theta - \frac{\theta^3}{3!}\right) + C_4\left(1 - \frac{\theta^2}{2!}\right) + C_5 \tag{2.49b}$$

$$w \simeq \frac{s}{r}\left[-C_1\left(\theta - \frac{\theta^3}{3!}\right) - C_2\left(1 - \frac{\theta^2}{2!}\right)\right] - C_3\left(1 - \frac{\theta^2}{2!}\right) + C_4\left(\theta - \frac{\theta^3}{3!}\right) \tag{2.49c}$$

Since $\eta = r\theta$ it can be shown that

$$H^{(1)}_{0j}(\eta) = H^{(1)}_{0j}(\theta) \tag{2.50a}$$

and

$$H^{(1)}_{1j}(\eta) = r\, H^{(1)}_{1j}(\theta) \tag{2.50b}$$

for j = 1,2 and employing Eqs. 2.48 it follows that the expression for $w(s,\eta)$ given by Eq. 2.45 can be expressed in the following alternate form

Approved for Public Release

Contrails

$$w(s,n) = w(s,\theta) = \sum_{i=1}^{2}\sum_{j=1}^{2} \left[H_{0i}^{(1)}(s)\, H_{0j}^{(1)}(\theta)\, w_{ij} \right.$$

$$H_{1i}^{(1)}(s)\, H_{0j}^{(1)}(\theta)\, w_{sij} + H_{0i}^{(1)}(s)\, H_{1j}^{(1)}(\theta)\, w_{\theta ij}$$

$$\left. + H_{1i}^{(1)}(s)\, H_{1j}^{(1)}(\theta)\, w_{s\theta ij} \right] \qquad (2.51)$$

with similar expressions for u and v. Thus, it is apparent from Eq. 2.51 that the assumed displacement states used in Section 2.3.1 (see Eq. 2.45) are bicubic in s and θ and they can therefore be specialized to represent the approximate rigid-body displacement states exhibited in Eqs. 2.49.

2.3.3 Circular Interpolation Functions - 48 Degrees-of-Freedom

The use of interpolation functions to generate assumed displacement states need not be restricted to polynomial type functions. For example, let

$$g(\theta) = C_0 + C_1\,\theta + C_2 \sin\theta + C_3 \cos\theta \qquad (2.52)$$

and evaluate $g(\theta)$ and $\frac{dg}{d\theta}(\theta)$ at the end points of a region[$\theta = 0$ and $\theta = \Delta\theta$] then

$$g(0) = C_0 + C_3 \qquad (2.53a)$$

$$g(\Delta\theta) = C_0 + C_1(\Delta\theta) + C_2 \sin(\Delta\theta) + C_3 \cos(\Delta\theta) \qquad (2.53b)$$

$$\frac{dg}{d\theta}(0) = C_1 + C_2 \qquad (2.53c)$$

$$\frac{dg}{d\theta}(\Delta\theta) = C_1 + C_2 \cos(\Delta\theta) - C_3 \sin(\Delta\theta) \qquad (2.53d)$$

Approved for Public Release

Contrails

Introducing the notation

$$g(0) = g_1, \quad g(\Delta\theta) = g_2, \quad \frac{dg}{d\theta}(0) = g_{\theta 1} \quad \text{and} \quad \frac{dg}{d\theta}(\Delta\theta) = g_{\theta 2}$$

and solving Eqs. 2.53 for C_0, C_1, C_2 and C_3 yields

$$C_0 = g_1 + \frac{g_{\theta 2} - g_{\theta 1}}{\sin \Delta\theta}$$

$$+ \left[\frac{(g_{\theta 2}-g_{\theta 1}) \sin \Delta\theta + g_{\theta 1}(1-\cos \Delta\theta-\Delta\theta \sin \Delta\theta)- g_{\theta 2}(1-\cos \Delta\theta)}{(1-\cos \Delta\theta)^2 - \sin \Delta\theta(\Delta\theta - \sin \Delta\theta)}\right] \frac{(1-\cos \Delta\theta)}{\sin \Delta\theta} \tag{2.54a}$$

$$C_1 = g_{\theta 1} + \left[\frac{-(g_2-g_1) \sin \Delta\theta-g_{\theta 1} (1-\cos \Delta\theta-\Delta\theta \sin \Delta\theta) + g_{\theta 2}(1-\cos \Delta\theta)}{(1-\cos \Delta\theta)^2 - \sin \Delta\theta(\Delta\theta-\sin \Delta\theta)}\right] \tag{2.54b}$$

$$C_2 = \frac{(g_2-g_1) \sin \Delta\theta + g_{\theta 1} (1-\cos \Delta\theta-\Delta\theta \sin \Delta\theta) - g_{\theta 2} (1-\cos \Delta\theta)}{(1-\cos \Delta\theta)^2 - \sin \Delta\theta (\Delta\theta-\sin \Delta\theta)} \tag{2.54c}$$

$$C_3 = - \left[\frac{g_{\theta 2} - g_{\theta 1}}{\sin \Delta\theta}\right]$$

$$+ \left[\frac{-(g_2-g_1) \sin \Delta\theta-g_{\theta 1} (1-\cos \Delta\theta-\Delta\theta \sin \Delta\theta) + g_{\theta 2} (1-\cos \Delta\theta)}{(1-\cos \Delta\theta)^2 - \sin \Delta\theta (\Delta\theta-\sin \Delta\theta)}\right] \frac{(1-\cos \Delta\theta)}{\sin \Delta\theta} \tag{2.54d}$$

Substituting C_0, C_1, C_2 and C_3 from Eqs. 2.54 into Eq. 2.52 and regrouping terms, $g(\theta)$ can be written in a form analogous to the first-order Hermite interpolation expression, that is

Approved for Public Release

Contrails

$$g(\theta) = \sum_{j=1}^{2} \left[S_{0j}^{(1)}(\theta)\, g_j + S_{1j}^{(1)}(\theta)\, g_{\theta j} \right] \tag{2.55}$$

where

$$S_{01}^{(1)}(\theta) = 1 - \frac{(1-\cos\Delta\theta)(1-\cos\theta) - \sin\Delta\theta\,(\theta - \sin\theta)}{(1-\cos\Delta\theta)^2 - \sin\Delta\theta\,(\Delta\theta - \sin\Delta\theta)} \tag{2.56a}$$

$$S_{02}^{(1)}(\theta) = \frac{(1-\cos\Delta\theta)(1-\cos\theta) - \sin\Delta\theta\,(\theta - \sin\theta)}{(1-\cos\Delta\theta)^2 - \sin\Delta\theta\,(\Delta\theta - \sin\Delta\theta)} \tag{2.56b}$$

$$S_{11}^{(1)}(\theta) = \theta - \frac{1-\cos\theta}{\sin\Delta\theta} + \frac{(1-\cos\Delta\theta-\Delta\theta\sin\Delta\theta)\left[(1-\cos\Delta\theta)(1-\cos\theta) - \sin\Delta\theta\,(\theta-\sin\theta)\right]}{\sin\Delta\theta\left[(1-\cos\Delta\theta)^2 - \sin\Delta\theta\,(\Delta\theta - \sin\Delta\theta)\right]} \tag{2.56c}$$

$$S_{12}^{(1)}(\theta) = \frac{1-\cos\theta}{\sin\Delta\theta} - \frac{(1-\cos\Delta\theta)\left[(1-\cos\Delta\theta)(1-\cos\theta) - \sin\Delta\theta(\theta-\sin\theta)\right]}{\sin\Delta\theta\left[(1-\cos\Delta\theta)^2 - \sin\Delta\theta(\Delta\theta-\sin\Delta\theta)\right]} \tag{2.56d}$$

It can be shown that the interpolation functions defined by Eqs. 2.56 have the following properties:

Approved for Public Release

Contrails

$$S^{(1)}_{0j}(\theta_k) = \delta_{jk} \; ; \qquad j = 1,2; \quad k = 1,2 \qquad (2.57a)$$

$$\frac{dS^{(1)}_{0j}}{d\theta}(\theta_k) = 0 \qquad j = 1,2; \quad k = 1,2 \qquad (2.57b)$$

$$S^{(1)}_{1j}(\theta_k) = 0 \qquad j = 1,2; \quad k = 1,2 \qquad (2.57c)$$

$$\frac{dS_{1j}}{d\theta}(\theta_k) = \delta_{jk} \; ; \qquad j = 1,2; \quad k = 1,2 \qquad (2.57d)$$

Now let f(s) be expressed in terms of first-order Hermite interpolation polynomials as follows

$$f(s) = \sum_{i=1}^{2} \left[H^{(1)}_{0i}(s) \, f_i + H^{(1)}_{1i}(s) \, f_{si} \right] \qquad (2.58)$$

and assume the usual product form

$$w(s,\theta) = f(s) \, g(\theta) \qquad (2.59)$$

where f(s) is given by Eq. 2.58 and g(θ) is given by Eq. 2.55. Solving for the corner values of w, $\frac{\partial w}{\partial s}$, $\frac{\partial w}{\partial \theta}$ and $\frac{\partial^2 w}{\partial s \partial \theta}$ it is found that

$$w_{ij} = w(s_i, \theta_j) = f_i \, g_j \qquad (2.60a)$$

$$w_{sij} = \frac{\partial w}{\partial s}(s_i, \theta_j) = f_{si} \, g_j \qquad (2.60b)$$

Approved for Public Release

Contrails

$$w_{\theta ij} = \frac{\partial w}{\partial \theta}(s_i, \theta_j) = f_i \, g_{\theta j} \tag{2.60c}$$

$$w_{s\theta ij} = \frac{\partial^2 w}{\partial s \partial \theta}(s_i, \theta_j) = f_{si} \, g_{\theta j} \tag{2.60d}$$

and therefore the assumed displacement state $w(s,\theta)$ may be expressed as follows

$$w(s,\theta) = \sum_{i=1}^{2} \sum_{j=1}^{2} [H_{0i}^{(1)}(s) \, S_{0j}^{(1)}(\theta) \, w_{ij} + H_{1i}^{(1)}(s) \, S_{0j}^{(1)}(\theta) \, w_{sij} + H_{0i}^{(1)}(s) \, S_{1j}^{(1)}(\theta) \, w_{\theta ij} + H_{1i}^{(1)}(s) \, S_{1j}^{(1)}(\theta) \, w_{s\theta ij}] \tag{2.61}$$

with similar expressions for $u(s,\theta)$ and $v(s,\theta)$.

The six linearly independent zero strain (rigid-body) displacement states exhibited in Eq. 2.48 are implied by the linearized strain-displacement relations for the cylindrical shell. A notable feature of assumed displacement states having the form given by Eq. 2.61 is that they can be specialized to represent the rigid body displacement states given by Eqs. 2.48 exactly.

The development of the discretized total potential energy expression for a 48 degree-of-freedom cylindrical shell element based upon assumed displacement states for u, v, and w of the form given by Eq. 2.61 follows the same steps as the development outlined in Section 2.3.1. That is, substituting the assumed displacement states (see Eq. 2.61) into the strain-displacement relations (Eq. 2.42) and then substituting into Eq. 2.43 and 2.44 yields a discretized total potential energy expression. The discretized total potential energy for the cylindrical shell element is similar in form to that for the plate element discussed in Section 2.2.1 and can be represented by Eqs. 2.11 and 2.12 with p replaced by c. Although explicit formulas for

Approved for Public Release

Contrails

the elements of the matrices K_{2c} , K_{3c} , and K_{4c} can be generated, they are too cumbersome to reproduce here.

The 48 degree-of-freedom cylindrical shell element discussed in this section exhibits the following attractive features: (a) it is theoretically possible to join this element together at any angle with the other 48 degree-of-freedom plate and cylindrical shell elements described herein (see Sections 2.1.1 and 2.3.1)†, (b) the 16 degree-of-freedom expansions used to represent the u and v displacements provide a good approximation of the middle surface stress state which can be important in dealing with buckling and postbuckling behavior, and (c) the assumed displacement states can be specialized to yield the six linearly independent zero-strain displacement states implied by the linearized strain-displacement equations exactly. Eigenvalue analyses of ordinary stiffness matrices (K_{2c}) based upon assumed displacement states of the form given by Eq. 2.61 yields six zero eigenvalues and six linearly independent eigenvectors representing the rigid-body modes.

In deciding between the cylindrical shell element described in this section and that described in Section 2.3.1 consideration should be given to the fact that the generation of the matrices K_{2c}, K_{3c}, and K_{4c} is more time consuming for the element described in this section. This is due to the increased complexity arising from the use of mixed polynomial and circular functions and to the necessity for double precision arithmetic in evaluating the elements of the matrices K_{2c}, K_{3c}, and K_{4c}. The need for double precision

---

† Note that interelement geometric admissibility cannot be satisfied along a common arc line interface between cylindrical shell elements based upon different forms of θ interpolation [i.e. $H_{0j}^{(1)}(\theta)$, $H_{1j}^{(1)}(\theta)$, or $S_{0j}^{(1)}(\theta)$, $S_{1j}^{(1)}(\theta)$].

Approved for Public Release

Contrails

arithmetic appears to be related to the fact that the transformation which carries the functions 1, θ, sin θ, cos θ (see Eqs. 2.52) into the interpolation functions $S_{0j}^{(1)}(\theta)$ and $S_{1j}^{(1)}(\theta)$ (see Eqs. 2.56) becomes singular as the subtended arc of the element ($\Delta\theta$) vanishes. The existing program (see Section 6) always employs double precision in evaluating the elements of the matrices K_{2c}, K_{3c} and K_{4c}.* However, in view of this difficulty, use of the cylindrical shell element described in this section is not recommended for cases where the subtended angle $\Delta\theta$ is less than 5°. This situation is not restrictive because it is known that the difference between the cylindrical shell element described in this section and that discussed in Section 2.3.1, vanishes in the limit as $\Delta\theta$ approaches zero. For $5° < \Delta\theta < 30°$ either element may be used. For $\Delta\theta > 30°$ the element described in this section is recommended while for $\Delta\theta < 5°$ the element described in Section 2.3.1 is recommended.

2.4 Implementation

The total potential energy for a structural system represented by an assemblage of discrete elements can be viewed as the sum of the contributions of the individual elements. The numerical prediction of the behavior of an assemblage of discrete elements may be viewed as a mathematical programming problem; that is, numerical solutions are to be generated by minimization of the total potential energy subject to certain equality constraints. The principle of minimum total potential energy states that of all possible geometrically admissible displacement states, those which locally minimize the total potential energy satisfy the equilibrium conditions, the natural

---

* Double precision is used only in computing the elements of the matrices K_{2c}, K_{3c}, and K_{4c}; the subsequent energy search phase of the program is carried out in single precision.

Approved for Public Release

Contrails

boundary conditions (stress or force) and the stability condition $\delta^2\Pi > 0$ and are therefore stable equilibrium positions[≠]. The total potential energy of an assemblage of discrete elements

$$\Pi = \sum_{k=1}^{N} \pi_k \tag{2.62}$$

where N is the total number of elements, is a function of all the degrees of freedom of all elements subject to the interelement geometric admissibility conditions and the displacement boundary conditions[+]. The satisfaction of geometric admissibility requirements leads to a set of linear equality constraints. These linear equality constraints reduce the number of degrees of freedom in the total potential energy expression.

Prior to seeking the minimum of the total potential energy, it may often be useful to further reduce the number of independent degrees-of-freedom by imposing additional conditions based upon an engineering insight into the anticipated behavior of the structure. For example, between two tangentially joined elements, continuity of middle surface strains may be anticipated in the absence of line tractions and curvature continuity may be expected in the absence of line moments. Force boundary conditions[*] may also be viewed as optional additional conditions. It should be clearly recognized that the use of additional conditions is not strictly required, however, employing them when appropriate, reduces the number of degrees-of-

---

≠ This statement recognizes the possible existence of relative minima in nonlinear problems and points up the fact that only "stable" solutions (in the $\delta^2\Pi > 0$ sense) will be found by minimization of the total potential energy.

\+ Displacement boundary conditions are the essential or imposed conditions of the variational formulation.

* Force boundary conditions are the additional or natural boundary conditions of the variational formulation.

Approved for Public Release

Contrails

freedom without a substantial change in the results obtained.

Imposing the interelement geometric admissibility conditions, the displacement boundary conditions and appropriate additional conditions leads to the total potential energy as a function of the independent degrees-of-freedom. Thus any of several powerful algorithms for the unconstrained minimization of a function of many variables may be employed to find a numerical solution to the structural analysis problem (see Section 4).

2.4.1 Geometric Admissibility

Since the assumed displacement states for u and v are continuous and the assumed displacement state for w is continuous and has continuous first derivatives ($\frac{\partial w}{\partial x}$, $\frac{\partial w}{\partial y}$), it follows that geometric admissibility is satisfied within the plate and shell discrete elements discussed in this report. To complete the satisfaction of the geometric admissibility requirement it is necessary to impose the interelement admissibility conditions and the displacement boundary conditions.

The assumed displacement states used here facilitate the satisfaction of interelement admissibility conditions. For example, consider the assemblage of two rectangular 48 degree-of-freedom thin plate elements joined at an angle ϕ as shown in Fig. 6. In this case geometric admissibility at the interface between elements I and II requires that

$$u^{II}(0,y_2) = \cos\phi\, u^{I}(a_1,y_1) - \sin\phi\, w^{I}(a_1,y_1) \qquad (2.63a)$$

$$v^{II}(0,y_2) = v^{I}(a_1,y_1) \qquad (2.63b)$$

$$w^{II}(0,y_2) = \sin\phi\, u^{I}(a_1,y_1) + \cos\phi\, w^{I}(a_1,y_1) \qquad (2.63c)$$

Approved for Public Release

Contrails

$$\frac{\partial w^{II}}{\partial x_2}(0,y_2) = \frac{\partial w^{I}}{\partial x_1}(a_1,y_1) \tag{2.63d}$$

Ignoring the distinction between y_1 and y_2 along the interface between the elements and defining $y_1 = y_2 = y$ the assumed displacement functions (see Eq. 2.8) reduce to the following expressions along the interface for the displacements appearing in Eq. 2.63a.

$$u^{II}(0,y) = \sum_{j=1}^{2} [H_{0j}^{(1)}(y)\, u_{1j}^{II} + H_{1j}^{(1)}(y)\, u_{y1j}^{II}] \tag{2.64a}$$

$$u^{I}(a_1,y) = \sum_{j=1}^{2} [H_{0j}^{(1)}(y)\, u_{2j}^{I} + H_{1j}^{(1)}(y)\, u_{y2j}^{I}] \tag{2.64b}$$

$$w^{I}(a_1,y) = \sum_{j=1}^{2} [H_{0j}^{(1)}(y)\, w_{2j}^{I} + H_{1j}^{(1)}(y)\, w_{y2j}^{I}] \tag{2.64c}$$

Substituting Eqs. 2.64 into Eq. 2.63a and noting that $H_{0j}^{(1)}(y)$ and $H_{1j}^{(1)}(y)$ are linearly independent, it is apparent that the geometric admissibility condition represented by Eq. 2.63a is satisfied along the entire common edge by imposing the following four equality constraints:

$$u_{1j}^{II} = \cos\phi\ u_{2j}^{I} - \sin\phi\ w_{2j}^{I} \quad ; \quad j = 1,2 \tag{2.65a}$$

$$u_{y1j}^{II} = \cos\phi\ u_{y2j}^{I} - \sin\phi\ w_{y2j} \quad ; \quad j = 1,2 \tag{2.65b}$$

In a similar manner the interelement geometric admissibility conditions

Approved for Public Release

Contrails

represented by Eqs. 2.63 b, c and d yield equality constraints as follows:

from Eq. 2.63b

$$v^{II}_{1j} = v^{I}_{2j} \quad ; \qquad j = 1,2 \tag{2.66a}$$

$$v^{II}_{y1j} = v^{I}_{y2j} \quad ; \qquad j = 1,2 \tag{2.66b}$$

from Eq. 2.63c

$$w^{II}_{1j} = \sin\phi \; u^{I}_{2j} + \cos\phi \; w^{I}_{2j} \quad ; \qquad j = 1,2 \tag{2.67a}$$

$$w^{II}_{y1j} = \sin\phi \; u^{I}_{y2j} + \cos\phi \; w^{I}_{y2j} \quad ; \qquad j = 1,2 \tag{2.67b}$$

and from Eq. 2.63d

$$w^{II}_{x1j} = w^{I}_{x2j} \quad ; \qquad j = 1,2 \tag{2.68a}$$

$$w^{II}_{xy1j} = w^{I}_{xy2j} \quad ; \qquad j = 1,2 \tag{2.68b}$$

Note that when the elements are joined by a hinge line then geometric admissibility does not require that the relative rotation between elements I and II be zero and the equality constraints due to Eq. 2.63d, that is Eqs. 2.68, are omitted. The equality constraints arising from the admissibility conditions represented by Eqs. 2.63a and c lead to linear combinations of the degrees-of-freedom, namely Eqs. 2.65 and 2.67. On the other hand, the admissibility conditions represented by Eqs. 2.63b and d lead to simple one to one linking conditions, namely Eqs. 2.66 and 2.68. All of the degrees-of-freedom involved in the equality constraints (Eqs. 2.65 through 2.68) implementing the interelement admissibility requirements (Eqs. 2.63) are on the common edge between elements I and II (see Fig. 6).

Approved for Public Release

Contrails

Two important special cases can be dealt with by specializing the foregoing relations. First consider the case where the elements I and II are joined tangentially so that the angle $\phi = 0$, $\cos \phi = 1$, $\sin \phi = 0$ and the geometric admissibility requirements (Eqs. 2.63) can be simplified accordingly. The equality constraints (Eqs. 2.65 through 2.68) implementing the interelement admissibility conditions are, for this special case ($\phi = 0$), all simple one to one linking conditions. The second special case is when the elements I and II are joined perpendicularly so that $\phi = 90°$, $\cos \phi = 0$, and $\sin \phi = 1$. Again the geometric admissibility requirements (Eqs. 2.63) can be specialized and the equality constraints (Eqs. 2.65 through 2.68) reduce to simple one to one linking conditions. The computer program described in Section 6 of this report is currently limited to assemblages of discrete elements connected together either tangentially ($\phi = 0$) or perpendicularly ($\phi = 90°$).

The assumed displacement states employed herein facilitate the satisfaction of a variety of imposed displacement boundary conditions. For example, consider implementing the requirement that the edge $x_2 = a_2$ of element II (see Fig. 6) be fully restrained, that is

$$u^{II}(a_2,y) = \sum_{j=1}^{2} [H_{0j}^{(1)}(y)\, u_{2j}^{II} + H_{1j}^{(1)}(y)\, u_{y2j}^{II}] = 0 \qquad (2.69a)$$

$$v^{II}(a_2,y) = \sum_{j=1}^{2} [H_{0j}^{(1)}(y)\, v_{2j}^{II} + H_{1j}^{(1)}(y)\, v_{y2j}^{II}] = 0 \qquad (2.69b)$$

$$w^{II}(a_2,y) = \sum_{j=1}^{2} [H_{0j}^{(1)}(y)\, w_{2j}^{I} + H_{1j}^{(1)}(y)\, w_{y2j}^{II}] = 0 \qquad (2.69c)$$

Approved for Public Release

Contrails

and

$$\frac{\partial w^{II}}{\partial x_2}(a_2,y) = \sum_{j=1}^{2} [H_{0j}^{(1)}(y)\, w_{x2j}^{II} + H_{1j}^{(1)}(y)\, w_{xy2j}^{II}] = 0 \qquad (2.69d)$$

where for convenience y_2 has been replaced by y. These displacement boundary conditions (Eqs. 2.69) lead to the following simple equality constraints:

$$u_{2j}^{II} = u_{y2j}^{II} = 0 \; ; \qquad j = 1,2 \qquad (2.70a)$$

$$v_{2j}^{II} = v_{y2j}^{II} = 0 \; ; \qquad j = 1,2 \qquad (2.70b)$$

$$w_{2j}^{I} = w_{y2j}^{II} = 0 \; ; \qquad j = 1,2 \qquad (2.70c)$$

$$w_{x2j}^{II} = w_{xy2j}^{II} = 0 \; ; \qquad j = 1,2 \qquad (2.70d)$$

In the case of full membrane restraint but simple support with respect to bending, the zeroing conditions exhibited in Eq. 2.70d would be ignored. In the event that membrane displacement tangent to the edge $x_2 = a_2$ of element II is not restrained, the zeroing conditions given by Eq. 2.70b would be ignored. Another useful displacement boundary condition is the requirement that $u^{II}(a_2,y)$ be uniform along the edge but of undetermined magnitude. By examining Eq. 2.69a it is found that this boundary condition can be implemented by imposing the following simple equality constraints:

$$u_{21}^{II} = u_{22}^{II} \qquad (2.71a)$$

and

$$u_{y21}^{II} = u_{y22}^{II} = 0 \qquad (2.71b)$$

Approved for Public Release

Contrails

Finally it should be noted that any prescribed displacement expressable in terms of a linear combination of the osculatory interpolation polynomials employed can be imposed by assigning appropriate numerical values to the degrees of freedom involved in the edge displacement relations (Eq. 2.69).

2.4.2 Additional Conditions

The previous section explains the procedure for assuring that the displacement state over an assemblage of discrete elements satisfies the geometric admissibility requirements. In this section a similar procedure for introducing optional additional conditions is outlined. In many situations the engineer in-charge will have some physical insight regarding the anticipated behavior of the structure being analyzed. By introducing appropriate additional constraints it is possible to reduce the number of independent degrees-of-freedom for a given modeling (idealization) without significantly changing the results of the analysis. For example, consider the case of two plate elements tangentially connected such as elements I and II in Fig. 6 when $\phi = 0$. The elements lie in the same plane and in the absence of line tractions on the common edge, it can be anticipated that the middle surface strains (ε_x, ε_y and γ_{xy}) as well as the rotation ($\theta_z = \frac{\partial v}{\partial x} - \frac{\partial u}{\partial y}$) will be continuous. Satisfaction of the interelement geometric admissibility requirement is achieved by making u, v, w and $\frac{\partial w}{\partial x}$ continuous along the interface as previously described (see Eqs. 2.63 with $\phi = 0$). In order to require continuous middle surface strains and rotation (θ_z) along the interface between elements I and II it is only necessary to introduce the additional conditions

Approved for Public Release

Contrails

$$\frac{\partial u^{II}}{\partial x_2}(0,y_2) = \frac{\partial u^{I}}{\partial x_1}(a_1,y_1) \tag{2.72a}$$

$$\frac{\partial v^{II}}{\partial x_2}(0,y_2) = \frac{\partial v^{I}}{\partial x_1}(a_1,y_1) \tag{2.72b}$$

which yield the following equality constraints between the degrees-of-freedom;

$$u^{II}_{x1j} = u^{I}_{x2j} \quad ; \qquad j = 1,2 \tag{2.73a}$$

$$u^{II}_{xy1j} = u^{I}_{xy2j} \quad ; \qquad j = 1,2 \tag{2.73b}$$

from Eq. 2.72a and

$$v^{II}_{x1j} = v^{I}_{x2j} \quad ; \qquad j = 1,2 \tag{2.74a}$$

$$v^{II}_{xy1j} = v^{I}_{xy2j} \quad ; \qquad j = 1,2 \tag{2.74b}$$

from Eq. 2.72b. Note that the implementation of middle surface strain and rotation continuity conditions involve only degrees of freedom associated with the common edge and simple one to one linking.

The geometric admissibility conditions and additional conditions where appropriate, have the effect of significantly reducing the number of independent degrees-of-freedom. For example, consider an assemblage of four coplanar 48 degree-of-freedom rectangular plate elements (see Fig. 7). At the outset there are 48 independent degrees-of-freedom associated with the interior node common to all four elements. It can be shown that by imposing the geometric admissibility conditions between the four elements, the number of independent degrees-of-freedom associated with the interior node is reduced to 22. Furthermore, if the middle surface strains and

Approved for Public Release

Contrails

rotations are made continuous between the four elements, by using the additional conditions, it will be found that the number of independent degrees-of-freedom associated with the interior node is reduced to 12.

More complex additional conditions may involve linear combinations of degrees-of-freedom not necessarily associated with the common edge. For example, consider again the case of two plate elements tangentially connected such as elements I and II in Fig. 6 with $\phi = 0$. In the absence of line moments, continuity of the bending moment M_x and the twisting moment M_{xy} along the common edge between elements I and II (see Fig. 6) may be anticipated. Satisfaction of the interelement admissibility conditions is sufficient to insure

$$\frac{\partial^2 w^{II}}{\partial x_2 \partial y_2}(0,y_2) = \frac{\partial^2 w^{I}}{\partial x_1 \partial y_1}(a_1,y_1) \tag{2.75a}$$

and

$$\frac{\partial^2 w^{II}}{\partial y_2^2}(0,y_2) = \frac{\partial^2 w^{I}}{\partial y_1^2}(a_1,y_1) \tag{2.75b}$$

Therefore it is only necessary to introduce the following additional condition

$$\frac{\partial^2 w^{II}}{\partial x_2^2}(0,y_2) = \frac{\partial^2 w^{I}}{\partial x_1^2}(a_1,y_1) \tag{2.76}$$

in order to have continuous bending moments M_x along the common edge between elements I and II. Implementation of the continuity condition on the curvature normal to the common edge can be shown to involve linear combinations of several degrees-of-freedom some of which are not associated with the interface line.

Approved for Public Release

Contrails

Since force boundary conditions are natural boundary conditions within a total potential energy formulation, they are usually treated as applied loads and are dealt with using the work equivalence approach. However, force boundary conditions may also be considered as optional additional conditions. For example, the requirement that the bending moment M_x along the edge $x_2 = a_2$ of element II equal a constant value $\bar{M}_x$ may be introduced as an additional condition

$$M_x(a_2,y_2) = -D[\frac{\partial^2 w^{II}}{\partial x_2^2}(a_2,y_2) + \nu \frac{\partial^2 w^{II}}{\partial y_2^2}(a_2,y_2)] = \bar{M}_x \qquad (2.78)$$

If the edge $x_2 = a_2$ of element II is simply supported then $w^{II}(a_2,y_2) = 0$ and the additional condition representing the uniform bending moment boundary condition reduces to

$$M_x(a_2,y_2) = -D[\frac{\partial^2 w}{\partial x_2^2}(a_2,y_2)] = \bar{M}_x \qquad (2.79)$$

Implementation of this optional additional condition will also involve linear combinations of several degrees-of-freedom some of which are not associated with the edge $x_2 = a_2$ of element II.

2.5 Examples

In this section some example problems are reviewed. These numerical solutions have been obtained using discrete element representations generated in the course of this research program. Three types of example problems are discussed. The first type exhibits nonlinear bending-membrane coupling and is characterized by the increasing slope of the load deflection curve (see Fig. 10). The specific example of this first class is a square clamped plate subject to a uniformly distributed transverse load. Example problems of the second type also exhibit nonlinear bending-membrane coupling, however they are

Approved for Public Release

Contrails

characterized by decreasing slope of the load end-shortening curve (prior to snap-through, see Fig. 13). The examples in this second group are flat, slightly curved, and curved panels subject to prescribed end-shortening. An interesting additional feature of the two curved panel examples is that they exhibit snap-through buckling. The third class of example problems is linear. One linear example problem is discussed, namely the pinched cylindrical shell of finite length. This example is included to illustrate numerically the influence of including exact rigid body modes in comparison with a good approximate representation.

It should be noted that solutions for other example problems have been documented. Linear clamped plate and linear pinched cylinder examples were reported in the interim report (Ref. 7). The influence of systematic refinement of the modeling was examined in both of these cases. The excellent convergence characteristics of the 48 degree-of-freedom plate (see Section 2.2.1) and cylindrical shell (see Section 2.3.1) elements were illustrated numerically in Ref. 7. Results for the pinched cylinder problem, including geometrically nonlinear terms in the strain displacement relations, were also given in Ref. 7. Static deflection results for skew cantilever plates subject to uniform transverse load were presented in Ref. 10. Additional static linear bending examples for cantilever and clamped rhombic plates were reported in Ref. 11. Some natural frequency predictions for clamped and cantilever rhombic plates were given in Ref. 11. Static deflection results for a uniformly loaded square clamped plate example, based on the 36 degree of freedom linear bending element (see Section 2.2.4) were given on p. 443 of Ref. 2.

2.5.1 Transversely Loaded Clamped Plate Example

Consider the clamped plate shown in Fig. 8 subject to a uniformly distributed transverse loading p_z. The clamped boundary conditions require

Approved for Public Release

Contrails

that u, v, w and the slope normal to the edge be zero on all four edges. The example plate has dimensions 20" x 20" x 0.1", modulus of elasticity E = 10.92 x 10^6 lbs/in^2 and Poisson's ratio ν = 0.3. Since the problem is doubly symmetric only one quadrant of the plate is considered. Four 48 degree-of-freedom discrete elements are used to represent a single quadrant of the plate (see Fig. 9). Imposing the boundary conditions and using additional conditions such that the middle surface strains and the rotation (θ_z) will be continuous between elements the number of independent degrees-of-freedom for this example is found to be 41. Solutions were obtained for each of several load intensities by applying the Fletcher-Powell algorithm for unconstrained minimization (see Section 4.1.1) to the total potential energy function. The midpoint transverse displacement (w_c) is given for load intensities (p_z) ranging from 0.2 psi to 2.0 psi in Table 1. The results obtained by a Ritz technique solution (see p. 421, Ref. 20) are also listed in Table 1. The agreement between the two solutions, exhibited in Table 1, is seen to be excellent. The load intensity versus midpoint transverse deflection data listed in Table 1, is presented graphically in Fig. 10. The increasing slope of the curve in Fig. 10 indicates that as the transverse displacement increases the membrane action grows in importance. It is apparent from Fig. 10 that linear theory would over estimate the deflection due to a particular load intensity with rapidly increasing error for higher load levels. A more detailed summary of the nodal displacements obtained using the 41 degree-of-freedom discrete element finite deflection analysis will be found in Table 11 of Ref. 7.

2.5.2 Panel End-Shortening Examples

Consider a simply supported rectangular panel subject to prescribed uniform end shortening δ (see Fig. 11). The displacement boundary conditions imposed are:

Approved for Public Release

Contrails

$$u(-A, y) = \delta \tag{2.80a}$$

$$u(+A, y) = -\delta \tag{2.80b}$$

$$w(\pm A, y) = w(x, \pm B) = 0 \tag{2.80c}$$

$$v(\pm A, y) = v(x, \pm B) = 0 \tag{2.80d}$$

The imposed displacement boundary conditions represented by Eqs. 2.80a and 2.80b imply that the edges $x = \pm A$ remain straight, that is $\frac{\partial u}{\partial y}(\pm A, y) = 0$. Doubly symmetric behavior of the panel is assumed and a single quadrant is modeled using four discrete elements (see Fig. 12). By linking degrees of freedom to insure geometric admissibility of the displacement pattern for the assemblage, using additional conditions so as to assure continuity of middle surface strains and rotation (θ_z), imposing the displacement boundary conditions and the symmetry conditions, the number of independent degrees-of-freedom reduces to 52. Numerical solutions were obtained for each of several prescribed end-shortening values (δ) by applying the Fletcher-Powell algorithm for unconstrained minimization (see Section 4.1.1) to the total potential energy function.

The load versus end-shortening plot obtained is represented by the solid line in Fig. 13 for the particular case where A = B = 12 in., h = 0.1 in., ν = 0.3, and E = 30 x 10^6 lb/in^2. The ordinate N is the equivalent uniform load required to maintain the displacement pattern induced by the imposed end-shortening δ and it is evaluated from the following expression:

$$N = \frac{1}{B}\int_0^B N_x\big|_{x=-A}\, dy = \frac{Eh}{B(1-\nu^2)}\int_0^B (\varepsilon_x + \nu\,\varepsilon_y)\,\big|_{x=-A}\, dy \tag{2.81}$$

Approved for Public Release

Contrails

where ε_x and ε_y are given in terms of the displacements by Eqs. 2.3. The discrete element analysis predicts a panel buckling load of 142.5 lbs/in while the formula given by Timoshenko in Ref. 21 (see p. 413) yields 144.5 lbs/in. The slope of the load vs. end-shortening plot decreases abruptly at the buckling load, however the elastic post-buckling behavior of the initially flat plate exhibits considerable additional load carrying capacity.

The second example problem in this group is a slightly curved cylindrical panel that differs from the previously discussed flat plate in only one respect; namely the radius of the panel is r = 500 in. rather than $r = \infty$. The displacement boundary conditions are given by Eqs. 2.80 with x replaced by s and y by $\eta = r\theta$. The panel is simply supported and the circumferential displacement of the edges $r\theta = \pm B$ and $s = \pm A$ is prevented while uniform longitudinal end-shortening ($\mp\delta$) is imposed on the edges $s = \pm A$. The behavior is assumed to be doubly symmetric and four cylindrical shell discrete elements are used to model one quadrant of the panel. Imposing interelement admissibility conditions, displacement boundary conditions, symmetry conditions, and additional conditions for middle surface strain and rotation continuity,numerical solutions are obtained by seeking the minimum of the total potential energy with respect to 52 independent degrees-of-freedom. Using the Fletcher-Powell minimization algorithm for each of several prescribed end-shortening values (δ) the displacement state throughout the panel was predicted.

The load versus end-shortening plot obtained is represented by the dashed line in Fig. 13 for the particular case r = 500 in., A = B = 12 in., h = 0.1 in., $\nu = 0.3$ and $E = 30 \times 10^6$ lbs/in^2. The ordinate is the equivalent uniform end load given by Eq. 2.81 with x replaced by s and y by $\eta = r\theta$. As the imposed end-shortening is increased the load required to maintain equilibrium increases along the prebuckled portion of the curve to

Approved for Public Release

Contrails

the point denoted by "a" in Fig. 13. Along the portion of curve between the origin and point "a" the slope of the curve is decreasing and clearly nonlinear. When an attempt is made to introduce additional end-shortening beyond point "a", a point on the post-buckled portion of the curve is obtained. This is a manifestation of the snap-through phenomenon. Additional points on the post-buckled portion of the load vs. end-shortening curve can be obtained by either increasing or decreasing the magnitude of the prescribed end-shortening. Note that when an attempt to generate a point on the post-buckled portion of the curve to the left of point "b" was made a jump to the prebuckled portion of the curve resulted. Furthermore, it was not possible, by energy minimization, to obtain points on a curve between "a" and "b" connecting the prebuckled and post-buckled portions of the load vs. end-shortening curve. This is because points on such a curve are associated with equilibrium displacement states that are not stable and therefore, do not correspond to local minima of the total potential energy.

The third example in this group is the same as the case of the slightly curved cylindrical shell panel except that the radius if 150 in.. As the end-shortening δ was increased, starting from the origin in Fig. 13, points on the curve joining the origin and point 1 were obtained; when an attempt was made to impose an end-shortening beyond point 1, a jump occurred to the curve 2-3. An attempt to extend this curve to the left of point 2 resulted in the generation of a point on curve 0-1, whereas an effort to extend this curve to the right of point 3 gave a point on the curve 4-5. Point 4 is as far to the left as this branch of the curve could be extended without a jump to curve 2-3 occurring. Curves joining points 1-2 and 3-4 could not be generated since displacement configurations corresponding to points on these curves are unstable and therefore do not correspond to local minima of the

Approved for Public Release

Contrails

total potential energy function. Some further insight into the behavior of this curved panel is offered by Fig. 14, which qualitatively illustrates displacement configurations corresponding to various portions of the load vs. end-shortening curve. The displacement patterns shown in Figs. 14a and b are essentially the same except that in Fig. 14 b the "dimpling inward" phenomenon has progressed to such a stage that the center deflection is negative. Figure 14c shows the displacement configuration after the first stage of the snap-through buckling of the panel manifested by a change in sign of the slope at the center of the edges $r\theta = \pm B$. In Fig. 14d the buckling pattern of the panel has undergone slope sign changes at all boundary points shown except at $(\pm A, \pm B/2)$. The displacement configuration illustrated in Fig. 14d suggests that another isolated portion of the load vs. end-shortening curve may exist; however, the generation of the curve has not been carried to an extent beyond that shown.

2.5.3 Pinched Cylindrical Shell

Consider a complete cylindrical shell of finite extent subject to self equilibrating concentrated loads as shown in Fig. 15. The loading P = 100 lbs.; dimensions L = 10.35 in., r = 4.953 in., h = 0.094 in.; and material properties for the particular example analyzed ($E = 10.5 \times 10^6$ lbs/in^2 and $\nu = 0.3125$) correspond to those for which experimental results are available (see Ref. 22 and Section 7.3 of this report). Taking advantage of symmetry, only one quadrant of the cylinder is modeled using cylindrical shell discrete elements. The displacement under the load for the particular example at hand is $w_p = -0.1084$ in. based upon the inextensional shell theory solution given by Timoshenko in Ref. 20 (see p. 501). Results for the predicted displacement under the load, for various idealizations shown in Fig. 16, are summarized in Table 2. For each of several modelings the number

Approved for Public Release

Contrails

of independent degrees-of-freedom as well as the displacement under the load obtained using each of the two distinct cylindrical shell elements described in this report, are summarized in Table 2. All of these results were obtained using additional conditions that require continuous mid-surface strains and rotation (θ_z) in addition to satisfaction of geometric admissibility conditions. It should be noted that for a fixed number of degrees of freedom the results obtained using the element discussed in Section 2.3.3, which permits an exact representation of the rigid body displacement states, offers only slightly better results. Furthermore, the solutions obtained using the element given in Section 2.3.1, which contains a good approximation of the rigid body modes, approach the alternative solutions as the modeling is refined. Based on these results, it does not appear that the additional computational effort involved in using the cylindrical shell element described in Section 2.3.3 is particularly rewarding in terms of improved prediction of the displacement behavior. It should be noted that the magnitude of the predicted displacements using modelings F, G and H exceed the displacement magnitude based upon the inextensional shell theory solution (i.e. w_p = - 0.1084 in.). This is not surprising, since the finite element analyses permit nonzero middle surface strains that are precluded in the inextensional shell theory solution. Finally, it is of interest to note that the displacement under the load for modeling G using the element described in Section 2.3.1, including geometric nonlinearity, was found to be -0.1114873 in. (see Ref. 7, p. 150).

Approved for Public Release

Contrails

SECTION 3

REISSNER ENERGY FORMULATION FOR A RECTANGULAR PLATE DISCRETE ELEMENT

3.1 Introduction

Each of the three commonly used formulations of the structural analysis problem is associated with a corresponding energy principle. The displacement method is related to the principle of minimum total potential energy, the force method is equivalent to the complementary energy approach, and the mixed force-displacement formulation corresponds to the Reissner energy principle (Ref. 23). The variational principle set forth in Ref. 23 states that of all possible states of stress and displacement that which makes the Reissner energy stationary satisfies the equilibrium equations and the force-displacement relations as well as the natural boundary conditions (both displacement and force) and is therefore the actual state of stress and displacement. It should be emphasized that the Reissner variational principle is a stationary principle rather than a minimum principle, therefore algorithms for seeking the minimum of a function of many variables may not be brought to bear directly.

The combined force-displacement approach is of interest for several reasons. In this approach both force and displacement unknowns are expressed in terms of assumed functions and therefore, force distributions are not obtained by differentiating approximate displacement results (as is the case in the displacement or potential energy method). Another characteristic of the combined force-displacement formulation is that both the equilibrium and force-displacement relations are satisfied approximately over the structure. It is also interesting to note that both force and displacement

Approved for Public Release

Contrails

boundary conditions are natural boundary conditions in the Reissner energy formulation and therefore the option to treat all boundaries conditions approximately exists. Qualitatively, the mixed force-displacement methods tend to treat force and displacement variables in a balanced or uniform manner.

3.2 Formulation

In this section of the Reissner energy formulation for a rectangular discrete element, including finite deflection bending-membrane coupling, is set forth. A linear membrane plate element and a linear bending plate element are in fact useful special cases of this formulation. Note that the Reissner energy for a typical interior element does not involve boundary condition contributions, however, these terms are important for elements on the boundary of the assemblage and they are therefore included in this development.

Assuming elastic isotropic plane stress behavior, the Reissner energy formulation for a rectangular plate element (see Fig. 1) is given by

$$\pi_R = \int_0^a \int_0^b \int_{-\frac{h}{2}}^{+\frac{h}{2}} \{[\sigma_x \varepsilon_x + \sigma_y \varepsilon_y + \tau_{xy} \gamma_{xy}] - \frac{1}{2E} [\sigma_x^2 + \sigma_y^2 - 2\nu \sigma_x \sigma_y + 2(1+\nu) \tau_{xy}^2]\} \, dz \, dy \, dx - W - S_1 - S_2 \qquad (3.1)$$

where it is understood that the strains ε_x, ε_y, and γ_{xy} are expressed in terms of the displacement variables (see Eqs. 2.3), W is the work done by external loads applied to the element, S_1 is the contribution due to force boundary

Approved for Public Release

Contrails

conditions, and S_2 is the contribution due to displacement boundary conditions. Introducing the strains in terms of the displacements (using Eqs. 2.3), expressing the stresses in terms of the force resultants

$$\sigma_x = \frac{N_x}{h} + z\frac{12}{h^3} M_x \tag{3.2a}$$

$$\sigma_y = \frac{N_y}{h} + z\frac{12}{h^3} M_y \tag{3.2b}$$

$$\tau_{xy} = \frac{N_{xy}}{h} + z\frac{12}{h^3} M_{xy} \tag{3.2c}$$

and integrating through the depth leads to the following expression for the element Reissner energy in terms of force resultants (N_x, N_y, N_{xy}, M_x, M_y, M_{xy}) and the displacements (u, v, w):

$$\pi_R = C_m + C_b + C_c - W - S_1 - S_2 \tag{3.3}$$

where

$$C_m = \int_0^a\int_0^b \{N_x \frac{\partial u}{\partial x} + N_y \frac{\partial v}{\partial y} + N_{xy}(\frac{\partial u}{\partial y} + \frac{\partial v}{\partial x}) - \frac{1}{2Eh}[N_x^2 + N_y^2 - 2\nu N_x N_y + 2(1+\nu) N_{xy}^2]\} \, dy \, dx \tag{3.4}$$

$$C_b = -\int_0^a\int_0^b \{M_x \frac{\partial^2 w}{\partial x^2} + M_y \frac{\partial^2 w}{\partial y^2} + 2 M_{xy} \frac{\partial^2 w}{\partial x \partial y} + \frac{6}{Eh^3}[M_x^2 + M_y^2 - 2\nu M_x M_y + 2(1+\nu) M_{xy}^2]\} \, dy \, dx \tag{3.5}$$

Approved for Public Release

Contrails

$$C_c = \frac{1}{2}\int_0^a\int_0^b \{N_x \left(\frac{\partial w}{\partial x}\right)^2 + N_y \left(\frac{\partial w}{\partial y}\right)^2 + 2 N_{xy} \frac{\partial w}{\partial x} \frac{\partial w}{\partial y}\} \, dy \, dx \qquad (3.6)$$

and the significance of W, S_1, and S_2 was previously discussed. Note that for a typical interior element the terms S_1 and S_2 vanish. However, for discrete elements on the boundary of an assemblage the contributions to the Reissner energy of the terms S_1 and S_2 must be considered assuming that the option to treat the corresponding boundary conditions as natural boundary conditions has been elected. Expressions for the contributions of the boundary conditions to the element Reissner energy are given in Appendix A.

Before generating a discretized form of the Reissner energy for a typical interior element it will be useful to remark on the physical significance of the first four terms in Eq. 3.3, namely C_m, C_b, C_c and W. The term C_m represents the contribution of the membrane forces (N_x, N_y, N_{xy}) and displacements (u, v) to the discrete element Reissner energy. This term taken by itself can be used to represent linear membrane behavior. The term C_b represents the contribution of the bending moments (M_x, M_y, M_{xy}) and the transverse displacement (w) to the discrete element Reissner energy. This term taken by itself can be used to represent linear small deflection plate bending behavior. The term C_c represents the bending-membrane coupling contribution to the discrete element Reissner energy and it involves only the membrane forces N_x, N_y, N_{xy} and the transverse displacement (w). It should be noted that C_m and C_b are quadratic while C_c is third degree. This should be compared with the total potential energy formulation given by Eq. 2.11 which is seen to contain quadratic (U_{2p}), third (U_{3p}), and fourth (U_{4p}) degree contributions. The term W represents the work done by loads

Approved for Public Release

Contrails

applied to the discrete element. Once the assumed displacement functions are selected, the generation of work equivalent load vectors for any particular loading on the discrete element is straight forward, the procedure being the same as in the potential energy formulation. The W contribution to the element Reissner energy is linear in the displacement unknowns.

The discrete representation of the Reissner energy for a typical interior rectangular discrete element is obtained by selecting assumed force and displacement patterns and then substituting these approximations into Eqs. 3.4, 3.5 and 3.6. The membrane displacements (u, v) and forces (N_x, N_y, N_{xy}) are bilinear over the discrete element, that is u, v, N_x, N_y and N_{xy} are expressed in terms of products of zeroth-order Hermite interpolation polynomials as follows

$$u(x,y) = \sum_{i=1}^{2} \sum_{j=1}^{2} H_{0i}^{(0)}(x) \, H_{0j}^{(0)}(y) \, u_{ij} \tag{3.7}$$

with a corresponding expression for v(x,y) and

$$N_x(x,y) = \sum_{i=1}^{2} \sum_{j=1}^{2} H_{0i}^{(0)}(x) \, H_{0j}^{(0)}(y) \, NX_{ij} \tag{3.8}$$

with similar expressions for $N_y(x,y)$ and $N_{xy}(x,y)$. The NX_{ij} represents 4 undetermined nodal parameters and the double index corner identification scheme is that shown in Fig. 1. Note that the zeroth order Hermite interpolation polynomials are given by Eqs. 2.26. The transverse displacement (w) and the moment resultants (M_x, M_y, and M_{xy}) are assumed to be bicubic over the discrete element, that is w, M_x, M_y, and M_{xy} are expressed in terms of products of first-order Hermite interpolation polynomials. The assumed displacement pattern for w(x,y) is the same as that given by Eqs. 2.8. The

Approved for Public Release

Contrails

bending moment $M_x(x,y)$ is approximated by

$$M_x(x,y) = \sum_{i=1}^{2} \sum_{j=1}^{2} [H_{0i}^{(1)}(x)\, H_{0j}^{(1)}(y)\, MX_{ij} + H_{1i}^{(1)}(x)\, H_{0j}^{(1)}(y)\, MX_{xij}$$

$$+ H_{0i}^{(1)}(x)\, H_{1j}^{(1)}(y)\, MX_{yij} + H_{1i}^{(1)}(x)\, H_{1j}^{(1)}(y)\, MX_{xyij}\,] \qquad (3.9)$$

with similar expressions for $M_y(x,y)$ and $M_{xy}(x,y)$. It should be noted that MX_{ij}, MX_{xij}, MX_{yij} and MX_{xyij} represent 16 undetermined nodal parameters, the subscripts x and y denote partial differentiation, and the double index corner identification scheme is the same as that shown in Fig. 1. The first-order Hermite interpolation polynomials are given by Eqs. 2.9

The discrete form of the membrane contribution to the element Reissner energy (C_m) is obtained by substituting the assumed functions for u, v, N_x, N_y and N_{xy} (see Eqs. 3.7 and 3.8) into Eq. 3.4 and integrating over the element. The result is

$$C_m = \underset{1\times 20}{\vec{X}_m^T}\ \underset{20\times 20}{Q_m}\ \underset{20\times 1}{\vec{X}_m} \qquad (3.10)$$

where the vector of membrane unknowns is defined by

$$\vec{X}_m^T = \lfloor u_{11}, u_{12}, u_{22}, u_{21}, v_{11}, \ldots, v_{21}, NX_{11}, \ldots, NX_{21},$$

$$NY_{11}, \ldots, NY_{21}, NXY_{11}, \ldots, NXY_{21} \rfloor \qquad (3.11)$$

and explicit formulas for the elements of the matrix Q_m are given in Appendix C of Ref. 12. The discrete representation of the bending contribution to the element Reissner energy is obtained by substituting the assumed functions for w, M_x, M_y and M_{xy} (see Eqs. 2.8 and 3.9) into Eq. 3.5 and integrating over the

Approved for Public Release

Contrails

element. The result is

$$C_b = \underset{1x64}{\vec{X}_b^T} \quad \underset{64x64}{Q_b} \quad \underset{64x1}{\vec{X}_b} \tag{3.12}$$

where the vector of bending unknowns is defined by:

$$\vec{X}_b^T = \lfloor w_{11}, w_{x11}, w_{y11}, w_{xy11}, w_{12}, \cdots, w_{xy12},$$
$$w_{22}, \cdots, w_{xy22}, w_{21}, \cdots, w_{xy21},$$
$$MX_{11}, \cdots, MX_{xy21}, MY_{11}, \cdots, MY_{xy21},$$
$$MXY_{11}, \cdots, MXY_{xy21} \rfloor \tag{3.13}$$

and explicit formulas for the elements of the matrix Q_b are given in Appendix C of Ref. 12.

The discrete form of the bending-membrane coupling contribution to the element Reissner energy is obtained by substituting the assumed functions for w, N_x, N_y, and N_{xy} (see Eqs. 2.8 and 3.8) into Eq. 3.6 and integrating over the element. The result is

$$C_c = \underset{1x12}{\vec{N}^T} \quad \underset{12x136}{Q_c} \quad \underset{136x1}{\vec{Y}_r} \tag{3.14}$$

where vector of membrane force unknowns is defined by

$$\vec{N}^T = \lfloor NX_{11}, NX_{12}, NX_{22}, NX_{21}, NY_{11}, \cdots, NY_{21}, NXY_{11}, \cdots, NXY_{21} \rfloor \tag{3.15}$$

and the vector $\vec{Y}_r$ contains as its elements the 136 possible products of the 16 degrees of freedom in the w(x,y) assumed displacement function taken in

Approved for Public Release

Contrails

pairs of two, that is

$$\underset{1x136}{\vec{Y}_r^T} = \lfloor w_{11}^2,\ 2w_{11}w_{x11},\ w_{x11}^2,\ 2w_{11}w_{y11},\ 2w_{x11}w_{y11},\ w_{y11}^2,\ \ldots,\ w_{xy21}^2 \rfloor \qquad (3.16)$$

Explicit formulas for the elements of the matrix Q_c are given in Appendix C of Ref. 12.

Combining the various contributions (Eqs. 3.10, 3.12, 3.14) the discrete representation of the Reissner energy for a typical interior rectangular discrete element is given by

$$\underset{1x1}{\pi_R} = \underset{1x20}{\vec{X}_m^T}\ \underset{20x20}{Q_m}\ \underset{20x1}{\vec{X}_m} + \underset{1x64}{\vec{X}_b^T}\ \underset{64x64}{Q_b}\ \underset{64x1}{\vec{X}_b} + \underset{1x12}{\vec{N}^T}\ \underset{12x136}{Q_c}\ \underset{136x1}{\vec{Y}_r} - \underset{1x24}{\vec{X}^T}\ \underset{24x1}{\vec{P}} \qquad (3.17)$$

where $\vec{X}$ contains the twenty-four displacement degrees-of-freedom that is

$$\underset{1x24}{\vec{X}^T} = \lfloor u_{11},\ u_{12},\ u_{22},\ u_{21},\ v_{11},\ \ldots,\ v_{21},\ w_{11},\ w_{x11},\ w_{y11},\ w_{xy11},$$
$$w_{12},\ \ldots,\ w_{xy12},\ w_{22},\ \ldots,\ w_{xy22},\ w_{21},\ \ldots,\ w_{xy21} \rfloor \qquad (3.18)$$

and the elements of the vector $\vec{P}$ are the work equivalent loads associated with each of the displacement degrees-of-freedom.

3.3 Implementation

The Reissner energy for a structural system represented by an assemblage of discrete elements can be formed by summing the contributions of the individual elements, that is

$$\Pi_R = \sum_{k=1}^{K} (\pi_R)_k \qquad (3.19)$$

Approved for Public Release

Contrails

Numerical solutions predicting the behavior of such an assemblage of discrete elements are to be generated by seeking a stationary value of Π_R subject to certain equality constraints. The equality constraints linking together various degrees-of-freedom arise as a result of imposing interelement geometric admissibility conditions and optionally requiring continuity of the force resultants between elements. The Reissner energy effort was limited to structures that could be represented by rectangular finite elements in a common plane and both displacement and force continuity between elements was always imposed.

Consider the interface between the coplanar elements I and II shown in Fig. 7. Continuity of the membrane displacements is expressed as follows

$$u^I(x,b) = u^{II}(x,0) \tag{3.20a}$$

$$v^I(x,b) = v^{II}(x,0) \tag{3.20b}$$

Substituting the assumed displacement functions (see Eq. 3.7), noting that the $H_{0i}^{(0)}(x)$ are linearly independent, it is apparent that Eqs. 3.20a and b will be satisfied along the entire common edge between I and II when

$$u^I_{i2} = u^{II}_{i1} \quad ; \qquad i = 1,2 \tag{3.21a}$$

$$v^I_{i2} = v^{II}_{i1} \quad ; \qquad i = 1,2 \tag{3.21b}$$

Continuity of the membrane forces between elements I and II is expressed as follows

$$N^I_x(x,b) = N^{II}_x(x,0) \tag{3.22a}$$

$$N^I_y(x,b) = N^{II}_y(x,0) \tag{3.22b}$$

$$N^I_{xy}(x,b) = N^{II}_{xy}(x,0) \tag{3.22c}$$

Approved for Public Release

Contrails

and these conditions can be implemented using the following simple equality constraints:

$$NX^{I}_{i2} = NX^{II}_{i1} \quad ; \quad i = 1,2 \tag{3.23a}$$

$$NY^{I}_{i2} = NY^{II}_{i1} \quad ; \quad i = 1,2 \tag{3.23b}$$

$$NXY^{I}_{i2} = NXY^{II}_{i1} \quad ; \quad i = 1,2 \tag{3.23c}$$

At a typical interior node, such as that common to elements I, II, III and IV in Fig. 7, the number of unknowns associated with the membrane behavior is reduced from 20 to 5 as a result of introducing displacement and force continuity conditions between discrete elements.

Continuity of displacement w and its first derivatives between the elements I and II is expressed as follows

$$w^{I}(x,b) = w^{II}(x,0) \tag{3.24a}$$

$$\frac{\partial w^{I}}{\partial y}(x,b) = \frac{\partial w^{II}}{\partial y}(x,0) \tag{3.24b}$$

Substituting the assumed displacement function (see Eqs. 2.8), noting that $H^{(1)}_{0i}(x)$ and $H^{(1)}_{1i}(x)$ are linearly independent, requiring that Eqs. 3.24a and b be satisfied along the entire common edge between I and II leads to the following simple equality constraints:

$$w^{I}_{i2} = w^{II}_{i1} \qquad i = 1,2 \tag{3.25a}$$

$$w^{I}_{xi2} = w^{II}_{xi1} \qquad i = 1,2 \tag{3.25b}$$

$$w^{I}_{yi2} = w^{II}_{yi1} \qquad i = 1,2 \tag{3.25c}$$

$$w^{I}_{xyi2} = w^{II}_{xyi1} \qquad i = 1,2 \tag{3.25d}$$

Approved for Public Release

Contrails

In a similar manner the undetermined nodal parameters involved in the expansions for M_x, M_y, and M_{xy} are linked thus assuring satisfaction of the following additional continuity conditions between elements I and II

$$M_x^{I}(x,b) = M_x^{II}(x,0) \tag{3.26a}$$

$$\frac{\partial M_x^{I}}{\partial y}(x,b) = \frac{\partial M_x^{II}}{\partial y}(x,0) \tag{3.26b}$$

$$M_y^{I}(x,b) = M_y^{II}(x,0) \tag{3.26c}$$

$$\frac{\partial M_y^{I}}{\partial y}(x,b) = \frac{\partial M_y^{II}}{\partial y}(x,0) \tag{3.26d}$$

$$M_{xy}^{I}(x,b) = M_{xy}^{II}(x,0) \tag{3.26e}$$

$$\frac{\partial M_{xy}^{I}}{\partial y}(x,b) = \frac{\partial M_{xy}^{II}}{\partial y}(x,0) \tag{3.26f}$$

It may be noted that conditions 3.26e and d assure continuity of the transverse shear resultant V_y while conditions 3.26a and f assure continuity of the transverse shear resultant V_x, that is:

$$V_y^{I}(x,b) = \frac{\partial M_{xy}^{I}}{\partial x}(x,b) + \frac{\partial M_y^{I}}{\partial y}(x,b) = \frac{\partial M_{xy}^{II}}{\partial x}(x,0) + \frac{\partial M_y^{II}}{\partial y}(x,0) = V_y^{II}(x,0) \tag{3.27a}$$

and

$$V_x^{I}(x,b) = \frac{\partial M_x^{I}}{\partial x}(x,b) + \frac{\partial M_{xy}^{I}}{\partial y}(x,b) = \frac{\partial M_x^{II}}{\partial x}(x,0) + \frac{\partial M_{xy}^{II}}{\partial y}(x,0) = V_x^{II}(x,0) \tag{3.27b}$$

At a typical interior node, such as that common to elements I, II, III, and IV in Fig. 7, the number of unknowns associated with the bending behavior is reduced from 64 to 16 as a result of employing the displacement and force

Approved for Public Release

Contrails

continuity conditions discussed.

The Reissner energy for a structural system represented by an assemblage of coplanar rectangular discrete elements may now be viewed as a function of a reduced set of independent variables ($\vec{Z}$). The problem to be solved may be stated as follows:

Given $\Pi_R(\vec{Z})$

Find $\vec{Z}^*$

such that $\Pi_R(\vec{Z}^*)$ is stationary.

An algorithm for seeking the stationary value of a function of several variables was set forth in Ref. 24 and further efforts along this same line were reported in Ref. 25. In the course of this investigation Powell's method (Ref. 24) was programmed and successfully tested on various simple (two variable) problems (see Ref. 12). Attempts to apply this algorithm to the solution of linear membrane plate problems formulated using the discrete element Reissner energy were unsuccessful. No satisfactory method for seeking the stationary value of Reissner energy functions of many variables was found in the course of this research program.

The Reissner energy formulation can be cast as an unconstrained minimization problem. This is accomplished by forming a residual function $\theta(\vec{Z})$, which is defined by

$$\theta(\vec{Z}) = \nabla\Pi_R{}^T \nabla\Pi_R = \sum_{i=1}^{N} [\frac{\partial\Pi_R}{\partial z_i}(\vec{Z})]^2 \qquad (3.28)$$

Clearly $\theta(\vec{Z})$ is positive for all $\vec{Z}$ and its minimum value will be zero when $\vec{Z} = \vec{Z}^*$ such that $\nabla\Pi_R(\vec{Z}^*) = 0$ which corresponds to the requirement that $\Pi_R(\vec{Z}^*)$ be stationary. Thus the problem may be stated in the following alternative form:

Approved for Public Release

Contrails

Given $\Pi_R(\vec{Z})$

Find $\vec{Z}^*$

Such that $\theta(\vec{Z}) = \nabla\Pi_R^T \cdot \nabla\Pi_R = \sum_{i=1}^{N} \left[\frac{\partial\Pi_R}{\partial z_i}(\vec{Z})\right]^2$ is a minimum.

Both the Fletcher-Powell and Fletcher-Reeves minimization algorithms (see Section 4.1.1) were employed in conjunction with this residual type formulation. Numerical results for some simple linear membrane problems were obtained, however, long running times were required and this approach was abandoned as prohibitively inefficient.*

The Reissner energy formulation can be used in conjunction with the Newton-Raphson technique. In effect the Reissner energy provides a convenient formulative device and it should be noted that the gradient $\nabla\Pi_R(\vec{Z})$ and the matrix of second partial derivatives $\frac{\partial^2\Pi_R}{\partial_i \partial z_j}(\vec{Z})$ employed in this computational scheme can be formed by summing the contributions from each of the discrete elements taken one at a time. The Newton-Raphson technique generates a sequence of vectors $\vec{Z}_1, \vec{Z}_2, \ldots, \vec{Z}_q, \vec{Z}_{q+1}, \ldots$ obtained by seeking the stationary value of the second order Taylor series expansion of Π_R about the current trial solution. That is given the trial solution vector $\vec{Z}_q$ the next vector in the sequence $\vec{Z}_{q+1}$ is given by

$$\vec{Z}_{q+1} = \vec{Z}_q + \Delta\vec{Z}_q \tag{3.29}$$

---

* It should be noted that the residual formulation using unconstrained minimization algorithms was abandoned before the profound influence of the scaling transformation set forth in Section 4.2 was recognized.

Approved for Public Release

Contrails

and $\Delta\vec{Z}_q$ is determined so that

$$\Pi_R(\vec{Z}_q + \Delta\vec{Z}_q) = \Pi_R(\vec{Z}_q) + \Delta\vec{Z}_q^T \nabla\Pi_R(\vec{Z}_q) + \frac{1}{2} \Delta\vec{Z}_q^T \left[\frac{\partial^2 \Pi_R}{\partial z_i \partial z_j}(\vec{Z}_q)\right] \Delta\vec{Z}_q \qquad (3.30)$$

is stationary with respect to $\Delta\vec{Z}_q$, that is such that

$$\nabla\Pi_R(\vec{Z}_q) + \left[\frac{\partial^2 \Pi_R}{\partial z_i \partial z_j}(\vec{Z}_q)\right] \Delta\vec{Z}_q = 0 \qquad (3.31)$$

Symbolically $\Delta\vec{Z}_q$ may be expressed as follows

$$\Delta\vec{Z}_q = - \left[\frac{\partial^2 \Pi_R}{\partial z_i \partial z_j}(\vec{Z}_q)\right]^{-1} \nabla\Pi_R(\vec{Z}_q) \qquad (3.32)$$

however it should be recognized that $\Delta\vec{Z}_q$ can be computed by solving the set of linear algebraic equations (Eqs. 3.31) and numerical inversion of the matrix of second partial derivatives is not required. The iterative procedure continues until $\nabla\Pi_R(\vec{Z})$ approaches zero and thus the change $\Delta\vec{Z}$ approaches zero (see Eqs. 3.31). Note that in the case of a linear membrane or bending problem the Newton-Raphson procedure converges in a single iteration. For the nonlinear problems discussed in the next section the method usually converged in 4 or 5 iterations. The principal shortcomings of using the Newton-Raphson method are that the procedure requires the storage of an nxn matrix and the solution of n simultaneous equations at each stage in the iterative procedure.

3.4 Examples

In this section numerical results for several example problems are discussed. All of these results were obtained using the discrete element Reissner formulation given in Section 3.2 and continuity of displacement and force variables was imposed in all cases as discussed in Section 3.3. A

Approved for Public Release

Contrails

linear membrane example, a linear plate example, a nonlinear transversely loaded plate problem, and a nonlinear prescribed end-shortening case are discussed.

3.4.1 Linear Membrane Example

Consider a beam of narrow rectangular cross section and unit width ($h = 1$ in.) supported at the ends $x = \pm\ell$ and subject to a uniformly distributed load of intensity q on the surface $y = -c$, as shown in Fig. 17. The force boundary conditions on the upper surface of the beam are

$$N_y(x,c) = 0 \tag{3.33a}$$

$$N_{xy}(x,c) = 0 \tag{3.33b}$$

and on the lower surface

$$N_y(x,-c) = -qh \tag{3.33c}$$

$$N_{xy}(x,-c) = 0 \tag{3.33d}$$

The force boundary conditions on the ends of the beam at $x = \pm\ell$ that correspond to the theory of elasticity solution are

$$N_x(+\ell,y) = \frac{3qh}{4c^3}\left(\frac{2}{3}y^3 - \frac{2}{5}c^2 y\right) \tag{3.33e}$$

$$N_{xy}(+\ell,y) = -\frac{3q\,h\ell}{4c^3}(c^2 - y^2) \tag{3.33f}$$

$$N_x(-\ell,y) = \frac{3qh}{4c^3}\left(\frac{2}{3}y^3 - \frac{2}{5}c^2 y\right) \tag{3.33g}$$

$$N_{xy}(-\ell,y) = +\frac{3q\,h\ell}{4c^3}(c^2 - y^2) \tag{3.33h}$$

Approved for Public Release

Contrails

The "exact" theory of elasticity solution of this problem is given in Ref. 26 (see p. 40). Numerical results for the particular case when h = 10 in., ℓ = 100 in., c = 8 in., E = 30 x 10^6 lbs/in^2, ν = 0.3 and q = 0.480 lbs/in^2 were obtained using the "exact" solution (Ref. 26). An approximate numerical solution for this particular problem was generated based on a discrete element Reissner energy analysis using a single step Newton-Raphson iteration. Considering symmetry about the y axis, the right hand side of the beam (see Fig. 17) was idealized using an assemblage of 8 rectangular discrete elements. All the boundary conditions were treated as natural boundary conditions with the exception of the two symmetry conditions $N_{xy}(0,y) = 0$ and $u(0,y) = 0$ which were imposed. The displacements are measured from the reference coordinate system x-y attached to the undeformed structure and therefore the v displacement of node 3 (see Fig. 17) is set to zero. For this modeling the Reissner energy is a function of 64 independent variables.

The displacement (u,v) and force (N_x, N_y, N_{xy}) results for the exact theory of elasticity solution (Ref. 26) and the approximate discrete element Reissner energy solution are both exhibited in Table 3. Note that the node numbers used in Table 3 correspond to the node numbering shown in Fig. 17. Comparing the two solutions tabulated in Table 3 it is seen that the approximate results are in substantial agreement with the exact results. The quality of the force results is gratifying. It is particularly interesting to note how well the force boundary conditions are satisfied even though they were treated as natural boundary conditions rather than as imposed boundary conditions. For example at nodes 5, 10 and 15 it is seen that the approximate solution gives N_y = -0.491 lbs/in., N_y = -0.49 lbs/in. and N_y = -0.49 lbs/in respectively, as compared with the exact value N_y = -0.48 lbs/in. Also at nodes 1, 6, and 11 along the free edge y = +c it is seen that both the N_y and N_{xy} values generated by the approximate analysis are small.

Approved for Public Release

Contrails

3.4.2 Linear Bending Example

Consider a fully clamped square plate subject to a uniformly distributed transverse load (see Fig. 8). A small deflection theory solution for this problem is given by Timoshenko in Ref. 20 (see p. 197). The example plate has dimensions 20" x 20" x 0.1", modulus of elasticity $E = 10.92 \times 10^6$ lbs/in^2, Poisson's ratio $\nu = 0.3$, and is subject to a load intensity $p_z = 1$ lb/in^2. The approximate solutions generated using a linear bending discrete element Reissner energy approach are compared with those given by the reference solution (Ref. 20). In view of the double symmetry a single quadrant of the plate is modeled using 4 square discrete elements (see Fig. 18). The approximate solutions were computed using a single step of Newton-Raphson iteration. An approximate solution was first obtained imposing the displacement boundary conditions along the clamped edges and then a second approximate solution was obtained treating the displacement boundary conditions along the clamped edges as natural boundary conditions (employing S_2 terms see Appendix A, Eqs. A9). In both of these approximate solutions the symmetry conditions were imposed on both the force and the displacement variables. A sampling of key results for this example is shown in Table 4. Complete results for the discrete element solutions will be found in Tables 4 and 5 of Ref. 12. When the clamped edge displacement boundary conditions are treated as natural boundary conditions, the force results predicted by the discrete element Reissner energy analysis are much closer to those given by the reference solution (Ref. 20). It should be noted that treating the clamped edge displacement boundary conditions as natural boundary conditions yields a discrete element formulation with 110 unknowns as compared with 86 unknowns, when these boundary conditions are imposed. For this example the displacement response was essentially insensitive to whether the clamped edge

Approved for Public Release

Contrails

displacement boundary conditions were treated as natural or imposed.

Finally, it should be recognized that although the reference solution and discrete element solution are in essential agreement the maximum deflection predicted is twice the plate thickness and is therefore well beyond the range of validity for small deflection plate theory. In the next section nonlinear finite-deflection theory results for this example problem are discussed.

3.4.3 Nonlinear Plate Bending Example

The fully clamped plate subject to uniform transverse load discussed in Section 3.4.2 was also analyzed using nonlinear finite deflection plate theory which includes bending-membrane coupling action. The four element idealization depicted in Fig. 18 was used, the displacement boundary conditions along the clamped edges were treated as natural boundary conditions, and symmetry conditions on both force and displacement variables were imposed. This four element idealization has 144 unknowns. Using the discrete element Reissner energy formulation in conjunction with the Newton-Raphson iteration scheme a numerical solution for this example with the transverse loading intensity p_z = 1 lb/in^2, was generated. This solution can be compared with the approximate nonlinear solution available in Ref. 20(see p. 421). Using 16 of the 48 degree of freedom nonlinear plate elements described in Section 2.2.1, to model a quadrant of the plate (see Fig. 19) a minimum potential energy solution was also obtained for this problem. The 16 element potential energy representation has 177 independent degrees-of-freedom and the results were obtained using the Fletcher-Powell minimization algorithm. A sampling of key results for this nonlinear plate bending example is shown in Table 5. Complete results for the discrete element Reissner energy solution will be found in Table 12 of Ref. 12. Examining Table 5 it is seen that the maximum

Approved for Public Release

Contrails

transverse displacements predicted by the three methods are identical to three significant figures. Maximum stress predicted by the discrete element Reissner energy solution is within 2% of the value predicted by the approximate solution in Ref. 20. The maximum stress predicted by the discrete element potential energy solution is about 6% under that given by the discrete element Reissner energy solution and about 8% below that given by the approximate solution in Ref. 20. A more detailed comparison of the Reissner energy results with the potential energy results for this example will be found in Tables 7 through 11 of Ref. 12. Finally, the nonlinear discrete element Reissner energy analysis was carried out for load intensities of $p_z = 0.5$ lb/in^2 and $p_z = 2.0$ lb/in^2. The transverse displacement is plotted versus load intensity in Fig. 20. The potential energy results discussed in Section 2.5.1 and the results due to Timoshenko Ref. 20 listed in Table 1 are both represented by the dashed line in Fig. 20. It is clear that these nonlinear load-displacement results are in very close agreement for all three methods and they are all substantially different from the results predicted by linear theory.

3.4.4 End-shortening of Flat Plate

In this section the flat plate subject to end-shortening previously discussed in Section 2.5.2 and shown in Fig. 11 is treated using a discrete element Reissner energy analysis. The displacement boundary conditions are given by Eqs. 2.80. The particular panel for which numerical results were obtained is identical with that treated in Section 2.5.2 that is A = B = 12, h = 0.1 in., $\nu = 0.3$, and $E = 30 \times 10^6$ lbs/in^2. Taking advantage of the double symmetry one quarter of the panel was modeled with four identical discrete elements. Imposing symmetry conditions and treating the edge boundary conditions as natural boundary conditions the number of unknowns in

Approved for Public Release

Contrails

the 4 discrete element Reissner energy formulation is found to be 142. The requirement that the edges subject to end-shortening ($x = \pm A$ in Fig. 11) remain straight is enforced by linking u displacement degrees of freedom however the magnitude of the end-shortening is not specified. The equivalent uniform end load is specified and then treated as a natural force boundary condition that is

$$S_1 = \int_0^B \bar{N}\, u\, dy \Big|_{x=-A} \tag{3.34}$$

where u is the undetermined uniform end-shortening. For various specified equivalent uniform end loads $\bar{N}$ solutions are obtained using the Newton-Raphson iteration procedure. A plot of equivalent uniform end ($\bar{N}$) versus midpoint transverse displacement w_o as shown in Fig. 21, based upon the four element Reissner energy results. The dashed curve marked Π_p in Fig. 21 shows the corresponding result based upon the 4 discrete element potential energy minimization solution discussed in Section 2.5.2. The buckling loads predicted by the Π_R solution, the Π_p solution and the Ref. 21 (see p. 413) solution are respectively; N_{cr} = 140 lb/in., N_{cr} = 142.5 lbs/in and N_{cr} = 144.5 lb/in. The finite element results are thought to be more nearly correct because they are based upon analyses involving more degrees of freedom (142 for Π_R and 52 for Π_p) than that given in Ref. 21. More detailed results for this example will be found in Ref. 12.

Approved for Public Release

Contrails

SECTION 4

MINIMIZATION ALGORITHMS

4.1 Introduction

The motivation for much of the work in energy search methods arose from the need to solve the highly nonlinear equilibrium equations associated with geometric nonlinearities caused by cubic and quartic displacement terms in the potential energy. By virtue of the principle of minimum potential energy many of the minimization algorithms from mathematical programming were directly applicable and an extensive bibliography through 1965 is contained in Ref. 1. After some initial work with relaxation type direct methods (Refs. 1 and 5), most recent efforts have been with gradient methods (Ref. 9) and in particular with the variable metric (Fletcher-Powell) and conjugate gradient (Fletcher-Reeves) algorithms. In general,gradient methods tend to be more efficient than non-gradient methods especially when the gradient is a computational byproduct of the function evaluation. The experience gained over a period of time in applying these algorithms to structural problems has led to some recent advances (Ref. 13) and new schemes that are reported in this section.

4.1.1 Gradient Methods

The conjugate gradient and variable metric algorithms can be viewed as unconstrained minimization methods or as procedures for solving systems of linear and nonlinear equations (see Refs. 13, 27 and 28). Mathematically these points of view are entirely equivalent although computationally there are subtle differences which will be discussed in a later section. Both methods proceed by minimizing the energy in a sequence of directions each somehow related to gradients of the energy function. The steps in the

Approved for Public Release

Contrails

conjugate gradient method from an initial guess vector $\vec{Z}_o$, are

$$\vec{P}_o = -\nabla\Pi_o = -\nabla\Pi(\vec{Z}_o) \tag{4.1a}$$

$$\vec{Z}_{i+1} = \vec{Z}_i + t_i \vec{P}_i \tag{4.1b}$$

$$\nabla\Pi_{i+1} = \nabla\Pi(\vec{Z}_{i+1}) \tag{4.1c}$$

$$\vec{P}_{i+1} = -\nabla\Pi_{i+1} + \beta_i \vec{P}_i \tag{4.1d}$$

where β_i is a positive scalar determined by an orthogonalization criteria and t_i is the smallest positive root of the directional derivative $\vec{P}_i^T \cdot \nabla\Pi(\vec{Z}_i + t\vec{P}_i)$ for prescribed $\vec{Z}_i$ and $\vec{P}_i$ and thus corresponds to the minimum of $\Pi(\vec{Z}_i + t\vec{P}_i)$ considered as a function of the scalar t. The one dimensional (linear) search for this root is the subject of the next section. In the case of an ordinary stiffness matrix $K^{\neq}$ a closed form solution for t_i is possible (Ref. 29) and a number of algebraically equivalent expressions may be formed, namely

$$t_i = \frac{|\nabla\Pi_i|^2}{\vec{P}_i^T K \vec{P}_i} = -\frac{\vec{P}_i^T \nabla\Pi_i}{\vec{P}_i^T K \vec{P}_i} = -\frac{\vec{P}_i^T \nabla\Pi_o}{\vec{P}_i^T K \vec{P}_i} \tag{4.2}$$

The scalars β_i are determined by the K-orthogonalization of the residual vectors (negative of the gradient)in the linear case and again a number of equivalent expressions are possible (Ref. 29), namely

---

$\neq$ The potential energy is then simply $\Pi = \frac{1}{2}\vec{Z}^T K \vec{Z} - \vec{Z}^T \vec{F}$.

Approved for Public Release

Contrails

$$\beta_i \equiv \frac{\left|\nabla\Pi_{i+1}\right|^2}{\left|\nabla\Pi_i\right|^2} = \frac{\nabla\Pi_{i+1}^T K \vec{P}_i}{\vec{P}_i^T K \vec{P}_i} = \frac{-\nabla\Pi_{i+1}^T K \nabla\Pi_i}{\vec{P}_i^T K \vec{P}_i} \tag{4.3}$$

If the orthogonalization is considered a separate process starting from $\nabla\Pi_o$ then a recursive formula is generated for $\nabla\Pi_{i+1}$ in terms of K and $\vec{P}_i$,

$$\nabla\Pi_{i+1} = \nabla\Pi_i + t_i K \vec{P}_i \tag{4.4}$$

However, the usual gradient definition of $\nabla\Pi(\vec{Z}_{i+1})$ results when $\vec{P}_i$ is the direction used to generate $\vec{Z}_{i+1}$ and $\nabla\Pi_o$ is $\nabla\Pi(\vec{Z}_o)$. All numerical results in this report use the current gradient $\nabla\Pi(\vec{Z}_{i+1})$. In nonlinear problems, as Eq. 4.1c indicates, the current gradient must be used by the definition of the algorithm. It can be shown in the linear case (Ref. 29) that the gradients are mutually orthogonal and as an important consequence the procedure converges in at most n steps where n is the dimension of K .

The variable metric method (Ref. 28) also used K-orthogonal directions but these directions are determined in quite a different manner. A square matrix H_i is computed at each step which accumulates information about the function $\Pi(\vec{Z})$ and ultimately converges to the inverse of K in linear problems. This matrix is used as a metric to transform the gradient directly into a new search direction and gives the method its name. The formulation of this procedure as given by Fletcher and Powell (Ref. 28) is:

$$\vec{P}_i = - H_i \nabla\Pi(\vec{Z}_i) \tag{4.5a}$$

$$\vec{S}_i = t_i \vec{P}_i \tag{4.5b}$$

where again t_i is determined so as to minimize $\Pi(\vec{Z}_i + t\vec{P}_i)$ for given $\vec{Z}_i$ and $\vec{P}_i$,

Approved for Public Release

Contrails

$$\vec{Z}_{i+1} = \vec{Z}_i + \vec{S}_i \tag{4.5c}$$

$$\vec{V}_i = \nabla\Pi(\vec{Z}_{i+1}) - \nabla\Pi(\vec{Z}_i) \tag{4.5d}$$

and

$$H_{i+1} = H_i + A_i + B_i \tag{4.5e}$$

$$A_i = \vec{S}_i \vec{S}_i^T / \vec{S}_i^T \vec{V}_i \tag{4.5f}$$

$$B_i = - H_i \vec{V}_i \vec{V}_i^T H_i / \vec{V}_i^T H_i \vec{V}_i \tag{4.5g}$$

The initial H_i is any positive definite matrix and the identity matrix is often used. The monotonic reduction of $\Pi(\vec{Z})$ at each step can be shown (Ref. 28) and n step convergence in linear problems follows from the K-orthogonality of the $\vec{S}_i$. In nonlinear problems H_i converges to an approximation of the inverse of the matrix of second partial derivatives so that in the limit its convergence characteristics resemble Newton's method. In the course of applying it to a wide variety of structural problems the method has proved very stable with storage and manipulation of a full H matrix its most serious handicap.

4.2 Scale Effects on Gradient Methods

4.2.1 Linear

A recent improvement in the efficiency of gradient methods (Ref. 13) was achieved not by finding better search directions but rather by transforming the function space itself. The characteristic invariants of the space for a linear problem are the eigenvalues of the stiffness matrix. These are proportional to the square of the principal axes of a constant energy

Approved for Public Release

Contrails

ellipsoid in the space. It is clear geometrically that an n-dimensional sphere is the optimal function space since one gradient move from any point in the space reaches the minimum. In general the conditioning number C_N of the matrix of second partials $[\frac{\partial \Pi}{\partial z_i \partial z_j}]$

$$C_N = \left|\lambda_{max}/\lambda_{min}\right| \tag{4.6}$$

where λ denotes an eigenvalue, is also a measure of the deviation of a function space from optimal. The closer C_N is to unity the better the space. As reported in Ref. 13 the presence of mixed derivative displacement terms, like w_{xy}, can cause huge variations in this number with simple changes in the physical units used. A solution to this dilemma was found to be a scaling transformation which by reducing C_N improves the efficiency of gradient methods. To understand the rationale of this transformation consider the before and after situation shown in Fig. 22 with respect to the Gerschgorin circles. Recall that Gerschgorin's theorem guarantees that every eigenvalue of the matrix A lies in at least one of the disks centered at a_{ii} and of radii $R_i \equiv \sum_{j \neq i} |a_{ij}|$ so that the circles in Fig. 22 indicate the possible range of eigenvalues. In the unscaled case the circles are not only large but are centered at widely different points which is the key to the solution. The circles for the scaled matrix are all centered at the same point and their radii are tightly bounded above. This was achieved by a scaling transformation which will now be described.

To minimize a positive definite quadratic form of the potential energy

$$\Pi(\vec{Z}) = \frac{1}{2} \vec{Z}^T K \vec{Z} - \vec{Z}^T \vec{F} \tag{4.7}$$

operate in the scaled coordinates

Approved for Public Release

Contrails

$$\underset{\sim}{\Pi}(\vec{Y}) = \frac{1}{2}\,\vec{Y}^T\,\underset{\sim}{K}\,\vec{Y} - \vec{Y}^T\,\vec{F} \tag{4.8}$$

where

$$\vec{Z} = D\,\vec{Y}\,, \qquad \vec{F} = D^T\,\vec{F}$$

$$\underset{\sim}{\Pi}(\vec{Y}) = \Pi(\vec{Z})\,, \qquad \underset{\sim}{K} = D^T\,KD \tag{4.9}$$

and

$$d_{ij} = \begin{cases} 0 & i \neq j \\ 1/(c\,\sqrt{k_{ii}}\,) & i = j \end{cases} \tag{4.10}$$

The circles for $\underset{\sim}{K}$ are all centered at $1/c^2$ and since c cancells out in the eigenvalue ratio for C_N, the particular value of c cannot effect the conditioning number for $\underset{\sim}{K}$. However by choosing $c = \sqrt{m}$, where m is the maximum number of nonzero elements in any row, the spectral radius of $\underset{\sim}{K}$ can be shown (Ref. 13) to be less than one

$$\rho(K) \equiv \max_i |\lambda_i| < 1 \tag{4.11}$$

This scaling transformation does not in general achieve the optimum C_N but does represent a standard form for positive definite matrices that eliminates ill-conditioning characterized by a large variation in the diagonal elements. A study of the influence of this transformation on the variable metric and conjugate gradient algorithms was made for the case of a linear plate bending problem using c = 1. A nine element idealization was used as shown in Fig. 23 with a_1, a_2, a_3 equal to 70, 70, 60. The convergence characteristics of the conjugate gradient method as illustrated in Fig. 24 indicate rapid convergence in less than n cycles (n = number of independent degrees of freedom)

Approved for Public Release

Contrails

while the unscaled problem failed to converge in 4n cycles. The same data for the variable metric method are shown in Fig. 25 and indicate a significant improvement. However, in this case the unscaled problem does converge and in approximately n cycles.

4.2.2 Nonlinear

The shapes of constant energy surfaces in a nonlinear space are not only more complex but are often not even convex. However, Taylor's theorem indicates that in the neighborhood of a relative minimum of the potential energy having positive definite second variation, the matrix of second partial derivatives

$$\left[\frac{\partial^2 \Pi}{\partial z_i \partial z_j}\ (\vec{Z})\right] = \left[\frac{\partial^2}{\partial z_i \partial z_j}\ (U_2 + U_3 + U_4 - W)\right] \qquad (4.12a)$$

that is

$$\left[\kappa_{ij}\ (\vec{Z})\right] = \left[K_{ij} + \frac{\partial^2}{\partial z_i \partial z_j}\ (U_3 + U_4)\right] \qquad (4.12b)$$

dominates the potential energy. Hence it is possible to define scaling for the nonlinear problem which is similar to that for the linear problem. In the nonlinear case, however, the scaling transformation is a function of $\vec{Z}$. In the geometrically nonlinear problems which have been studied, the diagonals of $\kappa_{ij}(\vec{Z})$ differed by factors of two or three with respect to the linear K_{ij} but they were the same order of magnitude. Computational experience to date indicates scaling based on K_{ij} to be as good as scaling based on $\kappa_{ij}\ (\vec{Z})$ in such situations. The present scaling procedure thus removes gross ill-conditioning but does not appreciably change the conditioning for variations in $\kappa_{ii}\ (\vec{Z})$ that are less than one order of magnitude.

There has also been some use of linear scaling for problems with material nonlinearities (Ref. 6) in conjunction with the variable metric

Approved for Public Release

Contrails

method. The diagonals of the flexibility matrix were used in this case since the complementary energy functional was being minimized. The improvement in the convergence characteristics of the variable metric method was comparable to that obtained in geometrically nonlinear problems. Results of these and other applications lead to the conclusions that:

(1) Convergence of the variable metric method can be significantly improved by linear scaling in both linear and nonlinear problems.

(2) The conjugate gradient method is a reliable algorithm in scaled coordinates for plate and shell problems.

4.3 Convergence Studies

4.3.1 Over-Discretized problems.

The conjugate gradient algorithm was applied to a linear plate bending problem to numerically study convergence vs. the number of degrees of freedom used for a square element grid. All numerical work employs the scaling transformation with c = 1. The 16 degree of freedom plate bending element of Reference 2 is capable of representing the energy and maximum displacement of a simply supported plate under uniform pressure with a very few elements. As more elements are used the problem quickly becomes "over-discretized" in the sense that only a fraction of the degrees of freedom present are needed to represent accurately the displacement field. The number of cycles required by the conjugate gradient method as a function of the number of degrees of freedom in this situation is shown in Fig. 26. The relationship is nearly linear with a slope considerably less than one. Since only square elements (i.e. uniform grids) were used in these cases, the rate of convergence is probably greatest for this particular element stiffness matrix. Typical run times on the 7094 for N = 100, 256 and 400 are

Approved for Public Release

Contrails

15, 81 and 180 seconds including formation of matrices. These results indicate that convergence occurs with $\bar{n} << n$ for over-discretized problems. A study made by Kowalik (Ref. 30) using a plane stress (membrane) element produced a similar result when he obtained convergence in 280 cycles for 680 degrees of freedom. This result was obtained without any reported scaling; however, most plane stress element stiffness matrices have equal diagonals if their planform is square and in general should not suffer seriously from scale effects. It is important to note that the conjugate gradient method storage requirements were only one (16 x 16) element stiffness matrix and a few vectors of dimension n for these square grids.

4.3.2 Ill-Conditioned Problems

The convergence characteristics of the variable metric and conjugate gradient methods in problems with essential ill-conditioning was investigated using four irregular element grids. These grids are shown in Fig. 23 and have the same (uneven) spacing in the x and in the y directions. These grids were chosen so as to produce stiffness matrices with high conditioning numbers independent of scale effects. The scaled and unscaled conditioning numbers (C_N) are given in Table 6 identified by the maximum element aspect ratio (a/b) for the grid.

For this study, convergence was defined as the cycle at which no further reduction could be made in the potential energy even in the direction of steepest descent. The number of cycles so required by the variable metric and conjugate gradient methods are plotted in Figs. 27 and 28 vs. $\log_{10} C_N$ and maximum element (a/b). These results indicate that (1) aspect ratio is a good measure of conditioning in these problems and (2) the number of cycles increases approximately linearly with both parameters. As Fig. 28 shows, well over n cycles (45 vs. 36) were required by the conjugate gradient

Approved for Public Release

Contrails

method for the case with largest C_N. In such ill-conditioned problems it is crucial that the sequence of conjugate directions be continued beyond cycle n and not aborted in favor of a steepest descent move at cycle n+1. The reason is that the very slow rate of convergence typical of many of the cycles at the beginning of an ill-conditioned problem will be repeated and ultimate convergence thereby significantly delayed. These remarks, of course, pertain to linear problems and the suggestion in Ref. 27 to return periodically to a steepest descent move may be well taken for nonlinear problems. Further results concerning the accuracy of the displacement field found in these linear cases may be found in Ref. 13.

4.4 The Linear Search Problem

4.4.1 Step Size Estimates

A factor strongly affecting the efficiency of gradient methods in nonlinear problems is the linear search that must be made in each new direction. The object of this search is to find the first positive root, t*, such that the directional derivative $(d\Pi(t))$ at $\vec{Z} + t\vec{P}$ in the direction $\vec{P}$,

$$d\Pi(t) \equiv \vec{P}^T \cdot \nabla\Pi(\vec{Z} + t\vec{P}) \tag{4.13}$$

vanishes or equivalently the first minimum of $\Pi(\vec{Z} + t\vec{P})$ on $0 < t$. A closed form solution for this root is known for linear problems so that an iterative search is required only in nonlinear cases. In the widely used cubic interpolation scheme of Davidon (Ref. 27, 28) and in a new scheme to be presented in the next section, the root is first bracketed by taking ever larger steps, h_i, until the directional derivative reverses sign. At every step, h_i, in this process a function and gradient evaluation are required.

Approved for Public Release

Contrails

The true computational cost of a gradient method then depends not only on the number of cycles (directions) but on this number weighed by the cost of each linear search.

A method for generating the first step size, h_1, in each new direction so that the bracketing can usually be accomplished in one or two steps has been developed. The essence of the scheme lies in making the process adaptive. The infinity norm of the current vector

$$||\vec{Z}_i||_\infty \equiv \max_j |Z_j| \tag{4.14}$$

is used to generate h_1 as

$$h_1 = c_i ||\vec{Z}_i||_\infty \tag{4.15}$$

where c_i is a parameter dependent on the history of all i-1 linear searches previously performed.

$$\begin{aligned} c_0 &= 1 \\ c_i &= (2)^{r-1} \left(\tfrac{1}{2}\right)^s c_{i-1} \end{aligned} \tag{4.16}$$

with

r = the number of increments required to bracket the root in cycle i-1.

s = the number of decrements required to insure $|d\Pi(t_a)| > 0.01 |d\Pi(t_b)|$; plus 1 if the search results in $t^* < t_a + 0.1 (t_b - t_a)$ at cycle i.

Within a few cycles, usually two, the value of c_i has adapted to the space and any further changes are infrequent. Because of this property the initial h_1 at cycle one is not critical. If for some reason a new direction does produce a drastic change in the linear search, the machinery necessary to adapt

Approved for Public Release

Contrails

to such a change is present. The object of this procedure is to bracket the root, t*, with a minimum effort subject to the constraint that the resulting interval be reasonably small in the sense defined by s.

4.4.2 Iterative Solution

Once a zero of the directional derivative has been bracketed the cubic fitting scheme of Davidon works reasonably well and is in wide use. The most common difficulty encountered is in satisfying the condition,

$$\left| \frac{d\Pi\ (t^*)}{||\vec{P}||_2 \cdot ||\nabla\Pi(\vec{Z} + t^*\vec{P})||_2} \right| < \varepsilon \qquad (4.17)$$

Geometrically this is the cosine of the "angle" between $\vec{P}$ and $\nabla\Pi(\vec{Z} + t^*\vec{P})$ which provides a convenient frame of reference in choosing ε for computations. Literally ε is a convergence criteria for accepting t* as a zero of the directional derivative. Since the cubic fit scheme seeks t* indirectly by interpolating the function $\Pi(t)$, it will have difficulty in those cases where the directional derivative crosses zero with a steep slope. A new iterative scheme has been developed based directly on $d\Pi(t)$, the slope of $\Pi(t)$. With t* bracketed as previously discussed in Section 4.4.1 the problem of finding the crossing is relatively straight forward. A combination Regula Falsi-Bisection procedure has been developed that works well under these starting conditions. If the function is quadratic the procedure is exact and if the function space is nonlinear but convex the procedure will always converge to the root. Let t_e be the current estimate to t*,

Approved for Public Release

Contrails

1. $t_e = t_a - d\Pi(t_a) \left\{ \frac{t_a - t_b}{d\Pi(t_a) - d\Pi(t_b)} \right\}$

2. If $d\Pi(t_e) \cdot d\Pi(t_b) < 0$

   then

   $t_b \rightarrow t_a$

   $t_e \rightarrow t_b$

   else

   $t_a \rightarrow t_a$

   $t_e \rightarrow t_b$

3. $t_e = \frac{1}{2}(t_a + t_b)$

4. If $d\Pi(t_e) \cdot d\Pi(t_b) < 0$

   then

   $t_b \rightarrow t_a$

   $t_e \rightarrow t_b$

   else

   $t_a \rightarrow t_a$

   $t_e \rightarrow t_b$

The iteration steps are 1, 2, 3, 4, 1, 2, 3, 4, ... until convergence as defined by Eq. 4.17 is achieved. Step 1 is basic Regula Falsi,steps 2 and 4 insure that the interpolation points always bracket the root and step 3 insures against slow convergence for strongly nonlinear problems. This is illustrated in Fig. 29 and clearly shows the need for step 3 when steps 2 and 4 are used. The flat part of the curve corresponds to a region in which the quadratic term in Π dominates. As t becomes large the higher order terms dominate, causing the directional derivative to sweep up in direct proportion.

Approved for Public Release

Contrails

It is this behavior that necessitates step 3 to maintain a good rate of convergence.

4.5 Termination Criteria

4.5.1 Minimum Function vs. Minimum Gradient in Finite Arithmetic

To discuss termination criteria for energy search algorithms it is helpful initially to distinguish between linear and nonlinear problems. In linear problems most gradient methods, like the conjugate gradient or variable metric, theoretically converge in at most n steps where n is the number of degrees of freedom. The proof of this results, when the gradient after n cycles is shown to be orthogonal to n linearly independent vectors and hence is the null vector. In actual computations with finite arithmetic, the chances of the gradient vector being null are nil. What one usually assumes is that when the energy is converged to η digits, the norm of the gradient is small enough to give a solution of the equilibrium equations accurate to $\xi \leq \eta$ digits. With η a finite value there are a number of displacement states that yield the same energy to η digits, but differ from each other after the ξ^{th} place. For example in some problems there may be several displacement states that are equal to only 4 digits but give the same energy to 8 places and it is impossible in such cases to get 5 digit accuracy with a termination criteria based entirely on the energy. On the other hand components of the displacement vector rarely converge at the same rate and the larger displacements are usually accurate to more than ξ places which tends to support an energy criteria. The same line of reasoning applies equally well to nonlinear problems except that the process theoretically converges (and the gradient becomes the null vector) only in the limit. Thus in most problems the choice of a termination criteria becomes a matter of picking a suitable value of η. As noted in Ref. 13 for linear plate bending problems it is possible to take η equal to the working precision of the

Approved for Public Release

Contrails

arithmetic without adding many extra cycles to the search. In practice both linear and nonlinear structural problems are usually run until no reduction in the energy can be made in the direction of steepest descent.

There occasionally are cases when the gradient is not as small as one would like even after the energy is converged to η places. If η is the working precision of the arithmetic then either a higher precision must be used or some alternative scheme employed as a terminal option to drive the gradient to zero independent of an energy criteria. While this last statement may sound paradoxical it is simply a recognition of the fact that several displacement states have the same energy to η places but have different gradients. To get from one of the states with a higher gradient to one with a lower gradient the iteration should be such that the norm of the gradient decreases monotonically. This iteration may cause the energy to increase initially, however, the values cannot change significantly from that previously found, since the equilibrium position is stable. One such scheme is presented in the next section.

4.5.2 Functional Iteration as a Terminal Option

The object of the energy search is to find the $\vec{Z}$ that solves the equilibrium equations $\nabla\Pi(\vec{Z}) = 0$. Consider the problem of solving this system of nonlinear equations starting from the $\vec{Z}$ found by the energy search algorithm. This may be viewed as a cleaning up operation for problems difficult to solve accurately by energy search. In this context it seems logical to ask that the algorithm used be free from any large matrix operations and that it be computationally less effort than the energy search. A form of functional iteration that is a nonlinear analog of Jacobi iteration fits these requirements and a strong argument for convergence can be made if nonlinear scaling is used. Define a functional iteration to solve the problem $\vec{Z} = \vec{g}(\vec{Z})$ by

Approved for Public Release

Contrails

$$\vec{Z}_{i+1} = \vec{g}(\vec{Z}_i) \qquad i = 0, 1, 2, \ldots \tag{4.18}$$

The contracting mapping theorem (see Ref. 31) implies that

If

$$||\vec{g}(\vec{Z}_o) - \vec{Z}_o|| \leq (1-L)\, r$$

and

$$||\vec{g}(\vec{Z}) - \vec{g}(\vec{Y})|| \leq L\, ||\vec{Z} - \vec{Y}|| \tag{4.19}$$

for all

$$\vec{Z}, \vec{Y} \text{ such that } ||\vec{Z} - \vec{Z}_o||, \; ||\vec{Y} - \vec{Z}_o|| \leq r$$

with

$$0 \leq L < 1, \qquad r > 0$$

Then

$$\lim_{i\to\infty} \vec{Z}_i \to \vec{Z} \tag{4.20}$$

In other words if the initial guess $\vec{Z}_o$ isn't too bad and if $\vec{g}$ has a Lipschitz constant less than one in the neighborhood of $\vec{Z}_o$ then the iteration converges to the unique solution in that neighborhood. If the component functions, g_i, of $\vec{g}$ are differentiable then Taylor's theorem gives as a Lipschitz constant

$$L = \max_{||\vec{Z}-\vec{Z}_0||\leq r} \left|\left| \left[\frac{\partial g_i}{\partial z_j} \right] \right|\right| \tag{4.21}$$

In the present problem,

$$\vec{g}(\vec{Z}) = \vec{Z} - \nabla\Pi(\vec{Z}) \tag{4.22}$$

where $\Pi(\vec{Z})$ is the potential energy function so that

Approved for Public Release

Contrails

$$\left[\frac{\partial g_i}{\partial z_j}\right] = \left[\frac{\partial}{\partial z_j}\left(z_i - \frac{\partial \Pi}{\partial z_i}\right)\right] \tag{4.23a}$$

$$\left[\frac{\partial g_i}{\partial z_j}\right] = \left[\delta_{ij} - \frac{\partial^2 \Pi}{\partial z_i \partial z_j}\left(\vec{Z}\right)\right] \tag{4.23b}$$

$$\left[\frac{\partial g_i}{\partial z_j}\right] = I - \kappa\left(\vec{Z}\right) \tag{4.23c}$$

and $\kappa(\vec{Z})$ is the matrix of second partials which in linear problems is simply the ordinary stiffness matrix. The eigenvalues of $\left[\frac{\partial g_i}{\partial z_j}\right]$ are $1 - \lambda_i(\vec{Z})$ where $\lambda_i(\vec{Z})$ are the eigenvalues of $\kappa(\vec{Z})$. Now if $\kappa(\vec{Z})$ is such that

$$\max_i \lambda_i \left(\vec{Z}\right) \leq 1 \tag{4.24}$$

then since $\kappa(\vec{Z})$ is positive definite by virtue of the principle of minimum potential energy,

$$0 \leq \zeta_i < 1 \tag{4.25}$$

where $\zeta_i = 1 - \lambda_i$ are the eigenvalues of $\left[\frac{\partial g_i}{\partial z_j}\right]$. Using the scaling criteria of Section 4.2 on $\kappa(\vec{Z})$ insures that Eq. 4.24 is satisfied so that a Lipschitz constant less than one has been shown at $\vec{Z}$. If the starting vector $\vec{Z}_0$ from energy search is near the solution then this indicates the following nonlinear Jacobi iteration is convergent in properly scaled coordinates,

$$\vec{Z}_{i+1} = \vec{Z}_i - \nabla\Pi\left(\vec{Z}_i\right) \qquad i = 0,1, \ldots \tag{4.26}$$

In the limited computational experience to date the scheme has always converged monotonically in the sense

$$\left|\left|\nabla\Pi\left(\vec{Z}_{i+1}\right)\right|\right|_2 < \left|\left|\nabla\Pi\left(\vec{Z}_i\right)\right|\right|_2 \tag{4.27}$$

The energy usually increases slightly the first few cycles and then decreases to a value very close to that found in the energy search.

Approved for Public Release

Contrails

SECTION 5

ANNULAR PLATE ELEMENT

5.1 Introduction

In this section the work reported in Section 2 is extended to the case of a flat plate element in the shape of a sector of an annulus. These elements may be joined with the rectangular plate and cylindrical shell elements reported previously. A special case of the annular plate element in which the circumferential dimension is large compared with the radial dimension is useful as a rib stiffener attached to cylindrical shells. Numerical results are presented and compared with known solutions for several linear example problems.

5.2 Development of the Element

The plate element developed in this section has the shape of a sector of an annulus, bounded by the arcs $r = r_1$ and $r = r_2$ and the rays $\theta = \theta_1$ and $\theta = \theta_2$ in a plane polar coordinate system (see Fig. 30). This shape makes it necessary to transform the strain-displacement relations for a flat plate in Cartesian coordinates (Eqs. 2.3) into polar coordinates, yielding*

$$\varepsilon_r = \frac{\partial u}{\partial r} + \frac{1}{2}\left(\frac{\partial w}{\partial r}\right)^2 - z\frac{\partial^2 w}{\partial r^2} \tag{5.1a}$$

$$\varepsilon_\theta = \frac{1}{r}\frac{\partial v}{\partial \theta} + \frac{u}{r} + \frac{1}{2r^2}\left(\frac{\partial w}{\partial \theta}\right)^2 - \frac{z}{r}\left(\frac{1}{r}\frac{\partial^2 w}{\partial \theta^2} + \frac{\partial w}{\partial r}\right) \tag{5.1b}$$

$$\gamma_{r\theta} = \frac{1}{r}\frac{\partial u}{\partial \theta} + \frac{\partial v}{\partial r} - \frac{v}{r} + \frac{1}{r}\frac{\partial w}{\partial r}\frac{\partial w}{\partial \theta} - \frac{2z}{r}\left(\frac{\partial^2 w}{\partial r \partial \theta} - \frac{1}{r}\frac{\partial w}{\partial \theta}\right) \tag{5.1c}$$

Here r, θ, and z are polar coordinates with corresponding displacement functions u, v, and w, and plane strain components ε_r, ε_θ, and $\gamma_{r\theta}$. The

* Alternatively, these equations may be derived from the set given in Ref. 7. for an arbitrary shell in curvilinear coordinates by substituting the appropriate expressions for the Lame parameters and principal radii of curvature.

Approved for Public Release

Contrails

assumptions implicit in these equations are:

(1) normals to the middle surface of the plate remain straight and normal during deformation,

(2) transverse shear deformation is negligible,

(3) the normal displacement w is constant through the thickness, and

(4) quadratic terms in u and v are small compared with quadratic terms in w.

Assumed displacement modes for the interior of this element are taken as sums of products of one-dimensional interpolation formulas, in the spirit of the work reported in Section 2. Thus, if f stands for either u, v, or w, we have

$$f(\xi,\eta) = \sum_{i=1}^{2} \sum_{j=1}^{2} \sum_{p=0}^{1} \sum_{q=0}^{1} F_{pi}(\xi)\, G_{qj}(\eta)\, f_{pqij} \qquad (5.2)$$

Here ξ and η are arc lengths in the radial and tangential directions, respectively; that is, $\xi = r$ and $\eta = r\theta$. The f_{pqij} are undetermined coefficients, and $F_{pi}(\xi)$ and $G_{qj}(\eta)$ are osculatory interpolation functions with the following properties:

$$F_{oi}(\xi_k) = \delta_{ik} \; ; \qquad G_{oj}(\eta_\ell) = \delta_{j\ell} \qquad (5.3a)$$

$$\frac{\partial F_{oi}}{\partial \xi}(\xi_k) = 0 \; ; \qquad \frac{\partial G_{oj}}{\partial \eta}(\eta_\ell) = 0 \qquad (5.3b)$$

$$F_{1i}(\xi_k) = 0 \; ; \qquad G_{1j}(\eta_\ell) = 0 \qquad (5.3c)$$

$$\frac{\partial F_{1i}}{\partial \xi}(\xi_k) = \delta_{ik} \; ; \qquad \frac{\partial G_{1j}}{\partial \eta}(\eta_\ell) = \delta_{j\ell} \qquad (5.3d)$$

Approved for Public Release

Contrails

where $\xi_k = r_k$, $\eta_\ell = r\theta_\ell$, δ_{ik} and $\delta_{j\ell}$ are Kronecker deltas, and i, k, j, ℓ take on values 1, 2.

A set of functions which satisfy the foregoing requirements is

$$F_{pi}(\xi) = (d)^p P_{pi}(\rho) \tag{5.4a}$$

$$G_{qj}(\eta) = (\rho d)^q S_{qj}(\theta) \tag{5.4b}$$

where the non-dimensionalized radial coordinate $\rho = r/d$ has been introduced, with $d = r_2 - r_1$. The $P_{pi}(\rho)$ are first-order Hermite interpolation polynomials given by

$$P_{01}(\rho) = \rho_2^2(-3\rho_1 + \rho_2) + 6\rho_1\rho_2\rho - 3(\rho_1 + \rho_2)\rho^2 + 2\rho^3 \tag{5.5a}$$

$$P_{02}(\rho) = \rho_1^2(3\rho_2 - \rho_1) - 6\rho_1\rho_2\rho + 3(\rho_1 + \rho_2)\rho^2 - 2\rho^3 \tag{5.5b}$$

$$P_{11}(\rho) = -\rho_1\rho_2^2 + \rho_2(\rho_2 + 2\rho_1)\rho - (2\rho_2 + \rho_1)\rho^2 + \rho^3 \tag{5.5c}$$

$$P_{12}(\rho) = -\rho_1^2\rho_2 + \rho_1(\rho_1 + 2\rho_2)\rho - (2\rho_1 + \rho_2)\rho^2 + \rho^3 \tag{5.5d}$$

Here ρ_1 is r_1/d and ρ_2 is r_2/d. These polynomials interpolate a function over the interval ρ_1 to ρ_2, in terms of the function values and first derivatives at the stations ρ_1 and ρ_2.

The functions $S_{qj}(\theta)$ may be chosen either as trigonometric interpolation formulas (written out in Eqs. 2.56 for the case $\theta_1 = 0$) or as first order Hermite interpolation polynomials. With the properties expressed in Eqs. 5.3 in mind, it is easily verified that the coefficients f_{pqij} in Eq. 5.2 are the values of

Approved for Public Release

Contrails

$$\frac{\partial^{p+q} f}{\partial \xi^p \partial \eta^q}$$

evaluated at the corner $\xi = \xi_i$, $\eta = \eta_j$. Substituting Eqs. 5.4 into Eq. 5.2 and choosing f = w for the sake of illustration yields

$$\begin{aligned} w(\rho,\theta) = \sum_{i=1}^{2} \sum_{j=1}^{2} [& P_{0i}(\rho)\, S_{0j}(\theta)\, w_{ij} \\ & + (d)\, P_{1i}(\rho)\, S_{0j}(\theta)\, w_{\xi ij} \\ & + (\rho d) P_{1i}(\rho)\, S_{1j}(\theta)\, w_{\eta ij} \\ & + (\rho d^2) P_{1i}(\rho)\, S_{1j}(\theta)\, w_{\xi\eta ij} \,] \end{aligned} \qquad (5.6)$$

w_{ij} is the displacement, $w_{\xi ij}$ and $w_{\eta ij}$ are the radial and tangential slopes, and $w_{\xi\eta ij}$ is the twist at the corner $\xi = \xi_i$, $\eta = \eta_j$. Along the edge $\theta = \theta_1$, Eq. 5.6 becomes, in light of the properties expressed in Eqs. 5.3,

$$w(\rho,\theta_1) = \sum_{i=1}^{2} [P_{0i}(\rho)\, w_{i1} + (d)\, P_{1i}(\rho)\, w_{\xi i1}] \qquad (5.7)$$

Thus the value of w along this edge depends only on the corner variables w_{11}, w_{21}, $w_{\xi 11}$ and $w_{\xi 21}$, so that continuity of w between two adjacent annular elements is assured by matching appropriate pairs of variables at the corners which bound such an edge. Furthermore, continuity of w between the straight side of an annular element and a rectangular plate element or a straight side of a cylindrical shell element can also be assured, since the latter two elements yield the same expression for w on such an edge as does Eq. 5.7.

Approved for Public Release

Contrails

Similarly, the slope $\frac{1}{(pd)} \frac{\partial w}{\partial \theta}$ along an edge $\theta = \theta_1$ is given by

$$\frac{1}{(pd)} \frac{\partial w}{\partial \theta} (\rho, \theta_1) = \sum_{i=1}^{2} [P_{0i}(\rho) w_{\eta i1} + (d) P_{1i}(\rho) w_{\xi\eta i1}] \qquad (5.8)$$

so that slope continuity between adjacent elements can also be assured by matching appropriate corner variables. Similar properties hold on edges $\rho = \rho_i$, that is, annular elements can be joined together along curved edges (provided they have the same center of curvature), or they may be joined to cylindrical shell elements at right angles.

Continuity of the u and v displacements is also assured by matching corner variables. It is not necessary to match derivatives of u and v across element boundaries, but this can be done in order to insure continuity of middle-surface strains on boundaries between annular elements when appropriate. However, when a rectangular element meets an annular element, these strain continuity conditions imply a linear constraint equation rather than a simple one-to-one linking of corner variables. This arises from the extra term in the tangential strain-displacement relation for the annular element. At the middle surface of a rectangular element,

$$\varepsilon_y = \frac{\partial v}{\partial y} + \frac{1}{2} \left(\frac{\partial w}{\partial y}\right)^2 \qquad (5.9)$$

while in an annular element,

$$\varepsilon_\theta = \frac{1}{r} \frac{\partial v}{\partial \theta} + \frac{u}{r} + \frac{1}{2r^2} \left(\frac{\partial w}{\partial \theta}\right)^2 \qquad (5.10)$$

Approved for Public Release

Contrails

The potential energy of an annular element, assuming linear elastic isotropic material behavior is

$$\pi_a = \frac{E}{1-\nu^2} \int_{-\frac{h}{2}}^{\frac{h}{2}} \int_{\theta_1}^{\theta_2} \int_{r_1}^{r_2} [\varepsilon_r^2 + \varepsilon_\theta^2 + 2\nu\, \varepsilon_r \varepsilon_\theta + \frac{1}{2}(1-\nu)\, \gamma_{r\theta}^2]\, r\, dr\, d\theta\, dz - W_a \qquad (5.11)$$

in which E is the modulus of elasticity, ν is Poisson's ratio, h is the plate thickness (assumed uniform), and W_a is the work done by loads applied to the discrete element. Substitution of the strain-displacement relations, Eqs. 5.1, into Eq. 5.11 yields quadratic, cubic, and quartic terms for the strain energy:

$$U_a = U_{2a} + U_{3a} + U_{4a} \qquad (5.12)$$

In principle, substitution of the assumed displacement modes and formation of stiffness matrices is carried out in the same manner as for the rectangular plate and cylindrical shell elements discussed in Section 2. However, the explicit appearance of the variable r in the strain-displacement relations and in the potential energy expression, the non-zero lower limits of integration,and the non-integer coefficients in the Hermite interpolation polynomials present complexities and numerical difficulties for the annular element which do not occur for the former elements.

A special case of this element in which the outer radius r_2 is not much larger than the inner radius, r_1 is useful in modeling rib stiffeners attached to cylindrical shells. The basic assumption made is that the radial strain $\varepsilon_r = 0$ over the entire element and the specialization then follows steps similar to those for the rectangular plate stiffener (see Section 2.2.2).

Approved for Public Release

Contrails

Application of this element to specific test cases is discussed in the next section.

5.3 Examples

Two test problems illustrating applications of the annular plate element to problems with linear, axially symmetric behavior are discussed.

A thick walled hollow cylinder subjected to internal pressure, illustrated in Fig. 31, is discussed in Article 26 of Ref. 26. A slice of the cylinder cut out by two adjacent cross sections can be treated as a plane stress problem. The cylinder has been modeled by a single element, by two elements (as shown by dotted lines in Fig. 31), and by five elements stacked radially. The condition of axially symmetric deformations, when imposed on the assumed displacement modes, eliminates all v_{ij}, $v_{\xi ij}$, $v_{\eta ij}$, $v_{\xi\eta ij}$, $u_{\eta ij}$, and $u_{\xi\eta ij}$ variables and requires that $u_{11} = u_{12}$, $u_{\xi 11} = u_{\xi 12}$, $u_{21} = u_{22}$, and $u_{\xi 21} = u_{\xi 22}$, leaving just two independent degrees-of-freedom for the one-element case. Table 7 lists maximum displacements and maximum stresses for three different cases, with approximate solutions for the three modelings compared with the exact solution of Ref. 26. Case 3 shows that more elements are needed to achieve good results as the ratio r_2/r_1 grows. This is due to the term $(r_2/r)^2$ which appears in the exact solution. As the size of the outer diameter relative to the inner diameter grows, more and more degrees-of-freedom are necessary to approximate this term well by polynomials.

An annular plate subject to various lateral loadings and support conditions is discussed in Article 17 of Ref. 20 (see in particular Fig. 36, p. 62, Ref. 20). Figure 32 shows the annular plate with the loads and support conditions for the first of ten cases for which solutions were

Approved for Public Release

Contrails

obtained. In each case results (obtained by two-element models) agree closely with the exact solutions reported in Ref. 20 as shown in Table 8.

Approved for Public Release

Contrails

SECTION 6

DESCRIPTION OF THE COMPUTER PROGRAM

6.1 Introduction

The computer program described in this section implements both the potential energy search method and the direct stiffness method of structural analysis for plate and shell structures which may be modeled adequately by assemblages of certain discrete elements. Geometric nonlinearities may be incorporated directly within these elements so that finite deflection, buckling and post-buckling behavior may be predicted. The Fletcher-Powell and Fletcher-Reeves function minimization algorithms are employed for the potential energy search. In addition, matrix inversion is available for linear solutions.

6.2 Program Capabilities and Limitations

6.2.1 Available Elements.

At present, this program contains six kinds of four-sided isotropic linear elastic plate and shell elements. Each is bounded by parametric curves in an orthogonal curvilinear x,y coordinate system.≠ Displacement states within each element are represented by assumed modes with certain generalized corner displacements as undetermined coefficients. Satisfaction of the geometric admissibility requirements of the principle of minimum potential energy is assured by assigning the same independent degree-of-freedom number to corresponding displacement variables where two element corners meet. With certain exceptions, enumerated below, the assumed modes are osculatory interpolation formulas, and each displacement function f(x,y)

≠ Throughout Section 6 and Appendix B the arc lengths are denoted x,y rather than ξ,η because the lower case Greek symbols are not available alpha-numeric characters for computer input-output.

Approved for Public Release

Contrails

has as undetermined coefficients the values of f and its derivatives with respect to x, y, and xy at each corner, for a total of sixteen. Here, f stands for either of the in-plane displacements u and v, or the transverse displacement w. Sixteen is the smallest number of modes assumed for interpolation of the displacement w. For u and v the smallest number of assumed modes is four. This choice is available as an option with certain elements. However, osculatory formulas (which interpolate a function and its first derivative) are preferred for interpolation of u and v for two reasons: first, this makes it possible to join elements together at right angles, and second, it has been found that the extra investment in computing time entailed by this choice pays off in better solutions (most notably, better membrane stress predictions). Similarly, an improvement in results for the bending displacement w is obtained by resorting to hyperosculatory interpolation formulas, with a total of thirty-six degrees of freedom. This option is available for certain elements, but its use with non-linear strain-displacement relations is not feasible.

Descriptions of the six available elements, illustrated in Fig. 33 follow.

6.2.1.1 Rectangular Plate Elements

Membrane displacements u(x,y) and v(x,y) may be interpolated over the interior of this element using either Lagrange (zeroth-order Hermite) polynomials with eight corner degrees-of-freedom or osculatory (first order Hermite) polynomials with thirty-two degrees of freedom (counting both u and v), or membrane action may be suppressed entirely. In the case of Lagrange interpolation, the four corner values of u and the four corner values of v are the undetermined coefficients. The bending displacement w(x,y) may be interpolated using osculatory polynomials with sixteen degrees of freedom or

Approved for Public Release

Contrails

hyperosculatory (second-order Hermite) polynomials with thirty-six degrees of freedom, or may be suppressed. In the case of hyperosculatory interpolation, the undetermined coefficients are w and its derivatives with respect to x, y, xy, xx, yy, xxy, xyy, and xxyy. It is recommended that only osculatory interpolation be used unless the structure is a simple unstiffened rectangular flat plate. Hyperosculatory interpolation is not allowed with non-linear problems.

6.2.1.2 Cylindrical Shell Elements

This element is bounded by two generators and two parallels of a circular cylindrical surface. Both membrane and bending displacements are interpolated using osculatory formulas, with a total of 48 degrees-of-freedom. Hermite polynomials are used in the axial direction, and either Hermite polynomials or circular interpolation functions may be specified for the circumferential direction. The latter include the functions sine and cosine, and contain exact representations of the zero-strain modes for the linear case. The polynomial interpolation functions give a good approximation of the zero-strain modes which improves as the circumferential dimension decreases. The trigonometric formulation becomes ill-behaved as this dimension decreases. Consequently, polynomial interpolation is recommended when the subtended angle falls below 5° while circular function interpolation is recommended when the subtended angle is greater than 30°.

6.2.1.3 Annular Flat Plate Elements

This element is bounded by two concentric arcs and two rays. As with the cylindrical element, either Hermite polynomials or circular functions are available for osculatory interpolation in the circumferential direction. The assumed modes for this element become ill-behaved as the ratio of the outer radius to the inner radius grows.

Approved for Public Release

Contrails

6.2.1.4 Rectangular Stiffener

Rectangular stiffener elements have been formulated as a special case of the rectangular flat plate element as discussed in Section 2.2.2. The stiffener is viewed as a plate attached at right angles to the panel being stiffened, with one edge coincident with the panel's middle surface. Since elements may be joined only along their edges, panels may be stiffened only along element boundaries.

6.2.1.5 Cylindrical Stiffener

This element bears the same relationship to the cylindrical shell element as the rectangular stiffener does to the rectangular plate. Thus a cylindrical stiffener is a special case of the cylindrical shell element with the circumferential dimension much larger than the axial dimension. This element is used only for stiffening annular plate elements.

6.2.1.6 Annular Stiffener

This element is a special case of the annular plate element with its outer radius not much larger than its inner radius. It is used as a rib stiffener on a cylindrical shell element.

6.2.2 Connection of Elements

When two elements meet along an edge, the corners which bound that edge on one element must coincide with those which bound it on the other element; that is, element edges may not overlap. Elements may be joined either tangentially or at right angles, and as many as four elements may have a single edge in common. If two elements share a curved edge, then they must be geometrically compatible. For example, the only elements which could abut a curved edge of a cylindrical shell element are (1) another cylindrical shell element with the same axis, radius of curvature, and circumferential dimension, or (2) an annular plate or annular stiffener element joined at right

Approved for Public Release

Contrails

angles, with the side joining the cylinder having the same radius as the cylinder, and the same circumferential dimension. When elements are joined at right angles, only osculatory interpolation should be used; otherwise interelement continuity will not be assured.

6.2.3 Specification of Boundary Conditions and Loads

Boundary conditions may be prescribed either as edge restraints or corner restraints. Symmetry conditions are included as possible edge restraints so that only a portion of a symmetric structure with symmetric loads need be modeled.

Various loadings may be prescribed on the faces of elements, along their edges, or at corners. Work equivalent load vectors are automatically calculated for a class of common loadings including point loads at corners, line loads along edges, and surface loads. For less common loadings, work-equivalent load vectors will have to be calculated by hand. All loads are considered positive in the direction of corresponding positive displacements. Multiple load conditions including automatic incrementation may be specified. Also, displacements may be imposed.

6.2.4 Solution Methods

The principal numerical tools in this program are the Fletcher-Powell and Fletcher-Reeves algorithms for minimization of an unconstrained function of n variables (Refs. 27 and 28). The Fletcher-Powell routine develops an n by n metric for the space, which is computed from information about the gradient of the function from previous iterations, while the Fletcher-Reeves routine accumulates this kind of information in a vector. The large matrix needed by Fletcher-Powell is generally a disadvantage. On the other hand, for problems exhibiting essential ill-conditioning Fletcher-Powell tends to converge in significantly fewer cycles than Fletcher-Reeves (Ref. 13).

Approved for Public Release

Contrails

Both routines exit when they find that searching in the negative gradient direction does not reveal a function value smaller (within the computer's single-precision limit) than the value at the current occupied point. This seemingly strict criterion has not led to wasted iterations in problems studied to date, except for problems so small that the time for an iteration is negligible.

As with most iterative solution methods, hitches can develop, even though the routines have been extensively tested. In particular, they should be given a "reasonable" starting solution. For most problems, either a zero solution or the solution of a slightly different load set will be used, which should eliminate this problem. For some types of buckling, however, a perturbed solution must be given. Otherwise, since this is a gradient method, an unstable "saddle point" might satisfy the exit criterion. Experience has shown that the best way to obtain a perturbed solution is to apply a small lateral load, which plays the same role as an initial imperfection in the laboratory. This lateral load can be removed once buckling has occurred.

The user should examine the intermediate output from the minimization routine and decide whether satisfactory convergence has been reached. In those rare cases where convergence is not satisfied, an inordinately large gradient vector usually makes this apparent. What constitutes a "large" gradient vector can best be learned by studying the results of converged problems. Another test of convergence is the amount of change of the function value in the last few iterations. This change should be in only the seventh or eighth decimal places. The program generates a scaling transformation which has handled adequately all conditioning problems studied to date. An

Approved for Public Release

Contrails

estimate of running time is almost impossible to give for this routine, since running times vary so widely from one case to another, depending on the amount of non-linearity in particular. The best advice in this regard is to study the running times of previous problems.

A matrix inversion routine is also incorporated in this program(Ref. 32). It can be used either to obtain solutions to linear problems, or to generate initial linear solutions to nonlinear problems, which are then turned over to one of the minimization routines for energy search. In the latter case, the inverse of the master stiffness matrix is used as an initial metric by the Fletcher-Powell routine. Running times for matrix inversion vary approximately with the cube of the number of degrees of freedom. Univac 1107 Fortran IV running time for a 210 x 210 matrix was 340 seconds.

6.2.5 Program Phases

The program is divided into three phases: setup phase, which reads the description of the problem, assigns independent degree-of-freedom numbers, and generates stiffness matrices; input/output phase, which reads and analyzes load specifications and prints displacements, strains, and stresses; and analysis phase, which seeks numerical solutions. For problems with linear strain-displacement relations either matrix inversion or energy search may be used. Nonlinear problems must use energy search; however, a linear solution may be obtained first, either by inversion or energy search, and this linear solution is used as a starting point for non-linear energy search. Note that non-linear problems are solved by a single call on a minimization routine so that no load incrementation is necessary. Nevertheless, incrementation may be desirable so that a load-deflection curve may be traced out. Furthermore, it is usually much more efficient to use incrementation so that energy search for each load can begin at the solution for a slightly smaller load.

Approved for Public Release

Contrails

6.2.6 Storage Limitations

As many as 50 elements and 250 independent degrees-of-freedom can be handled. When storage requirements exceed core capacity, the program automatically sets up temporary external storage on drum (disk). On the IBM 7044/7094, matrix inversion problems are limited to 200 degrees of freedom. For nonlinear problems, running times rather than storage requirements are the real limitations.

6.3 Modeling Structures

6.3.1 Choice of Element Properties

The user should model his structure with as few elements as possible consistent with his insight into the anticipated behavior. Often, the spacing of stiffeners is so close that only one element is needed between stiffeners. Another consideration is the shape of expected buckling modes (recall that osculatory interpolation fits a cubic in each direction). A small number of elements should be tried first, and the grid refined if this seems advisable. Sometimes non-linearity can be suppressed in some elements (such as stiffener elements), and this can cut running time substantially. However, no intraelement membrane-bending coupling will be effective in flat plate elements unless nonlinearity is specified.

6.3.2 Specification of the Layout of the Structure

The elements of the structure are to be numbered consecutively (1, 2, ...), with a right handed orthogonal curvilinear x-y-z coordinate system attached to each element in accordance with the following rules, which are illustrated in Fig. 33:

6.3.2.1 Rectangular Plate and Stiffener Elements

Attach an x-y-z coordinate system at any corner, with the element lying in the first quadrant of the x-y plane. For stiffener elements, the

Approved for Public Release

Contrails

x axis must lie on the short side.

6.3.2.2 Cylindrical Shell and Stiffener Elements

Attach the coordinate system at either of two corners such that the x axis lies on a straight edge, the y-axis on a curved edge, and the z-axis points outward from the axis of the cylinder. The y coordinate measures distance in the circumferential direction, not an angle.

6.3.2.3 Annular Plate or Stiffener Elements

Attach the coordinate system such that the x-axis points outward from the pole, the y-axis points counterclockwise along the inner arc, and the z-axis is perpendicular to the plate. Again, the y coordinate measures distance, not an angle. For this element, an r-θ coordinate system is more convenient for some purposes. In this system, r is equal to x plus the inner radius, and θ is y/r, the angular coordinate.

Next, the corners at each element must be numbered from 1 to 4, beginning from the origin of coordinates and proceeding clockwise as viewed from the positive z side. The edges are then numbered clockwise from 1 to 4 starting with the left edge. Edge 1 will connect corners 1 and 2, edge 2 corners 2 and 3, etc. These rules are illustrated in Fig. 33.

Perhaps the most difficult input problem is specifying the topology of the structure. The convention adopted herein is believed to be fairly easy to use, while still allowing elements to be joined tangentially or at right angles. Imagine cutting the structure into elements and then putting it back together element by element. A first element would be chosen, and a second element would be attached to it along some edge. A third element would then be attached to one of these, and perhaps to both. Continuing in this manner, the entire sturcture would be assembled. If three elements meet

Approved for Public Release

Contrails

at an edge, it is not necessary to prescribe three relationships, although this would produce no error. It would be sufficient to say that element A joins element B and element B joins element C, and this would automatically imply that A joins C. Each time an element is added this way, the following information should be recorded: which two elements are joined, the corner numbers that bound the edge on which they are joined, and the relationship between the coordinate axes of the two elements (for further details, see Appendix B.1, data set S1). Using this information, the program automatically imposes the constraints necessary for geometric admissibility and assigns degree-of-freedom numbers. In addition to admissibility, it normally imposes some additional continuity between elements. For osculatory interpolation of membrane displacements, the program imposes continuity of normal and shear strains at the middle surface across boundaries between coplanar elements. It may sometimes be desirable to suppress this continuity, however, and an option is provided for this. In particular, whenever two coplanar elements are met by a third perpendicular element along their common edge, this third element will in general cause a discontinuity in strain between the coplanar elements by picking up some of the load. For hyperosculatory interpolation, continuity of bending moments between elements is also imposed. No option is provided to suppress this. There is an option to specify that two elements are joined by a hinge, however.

6.3.3 Choice of Loadings and Boundary Conditions

The goal of most runs will be to generate some sort of load-displacement curve. Often this curve will have many branches, and a number of runs will be required to trace out all the desired branches. It is suggested that fairly small load incrementation steps be taken. During linear

Approved for Public Release

Contrails

portions of a curve, this should not consume excessive time if the solution vector is extrapolated linearly along with the load vector. Users who cannot see their output until the run is finished should prescribe only a small range of loads for each run unless they are fairly sure of the points where bifurcation or snap-through will occur. Restart procedures are provided to facilitate this.

Boundary conditions sufficient to preclude rigid-body displacements should always be prescribed, even when loads are self-equibrating. Symmetry conditions should be specified wherever possible.

6.4 Input Data

Input data decks are divided into two groups: specification cards, which describe the structure and prescribe certain program options, and load cards, which define a set of forces and imposed displacements to be analyzed. For each problem to be run in a given job, a set of specification cards is provided, followed by one or more sets of load cards. These sets are punctuated by a separator cards, which are of five kinds:

The title card identifies the current problem. Control is passed to the setup phase, which reads either a specification group or a restart card (see Section 6.4.2). Upon exit from the setup phase, independent degrees of freedom will have been assigned and stiffness matrices will have been generated and written on drum (disk).

The restart card may take the place of the specification group, and indicates that the result of the setup phase of a previous run is to be read from tape.

Approved for Public Release

Contrails

The loads card passes control to the input/output phase of the program which will read a group of load cards and generate a work-equivalent load vector, after which the analysis phase will take control.

A new problem card indicates that an entirely different problem is to be run next. It is followed immediately by a title card.

The stop card is the last card of the deck. Detailed rules for punching separator cards, specification cards, and load cards may be found in Appendix B.

The flow chart in Fig. 34 illustrates the use of separator cards, and how they control flow among program phases. Note that a specification group may be followed immediately by a stop card or a new problem card, in which case no analysis will be performed. This can be useful: the user can examine the output from the setup phase, and if it seems in order, run the problem with restart option, with very little lost time.

Approved for Public Release

Contrails

SECTION 7

EXPERIMENTAL PROGRAM

7.1 Introduction

One of the primary practical applications of the analytical research reported here is the development of a capability for analyzing the behavior of a structure under loads above those at which buckling first occurs in some element or portion of the structure. For example, in indeterminate trusses the structure's behavior is often satisfactory above the load for initial buckling. The same statement is true for stiffened panels. Thus, a more reasonable limitation on structural behavior is to limit deflections rather than to prohibit buckling. This holds for all structures having substantial reserve stiffness and strength above the first buckling load.

Capability for the nonlinear analysis of structures has been developed in this project and its previous phase. Verification of this capability is difficult because "exact" solutions are available for only the simplest cases. Only a limited number of tests have been carried to loads substantially above first buckling. Test results have been presented in Refs. 33 and 34 for some frame structures. Most of the specimens tested could be described as "fixed-jointed" trusses. That is, they consisted of members assembled to form triangles and arranged so that if the ends were pinned they would be determinate trusses. None of the tests reported in the foregoing references were on structures having substantial post buckling stiffness.

The goal of the experimental portion of this research program was to obtain test results to compare with the analytically predicted behavior. All tests were designed specifically to verify particular aspects of the analytical capability. Usually specimens having substantial post-buckling stiffness and

Approved for Public Release

Contrails

strength were selected. The procedure was cyclic in character. A test was conceived, designed and performed. The test results were compared with the analytical results. If agreement was not satisfactory the test and the analysis were examined critically and modifications were made. In some cases, it was necessary to modify the test several times. The test results reported were those from the last cycle in this process. Some of the difficulties are discussed and the unsuccessful specimen designs reviewed.

The experimental structures may be divided into three categories; planar trusses and frames, a cylindrical shell and integrally stiffened plates. The trusses and frames consisted of a shallow two bar truss, a three bar truss and a simple frame with a diagonal brace. Most of the tests were concerned with nonlinear behavior due to buckling and finite deflections. Nonlinearities of material behavior were avoided. The direction of loading was unchanged through large deflections.

The two bar truss was designed so that "snap-through" could occur with the material remaining in the elastic region. Due to the large member rotations involved the analysis capability is severely challenged. Since the load-deflection curve for this structure has a region of negative slope, stability of the specimen and test system must be considered. Displacements were induced using a test fixture which was effectively rigid. Considerations for the testing of such systems are discussed in Ref. 35. A simple three bar truss was tested with proportions such that one member buckles much earlier than the others. Thus, a substantial portion of the load deflection curve is beyond the first buckling load. The planar frame was designed so that a wide variety of loading conditions could be applied.

Approved for Public Release

Contrails

A single cylindrical shell was tested under the action of self equilibrating, concentrated loads acting along a diameter (see Fig. 54). This test will be referred to in the subsequent discussion as the "pinched cylinder". It was performed to correlate measured and computed strains. Finite element analyses have often been substantiated by comparing measured and analytical deflections. For many design applications strains constitute a more useful comparison. It should be noted that the current computer program does not permit the introduction of curvature continuity between elements as an additional condition therefore the analytical results will exhibit small surface strain discontinuities. The pinched cylinder specimen was available from a previous test reported in Ref. 22. However, in the previous test only deflections were measured. The same specimen was instrumented for selected strain measurements.

A number of stiffened plates were tested under the action of either transverse or in-plane loads. The specimens were proportioned so that stiffener buckling occurred in the linear range of the material. Extensive deflection and strain data are reported and are available for correlation with results generated by future computational effort.

7.2 Truss and Frame Tests

7.2.1 Design and Construction of Specimens

The snap-through planar truss was proportioned so that only one member buckled as the node point was displaced. Thus, the center node essentially traversed the arc of a circle centered on the support of the unbuckled bar. The structure was displaced from its unloaded position to the point where the buckled member becomes straight again. At this point the member forces shift from compression to tension and some deflection will occur due to unavoidable slack in the joints. The configuration tested is shown in Fig. 35 and a

Approved for Public Release

Contrails

detailed drawing with important dimensions of the specimen and test setup is shown in Fig. 36. A general view of the test is shown in Fig. 37.

The node of the truss was held between two bars parallel to the non-buckling member with a closed rectangular yoke. It was attached to the yoke between two tension force transducers and a prestress force was induced in the system such that the transducers always remained in tension. The three parallel bars consisting of the unbuckled truss member and the two guide bars, all hinged at their ends, were then rotated by inducing a displacement at the yoke. The force required to hold the truss in a particular position can be determined by monitoring the two force transducers. This system assured that the direction of the applied load remained unchanged over large displacements. The testing frame was effectively rigid so that considerations mentioned in Ref. 35 for system stability were satisfied. A single buckled member was used because a symmetric buckled configuration could not be maintained without some guides for the displaced node point. Attempts to test a structure in which both members buckled simultaneously and equally were unsuccessful. However, the unsymmetric system worked very well.

The truss members were constructed of a heat treated steel having a yield point of 140 kips/in^2. Considerable care was exercised to maintain member straightness during heat treating. Since the members had to be hung vertically from one end during the process only a limited member length could be treated. A high yield stress which permits large elastic strains, was necessary to permit significant member curvature during buckling. The member ends were clamped into end fittings containing precision bearings to provide the hinged ends. The end fittings were of steel to reduce the fitting flexibility to the minimum. The entire system was attached to a

Approved for Public Release

Contrails

one inch thick aluminum plate. The buckled structure is shown in Fig. 38.

The three bar truss configuration was designed so that one member picked up more force than the others and then buckled at an applied load considerably below the applied load required to buckle the next member. The specimen selected is shown in Fig. 39. The members were of aluminum alloy 7075-T651 and the end fittings of mild steel. The joint at the point of load application was constructed using miniature precision bearings similar to those used in the two bar truss. The member ends at the support nodes were constructed of hardened steel knife edges.

One of the most difficult problems faced in the truss experimental work was the slack and flexibility in the pinned joints. For the original design of the three bar truss the structural deformation characteristics were dominated by flexibility of the joints. Pinned joints constructed using bearings were usually too flexible for use in truss structures in the linear regime. In the first of end fittings designs aluminum was used for ease in manufacture. The use of steel increased the joint stiffnesses. Finally,for this specimen, bearings were replaced by the steel knife edge supports. They proved to be quite stiff and were easier to adjust than the bearing joints. The very small amount of slack in precision bearings (about 0.001 in) was in excess of that which could be tolerated. It was difficult to avoid slack at the knife edge supports. Thus, when the structure was loaded assembly forces resulted. These forces were not easily detected due to the very low member buckling stresses. The use of knife edge supports made it possible to adjust the fitup by introducing shim stock between the knife edge and its support. A photograph of the structure and test setup is shown in Fig. 40.

Approved for Public Release

Contrails

This system was quite successful in dealing with most of the problems met in attempting to test an indeterminate truss. Steel was used for the earlier specimens but the lower modulus of elasticity of aluminum was found to be desirable because larger members could be used to produce larger strains prior to buckling but no increase in the buckling load. The very small deflections occurring at the node prior to buckling made the structure difficult to test.

The configuration used and the loading conditions for the frame specimen are shown in Fig. 41. The configuration was selected for its simplicity and for the variety of possible loading conditions. The member thicknesses permitted large deflections of the structure without exceeding the yield point of the material. Also by using slender members the end forces were kept small and it was possible to construct end connections which were essentially rigid. However, the use of slender bars for the horizontal member and the two vertical members resulted in rather small structural stiffnesses after buckling of the diagonal member. The members were fabricated of 7075-T651 aluminum and the end fittings of steel. The structure was attached to a heavy aluminum plate for testing. Details of the specimen are shown in Fig. 42. Figure 43 is a photograph of the test setup. The buckled structure is shown in Fig. 44.

7.2.2 Instrumentation and Test Procedure

The most difficult instrumentation problem in this portion of the project was accurate measurement of very small deflections. In the linear range of truss behavior the accuracy of displacement measurements had to be of the order of 100 microinches. Since the applied loads were small it was important that the displacement measurement device not apply a force to the structure. The most successful system involved the use of an LVDT. Friction

Approved for Public Release

Contrails

was eliminated and the force applied to the structure by the transducer during displacement was certainly small. The output was taken either on a meter or into an X-Y plotter with the output of a force transducer. The use of dial indicators was attempted but they were only satisfactory for large displacements.

A number of force transducers were constructed for specific applications. They had a U-shaped configuration with foil resistance strain gages on both the inside and outside at the base of the U. The transducer can be seen in Fig. 43. It is possible to obtain almost any desired sensitivity along with substantial stiffness using this device. Output was taken either on a manual balance strain indicator, a self-balancing digital indicator, or with an X-Y plotter with the displacement output from the deflection transducer. All specimens were loaded by inducing a displacement rather than a force at the loaded node.

The snap-through specimen was tested to a displacement equal to twice the rise of the structure. Displacement measurements were made with a dial gage. Due to the arrangement of the force transducers the dial gage did not apply any force to the structure since it measured the displacement of the yoke. The force transducers were stiff enough so that there was no important difference between the yoke displacement and the truss node displacement. The displacement was applied in increments and readings of force and displacement were made. The linear portion of the load deflection curve was of little interest and no attempt was made to measure it. Sufficient accuracy could not have been obtained using a dial gage to make such measurements.

The instrumentation was the same for the three bar truss and the frame. Load deflection curves were obtained directly with the X-Y plotter. The test was performed by applying displacements continuously. A photograph of this

Approved for Public Release

Contrails

test setup is shown in Fig. 45. This instrumentation arrangement had the advantage that the test results could be evaluated immediately. Strain gages were attached to the members to monitor forces. Bending strains could be measured but the axial strains associated with buckling were so small that they could not be satisfactorily measured.

7.2.3 Results and Correlation

The results for two tests on the snap-through truss are given in Fig. 46 and 47. The correlation between theoretical and experimental results for the one inch rise structure is fairly good. Experimental error can arise from two sources. The force transducers should have been somewhat more sensitive since the 0.3 lbs. difference in buckling loads represents about six microinches strain output on the force transducer. However, the experimental results yielded a smooth curve with little data scatter. The second source of experimental error stems from the precision bearing flexibility. This factor would produce more flexibility in the structure than assumed in the analysis. The experimental curve also passes through zero load at one inch deflection. Elementary analysis shows that buckling occurs at 2.98 lbs.

The experimental results for the 2.25 inch rise structure shown in Fig. 47 are probably more accurate. Good agreement is obtained on buckling load. The elementary theoretical buckling load is 6.68 lbs.

The three bar planar truss was a very difficult one to test. In view of this fact the agreement shown in Fig. 48 between experimental and analytical results was excellent. The first buckling load is very sensitive to the existence of slack at the supports. Using the techniques described in Section 7.2.2 the results shown were obtained.

Approved for Public Release

Contrails

The stiffness obtained in the experiment was 64.9 kips/in before buckling and 34.7 kips/in after buckling compared with 74.9 kips/in and 35.9 kips/in respectively for the analytical prediction. The precision bearings at the loaded node probably accounted for most of the difference in the stiffnesses. The experimental first buckling load of 32.5 lbs. compares with 38.1 lbs. for the theoretical value. The upper analytical predicted buckling 58.9 lbs. compares with an experimental value of 58.8 lbs. An analytical check was also made by removing the buckled member and replacing it with its Euler buckling load. The resulting two bar planar truss was analyzed to determine the applied load at which the second member would buckle. The computed load (59 lbs.) was in excellent agreement with both the analytical and the experimental results.

The experimental results for the diagonally braced planar frame are shown in Figs. 49, 50, 51 and 52. Correlation of analytical with experimental results was carried out for one loading condition and is shown in Fig. 49. The curves follow each other quite closely. It might be expected that the experimental results would be more flexible than the analytical prediction, since perfect restraint is not achieved in the experimental set up. In this case the slender members required only small forces to restrain their ends. However, the end fittings clamped a portion of the member effectively shortening its length. This perhaps explains the somewhat higher stiffness measured.

7.3 Pinched Cylinder

7.3.1 Description of Specimen, Instrumentation and Testing

A short piece of cylindrical shell was tested by Guyan (Ref. 22) under the action of diametrically opposed concentrated loads. Deflections were measured on a diameter between the loads and on an end diameter. This same model was still available and was instrumented with strain gages so that

Approved for Public Release

Contrails

strains, in addition, to deflections could be measured. The primary goal was to correlate strain measurements at selected locations with the analytical prediction. The specimen used had been obtained from a longer piece of commercial extruded tubing. It is shown with strain gages in Fig. 53. The specimen dimensions and some other details are given in Fig. 54. It should be noted that specimen dimensional tolerances are quite large. The ratio of diameter to wall thickness is about 100 and the ratio of diameter to length is approximately 1.

Strains were measured along two edges of one octant of the specimen. The gage locations and their number designations are given in Fig. 55. Gage numbers and locations are further defined in Table 9. Since all strain measurements were made on lines of symmetry the direction of the principal strains were known and therefore two element rosettes were adequate. Electric resistance strain gages were used and they were attached with Eastman 910 adhesive. Rosettes were applied in pairs, inside and outside, back to back.

The test setup is shown in Fig. 56. The loads were applied through steel balls. The deflections measured were the deflection between the load points and the deflection along a diameter parallel to the loading line at the edge of the specimen. The loads were applied incrementally and deflection and strain readings were taken at each increment.

7.3.2 Results and Correlation

Experimental values for strain were recorded at eleven load levels. The measured strain and displacement data is reported in tabular form in Table C1 of Appendix C. This data showed excellent linearity when plotted versus load, exhibiting very little scatter. Some representative examples of load strain curves are also given in Figs. C1 through C4 of Appendix C.

Approved for Public Release

Contrails

Using cylindrical shell discrete elements of the type described in Section 2.3.1, the cylinder was modeled as shown in Fig. 57. The strain results for measured and predicted values are summarized in Figs. 58, 59 and 60. The lines shown in these figures were drawn to make the results easier to follow. It should be noted that the analytical results exhibit discontinuities in the surface strains because the current computer program does not permit the use of additional conditions implementing curvature continuity.

7.4. Stiffened Plates

7.4.1 Design and Construction of Specimens

This phase of the experimental program was concerned with the design and testing of stiffened plate structures. The objective of the stiffened plate program was to perform tests on models that exhibit significant post-buckling stiffness and strength while maintaining elastic behavior in the structural material under all loads.

There are almost unlimited possibilities in the design of stiffened plate test specimens. Stiffeners can be used on one or both sides of the plate, their thickness to depth ratio can vary over a wide range. Stiffeners can be oriented in one or two principal directions or they can be skewed. In addition, boundary conditions on the plates and various load conditions can change the character of the buckling behavior of a given plate. Obviously, no one plate model is representative of stiffened plates in general.

Approved for Public Release

Contrails

The specimens ultimately chosen for this program were generally quite similar, with stiffener number, stiffener position and type of loading the main variables. They had stiffeners on one side only and were subjected to either transverse or in-plane loads. An attempt was made to select specimens which could be accurately and easily modeled for analysis.

In all, five plate models were constructed. A preliminary unstiffened model consisted of a square uniform thickness aluminum plate with an edge beam of uniform dimension on all four sides. This model was designed for transverse loading. The edge beam was designed to offer edge restraint between a clamped and a free edge. Figure 61 is a photograph of the specimen and Fig. 62 gives details and dimensions. The purpose of the preliminary model was to investigate the type of boundary conditions to be used in the experimental program. Results from this model indicated that edge beams that contribute greatly to overall stiffness create problems in modeling the structure with the repertoire of discrete elements currently available. For this reason, none of the succeeding four models used edge beams to obtain primary stiffness, but only to impose boundary conditions on relatively "inactive" edges.

The first stiffened plate is shown in Fig. 63. Dimensions and a detail drawing are given in Fig. 64. The model is intended for transverse loading and is simply supported along each edge beam and the two remaining sides are free edges. It has one transverse stiffener and one longitudinal stiffener. The edge beam permits end rotation and constant displacement in the plane of the plate.

Approved for Public Release

Contrails

The thickness to depth ratio of the longitudinal stiffeners was originally 12 and was later changed to 30. The second stiffened plate is depicted in Fig. 65. Details and dimensions are shown in Fig. 66. This model, also intended for loading normal to the plane of the plate, has one transverse stiffener and two longitudinal stiffeners. There is one longitudinal stiffener on each free edge, otherwise this specimen is generally similar to the first model.

The third stiffened plate is shown in Fig. 67. Details and dimensions are shown in Fig. 68. This plate, while intended for transverse loads, is somewhat different from the first two plates. The overall depth of the specimen is 1.250 inches instead of about 0.9 inches. There are 3 longitudinal stiffeners and one transverse stiffener, all with a thickness to depth ratio of 29. Like the other two transversely loaded models, this model has a heavy edge beam on the simply supported sides.

The second and third specimens for transverse load were constructed to give additional insight into behavior of this particular type of stiffened plate configuration. By adding additional longitudinal stiffeners to these two models, more overall strength is obtained, in addition, a more uniform stress field is developed in the plate.

The fourth stiffened plate was intended for inplane loading. This specimen is pictured in Fig. 69 and details are shown in Fig. 70. It is a square plate with identical vertical and horizontal stiffeners with thickness to depth ratio of 12.7. The inplane loads are applied in the direction of the vertical stiffener on the top and bottom edge. These edges are free to displace in any direction. The two sides are restrained by edge beams but are free to move relative to the test fixture.

Approved for Public Release

Contrails

The stiffener orientation chosen was the simplest possible, with the thought that if the edge beams made analysis difficult due to modeling problems, they could be removed. The stiffeners were designed to buckle at about 25,000 psi by assuming them to be simply supported along the plate edge, free on the other edge, and selecting the thickness accordingly. This same procedure was used for the transversely loaded models, hence the critical stiffener buckling stress was about the same for all stiffened plate models. The desired behavior of the inplane loaded model was for the vertical stiffener on the plate to buckle under load. Various eccentricities of inplane load on this model cause different amounts of bending and should give various types of behavior.

The first stiffened plate specimen for transverse loading was essentially the same configuration as the inplane model. Smaller stiffener thicknesses were necessary on the transversely loaded specimens since the stiffeners are under a triangular stress distribution, due to bending, instead of the nearly uniform stress distribution in the case of the inplane specimen.

All models, except the pinched cylinder were machined from solid pieces of 7075-T651 aluminum. This material has a yield point of 73,000 lbs/in^2 and an ultimate strength of 83,000 lbs/in^2. In general, the maximum stress reached in any test was about 35,000 lbs/in^2, so that the material remained in the elastic range at all times. Tolerances on all dimensions were held to 0.001 in. except as noted in the detail drawing for each specimen (Figs. 64, 66, 68 and 70).

Approved for Public Release

Contrails

7.4.2 Instrumentation and Test Procedure

The primary results desired for all models were load-deflection behavior at different points on the models and load-strain behavior in regions of buckling and high stress. Deflections were measured with dial indicators of either 0.0001 in. sensitivity or 0.001 in. sensitivity as needed. Electric resistance strain gages of the foil type were used to record strains. Grid sizes were 1/4 in., or smaller in the region of high strain gradients. Adhesives used were Eastman 910 except on the inplane specimen. They were attached with BR-600 adhesive and heat cured. Figure 71 shows the gage locations for the inplane stiffened plate model. Figures 72 and 73 show the gage locations for two of the transversely loaded stiffened plates discussed previously.

The strain gage locations for the unstiffened plate can be seen in Fig. 74. The primary reasons for location of strain gages was to monitor highly stressed areas of the plates under test to avoid damaging the models, to check boundary conditions, or to record strains at locations that are nodes of subelements in the discrete element analyses.

Test devices and fixtures used were simple. These are best shown by photographs and diagrams. The test fixture and test orientation of the preliminary model (unstiffened plate, Fig. 61) is shown in Figs. 75 and 76. This model was supported on hard steel balls. They were brinelled into brass blocks and into the model to make the supports as stiff as possible. Displacements were induced by a micrometer screw as shown. In series with this micrometer screw was a small load cell to monitor load. Lateral deflection of the edge beams was measured with vernier calipers, while deflections other than the deflection under the central load were measured with dial indicators.

Approved for Public Release

Contrails

The inplane stiffened plate was loaded through steel balls and aluminum blocks machined to fit the tee formed by the end of the stiffener and the plate edge. This test, along with all the transverse loading tests were conducted on a 5,000 lb. screw type testing machine. This machine was well suited to buckling tests, since a displacement is induced rather than a load. This characteristic makes the possibility of damaging a specimen remote. The stiffness of the cross head is 10^6 lbs/in for a concentrated load in the center. This effect was compensated in the case of the inplane loaded specimen. The point of load application for this model was varied from the plate to the top edge of the stiffener to give various amounts of bending.

The test for all three transversely loaded stiffened plates were nearly identical, except for the number and location of loads applied to each. These plates were simply supported on round steel bars as shown in Figs. 78, 79, and 80. The transverse loading was applied as concentrated load(s), at the junction(s) of the longitudinal and transverse stiffeners on each model. The loading points are shown in Figs. 66, 68, and 70. Displacement was induced by the testing machine, through the buckling range, until a preselected maximum stress (approximately 30,000 lbs/in^2) was reached. Deflections and strains were read at 20 to 30 load levels in most tests. All deflections in the transverse loading tests were measured with dial indicators.

Approved for Public Release

Contrails

7.4.3 Results

The results of strain measurements are given in tabular form and some representative results are shown graphically in Appendix C. Load deflection curves for each specimen are shown in Figs. 81 through 85. The load deflection curve for the unstiffened plate (Fig. 81) is given with the theoretical curves for a simply supported small deflection analysis and a finite deflection clamped plate analysis.

Photographs of buckled stiffeners for the transversely loaded specimens are shown in Figs. 86, 87, and 88. The buckled deflection of the inplane loaded specimen had a maximum value of about 0.01 inches and was too small to be visible in the photograph. The results of the stiffened plate tests show that all four structures exhibited significant post-buckling stiffness. In addition, some of the strain results are decidedly non-linear, due to buckling and finite deflection effects. The overall behavior of the three transversely loaded specimens was quite similar with one notable exception. The primary buckling mode of the plate with two longitudinal stiffeners has two small waves instead of one wave, as is the case in the other two models. This is shown in the photographs of the buckled specimens (Figs. 86, 87, and 88).

Approved for Public Release

Contrails

SECTION 8

CONCLUSIONS

The research program reviewed in this report has demonstrated that the energy search approach to structural analysis can be successfully applied to the prediction of geometrically nonlinear behavior in plate and shell type structures. Numerical examples demonstrate the ability of the various plate and shell elements generated to deal with problems exhibiting:

(a) nonlinear bending-membrane coupling,

(b) stable post buckling behavior,

(c) various stable branches on a post-buckling load vs. end-shortening curve.

A laboratory-type experimental program has provided data for comparison with current and future analytical behavior predictions. Satisfactory correlation has been achieved for several planar truss and frame specimens exhibiting various geometrically nonlinear behavior characteristics. Experimental results are reported for several plate, shell and stiffened plate configurations however only a limited comparison was possible within the scope of the present effort. Additional computational effort using the computer program described in Section 6 will be necessary, particularly for the stiffened plate cases.

It can be concluded that assumed displacement patterns formed from products of one-dimensional interpolation functions can be used to generate a useful class of shell discrete elements including geometric nonlinearity. In particular 48 degree-of-freedom rectangular plate, cylindrical shell, and annular plate discrete elements have been developed and evaluated numerically.

Approved for Public Release

Contrails

These elements can be joined together at arbitrary angles, although the current computer program is limited to tangential and right angle joining. Satisfaction of interelement geometric admissibility requirements is straightforward. The element assumed displacement states also facilitate the optional use of additional conditions such as middle surface strain continuity, based on physical insight. These 48 degree-of-freedom elements provide a good approximation of the middle surface stress state which enhances the ability to predict buckling and post-buckling behavior. The generation of a linear bending parallelogram element using products of one dimension interpolation functions suggests that extension of the work reported herein to oblique coordinates is feasible. The approach is, however, currently restricted to elements for which opposite edges are parallel.

The zero-strain rigid-body mode question has been examined within the context of the linear cylindrical shell discrete element. Using first-order Hermite interpolation polynomials in the circumferential ($\eta=r\theta$) direction gives a good approximation of the rigid-body modes and using osculatory interpolation based on the functions (1, θ, sin θ, cos θ) includes exact representation of rigid-body modes. For subtended angles $\Delta\theta$ between 5° and 30° either element may be used. The element based on circular function interpolation involves additional effort due to the more complicated functions and the need to use double precision arithmetic and it tends to produce only slightly better results. For cylindrical shell elements with subtended angles $\Delta\theta$ greater than 30° it is recommended that only circular interpolation functions be employed and for cylindrical shell elements with subtended angles $\Delta\theta$ less than 5° it is recommended that only the polynomial interpolation functions be used.

Approved for Public Release

Contrails

While the major portion of this research program was based upon the principle of minimum potential energy, an exploratory study based upon the Reissner energy principle was carried out. The Reissner energy method appears attractive because: (1) it permits a balanced approach in which force and displacement variables are both approximated using products of one dimensional interpolation functions; (2) both equilibrium and force-displacement relations are satisfied approximately; (3) both force and displacement boundary conditions may be treated as natural boundary conditions; and (4) both interelement geometric admissibility and interelement force equilibrium conditions are easily satisfied. A 84 degree-of-freedom discrete element Reissner energy formulation for a rectangular plate was carried out based upon bilinear approximations, for the membrane unknowns (u, v, N_x, N_y, N_{xy}) and bicubic approximations for the bending unknowns (w, M_x, M_y, M_{xy}). This formulation includes geometric nonlinearity arising from the second degree terms in the finite deflection strain-displacement relations,however, the highest degree terms in the Reissner energy are only cubic as contrasted with the quartic terms in the potential energy formulation. The 84 degree-of-freedom discrete element formulation is specialized to yield a 20 degree-of-freedom linear membrane discrete element and a 64 degree of freedom linear plate bending element. The numerical examples indicate that: (a) good quality force and displacement predictions are obtained, (b) better overall results can often be obtained by treating force and/or displacement boundary conditions approximately as natural boundary conditions rather than by satisfying them exactly as imposed boundary conditions, (c) buckling and stable post-buckling behavior predictions can be obtained as a result of including geometric nonlinearity in the formulation. A satisfactory algorithm for finding the stationary value of a function of many variables was not found in the course

Approved for Public Release

Contrails

of this investigation. An alternative formulation based upon minimizing a residual function was found to be inefficient and numerical solutions based upon the Reissner energy formulation were accomplished using the Newton-Raphson method. While this method is efficient it requires storage of an nxn matrix $[\frac{\partial^2 \Pi_R}{\partial z_i \partial z_j}]$ and solution of a set of n simultaneous equations for each iteration cycle. This severely limits the number of variables that can be handled without recourse to auxilliary storage. The rectangular plate discrete element Reissner energy formulation given is also limited to structures that can be modeled using coplanar elements since different levels of interpolation were employed to approximate the membrane (u, v, N_x, N_y, N_{xy}) and bending (w, M_x, M_y, M_{xy}) unknowns. As pointed out in Section 3 the residual function formulation was abandoned prior to recognizing the strong influence variable scaling can have on the convergence characteristics of unconstrained minimization algorithms and it is recommended that this approach be reexamined employing variable scaling transformations.

Energy search methods for structural problems, based on gradient minimization algorithms, have been shown computationally competitive with conventional solution procedures. An important factor contributing to this result was the discovery of a strong scale effect on the convergence of gradient methods which can be controlled by the diagonal scaling criteria presented in Section 4. A study of the convergence properties of the conjugate gradient method in over-discretized problems indicate convergence in $\bar{n} << n$ cycles where n is the total number of independent degrees-of-freedom. A structural problem with several hundred degrees of freedom has been efficiently solved with this method and because no assembled matrices are required much larger problems are feasible without recourse to auxiliary storage equipment.

Approved for Public Release

Contrails

A new linear search procedure has been developed based entirely on the directional derivative which is exact for linear problems. This approach eliminates orthogonality problems that sometimes arise in function fitting schemes. A nonlinear analog of Jacobi iteration was formulated and analyzed for use as a terminal option with energy search procedures. This option provides a capability for further reducing the gradient.

A computer program has been generated which draws together most of the important separate contributions made within the minimum potential energy framework during the course of this research program. The program implements discrete element finite deflection analysis of a class of structures that can be modeled as assemblages of plate, cylindrical shell, and annular plate elements connected together tangentially or at right angles. Flexibility in application has been built into this program by providing a variety of options. For example, algorithmic options include Fletcher-Reeves or Fletcher-Powell minimization with scaling and matrix inversion for linear problems. Ease of data preparation and optimization of coding and storage allocation are also notable characteristics of this program.

Several specific topics that are thought to merit further investigation are now discussed.

(1) A general equality constraint capability should be developed and implemented within the context of the minimum total energy formulation so as to facilitate:
   (a) joining elements at arbitrary angles,
   (b) the use of curvature continuity additional conditions,
   (c) the optional introduction of interelement equilibrium conditions,
   (d) the exact satisfaction of force boundary conditions on an optional basis.

Approved for Public Release

Contrails

(2) The residual function formulation which transforms the Reissner energy formulation into an unconstrained minimization problem should be reexamined making use of the scaling transformation ideas set forth in Section 4.

(3) A more extensive body of computational experience with the computer program described in Section 6 should be pursued. In particular it is suggested that some large linear problems be undertaken and that further computational effort be directed toward correlation of the post-buckled stiffened plate experimental results reported in Section 7.

(4) Increased emphasis should be placed upon evaluating the quality of stress predictions possible within the potential energy minimization framework. There is insufficient evidence, at this juncture, to conclude that a Reissner energy formulation gives better stress results than a potential energy formulation for approximately the same number of unknowns (degrees of freedom).

(5) The potential energy parallelogram plate element formulation should be extended to include linear membrane and geometric nonlinearities, thus facilitating the representation of multi-cell swept-back box-beam structures.

Several general areas for further work come to mind as a result of this research program. Effort should be directed toward extending the use of various interpolation function displacement patterns to other elements such as conical and toroidal shell elements including geometric nonlinearity. Sandwich plate and shell elements including transverse shear deformation, unbalanced anisotropic faces (representative of thin laminated

Approved for Public Release

Contrails

fiber composite skins), and geometric nonlinearity merit investigation. Consideration should be given to physically nonlinear behavior within the context of minimum potential energy formulations, the goal being to cope efficiently with both geometric and material nonlinearities. Finally, efforts to improve computational efficiency for discrete element nonlinear structural analysis by function minimization, should be continued.

Approved for Public Release

Contrails

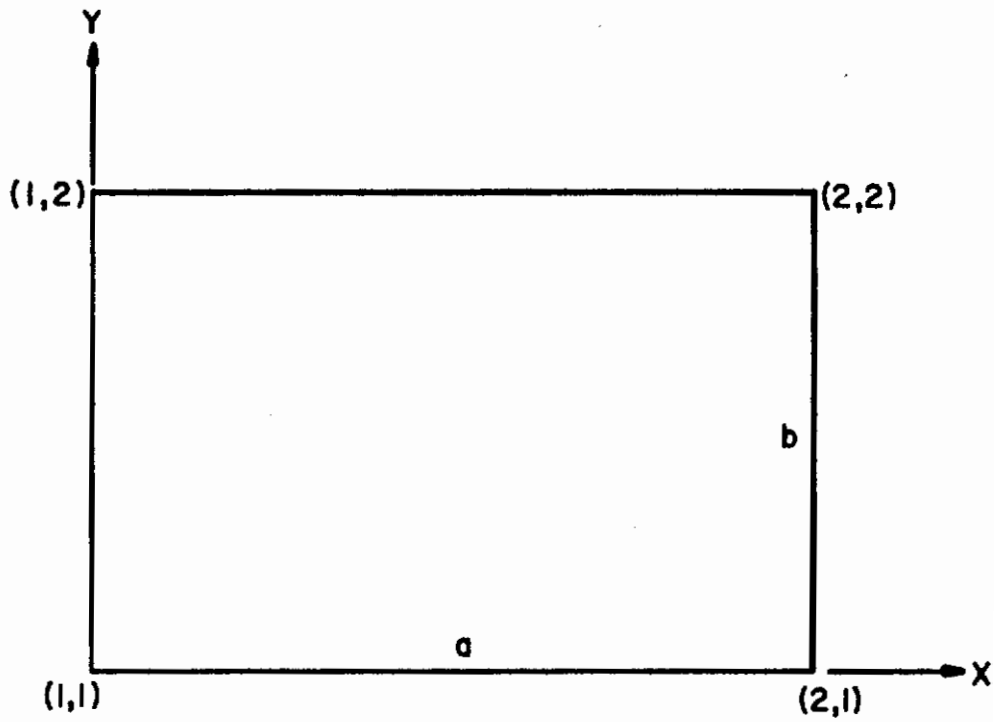

Figure 1. Rectangular Plate Discrete Element

Approved for Public Release

Contrails

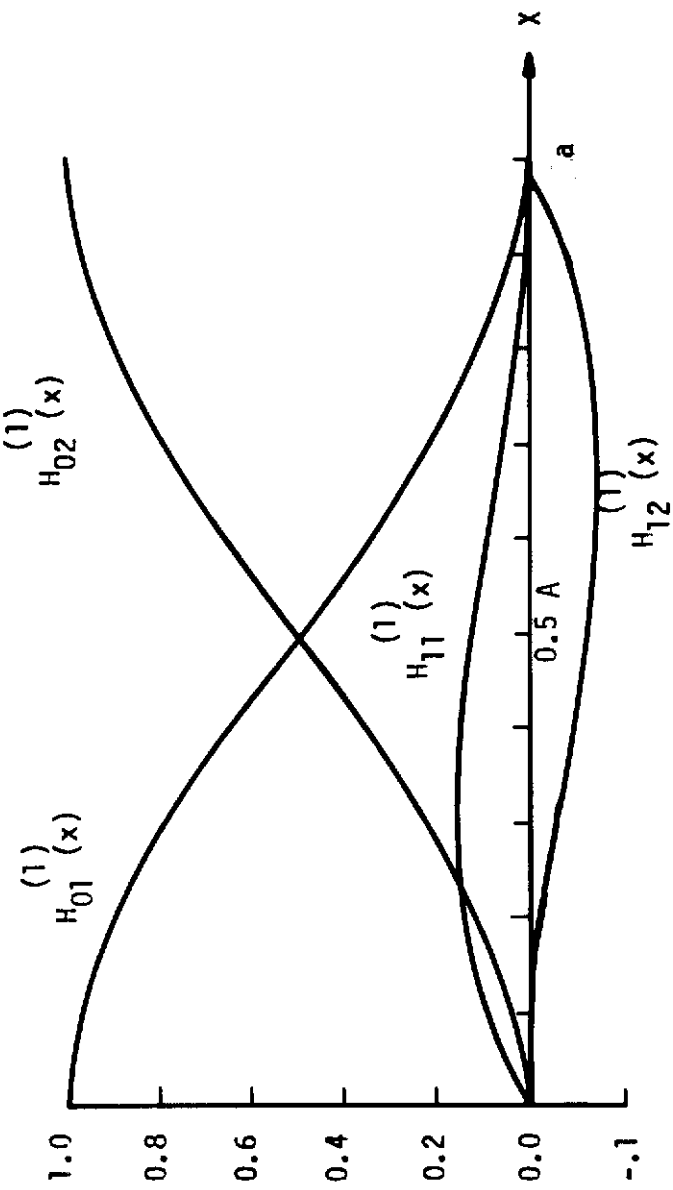

Figure 2. First Order Hermite Interpolation Polynomials

Approved for Public Release

Contrails

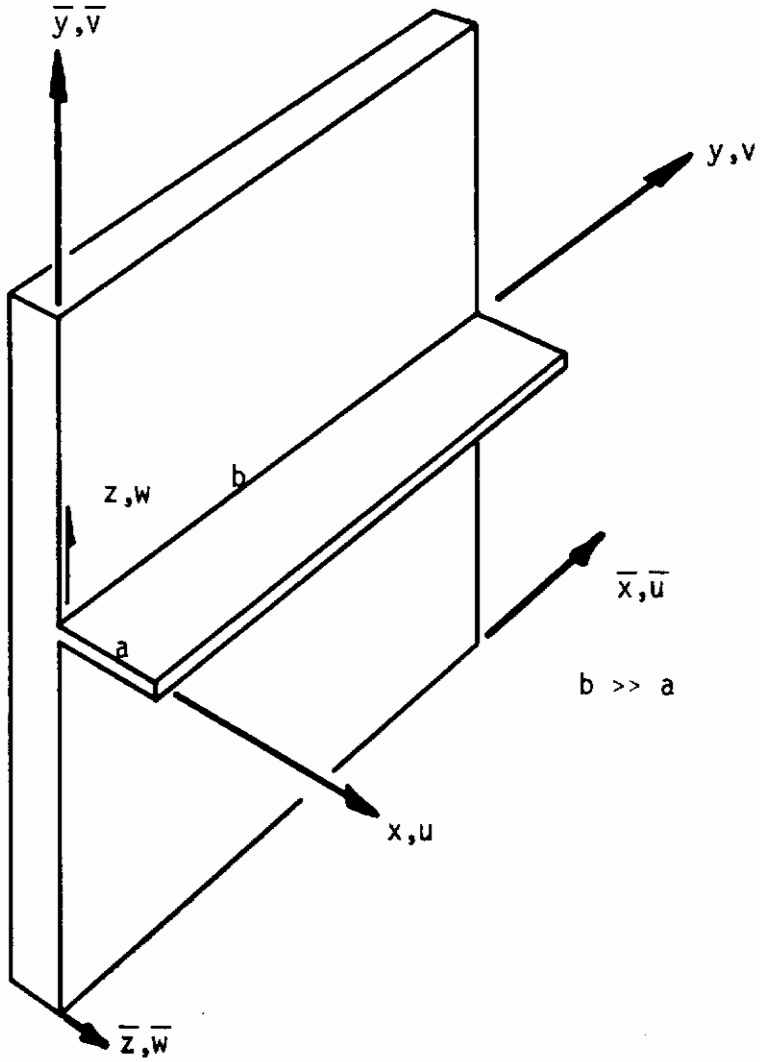

Fig. 3 Integral Stiffener of Rectangular Cross Section

Approved for Public Release

Contrails

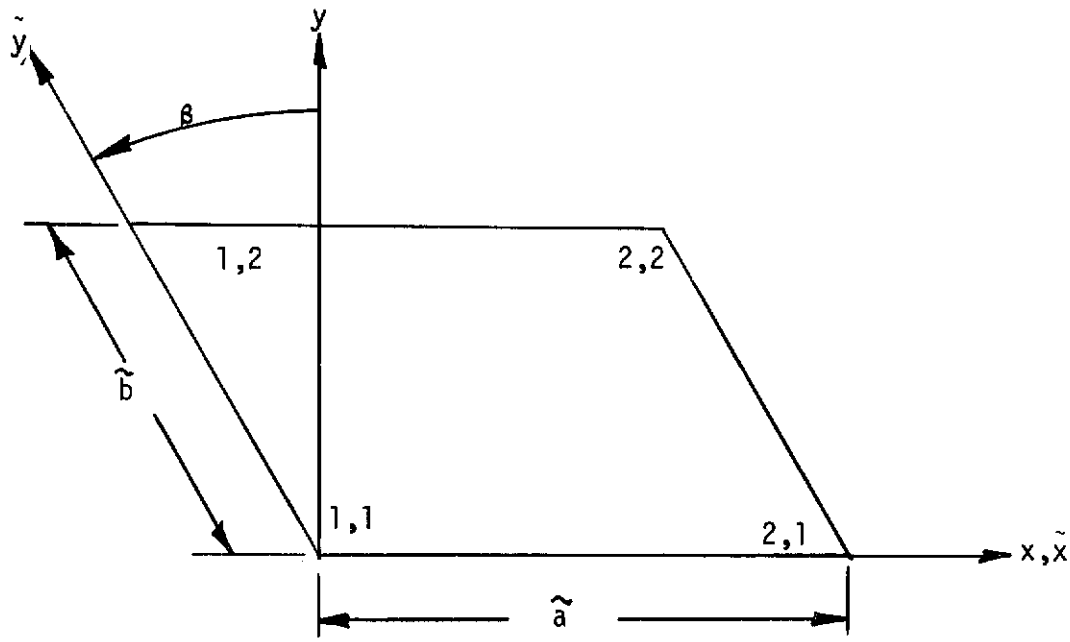

Figure 4. Parallelogram Plate Discrete Element

Approved for Public Release

Contrails

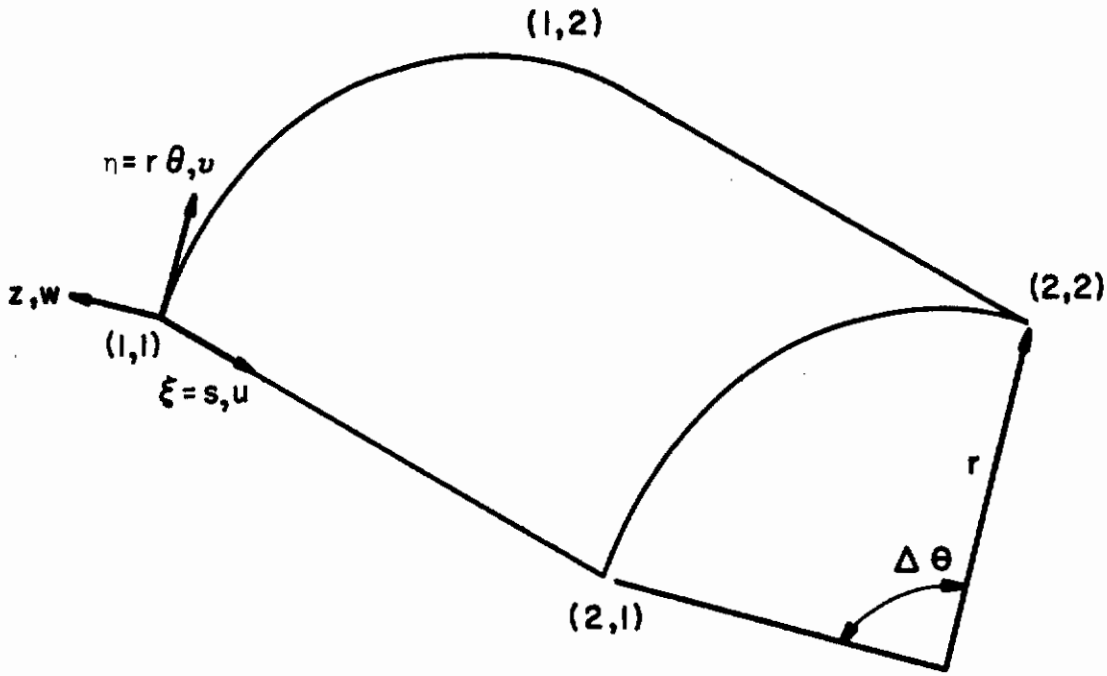

Figure 5. Cylindrical Shell Discrete Element

Approved for Public Release

Contrails

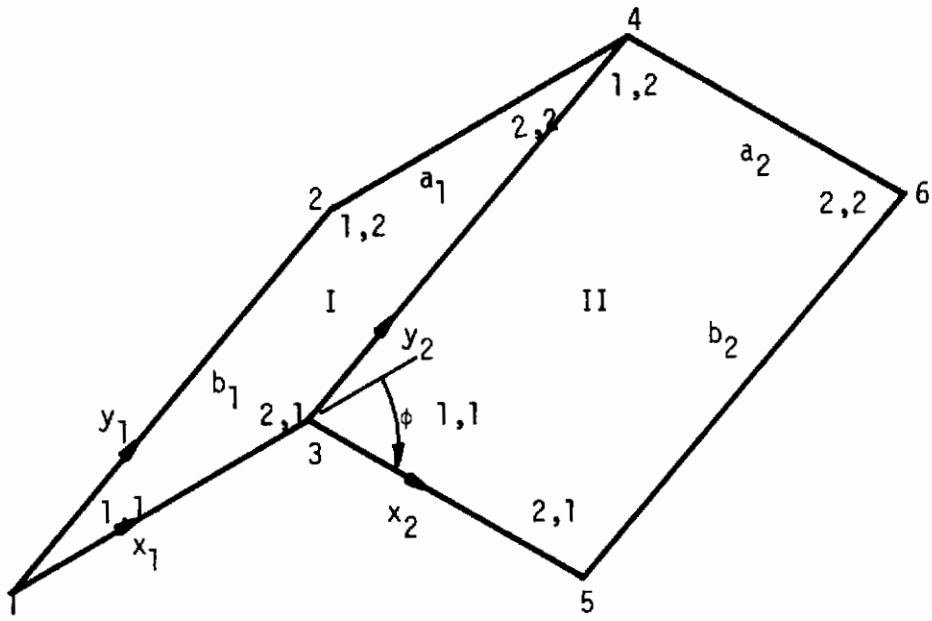

Figure 6. Two Rectangular Plate Elements Joined at an Arbitrary Angle

Approved for Public Release

Contrails

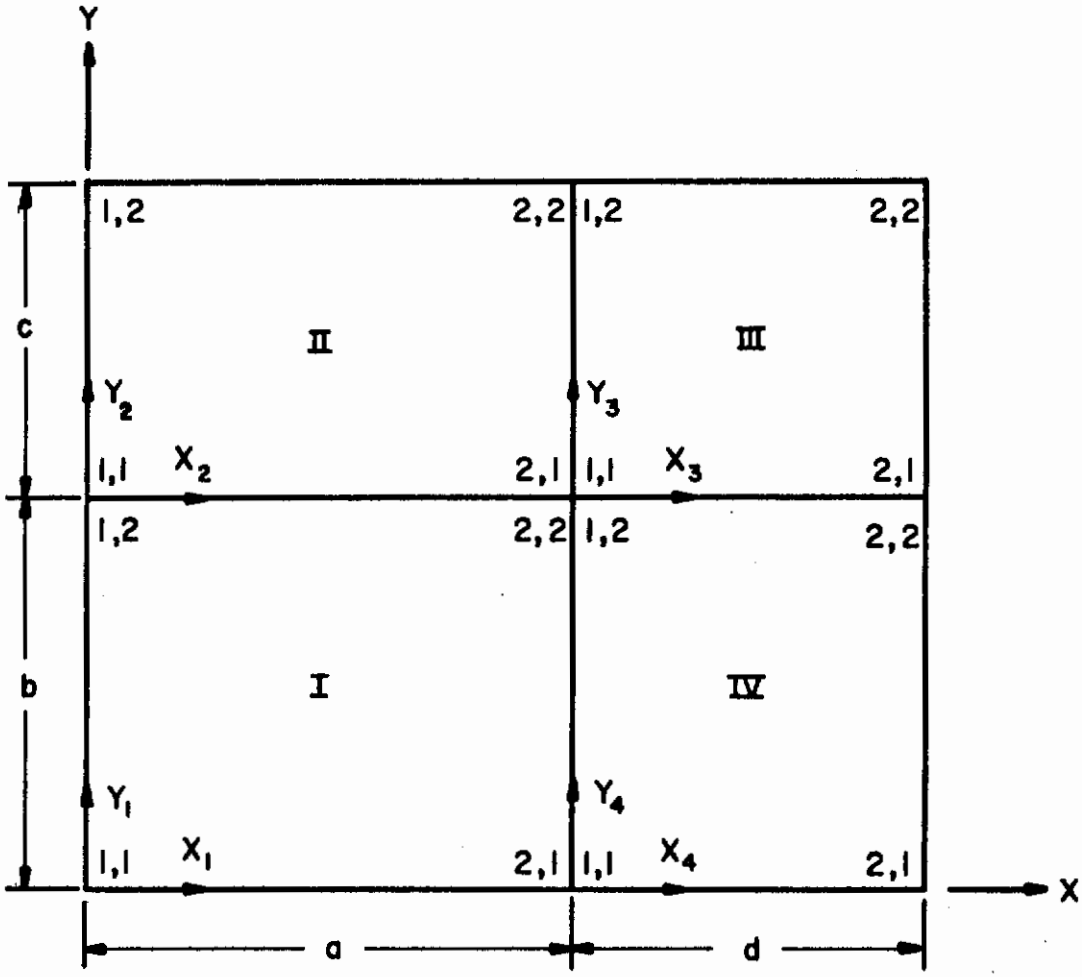

Figure 7. Four Coplanar Rectangular Plate Elements

Approved for Public Release

Contrails

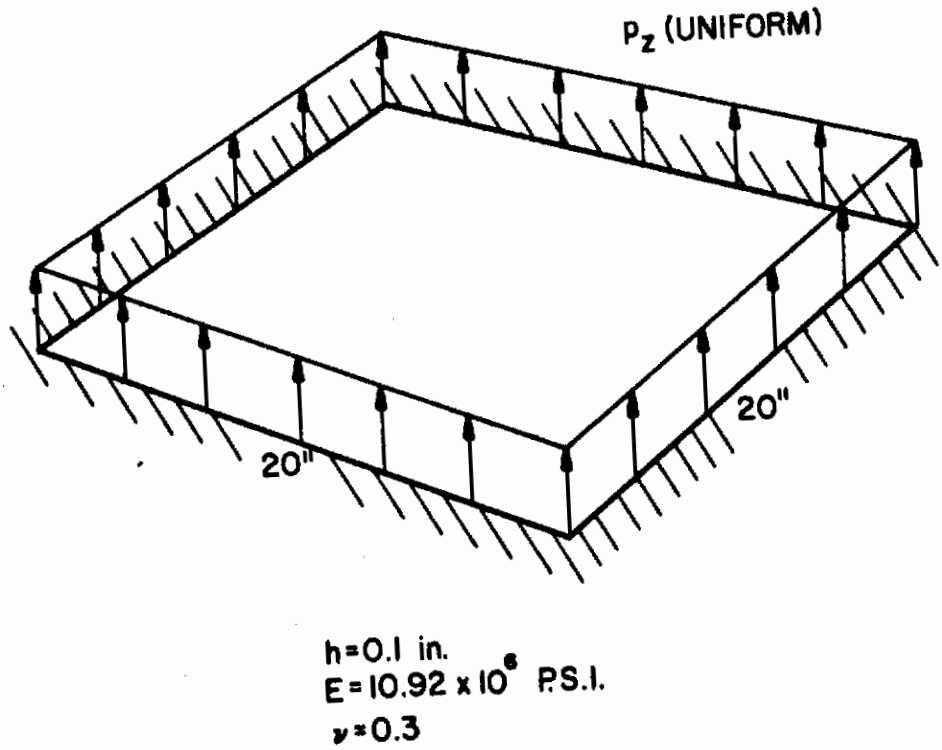

Figure 8. Clamped Plate Subject to Uniformly Distributed Load (p_z)

Approved for Public Release

Contrails

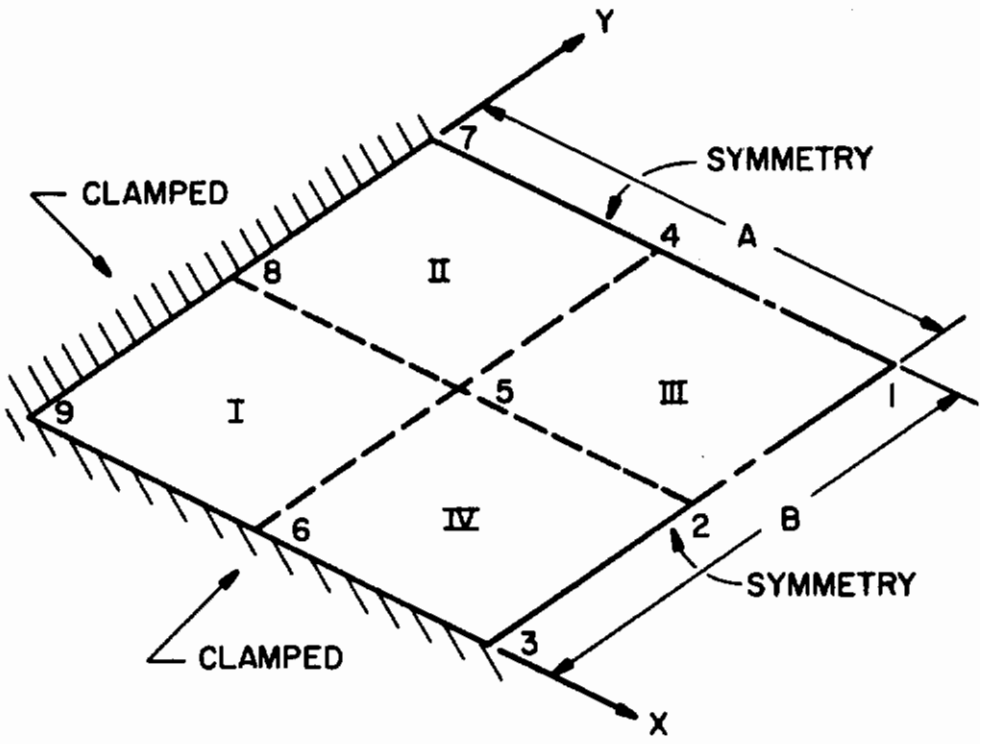

Figure 9. Quarter Clamped Plate

Approved for Public Release

Contrails

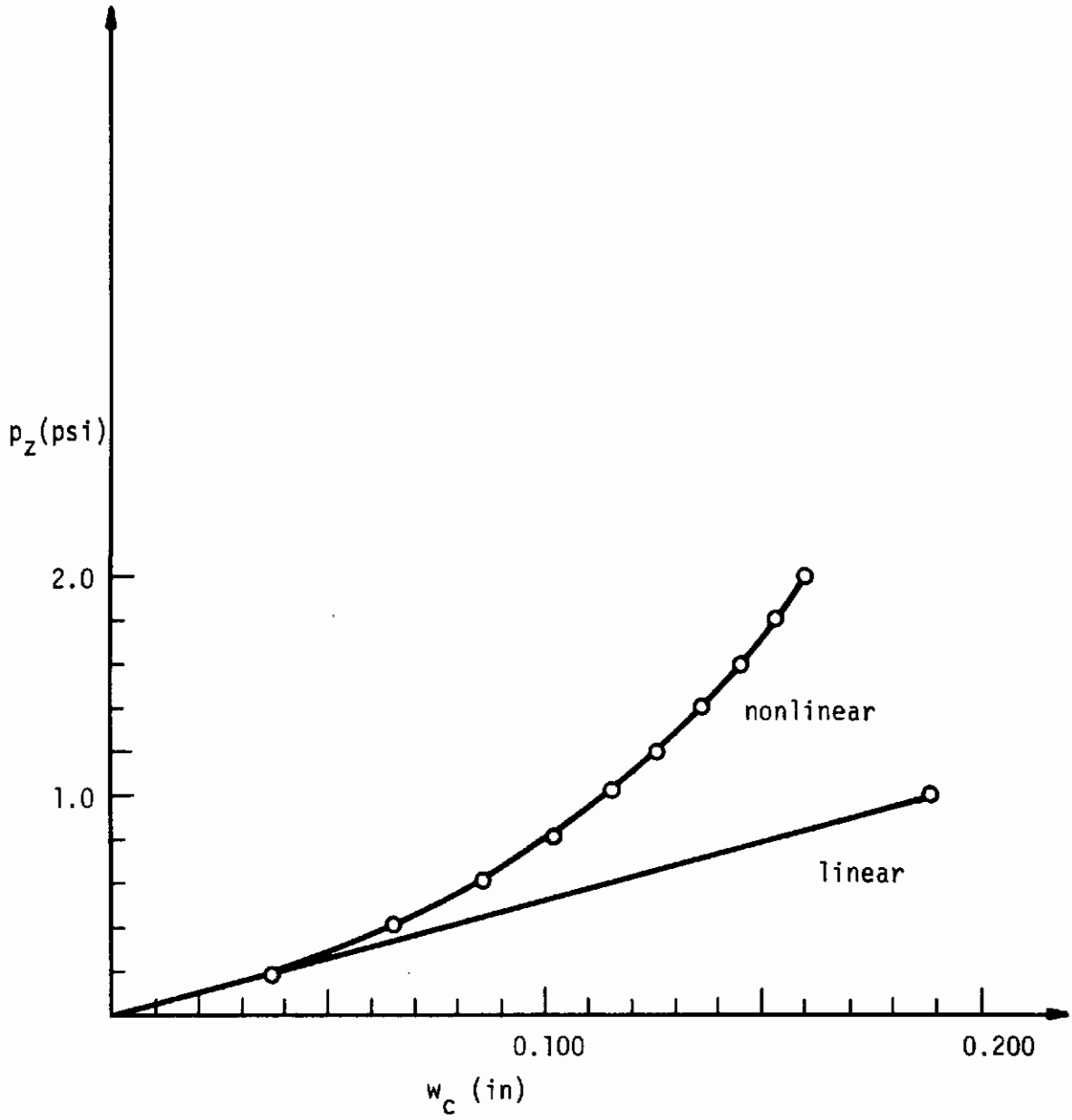

Fig. 10 Load Intensity vs. Midpoint Deflection for Uniformly Loaded Clamped Plate

Approved for Public Release

Contrails

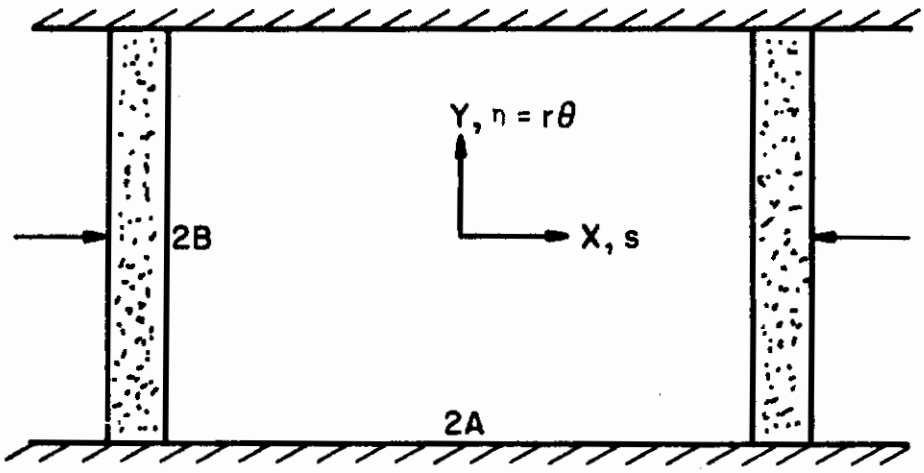

Figure 11. Rectangular Panel Subject to End-Shortening

Approved for Public Release

Contrails

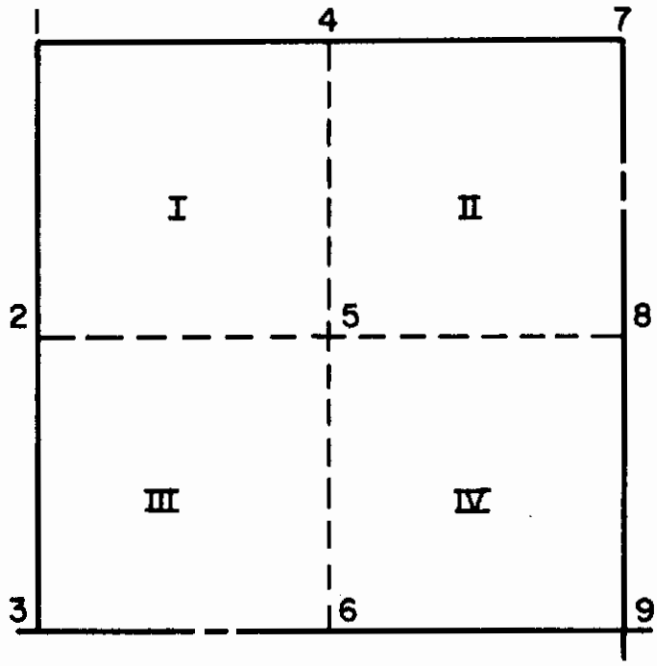

Figure 12. Modeling of One Quadrant for Panel End-Shortening Cases

Approved for Public Release

Contrails

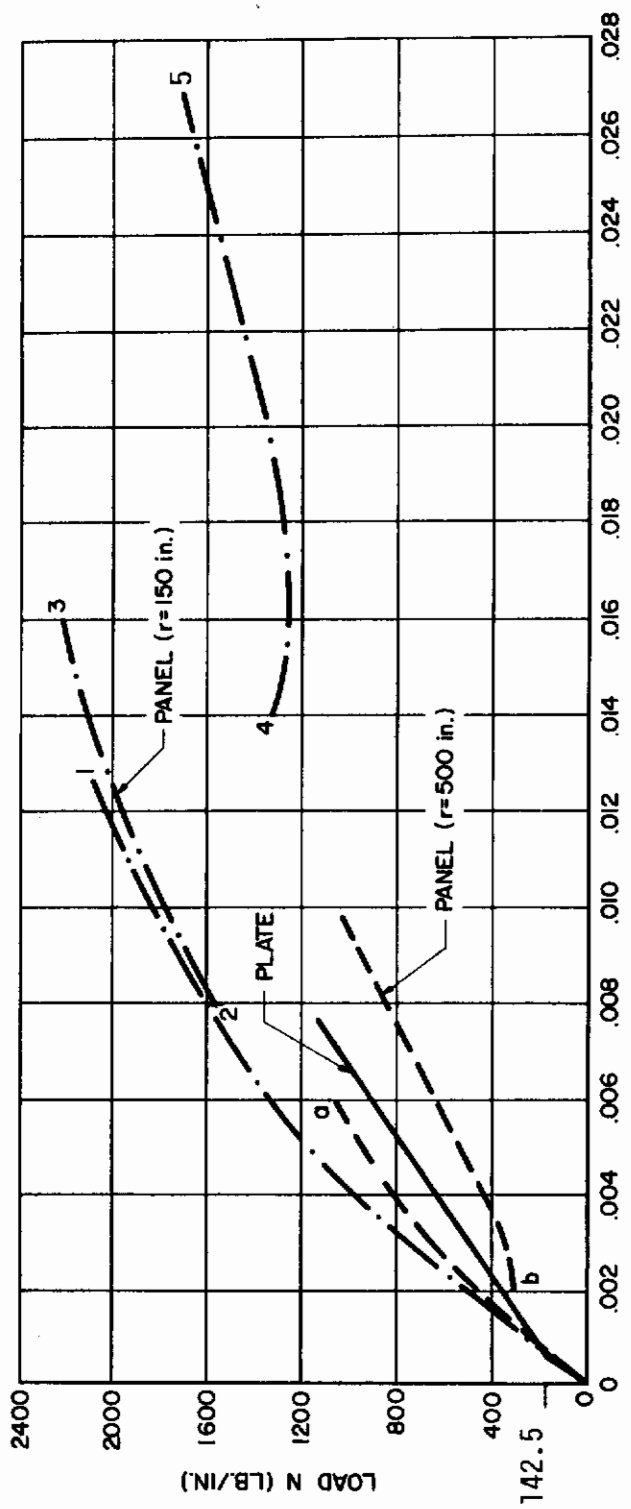

Figure 13. Load vs. End-Shortening

Approved for Public Release

Approved for Public Release

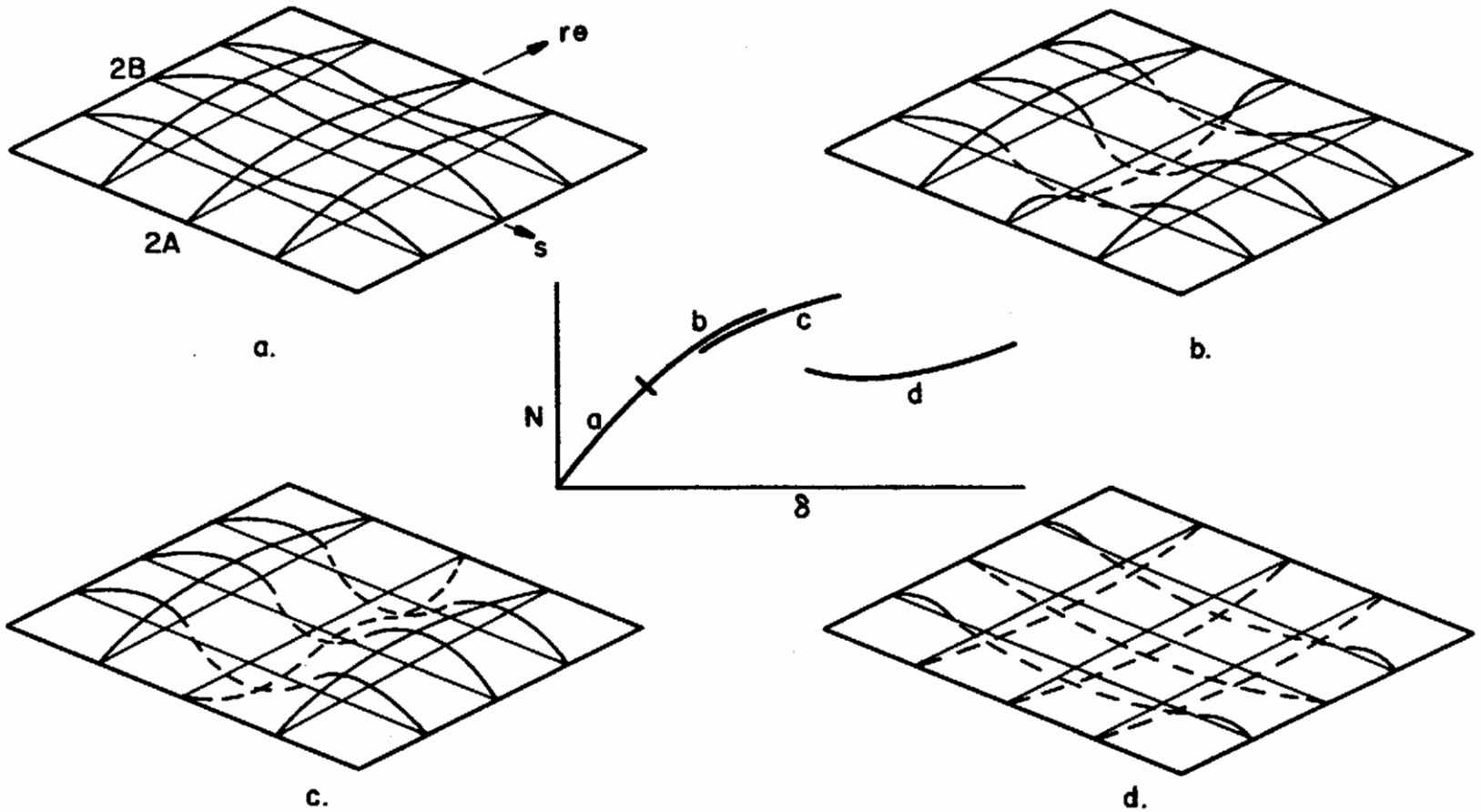

Figure 14. Curved Panel Displacement Configurations (r = 150 in.)

Contrails

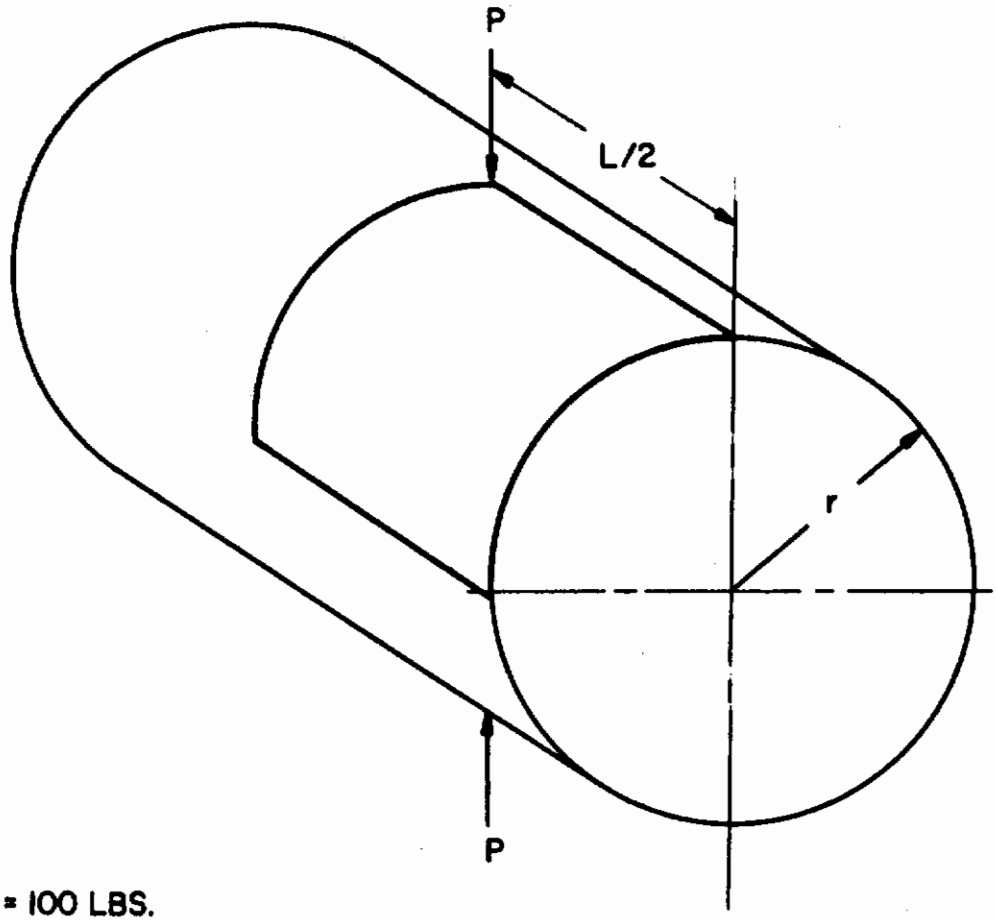

P = 100 LBS.
L = 10.35 IN.
r = 4.953 IN.
h = 0.094 IN.
ν = 0.3125
E = 10.5×10^6 P.S.I.

Figure 15. Pinched Cylindrical Shell

Approved for Public Release

Contrails

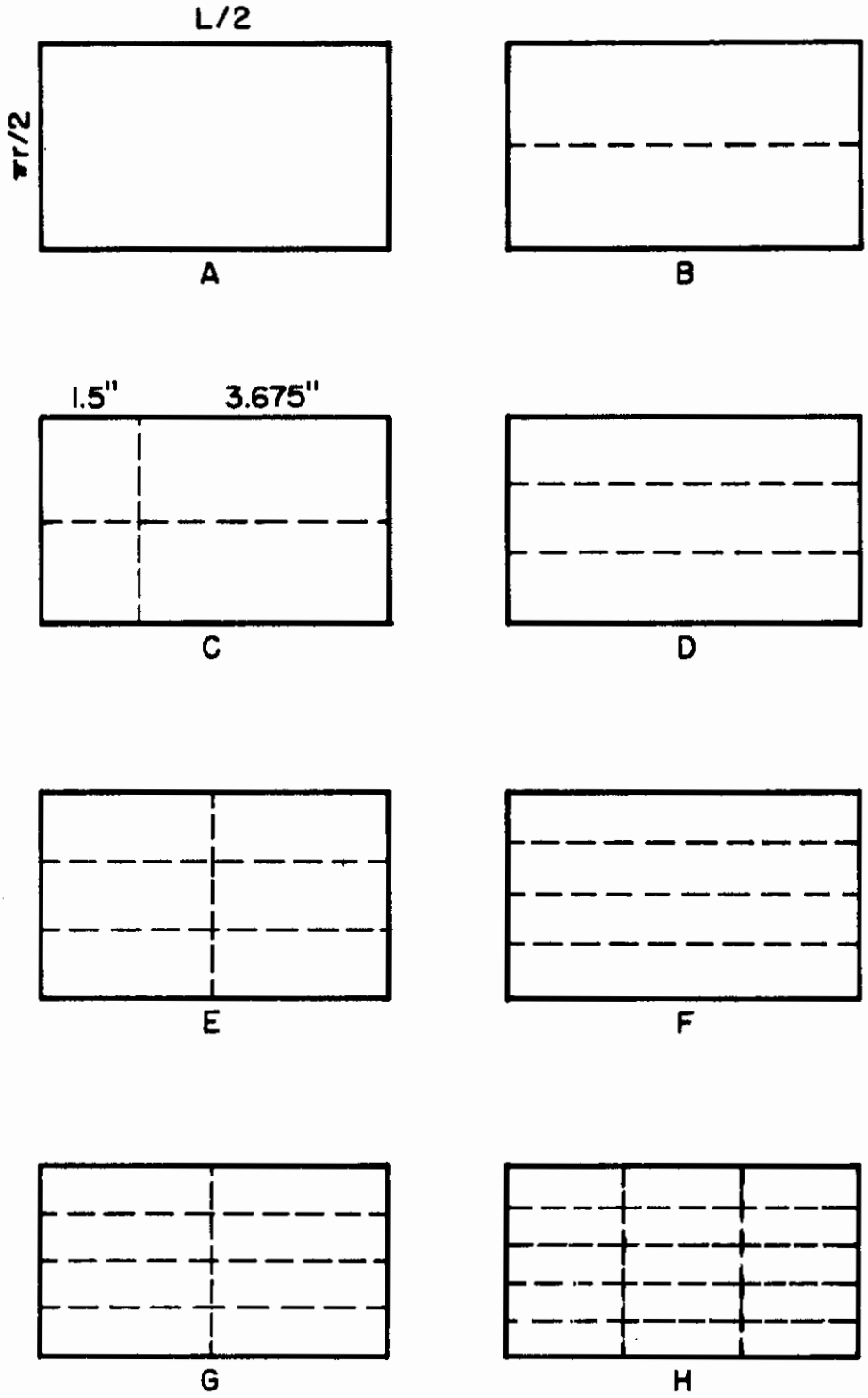

Figure 16. Octant Modelings Pinched Cylindrical Shell

Approved for Public Release

Contrails

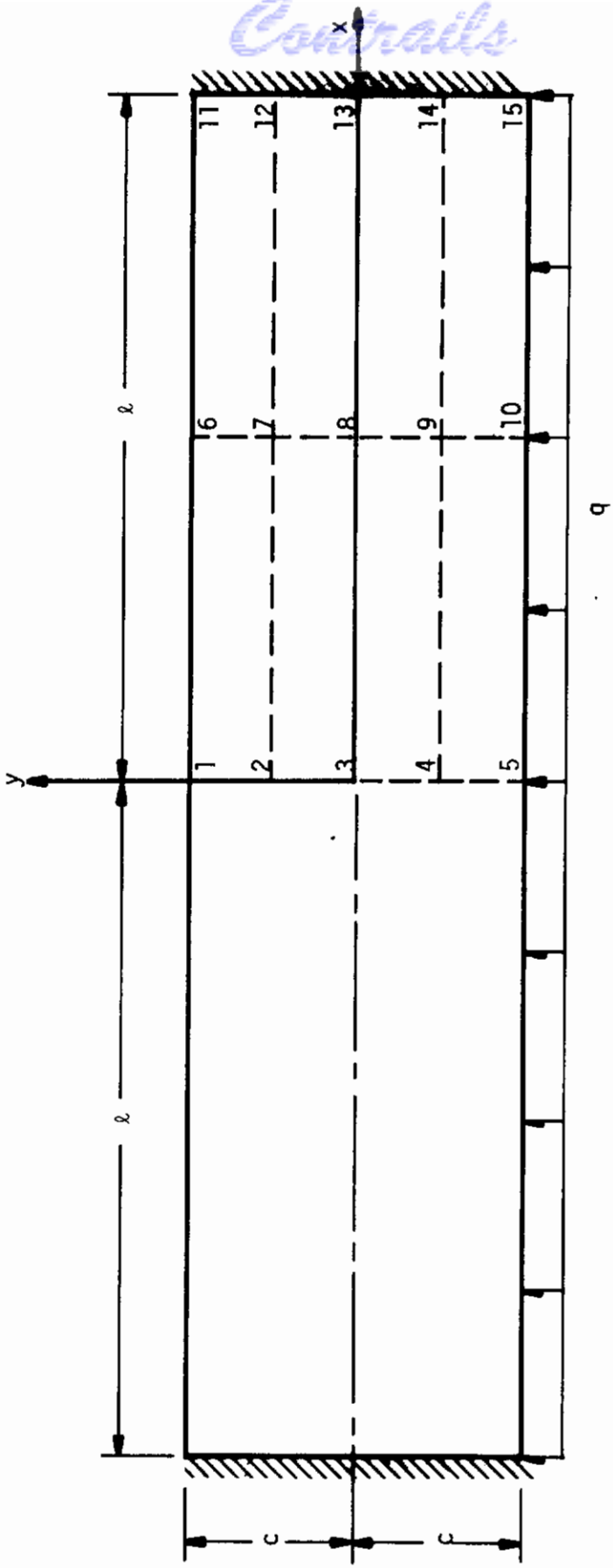

Figure 17. Linear Membrane Example - Π_R - (Section 3.4.1)

Approved for Public Release

Contrails

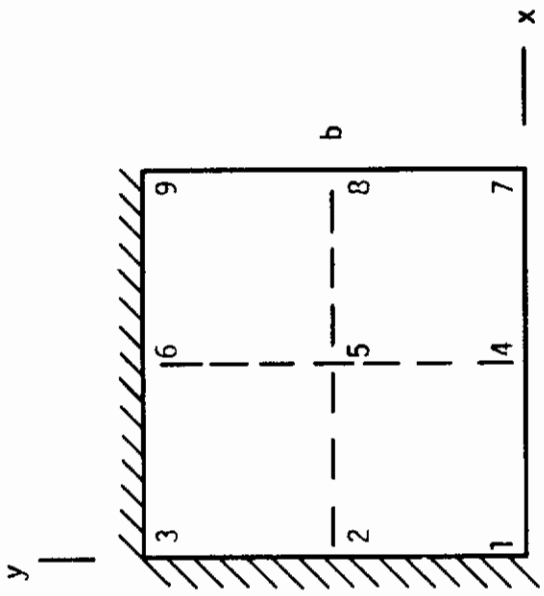

Figure 18. 2 x 2 Discrete Element Idealization - Π_R - (Section 3.4.2)

Approved for Public Release

Contrails

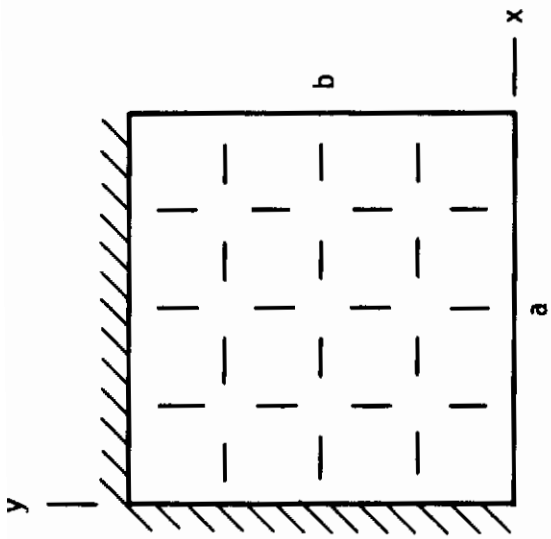

Figure 19. 4 x 4 Discrete Element Idealization

Approved for Public Release

Contrails

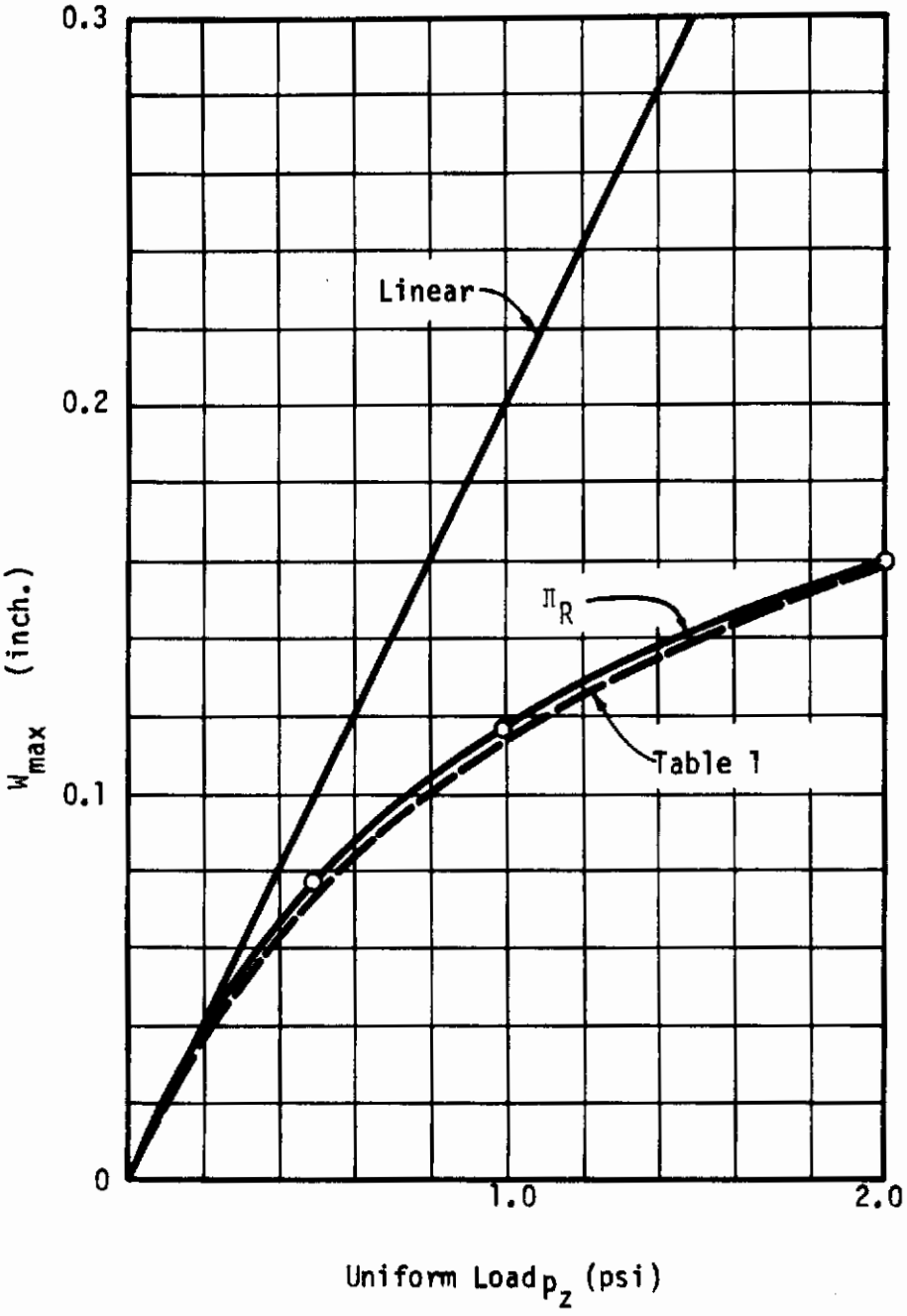

Figure 20 Maximum Displacement vs. Uniform Load

Approved for Public Release

Contrails

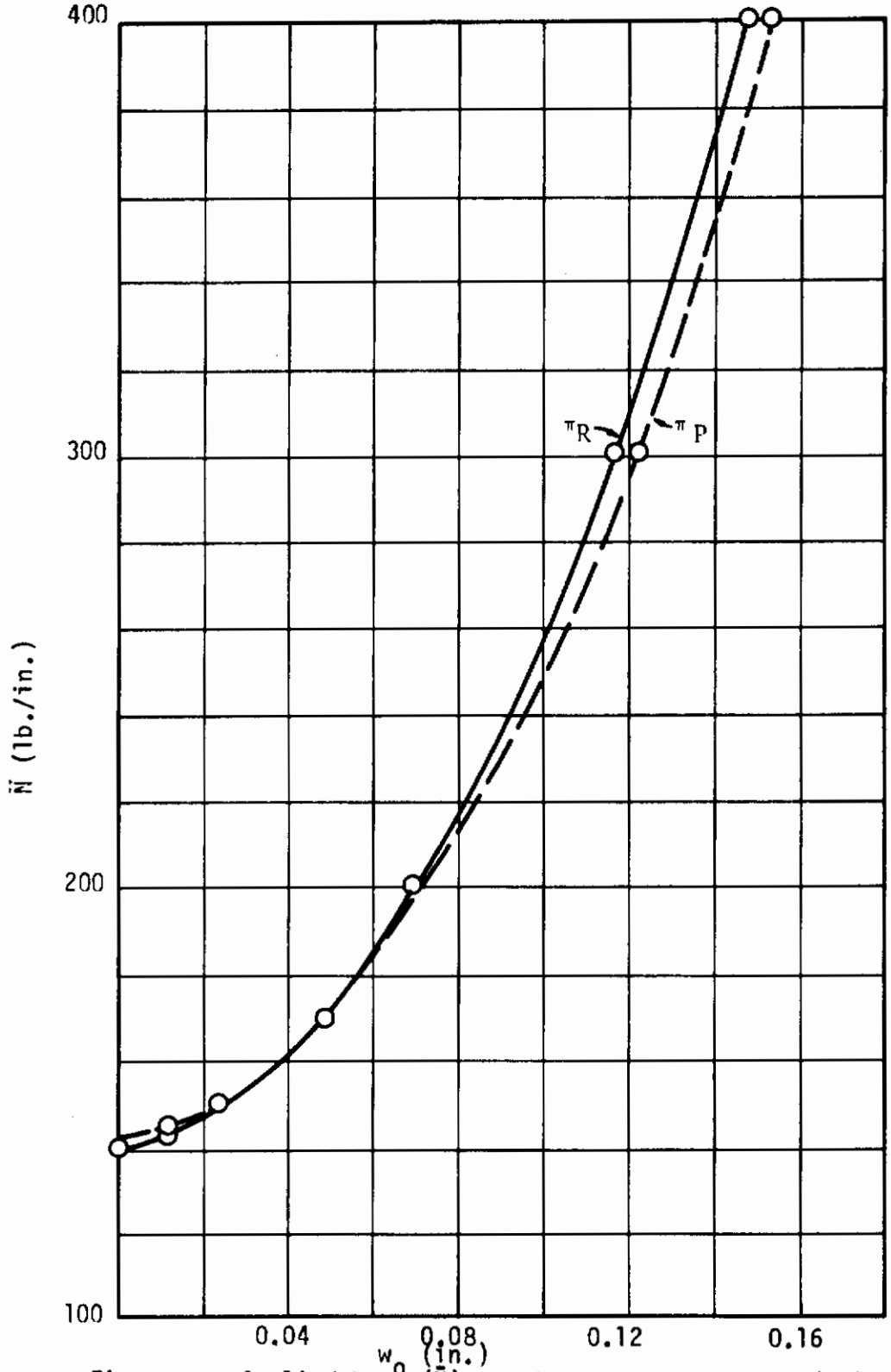

Figure 21. Applied Load ($\bar{N}$) vs. Center Displacement (w_0)

Approved for Public Release

Contrails

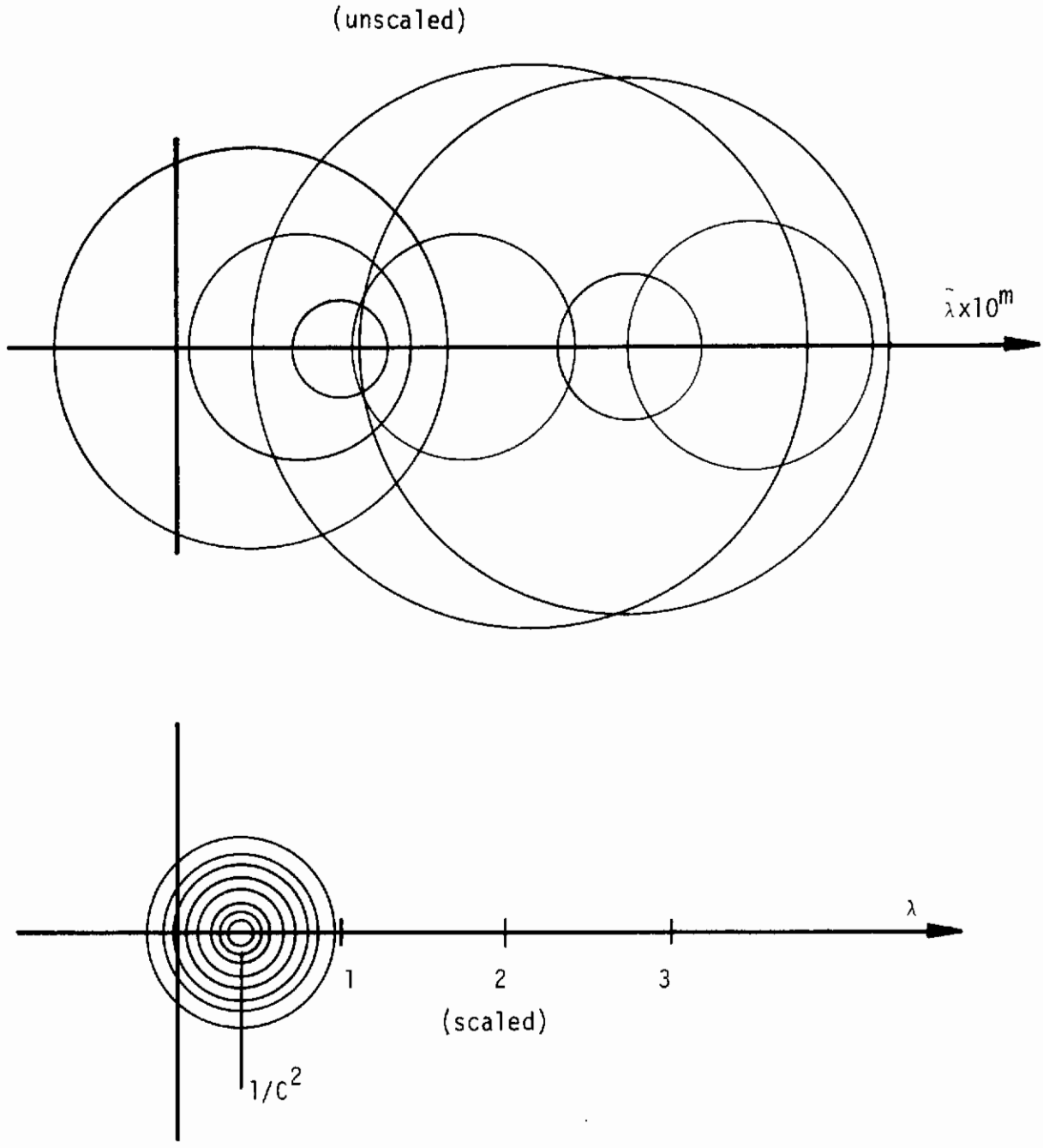

Figure 22. Gerschgorin Circles for K and $\tilde{K}$

Approved for Public Release

Contrails

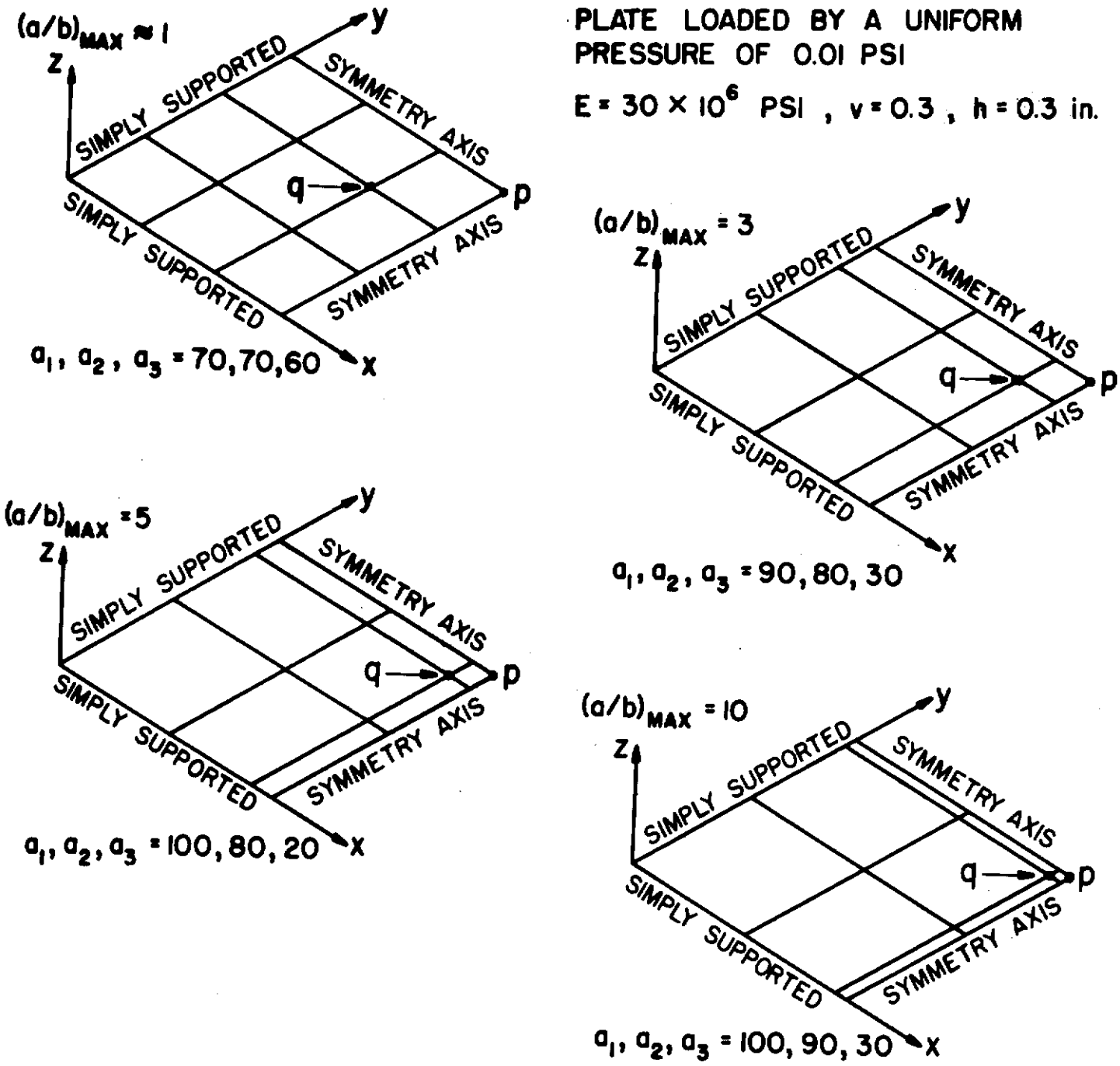

Figure 23. Nine Element Idealization of Simply Supported Plate

Approved for Public Release

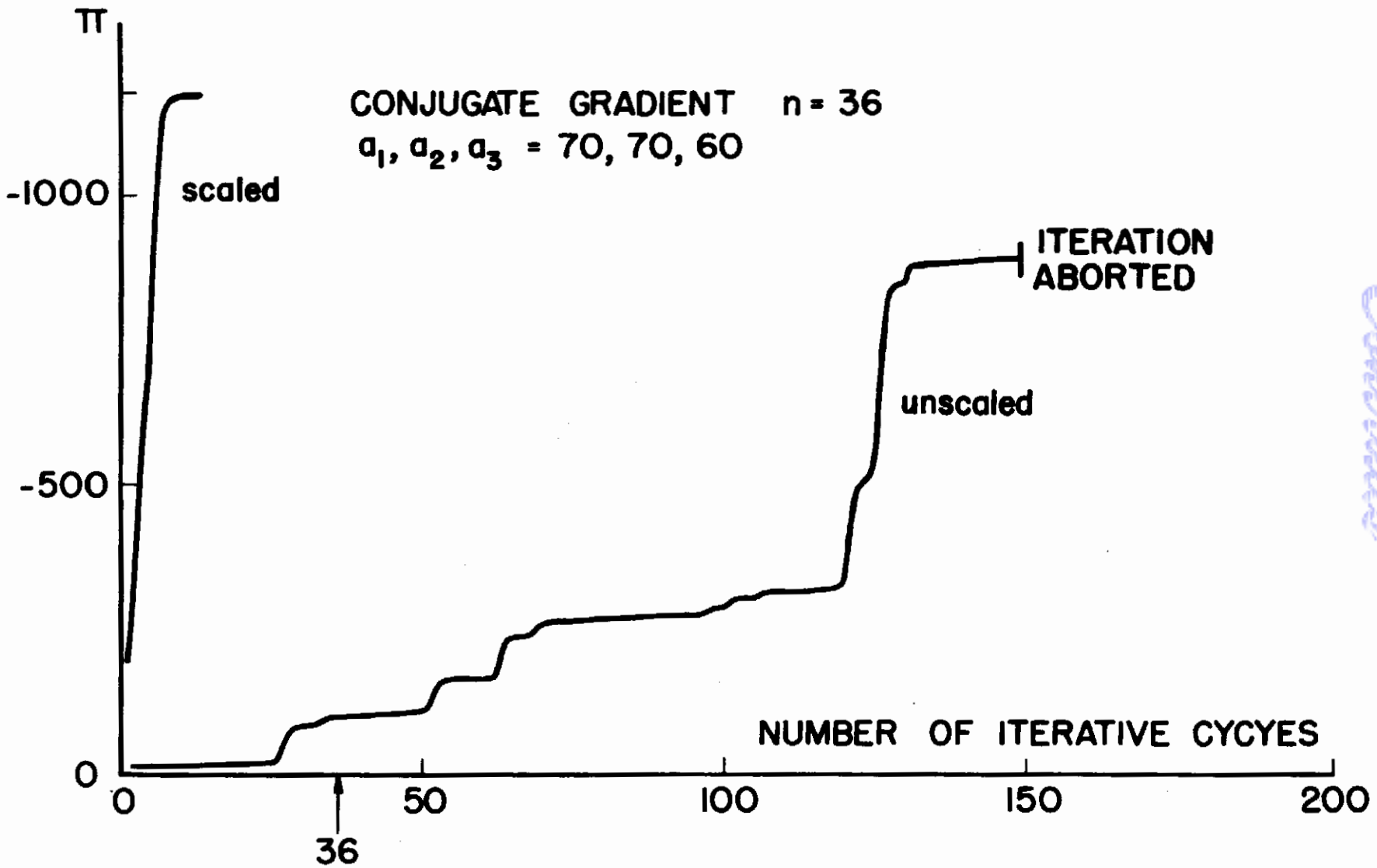

Figure 24. Potential Energy vs. Number of Cycles
(Conjugate Gradient - Fletcher-Reeves)

Approved for Public Release

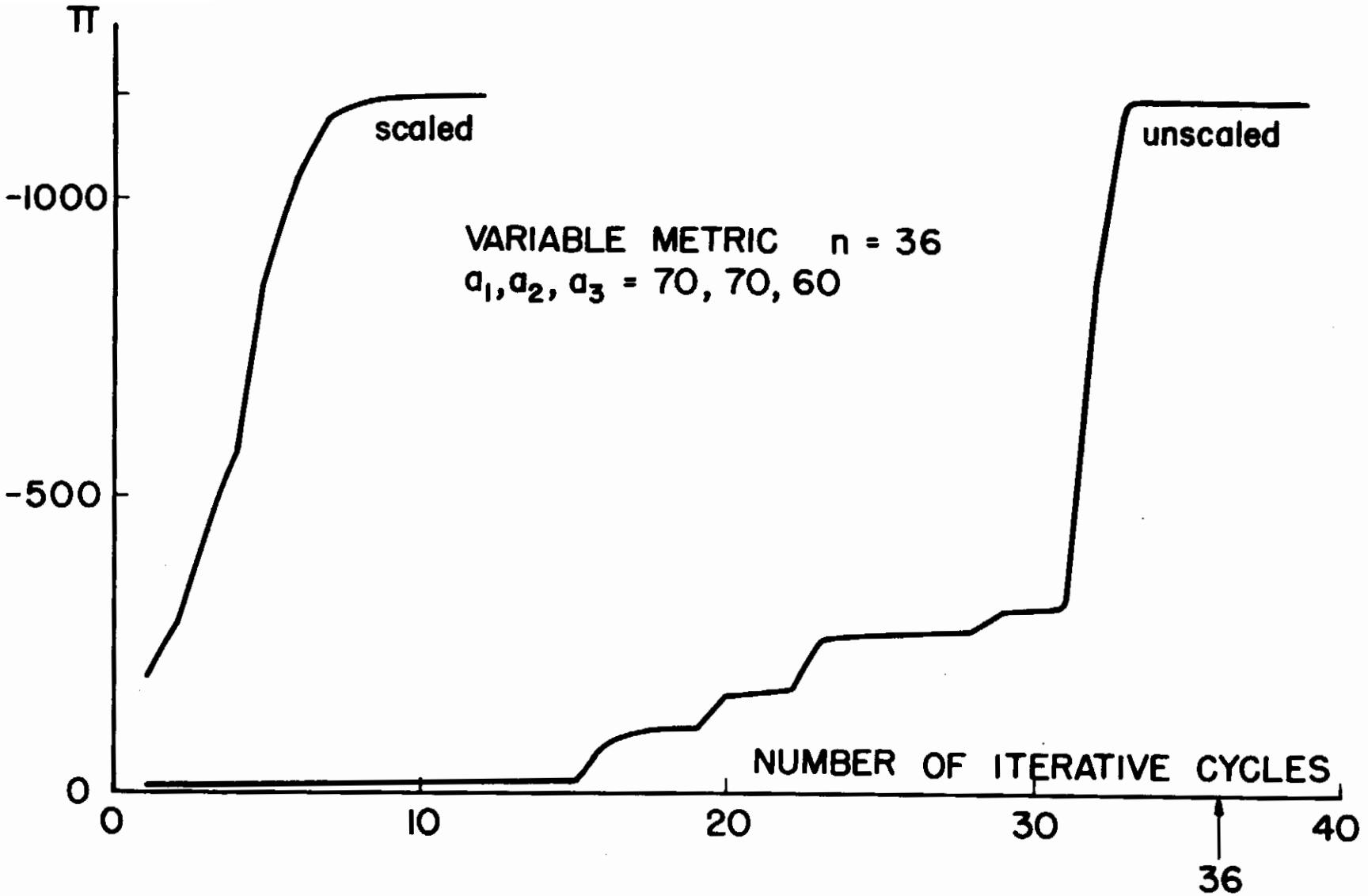

Figure 25. Potential Energy vs. Number of Cycles
(Variable Metric - Fletcher-Powell)

Approved for Public Release

Approved for Public Release

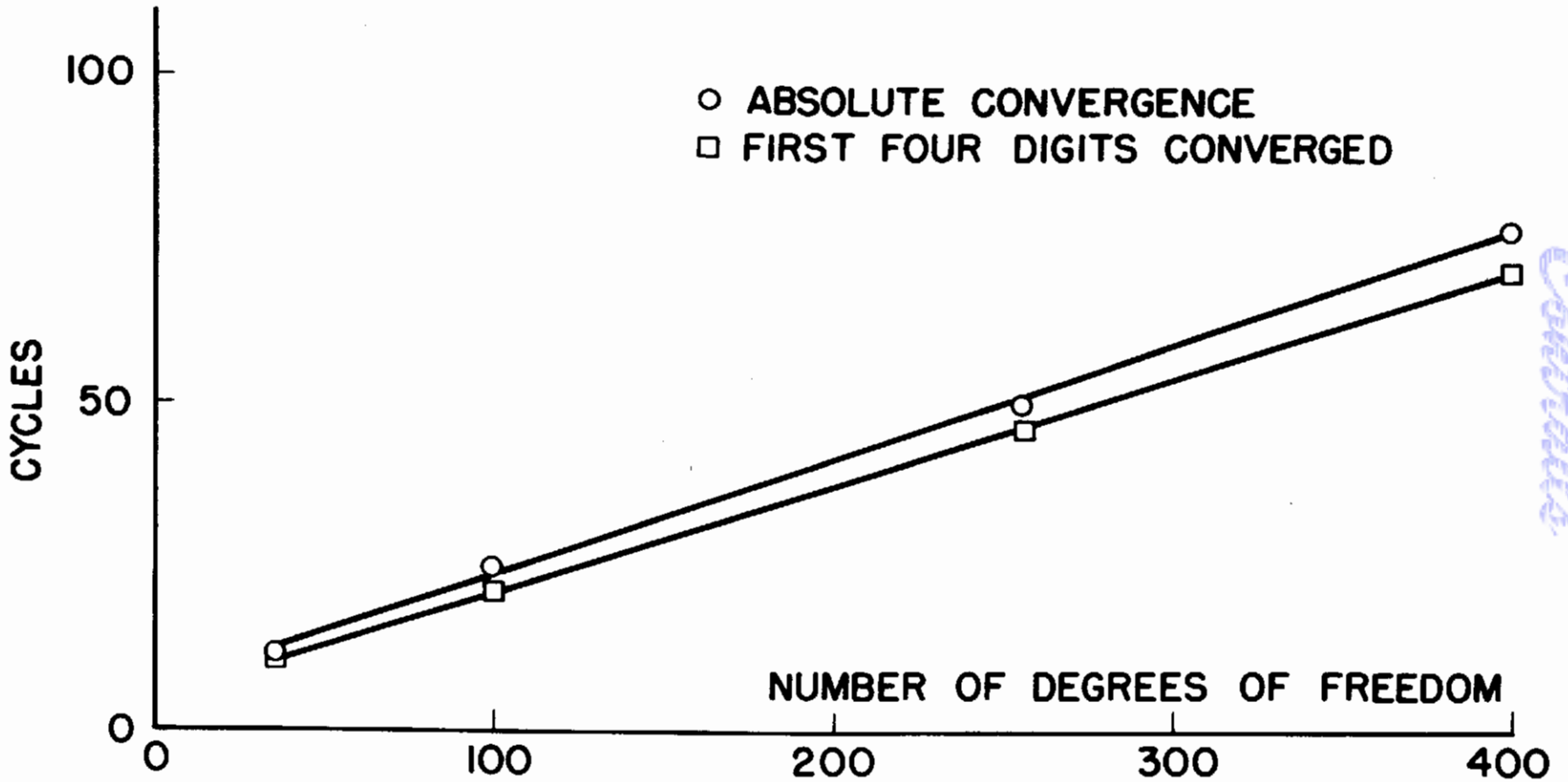

Figure 26. Convergence of the Conjugate Gradient Method with Increasing Degrees of Freedom

Contrails

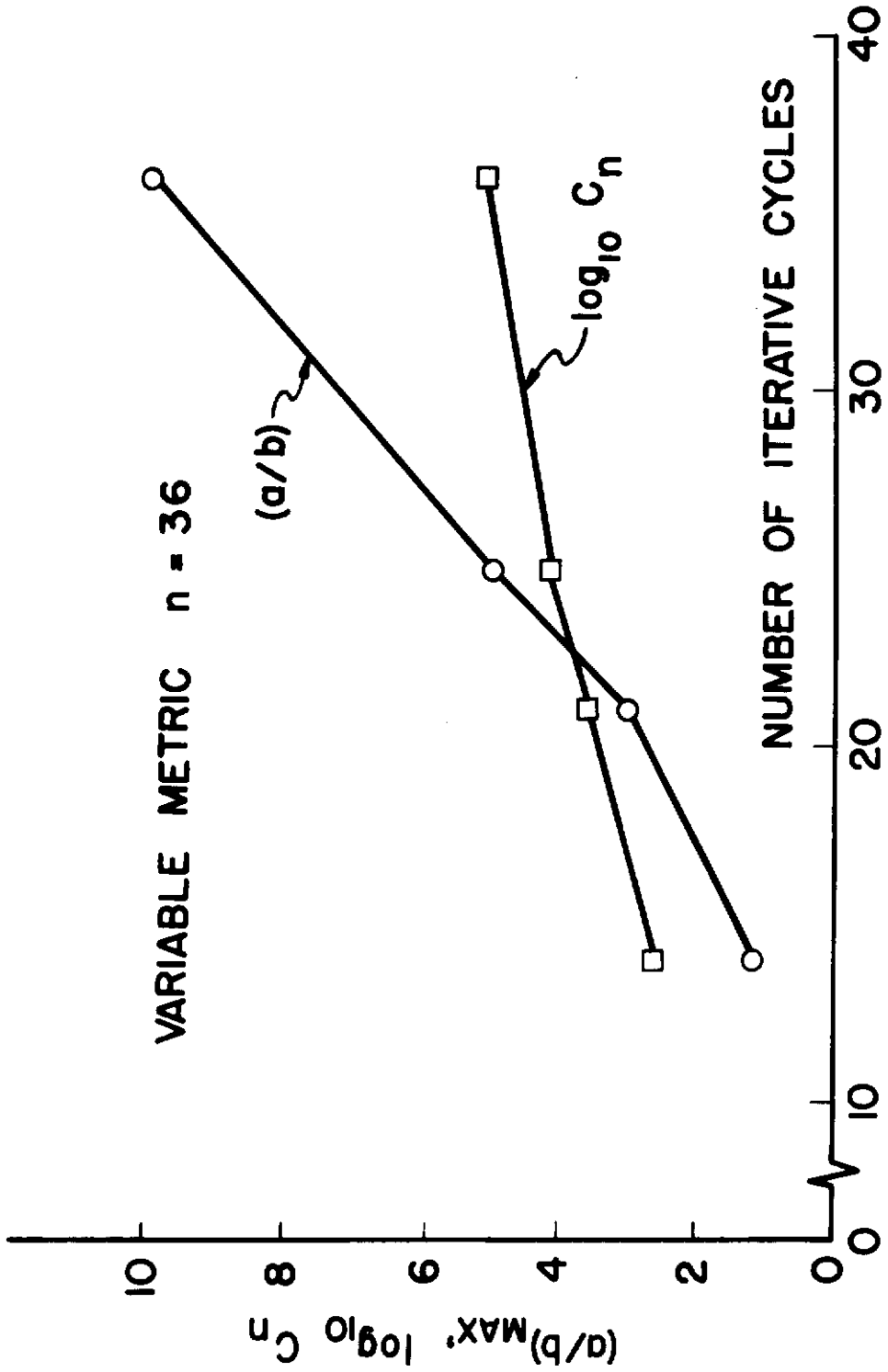

Figure 27. Convergence of the Variable-Metric Method with Increasing-aspect-ratio Grids

Approved for Public Release

Contrails

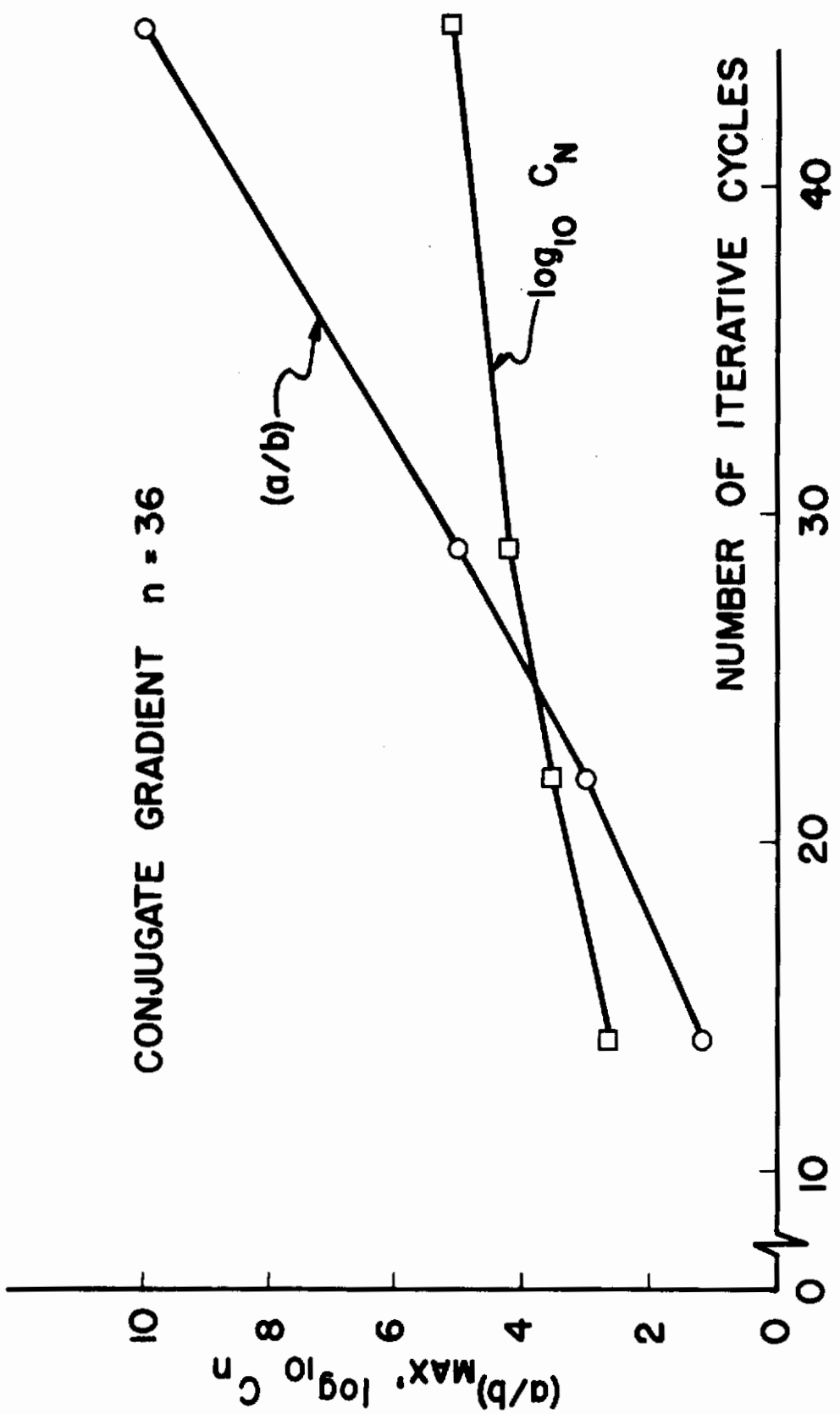

Figure 28. Convergence of the Conjugate Gradient Method with Increasing-aspect-ratio Grids

Approved for Public Release

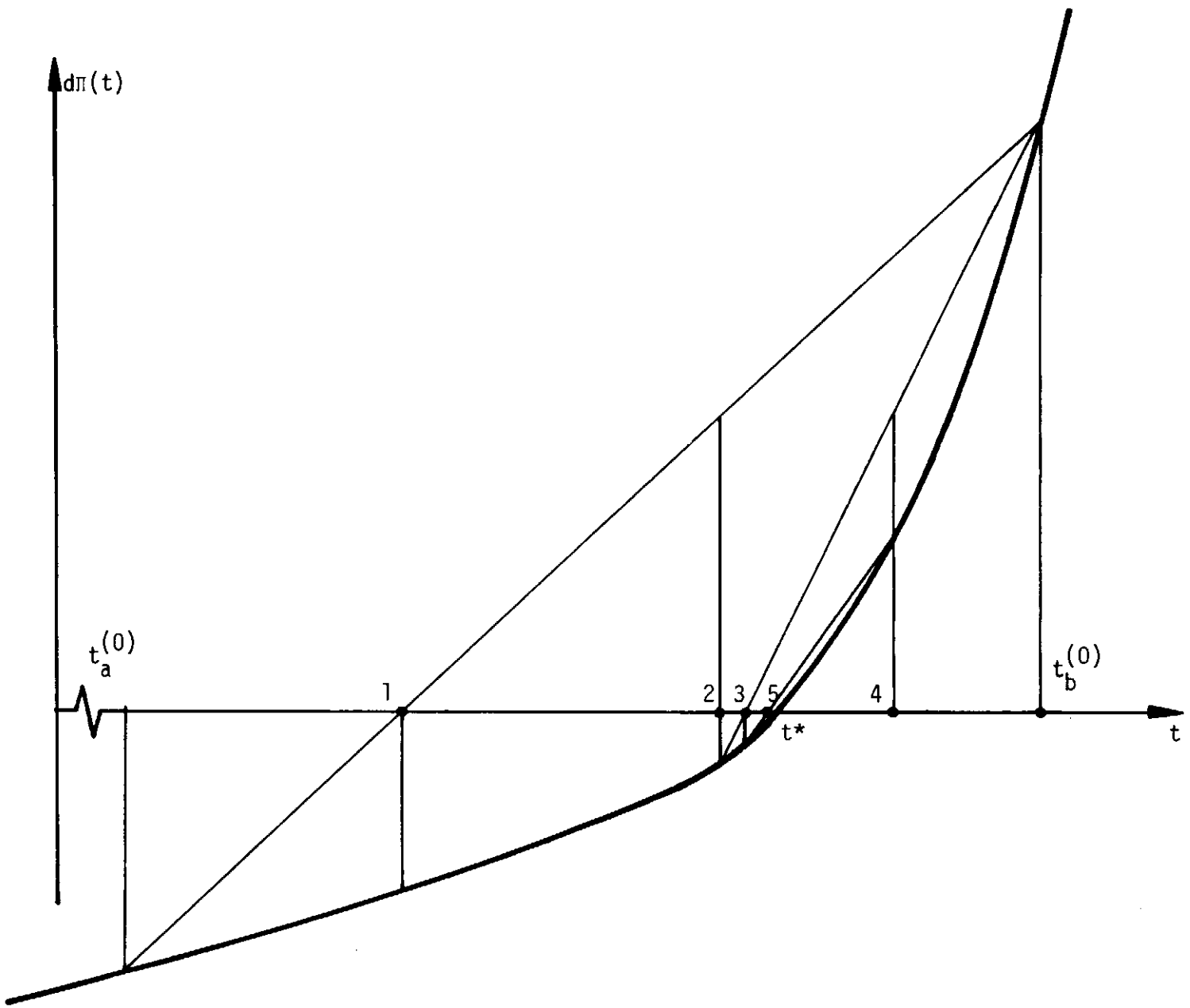

Figure 29. Illustration of the Regula Falsi-Bisection Linear Search Procedure (Section 4.4.2)

Approved for Public Release

Contrails

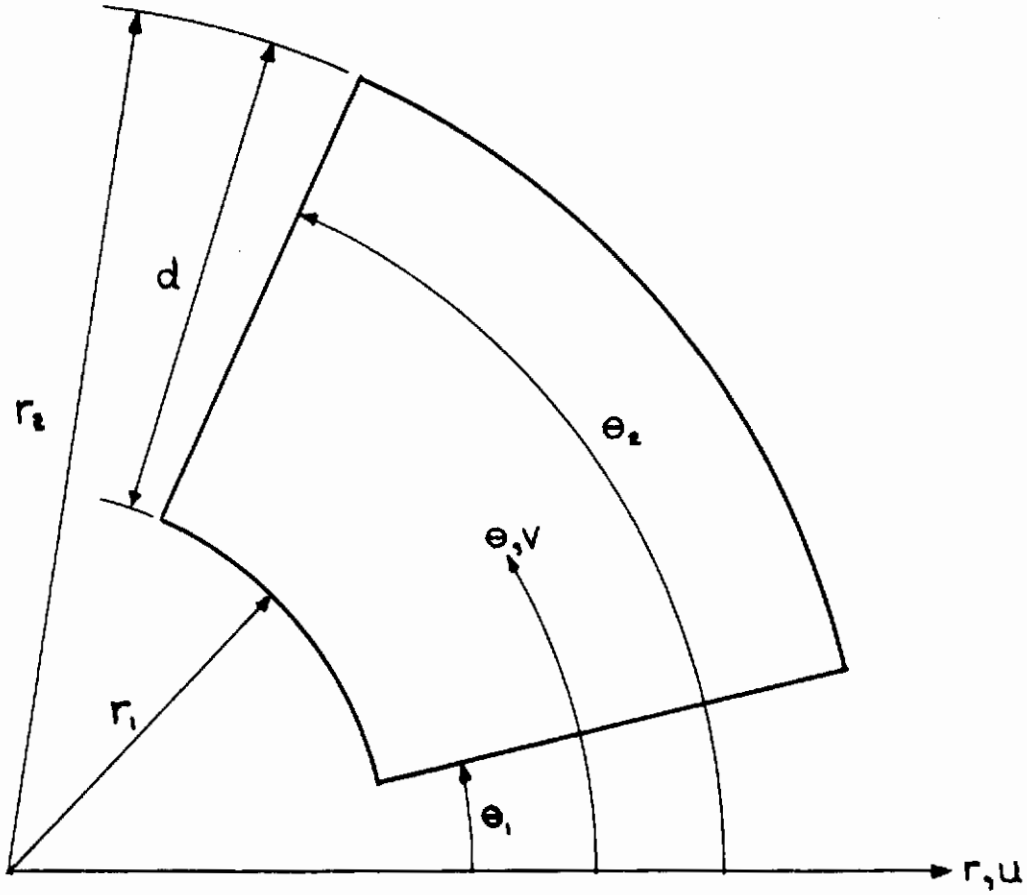

Figure 30. Annular Plate Discrete Element

Approved for Public Release

Contrails

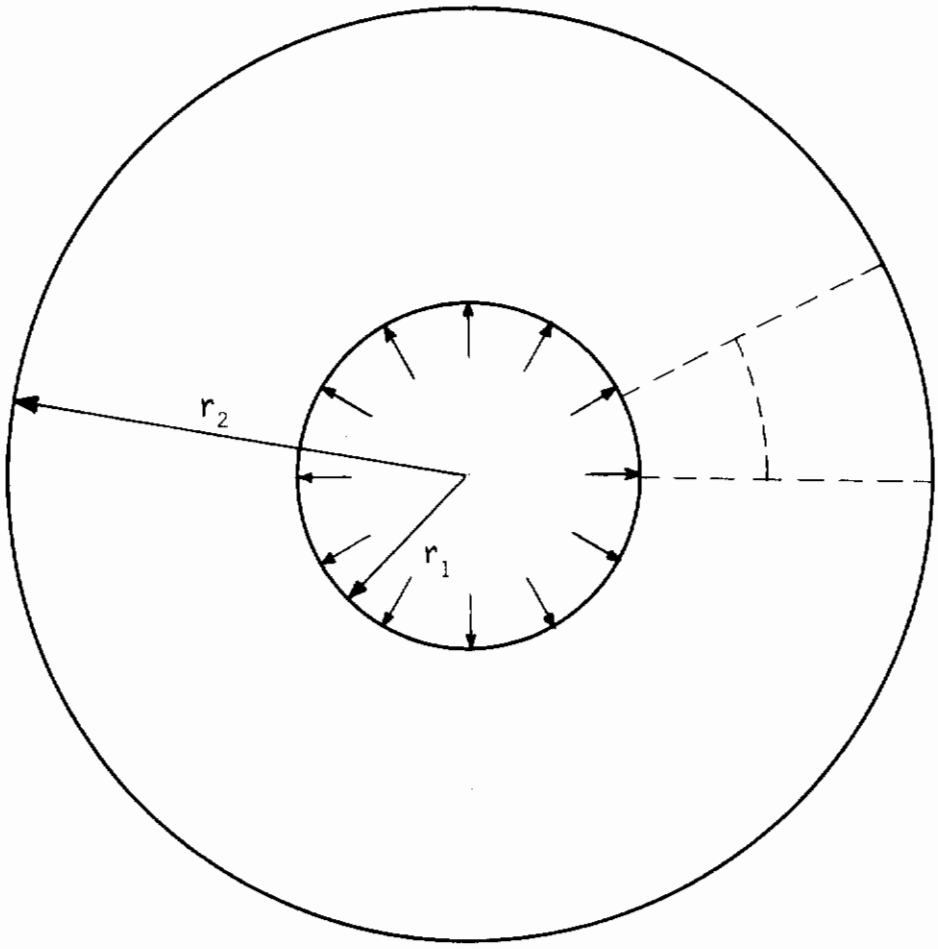

Figure 31. Thick Cylinder Subject to Internal Pressure

Approved for Public Release

Contrails

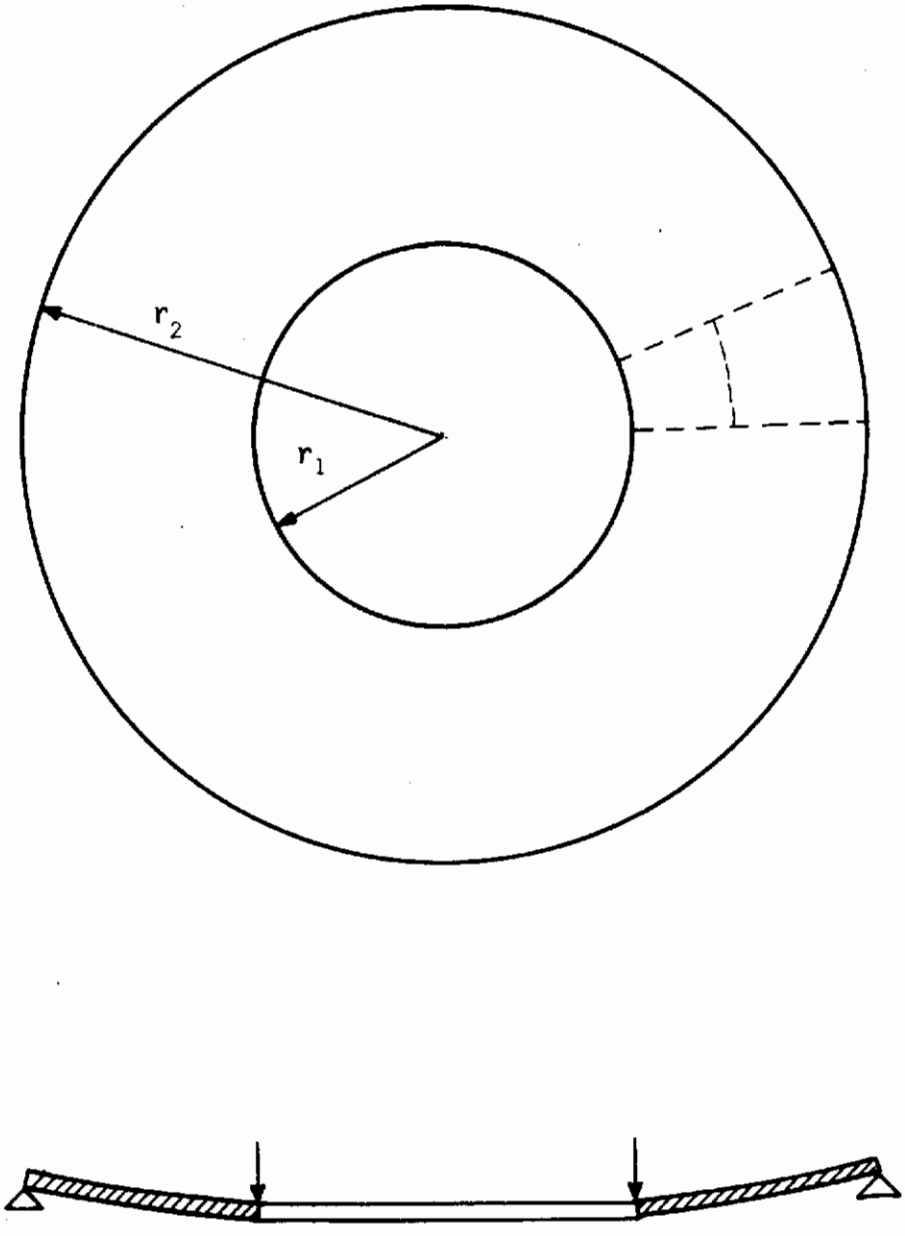

Figure 32. Annular Plate Example - Case 1

Approved for Public Release

Contrails

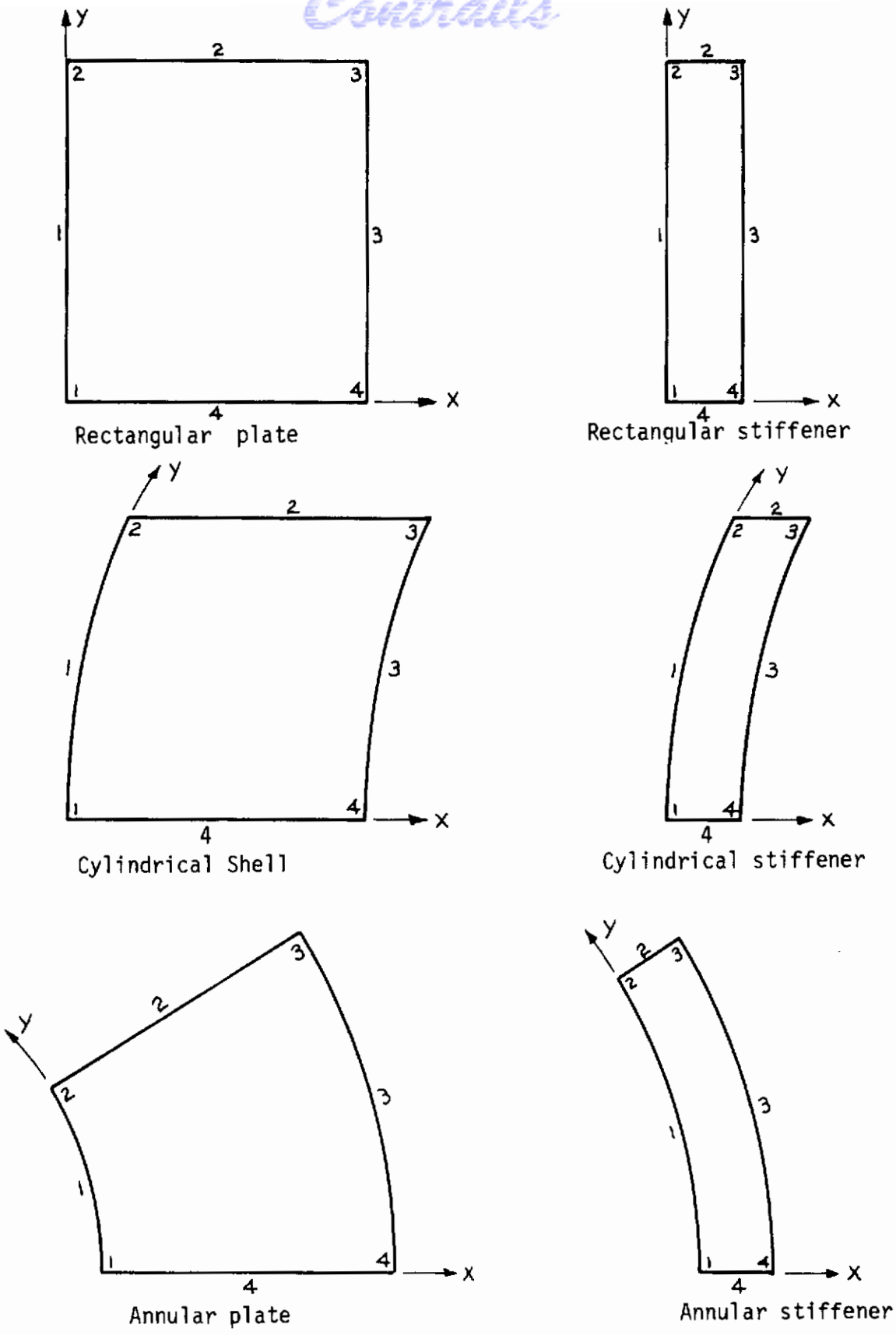

Fig. 33 Elements Available in Computer Program

Approved for Public Release

Contrails

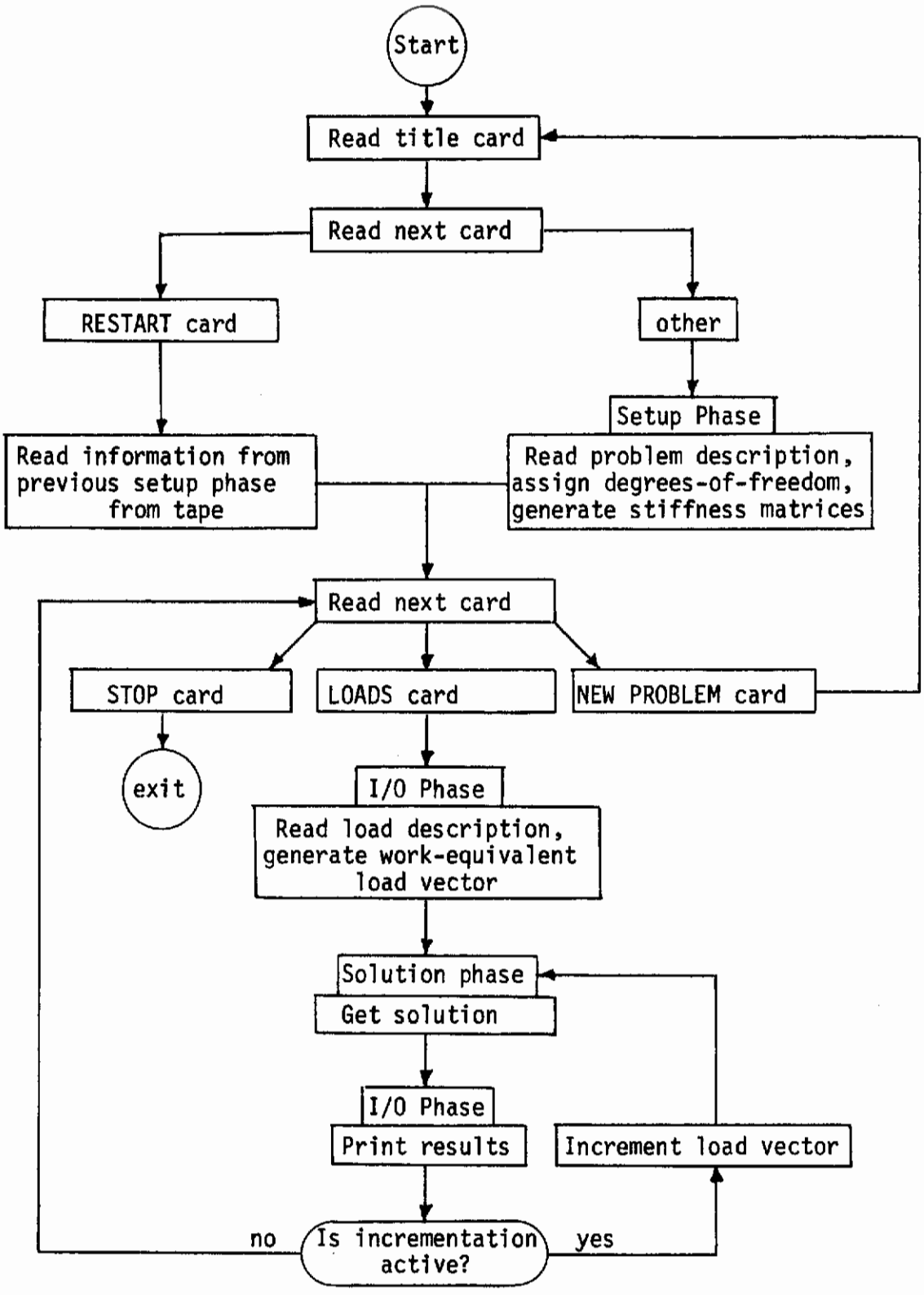

Fig. 34 Flow of Control Among Program Phases

Approved for Public Release

Contrails

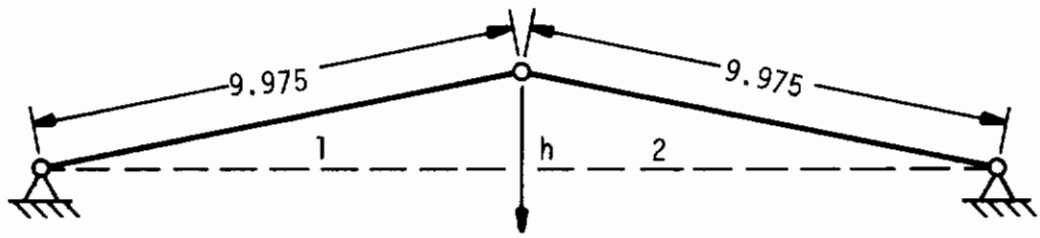

Member	Width	Thickness
1	0.050"	0.050"
2	0.050"	0.187"

h(rise) 2.25" and 1"

Figure 35. Snap-Through Truss

Approved for Public Release

Contrails

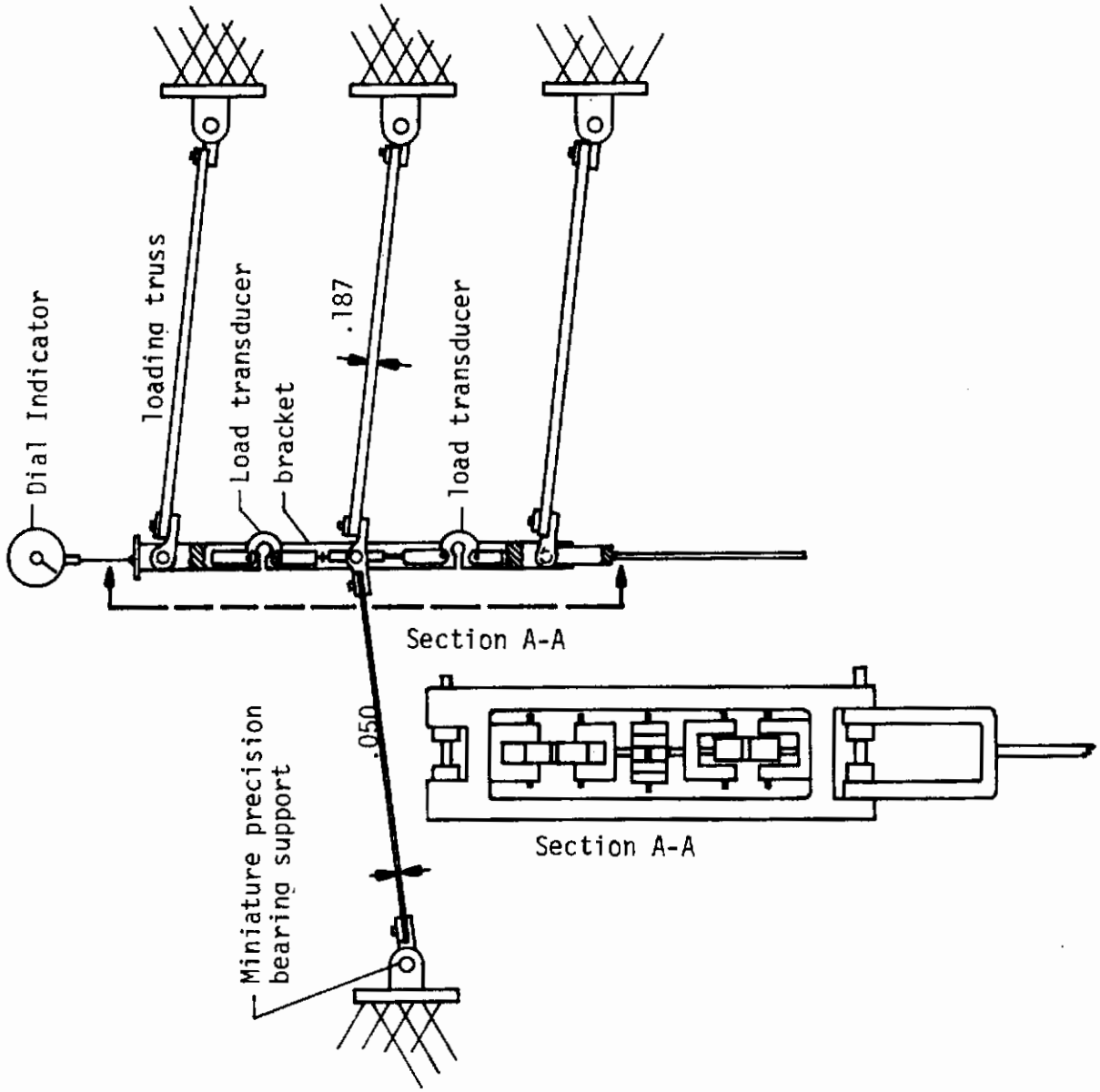

Fig. 36 Snap-Through Truss and Test Setup Details

Approved for Public Release

Contrails

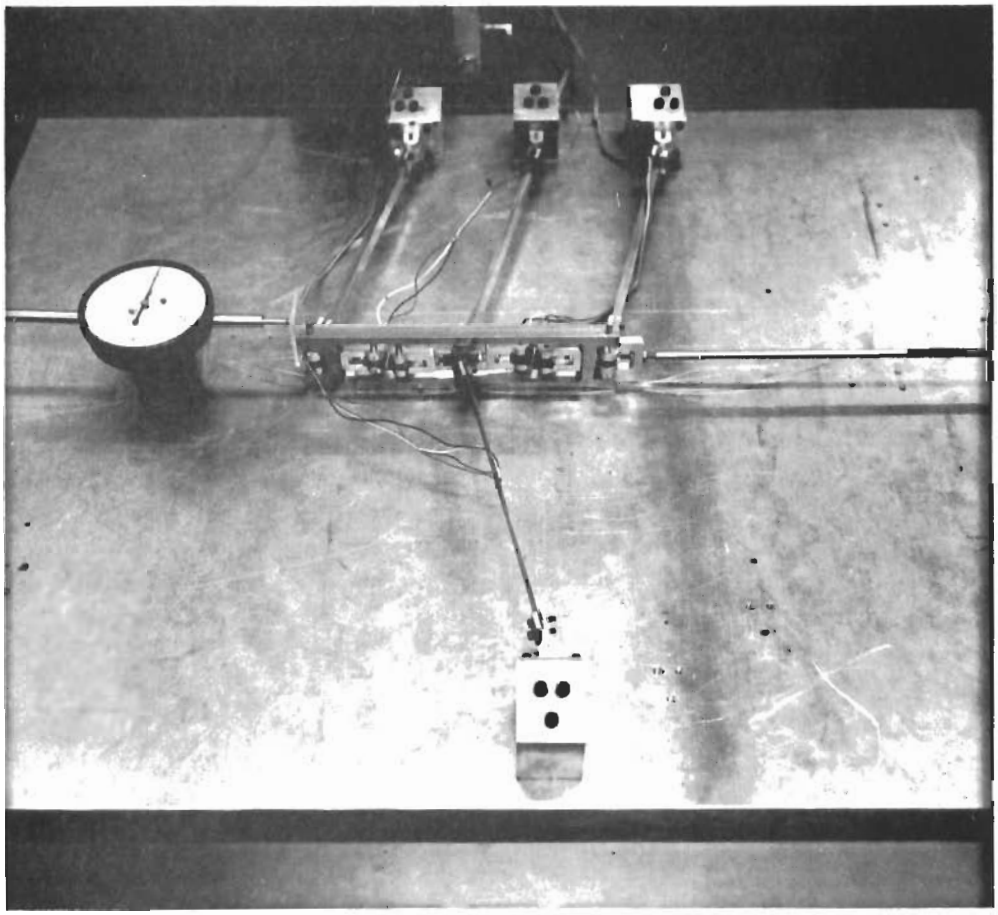

Fig. 37 Photograph of Snap-through Test

Approved for Public Release

Contrails

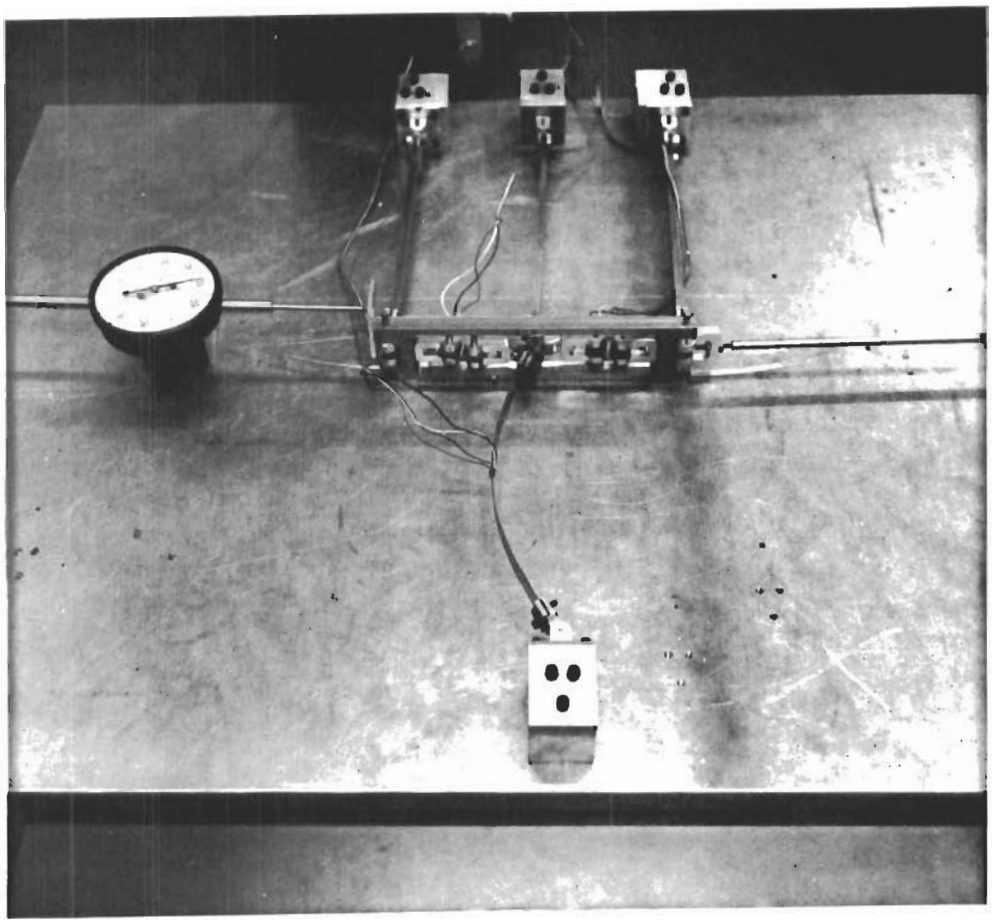

Fig. 38 Buckled Snap-Through Truss

Approved for Public Release

Contrails

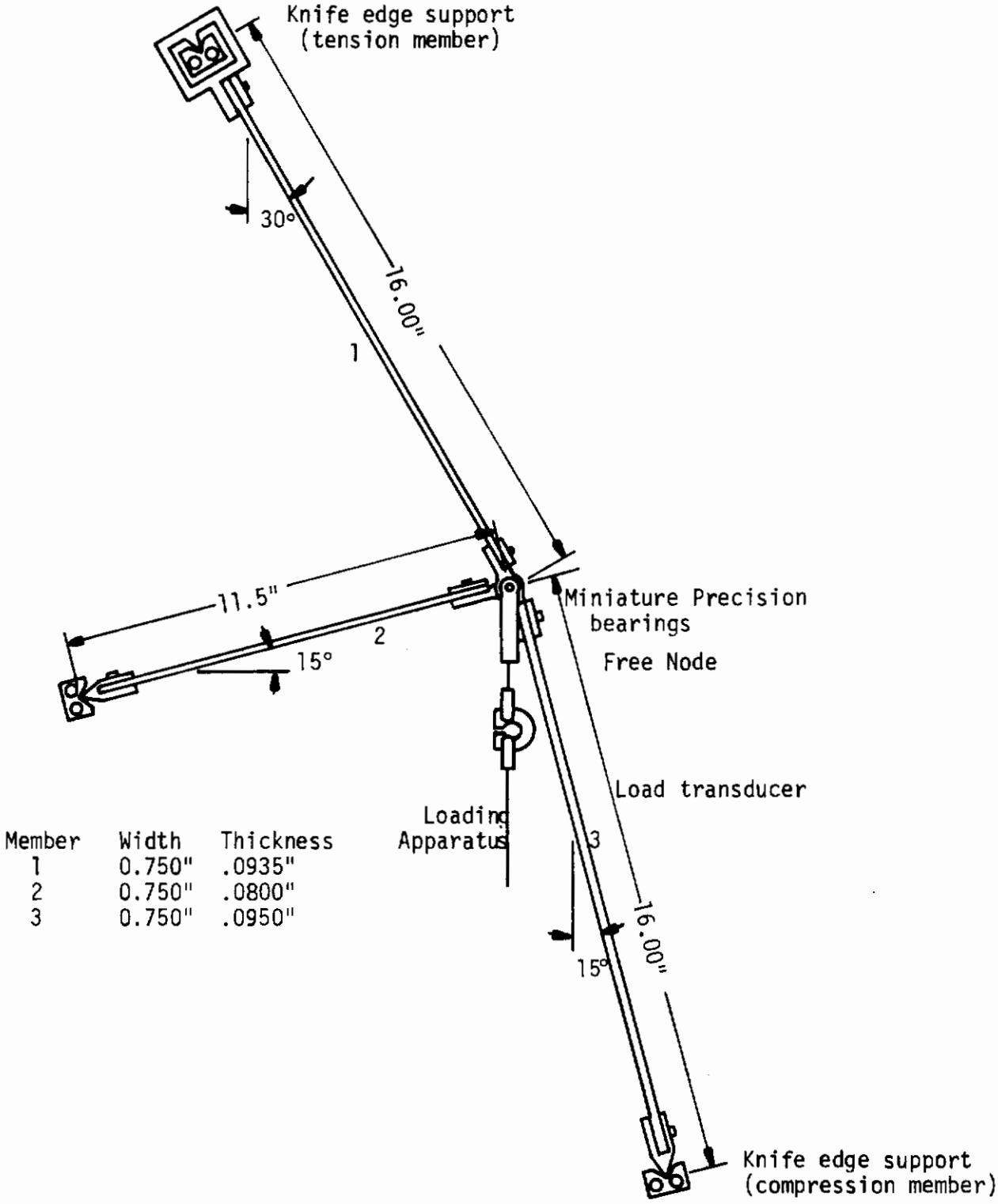

Member	Width	Thickness
1	0.750"	.0935"
2	0.750"	.0800"
3	0.750"	.0950"

Fig. 39 Three Bar Truss Specimen

Approved for Public Release

Contrails

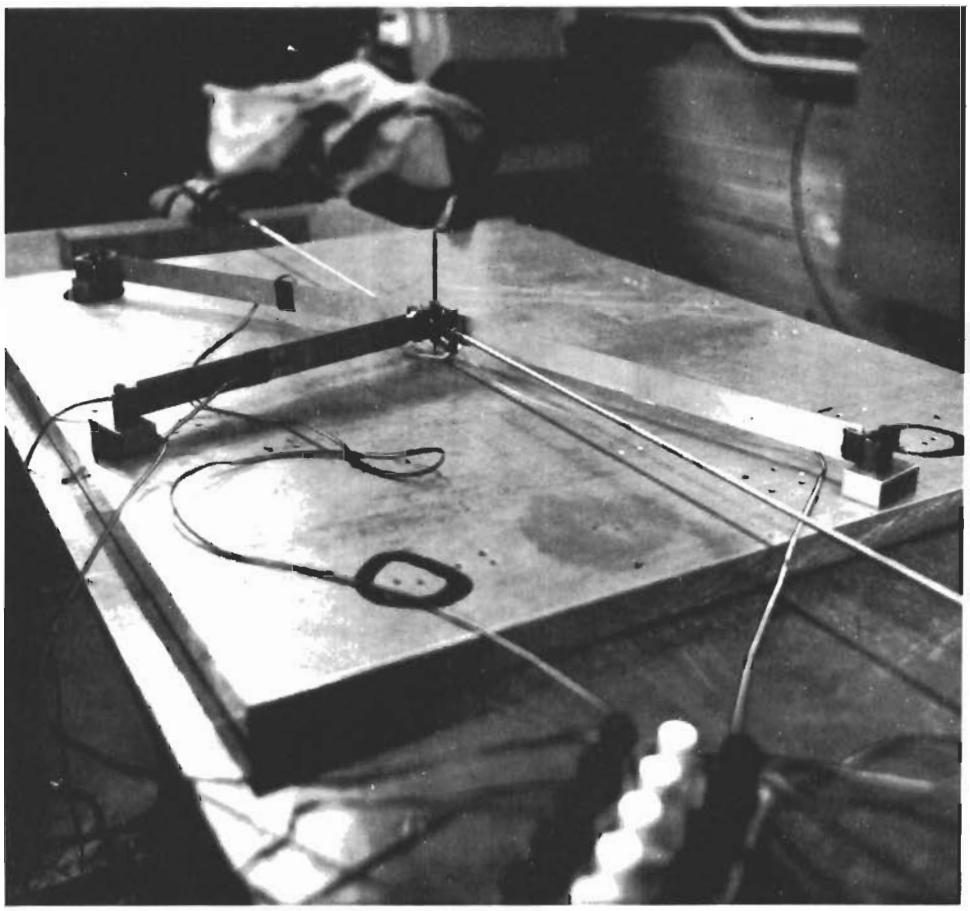

Fig. 40 Photograph of Three Bar Truss Test

Approved for Public Release

Contrails

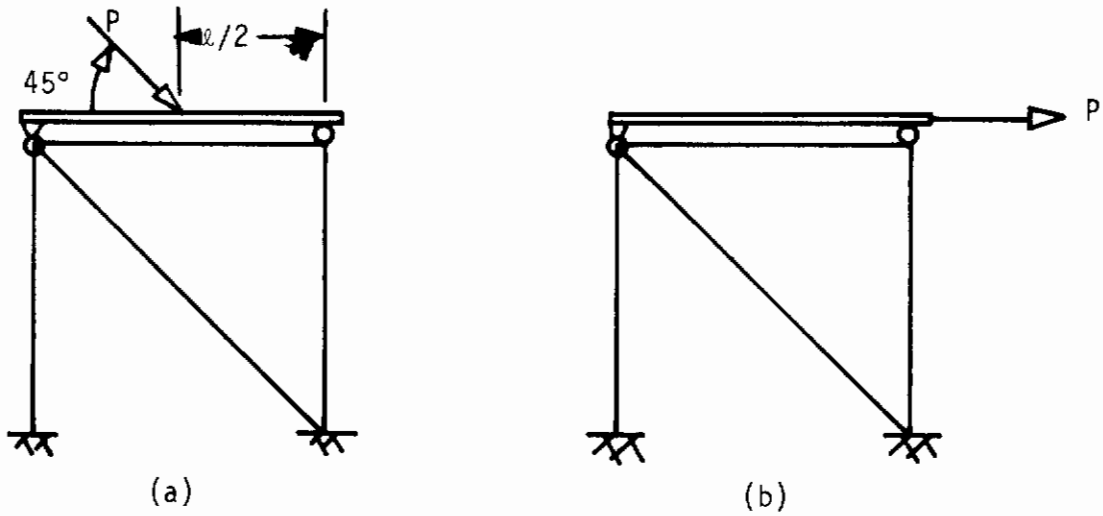

(a) (b)

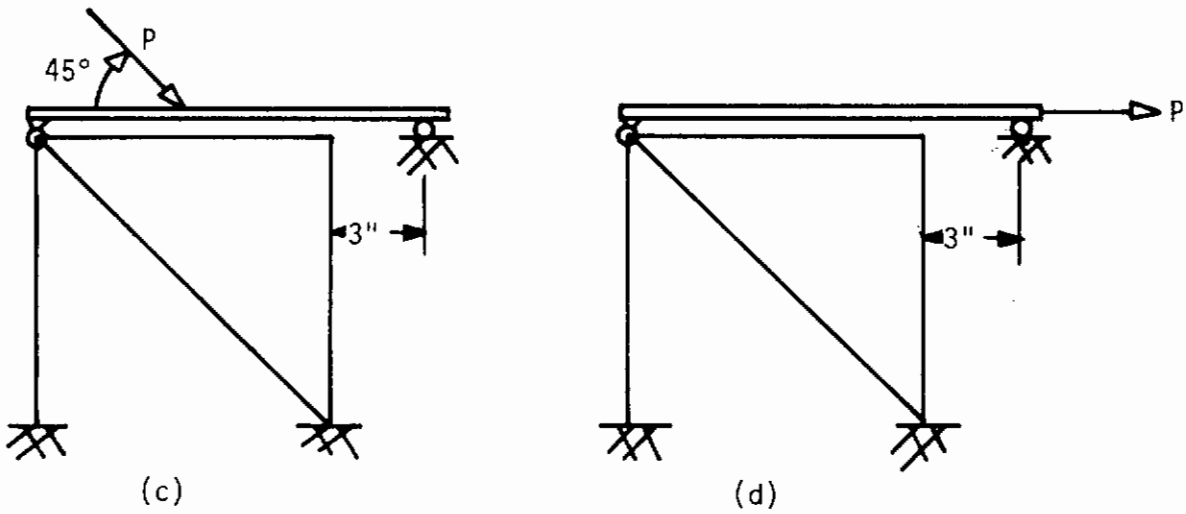

(c) (d)

Fig. 41 Frame Configuration and Loading Conditions

Approved for Public Release

Contrails

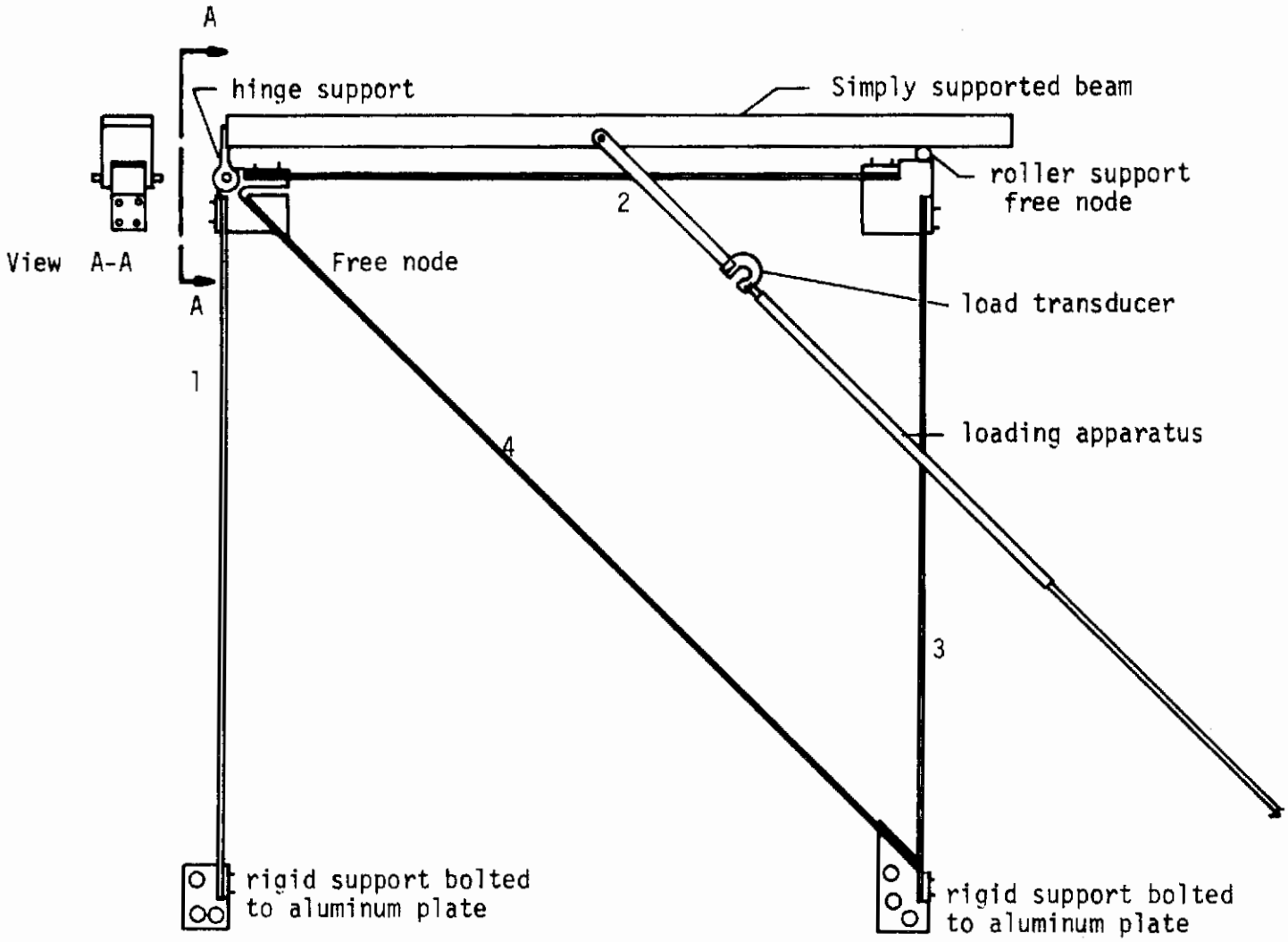

Member	Length	Width	Thickness
1	16.532"	0.750"	0.0625"
2	15.062"	0.750"	0.0625"
3	16.532"	0.750"	0.0625"
4	23.000"	0.750"	0.0625"

Fig. 42 Frame Specimen Details

Approved for Public Release

Contrails

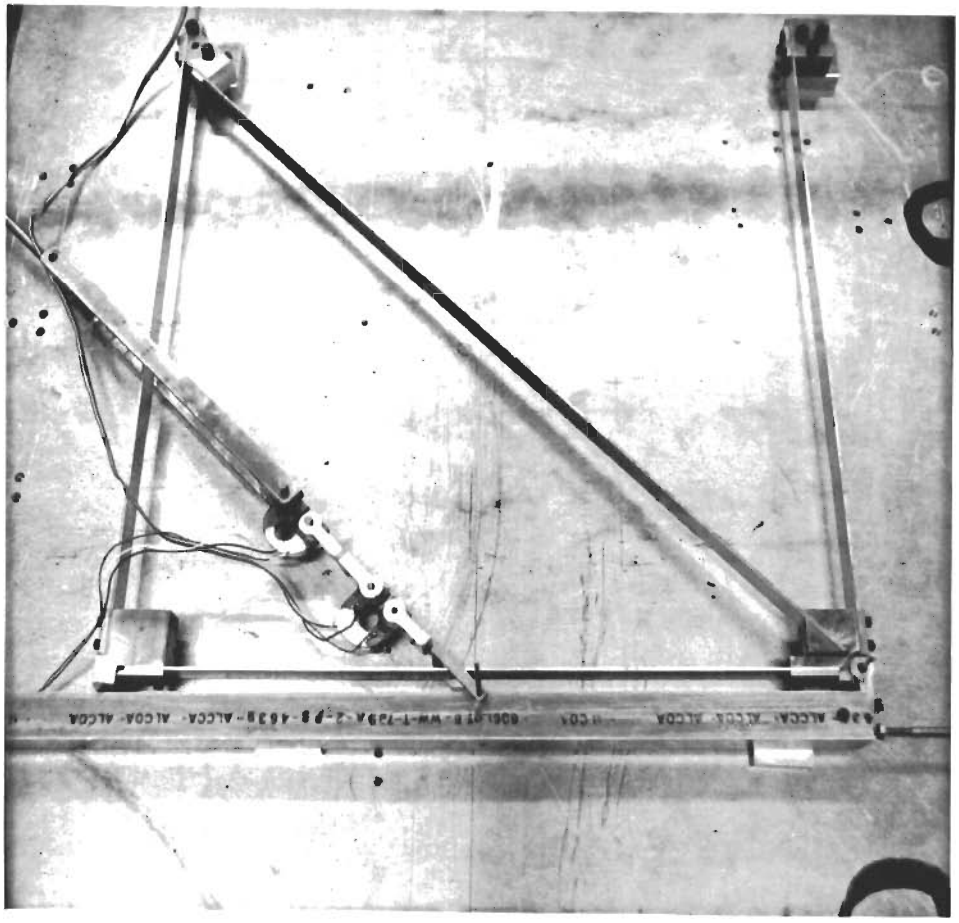

Fig. 43 Photograph of Frame Test Setup

Approved for Public Release

Contrails

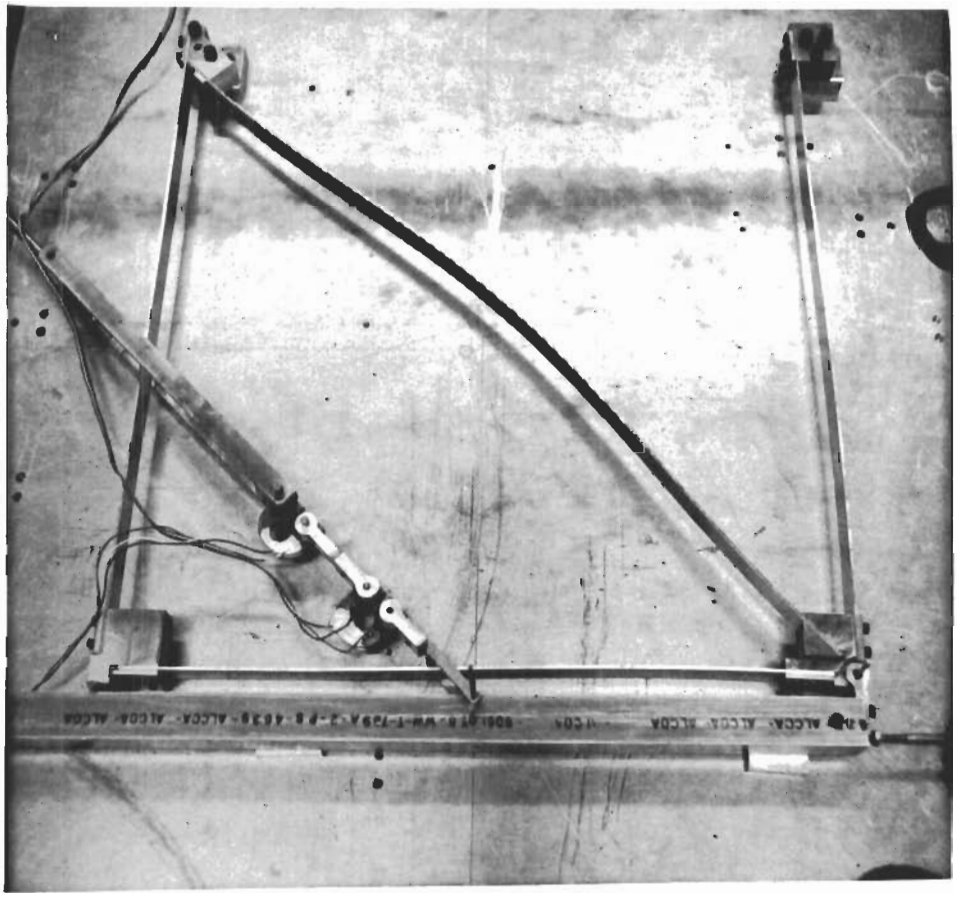

Fig. 44 Photograph of Displaced Frame

Approved for Public Release

Contrails

Fig. 45 Photograph of Typical Test Setup and Instrumentation

Approved for Public Release

Contrails

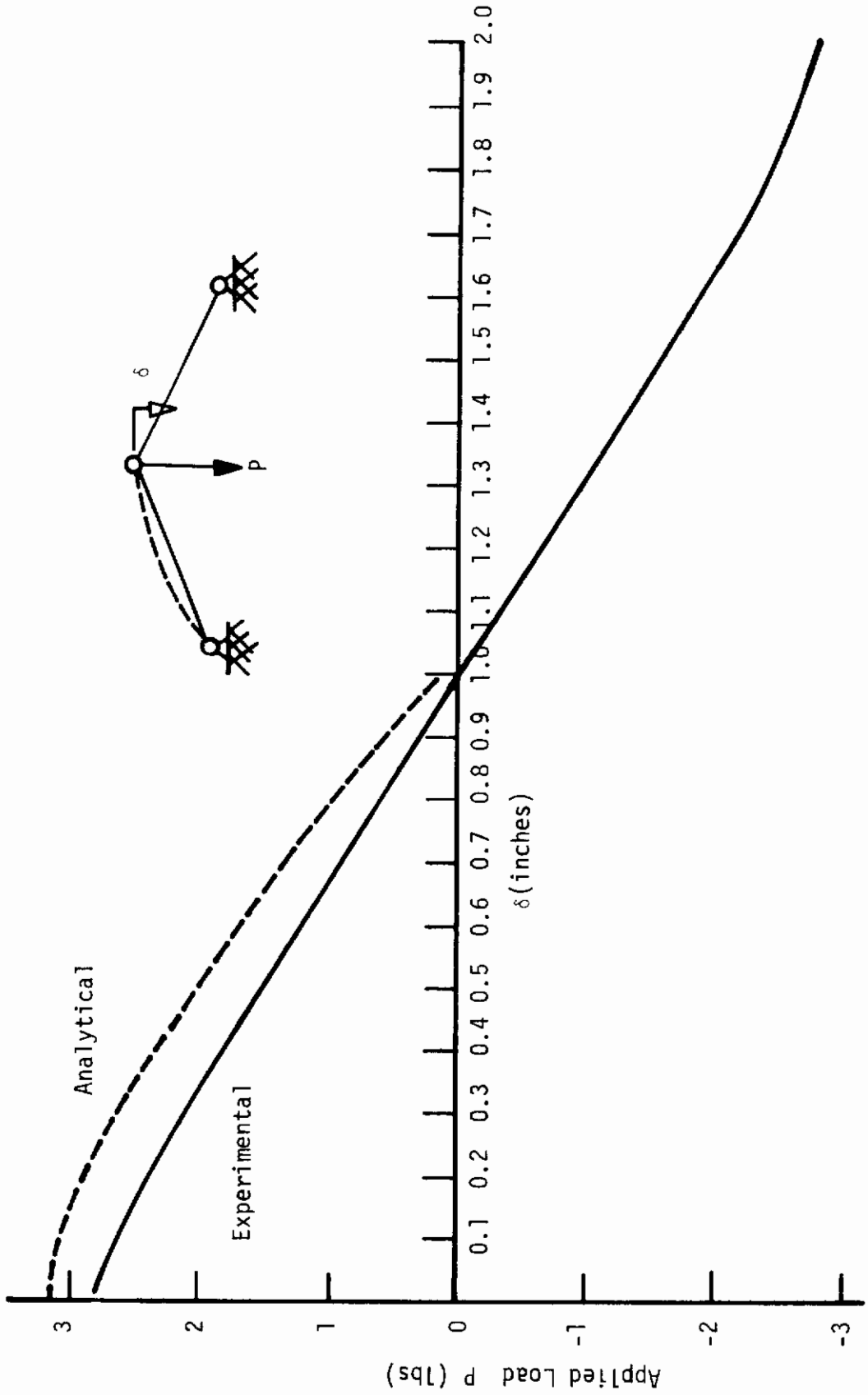

Fig. 46 Load Deflection Correlation for One Inch Rise Snap-Through Truss

Approved for Public Release

Contrails

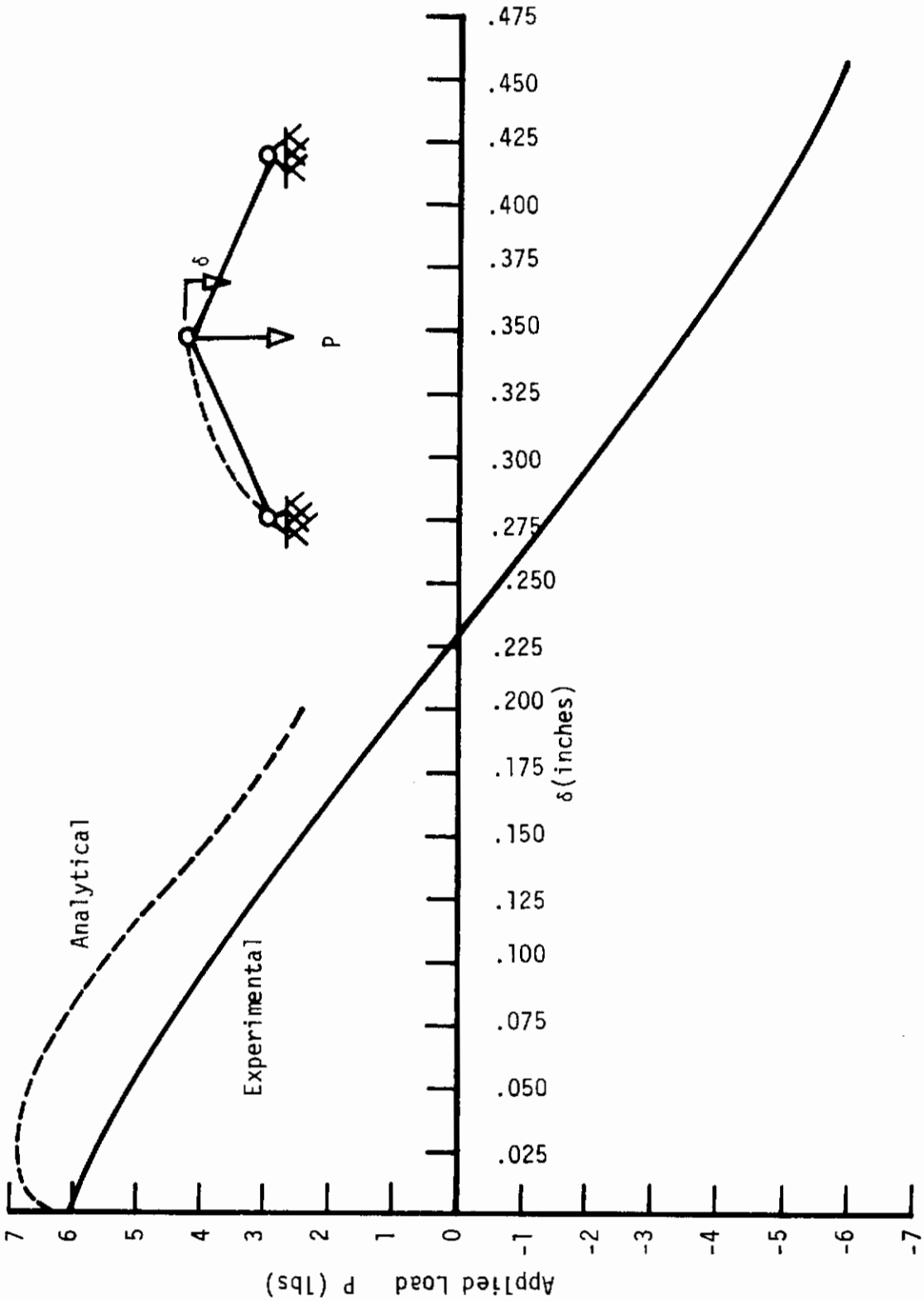

Fig. 47 Load Deflection Correlation for 2.25 Inch Rise Snap-Through Truss

Approved for Public Release

Contrails

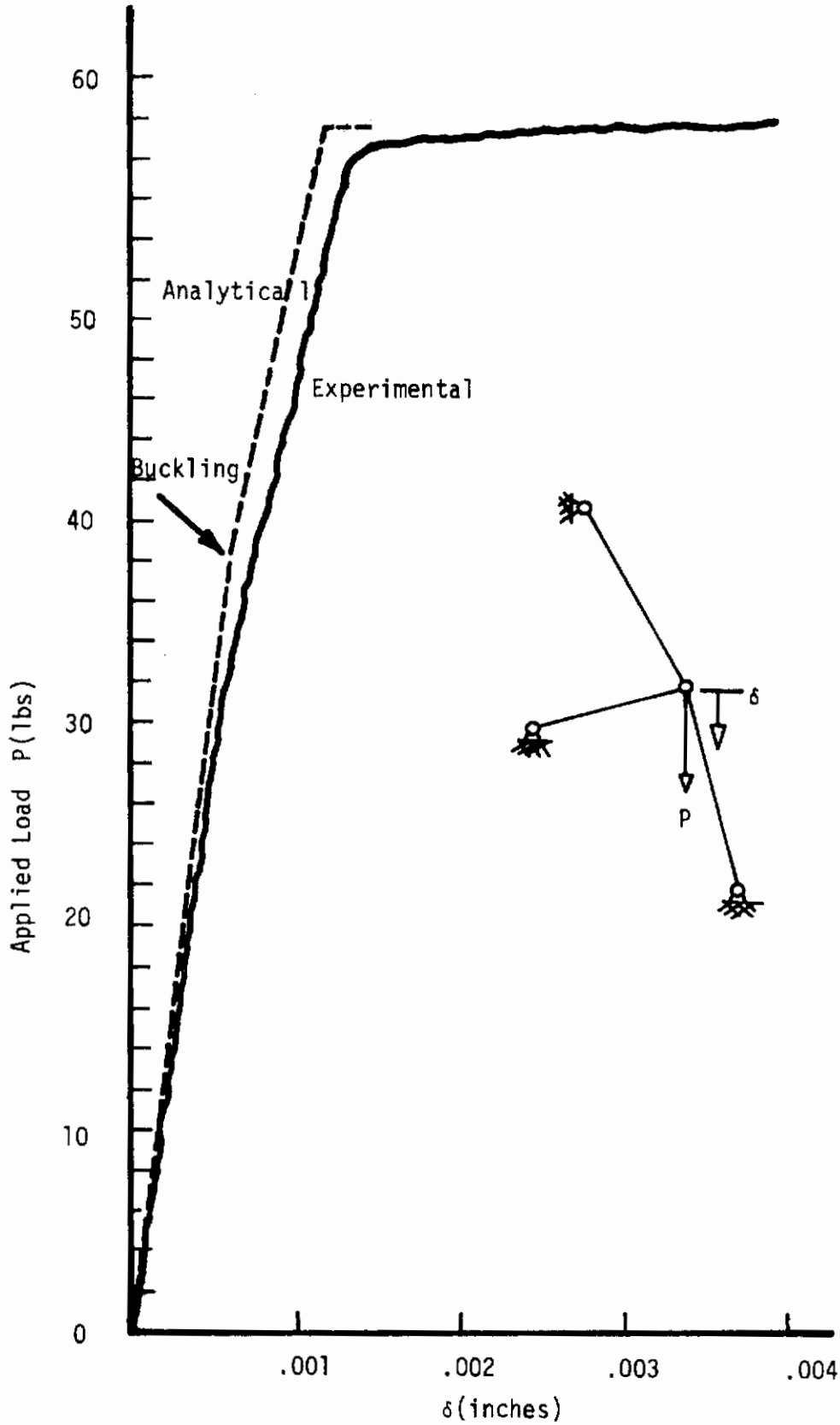

Fig. 48 Load Deflections Correction for the Three Bar Truss

Approved for Public Release

Contrails

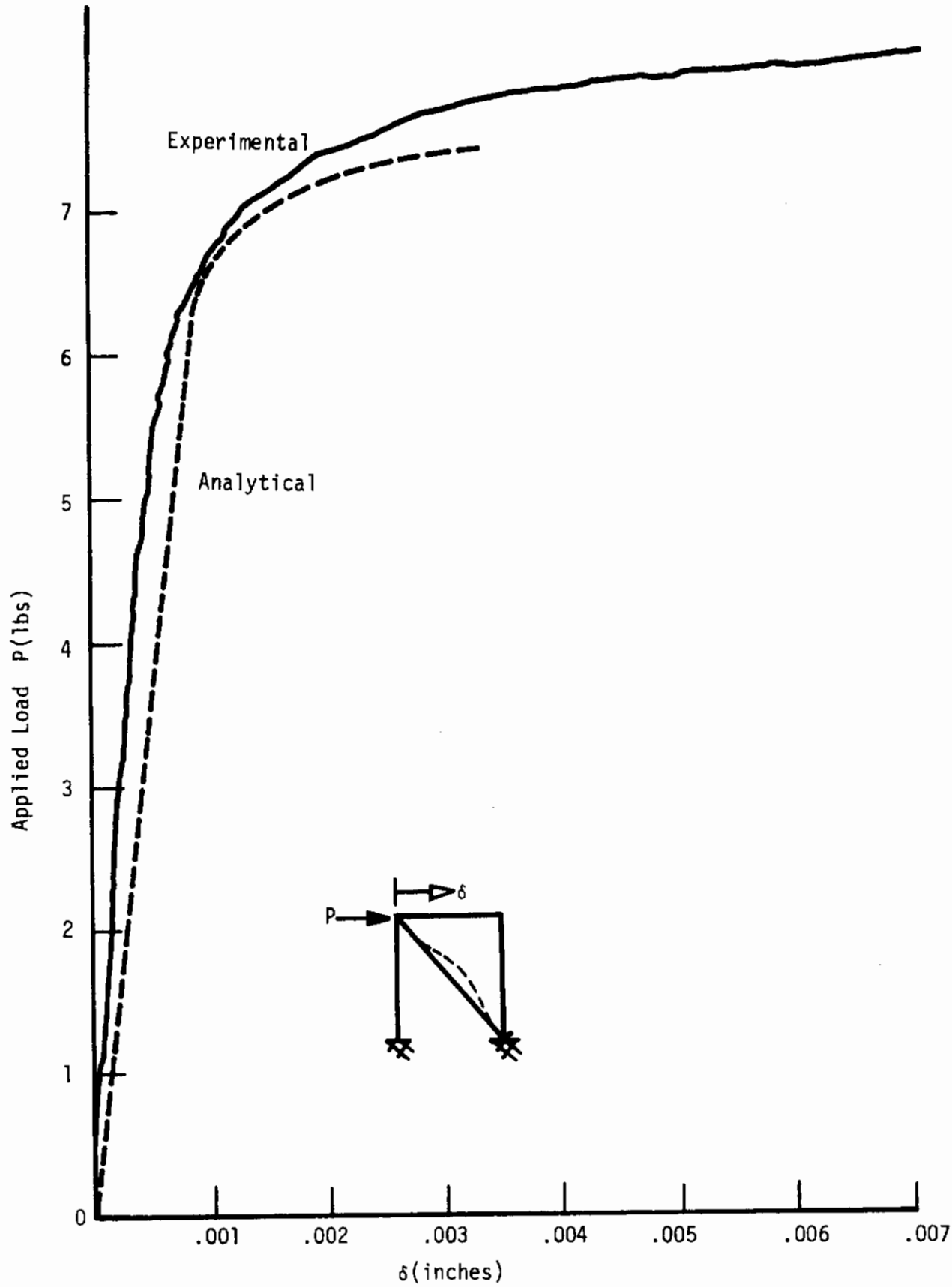

Fig. 49 Load Deflection Correlation for the Planar Braced Frame

Approved for Public Release

Contrails

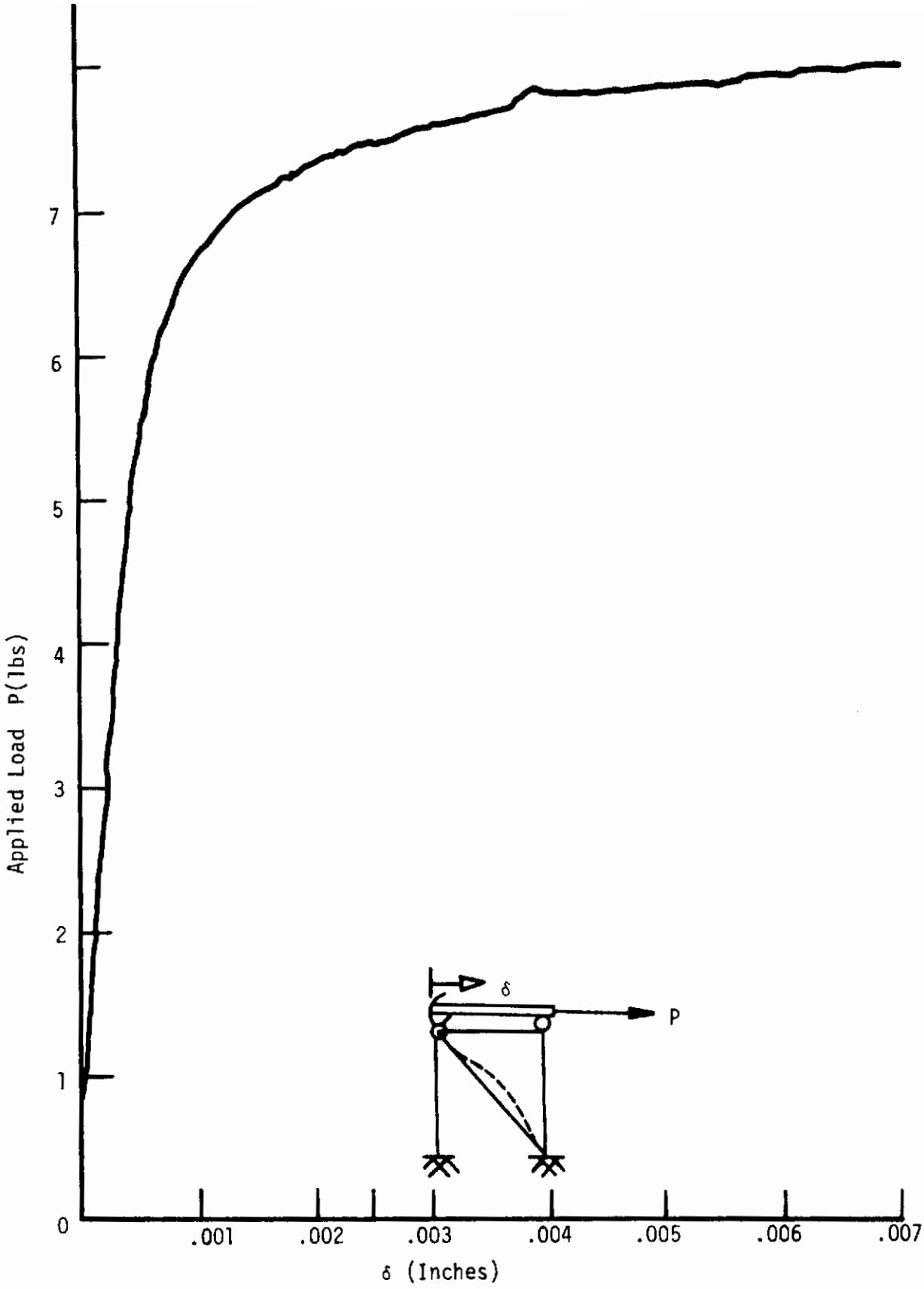

Fig. 50 Load Deflection Results for Test Number 2 on the Planar Braced Frame

Approved for Public Release

Contrails

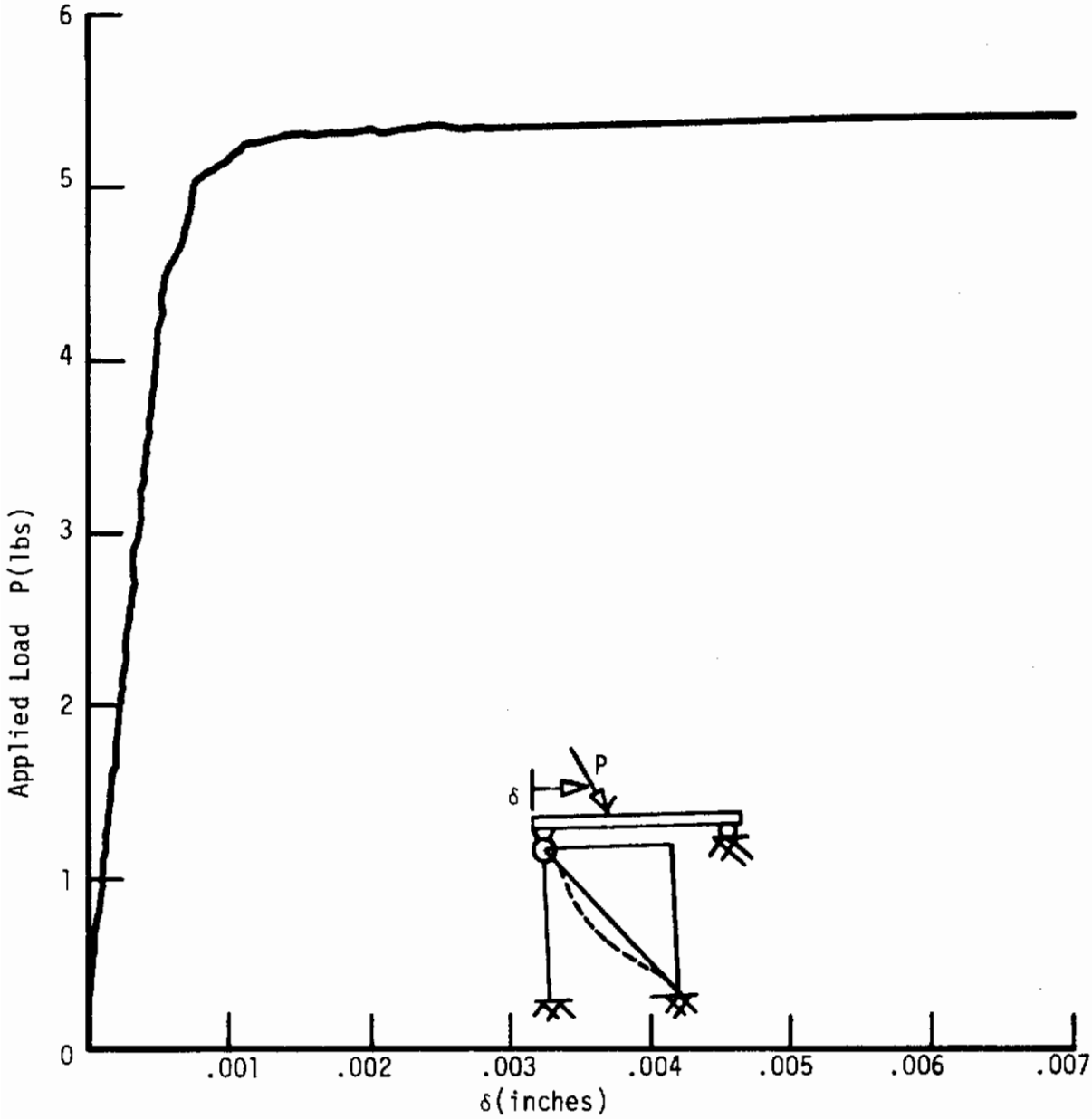

Fig. 51 Load Deflection Results for Test Number 3 on the Planar Braced Frame

Approved for Public Release

Contrails

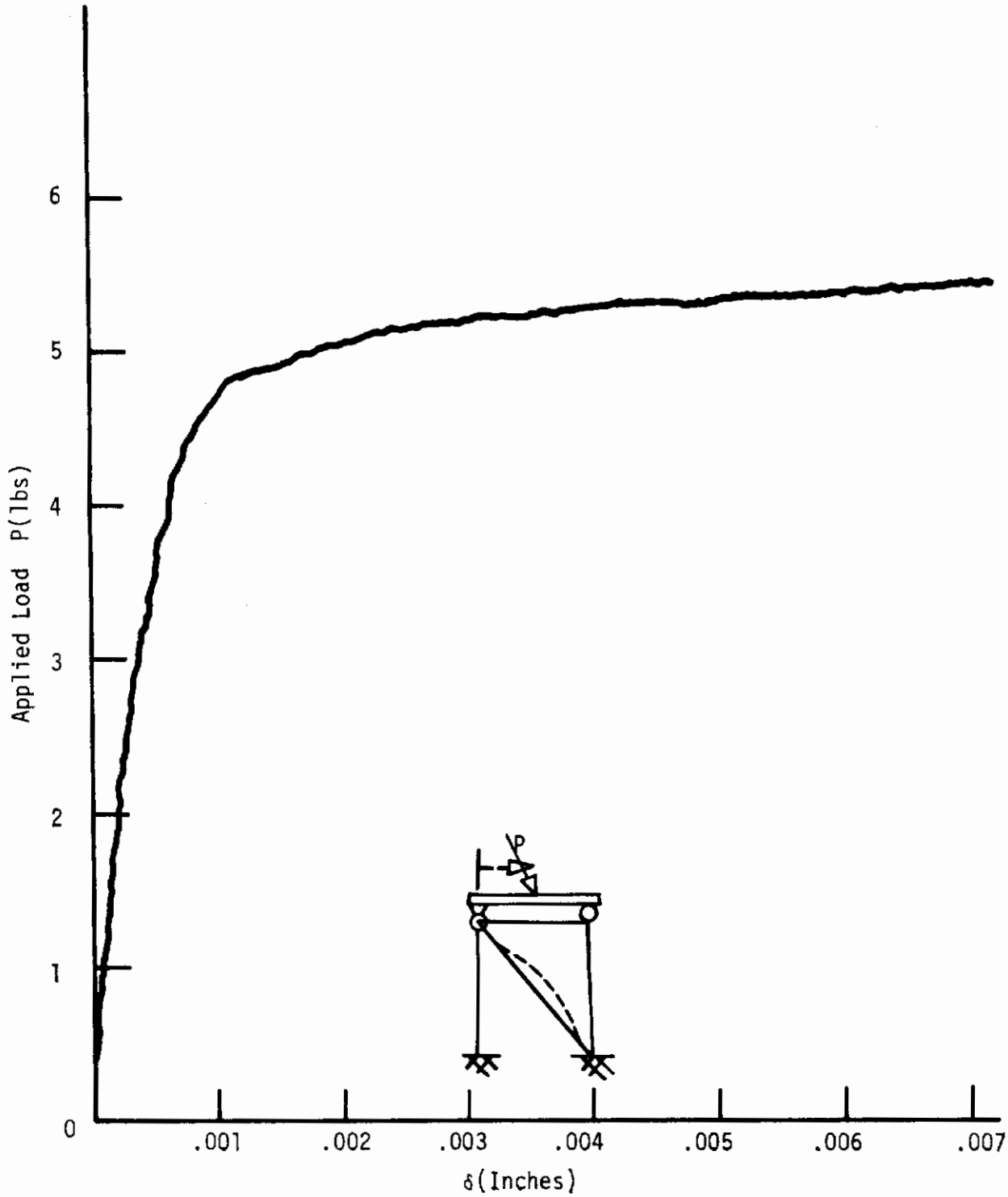

Fig. 52 Load Deflection Results for Test Number 4 on the Planar Braced Frame.

Approved for Public Release

Contrails

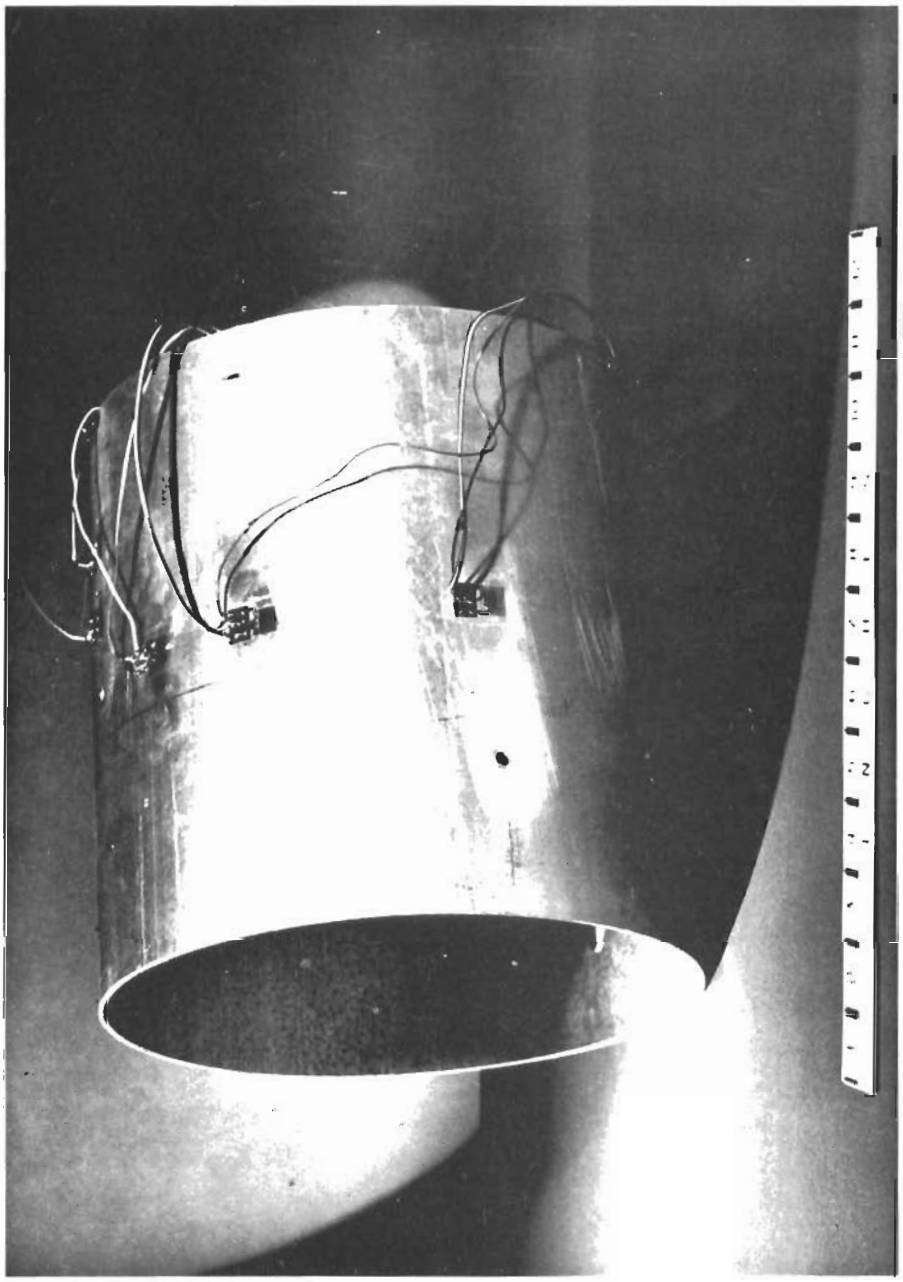

Fig. 53 Pinched Cylinder Specimen, Outer Strain Gages.

Approved for Public Release

Contrails

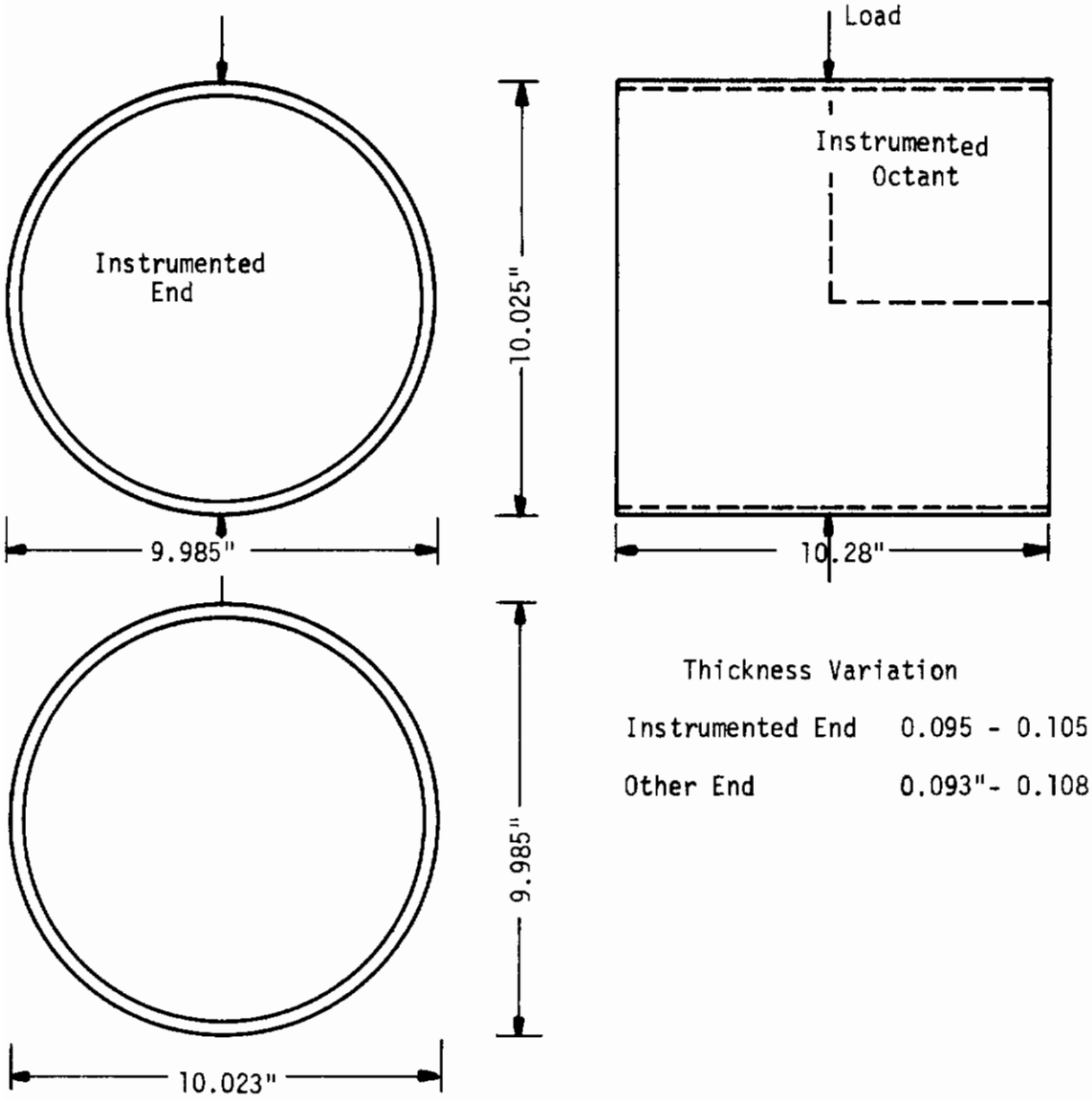

Thickness Variation

Instrumented End	0.095 - 0.105
Other End	0.093"- 0.108

Imperfections 5 - 0.025" Holes at Various Locations

Material - Aluminum - Unknown Properties

Fig. 54 Pinched Cylinder, Dimensions, Details and Loads

Approved for Public Release

Contrails

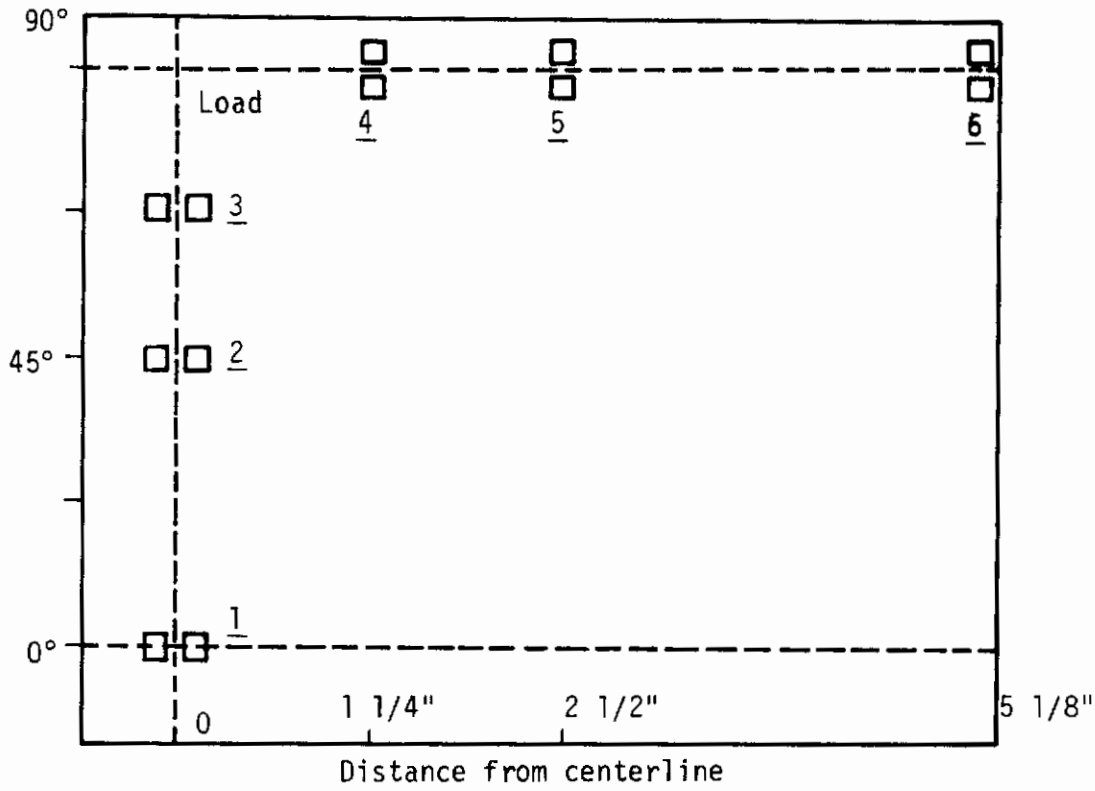

Flattened Side View of Instrumented Octant, Top Surface

□□ Indicates two element, quarter inch rosette.

NOTE: Strain gage rosettes were applied to the inner surface of the specimen, directly back to back of the outer rosettes.

Rosette Number	Comparable Inside Rosette
1	7
2	8
3	9
4	10
5	11
6	12

Fig. 55 Pinched Cylinder Strain Gage Orientation

Approved for Public Release

Contrails

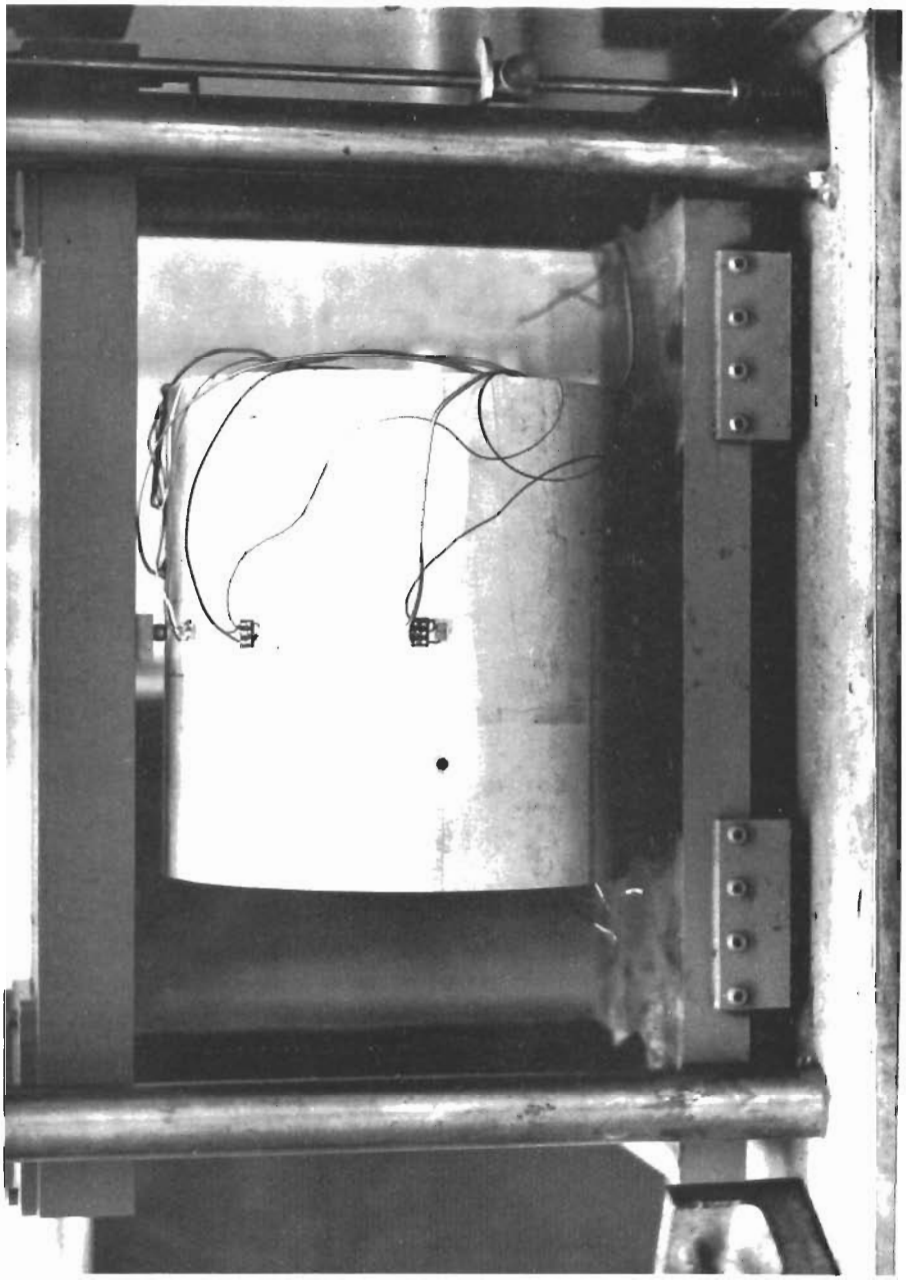

Fig. 56 Pinched Cylinder Undergoing Test.

Approved for Public Release

Contrails

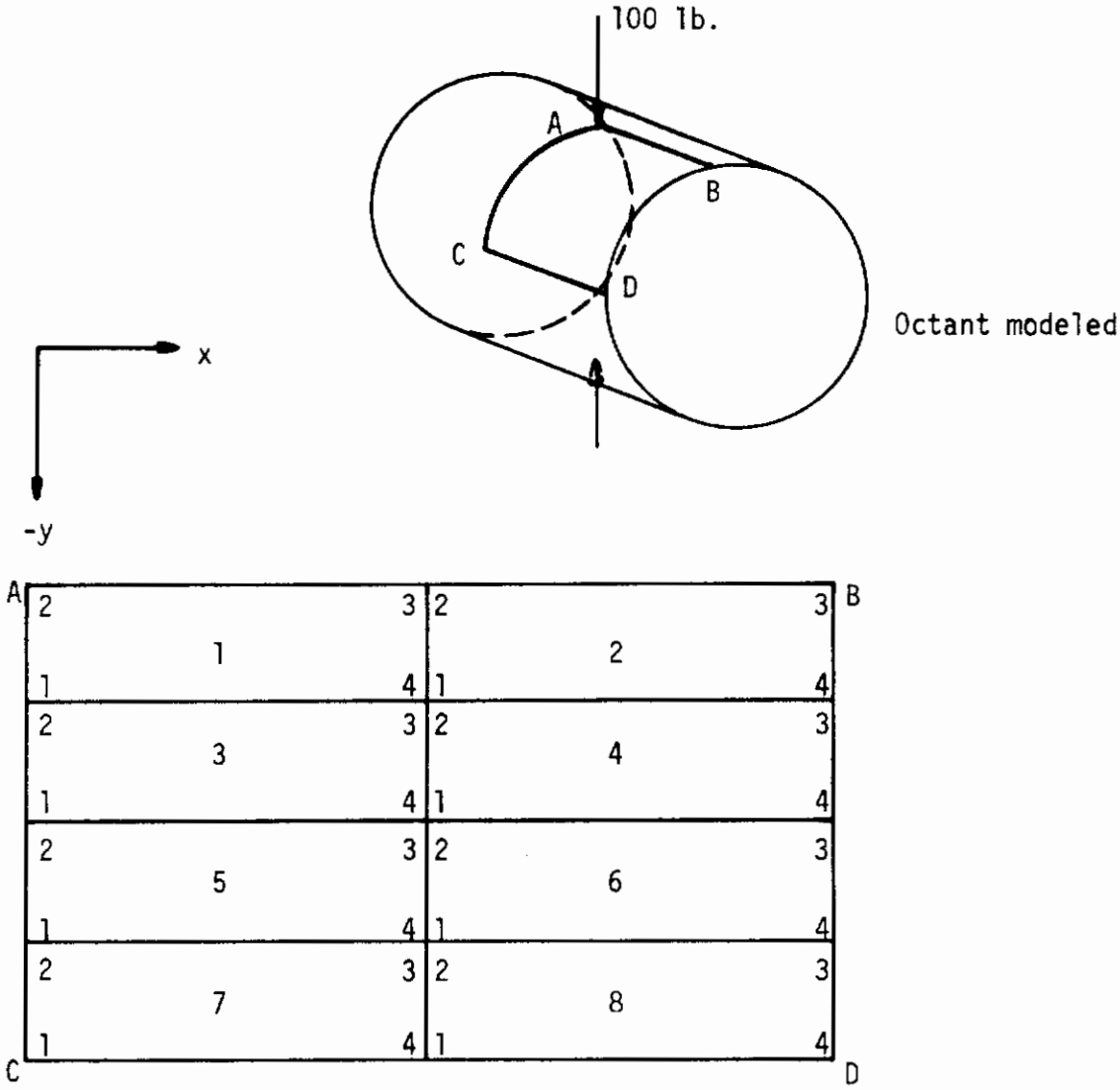

Fig. 57 Finite Element Representation of Pinched Cylinder

Approved for Public Release

Contrails

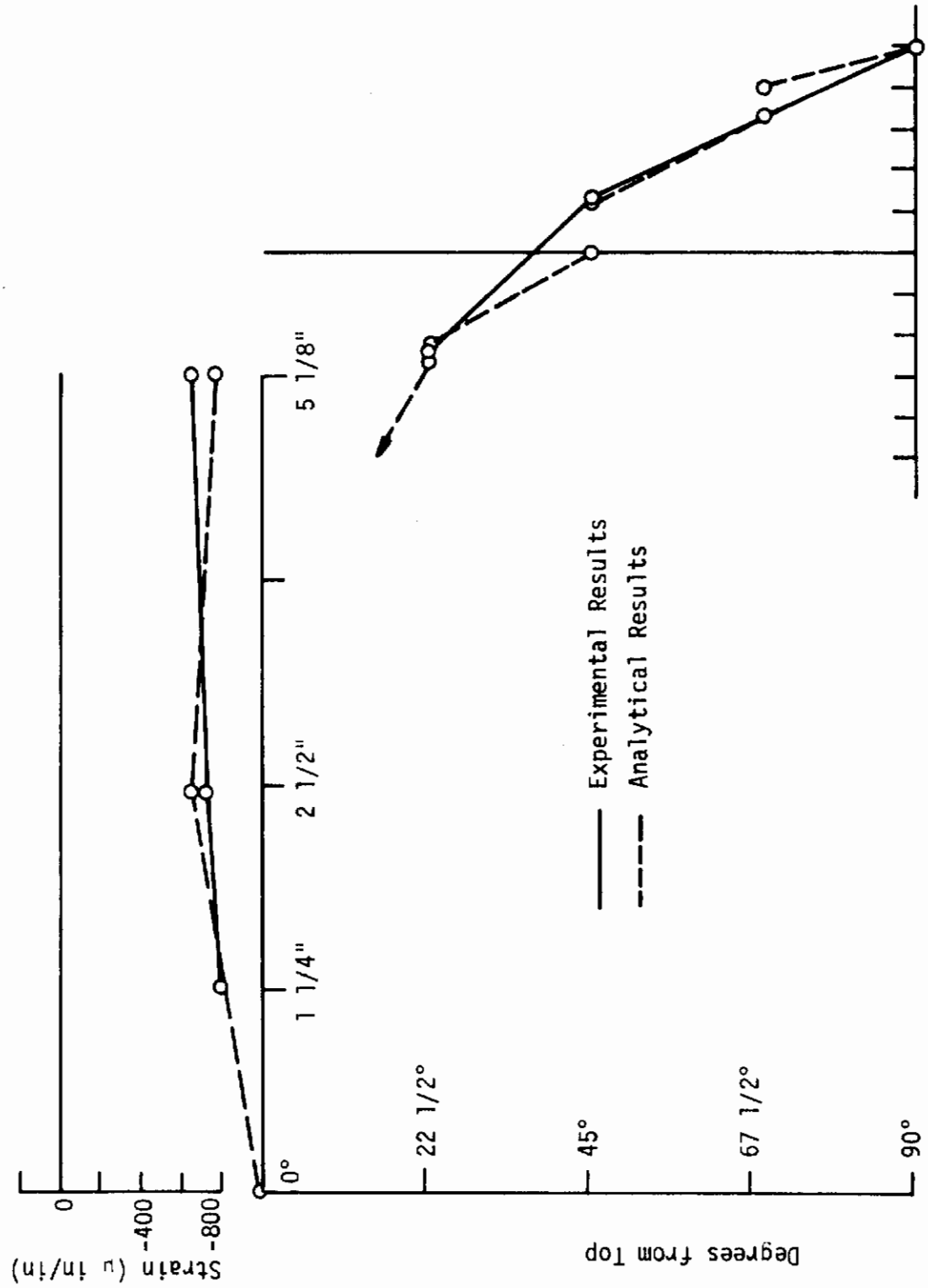

Fig. 58 Strains on Outer Surface of Pinched Cylinder, Circumferential Direction

Approved for Public Release

Contrails

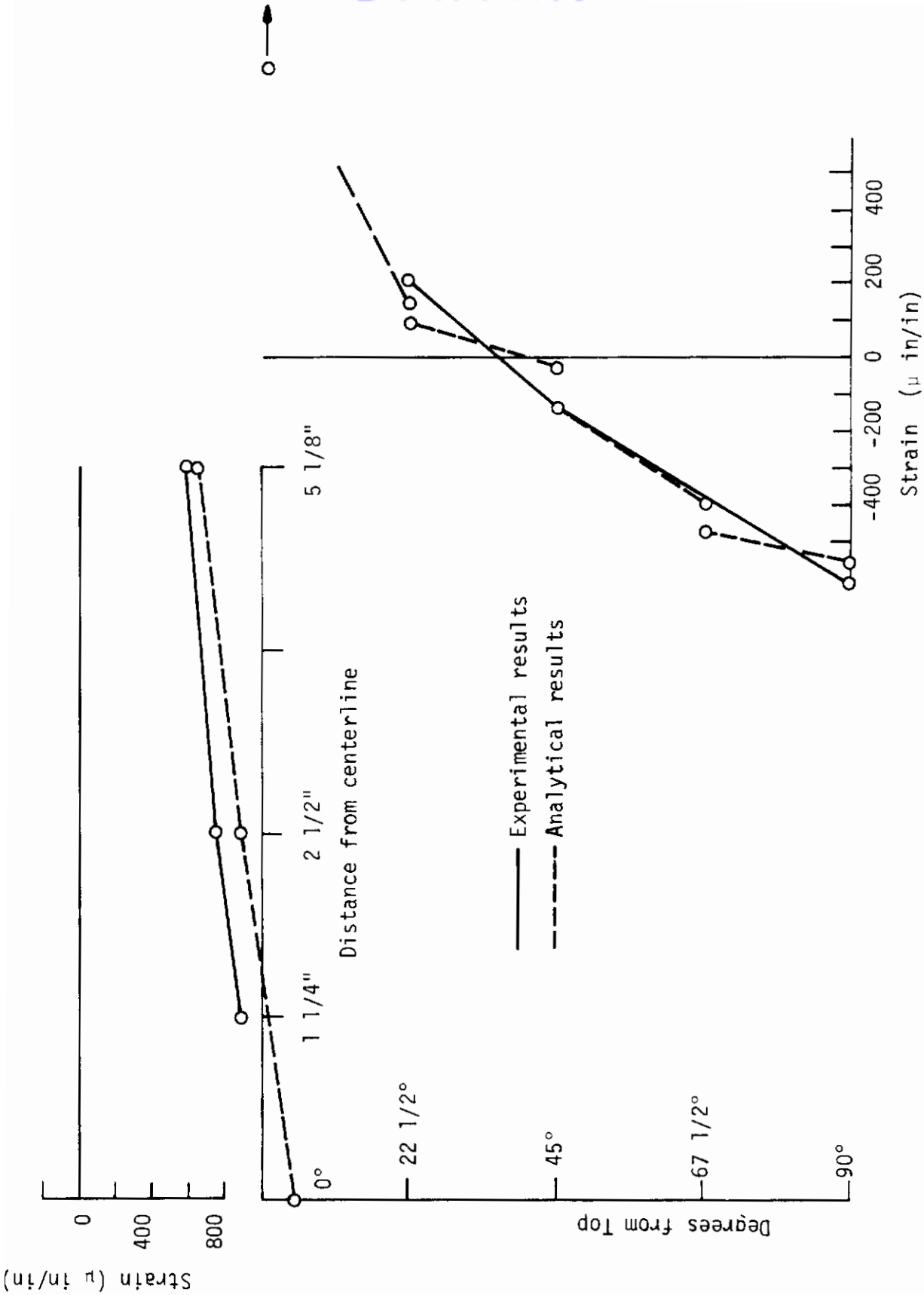

Fig. 59 Strains on Inner Surface of Pinched Cylinder, Circumferential Direction

Approved for Public Release

Contrails

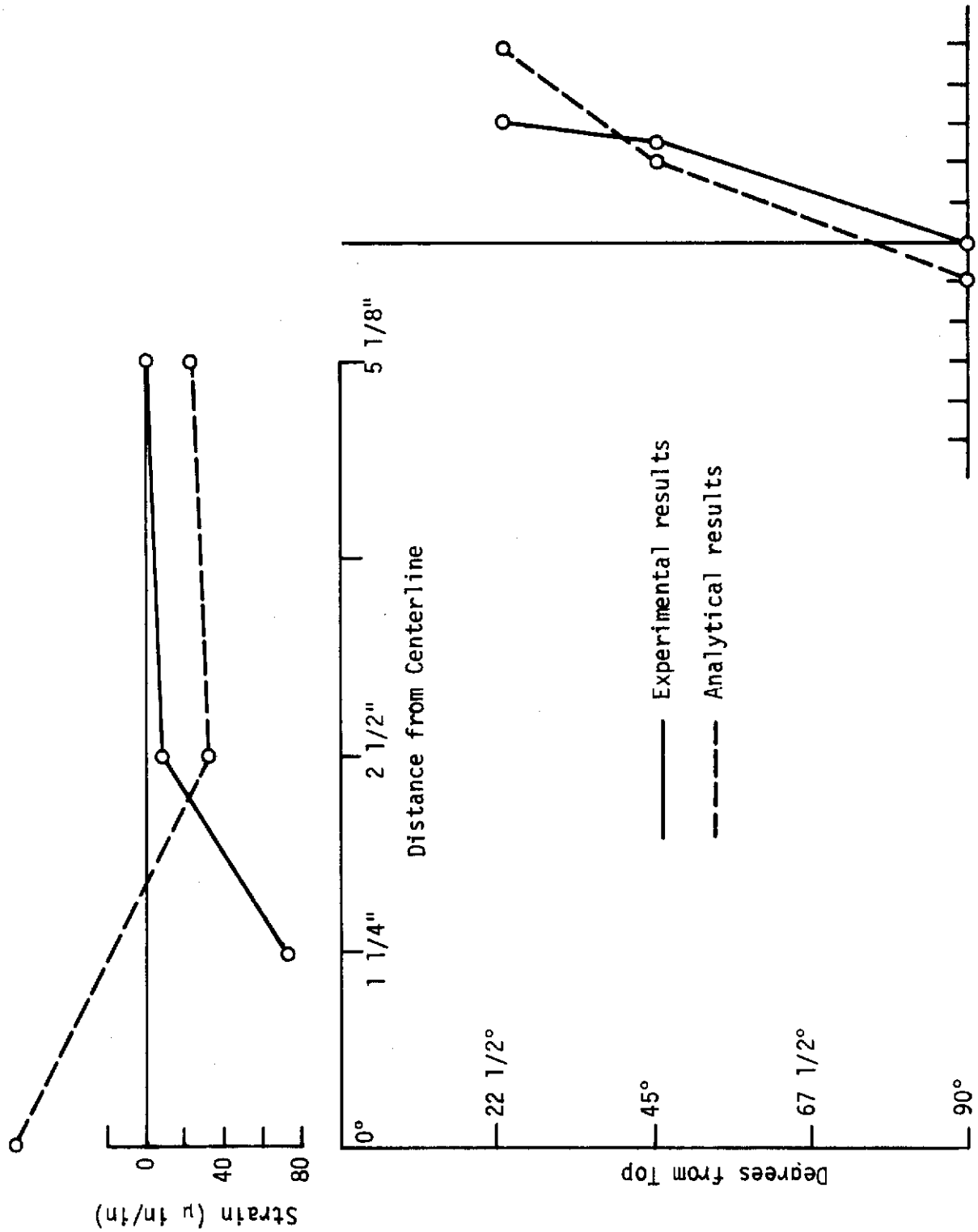

Fig. 60 Strains on Middle Surface of Pinched Cylinder, Longitudinal Direction

Approved for Public Release

Contrails

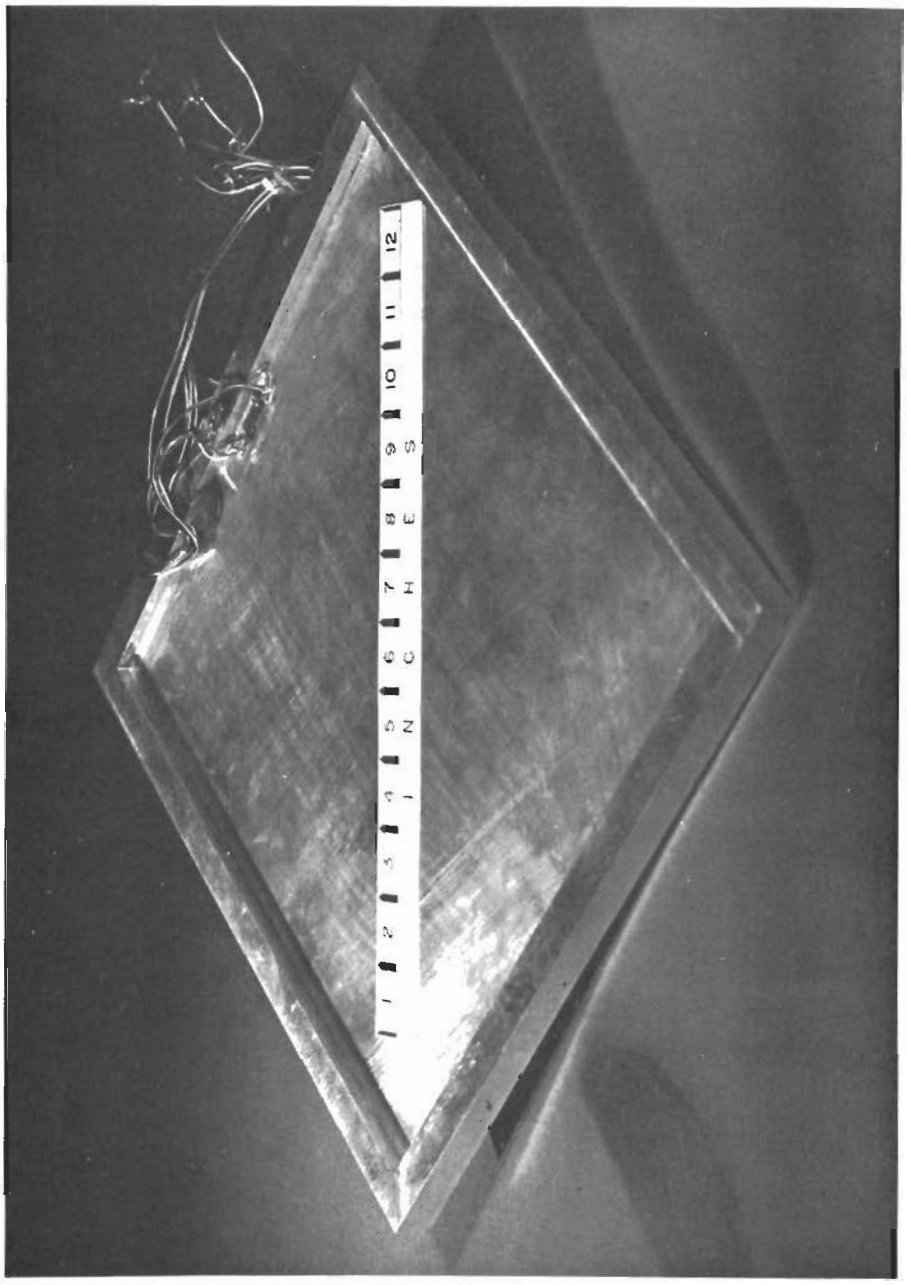

Fig. 61 Rectangular Plate with Elastic Edge Beams, Transverse Loading.

Approved for Public Release

Contrails

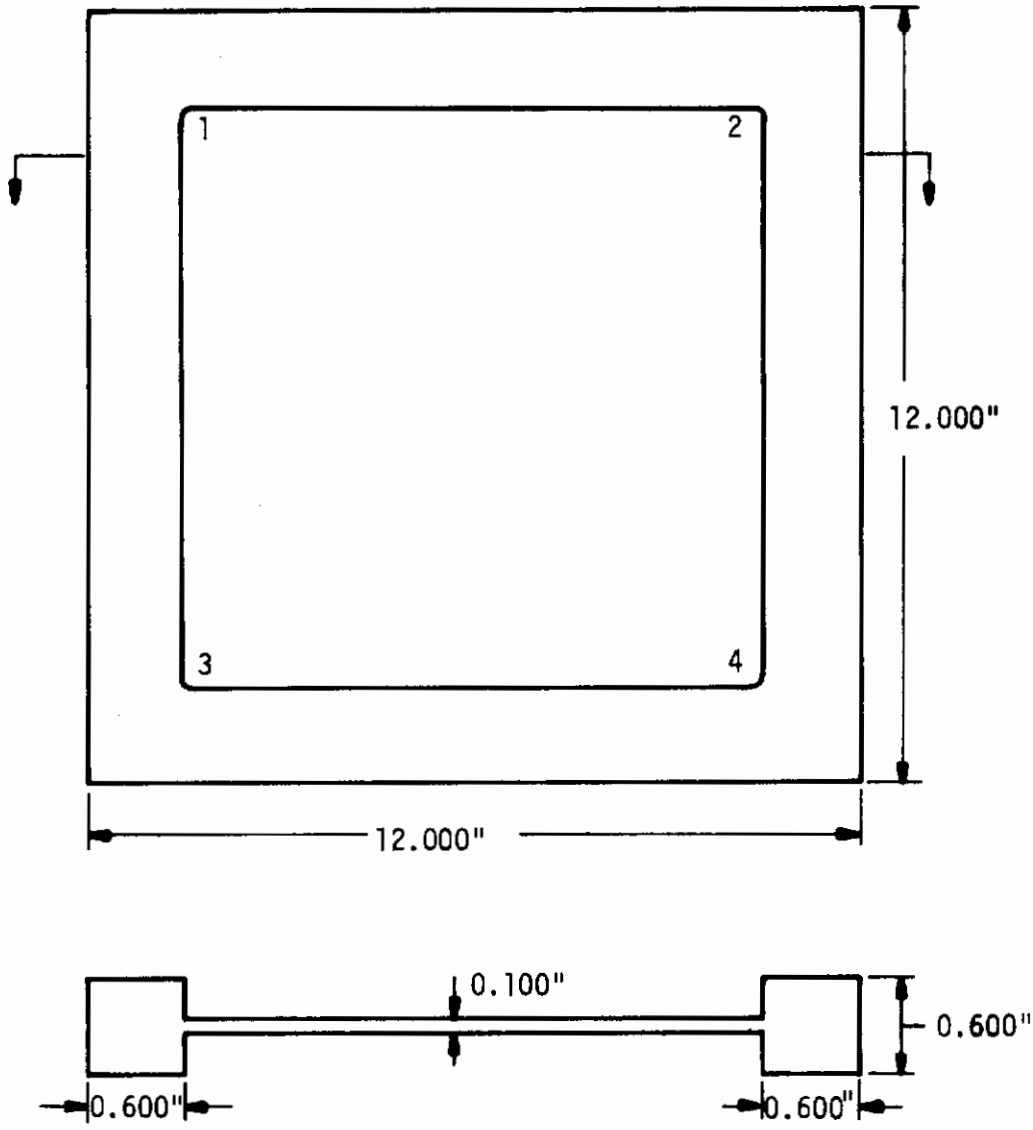

Edge beam 0.600 x 0.600 throughout

Plate Thickness (in)	Quadrant
0.100	1
0.100	2
0.100	3
0.100	4
Vertical fillets	1/8" radius

Fig. 62 Rectangular Plate, Details and Dimensions

Approved for Public Release

Contrails

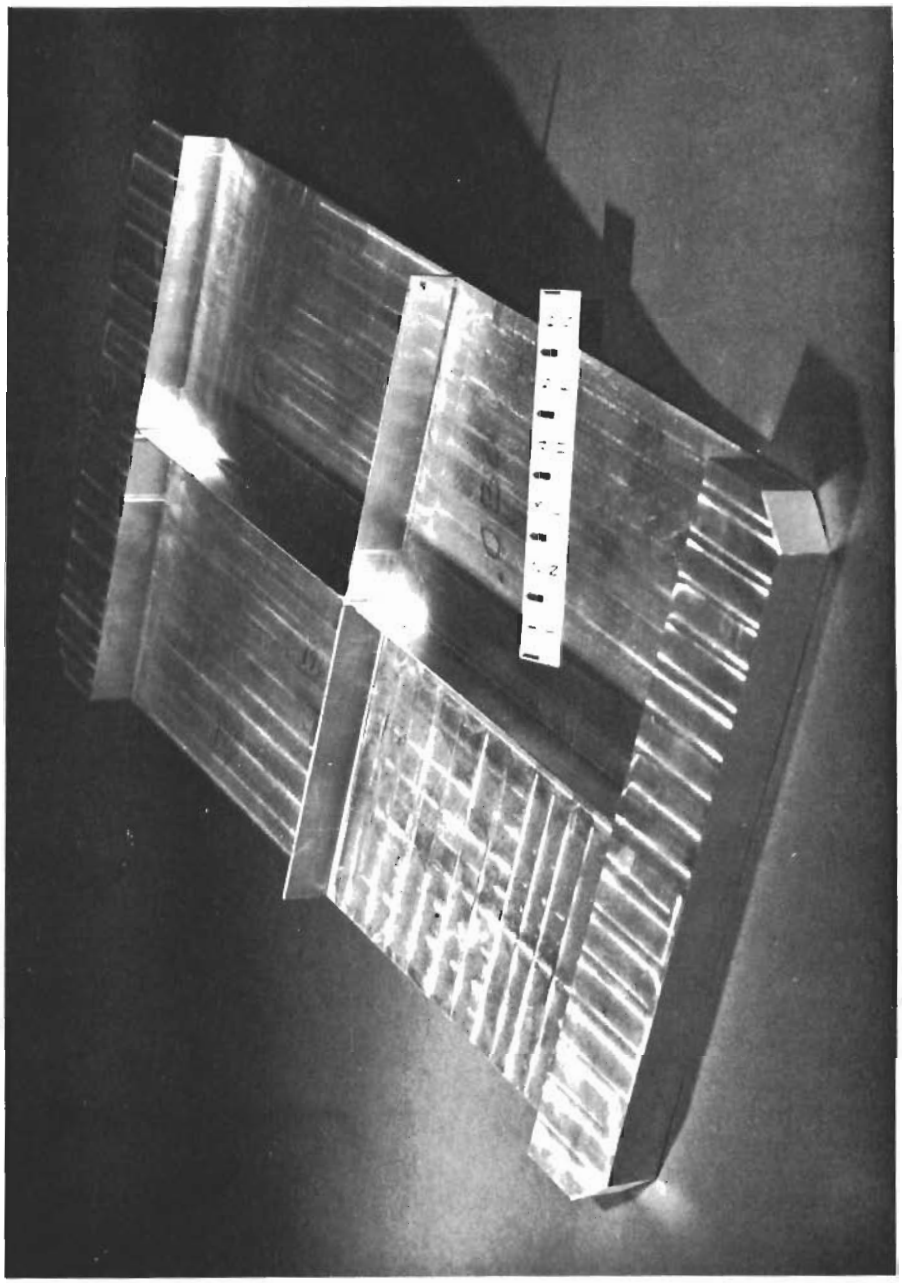

Fig. 63 Stiffened Plate Number 1, One Longitudinal Stiffener, One Transverse Stiffener, Transverse Loads.

Approved for Public Release

Contrails

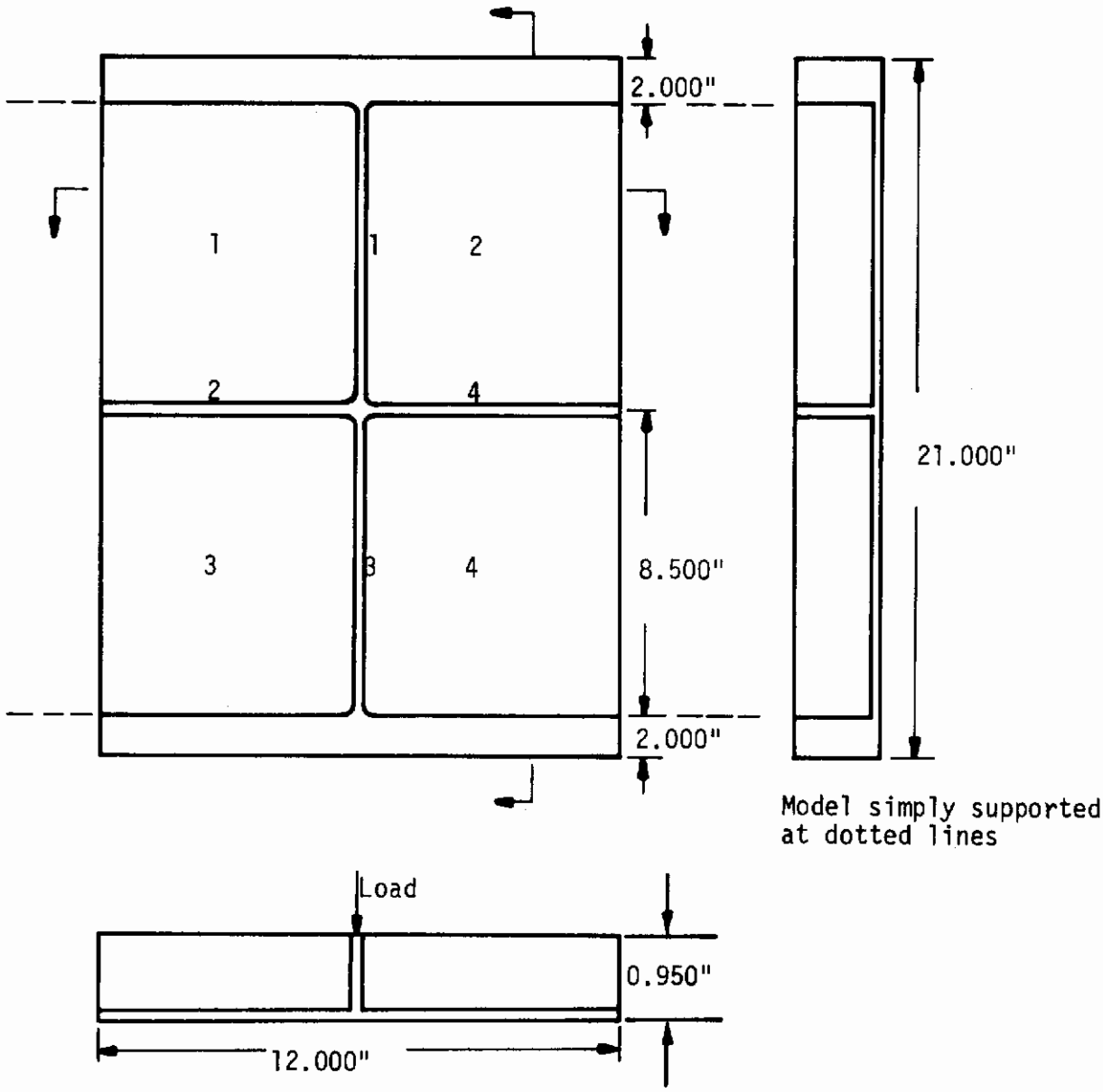

	Dimensions	Thickness (in)
Stiffener	1	0.030
	2	0.075
	3	0.030
	4	0.075
Plate Panel	1	0.050
	2	0.050
	3	0.050
	4	0.050

Vertical fillets 1/8" radius

Fig. 64 Stiffened Plate Number 1, Dimensions, Details and Loads.

Approved for Public Release

Contrails

Fig. 65 Stiffened Plate No. 2, Two Longitudinal Stiffeners, One Transverse Stiffener, Transverse Loads.

Approved for Public Release

Contrails

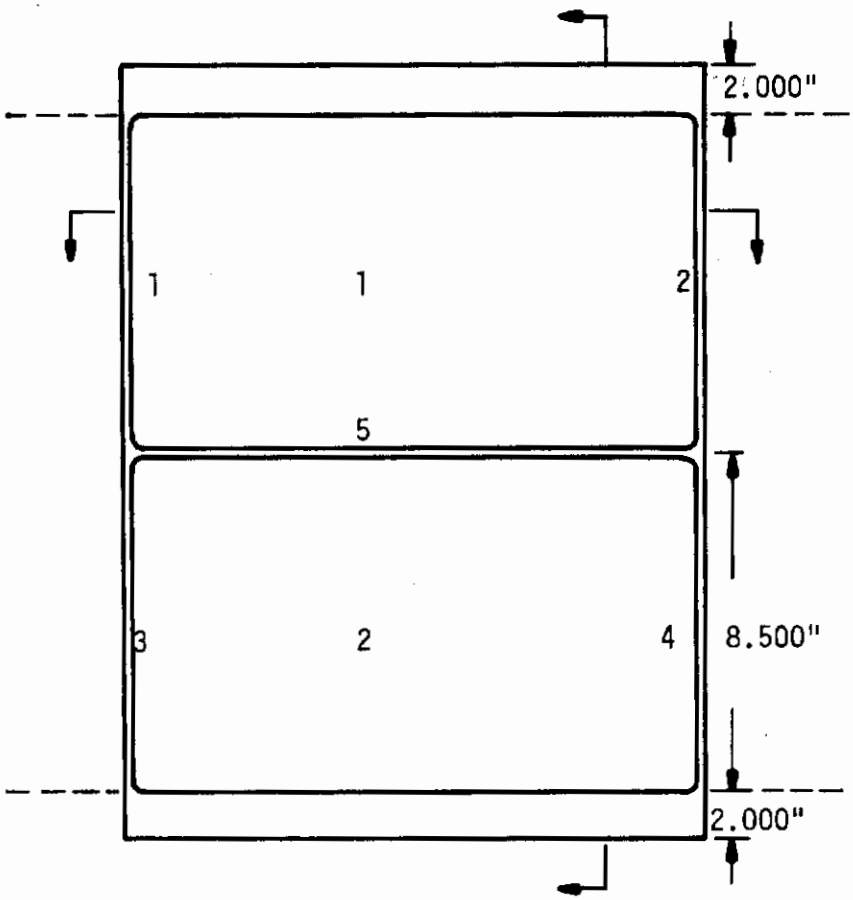

Two equal loads

Model simply supported at dotted lines

Dimensions		Thickness (in)
Stiffener	1	0.030
	2	0.030
	3	0.030
	4	0.030
	5	0.060
Plate Panel	1	0.050
	2	0.050

Vertical fillets 7/16" radius

Overall height variation - NIL

Fig. 66 Stiffened Plate Number 2, Details, Dimensions and Loads

Approved for Public Release

Contrails

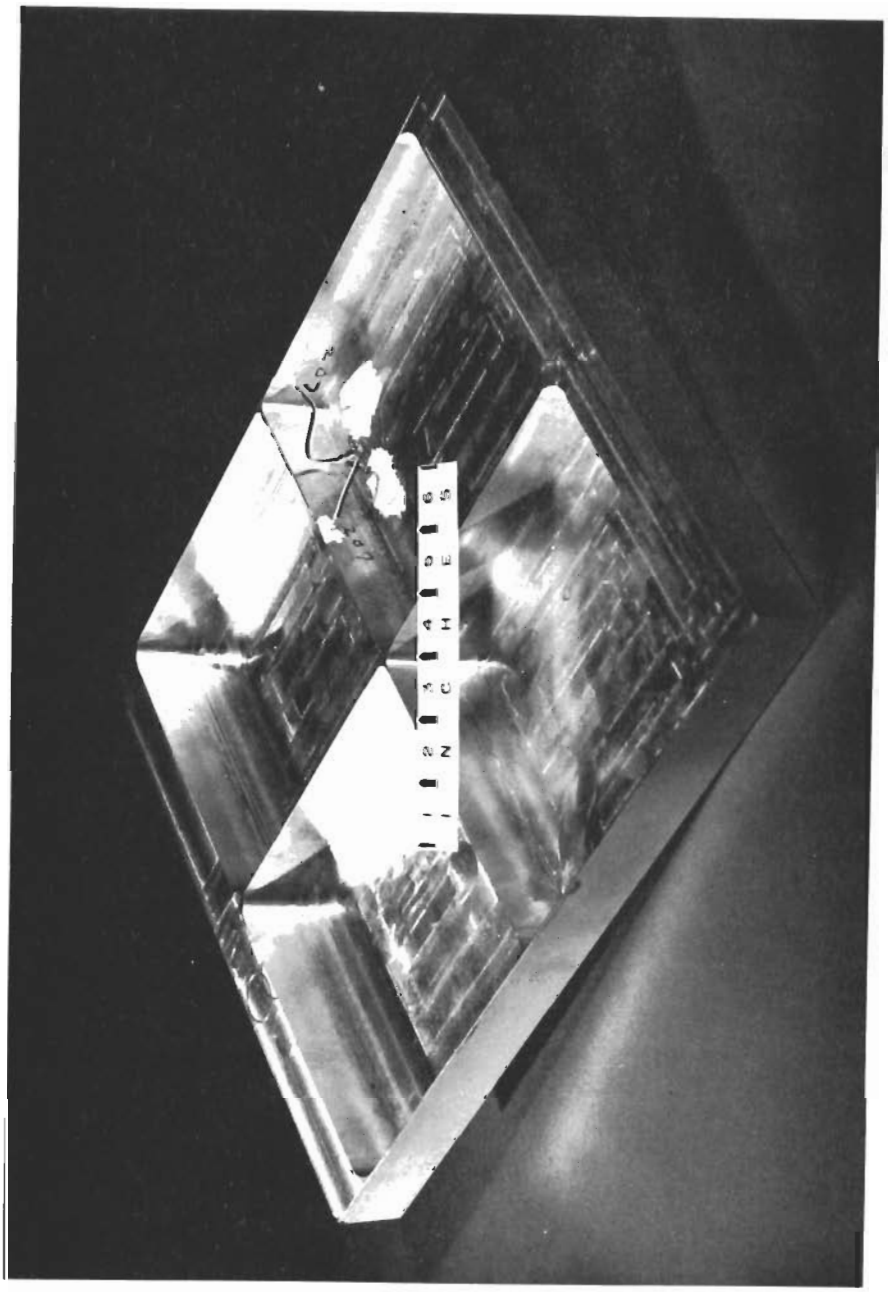

Fig. 67 Stiffened Plate No. 3, Three Longitudinal Stiffeners, One Transverse Stiffener, Transverse Loads.

Approved for Public Release

Contrails

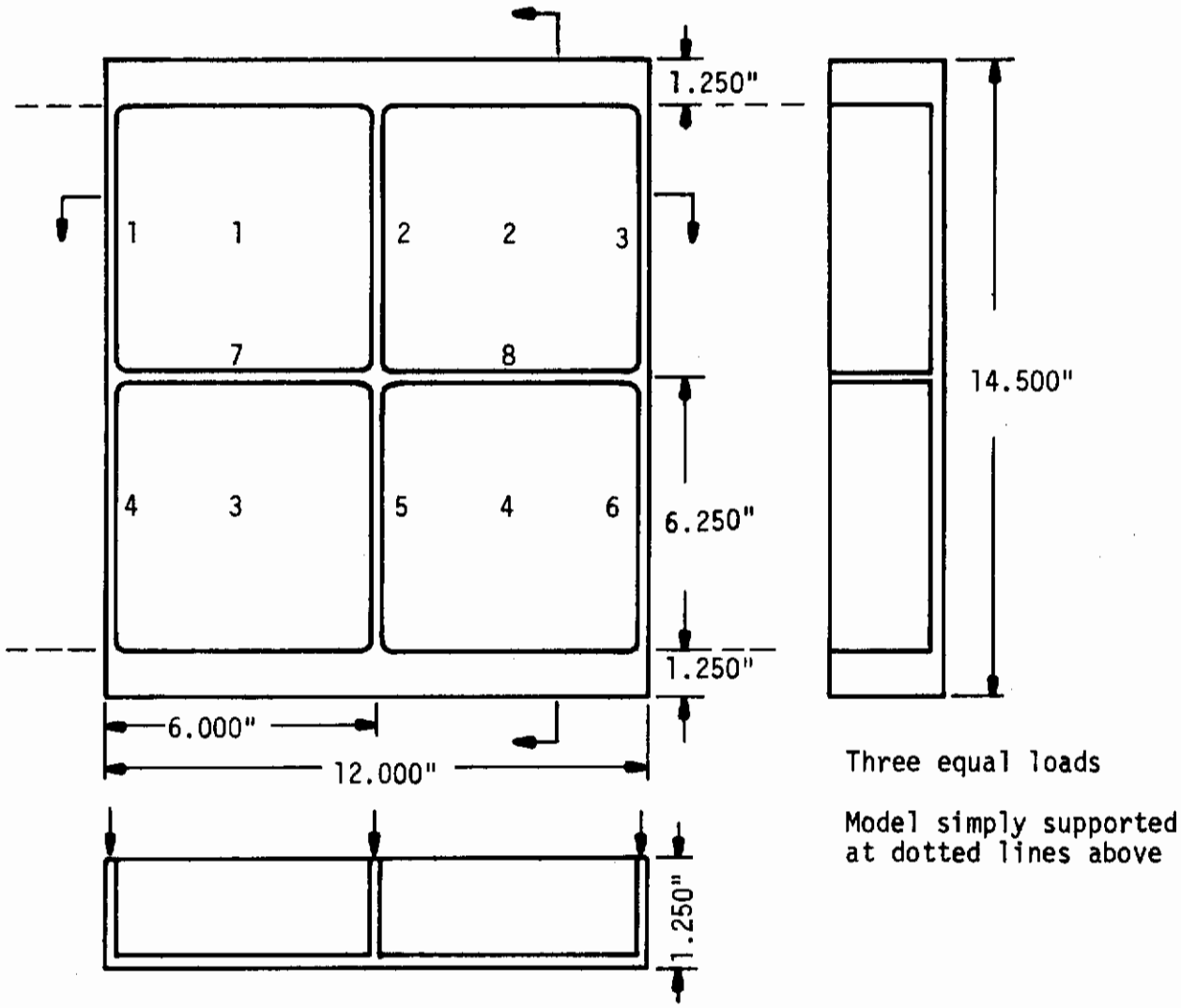

	Dimensions	Thickness (in)
Stiffener	1	0.040
	2	0.040
	3	0.040
	4	0.040
	5	0.040
	6	0.040
	7	0.040
	8	0.040
Plate Panel	1	0.100
	2	0.100
	3	0.100
	4	0.100

Vertical fillets.

Center span	3/16" radius
ends	7/16" radius

Fig. 68 Stiffened Plate Number 3, Details, Dimensions and Loads.

Approved for Public Release

Contrails

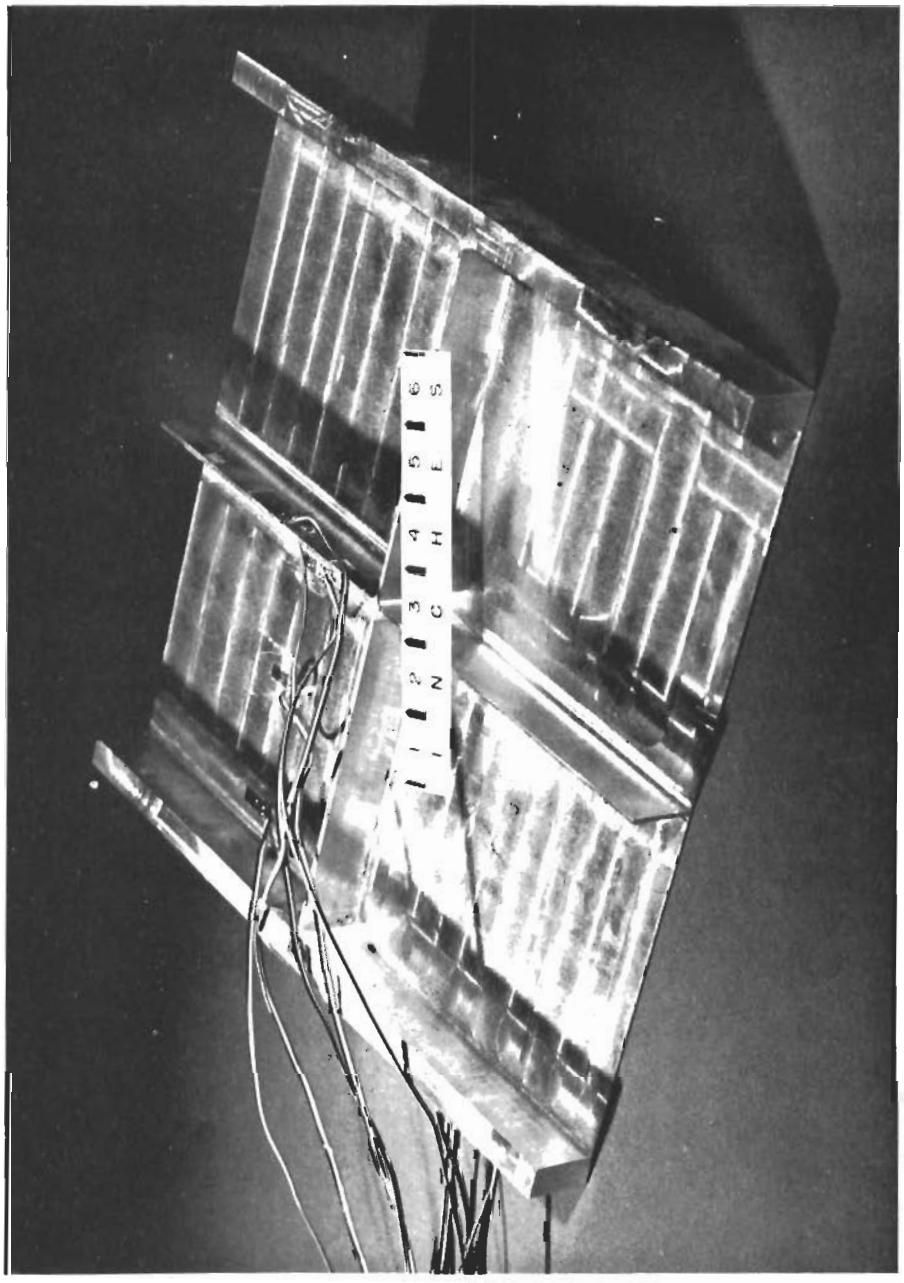

Fig. 69 Stiffened Plate No. 4, One Vertical Stiffener, One Horizontal Stiffener, Inplane Loads.

Approved for Public Release

Contrails

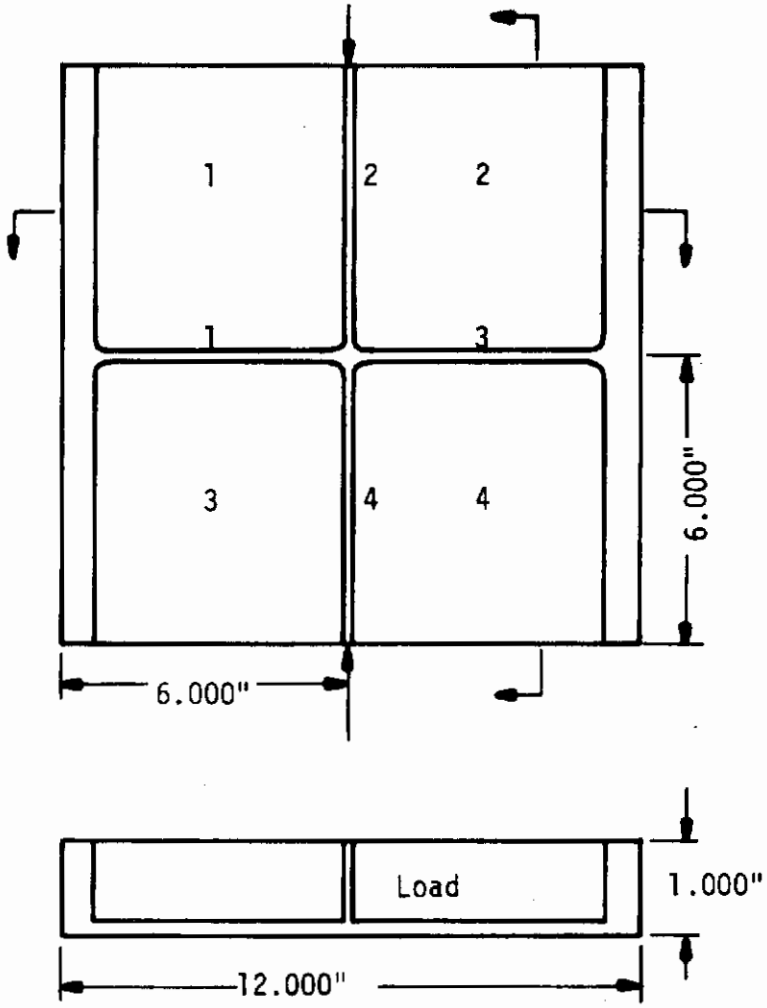

Nominal stiffener dimensions 0.950" x 0.075"

Dimensions		Thickness (in)
Left edge beam		0.500
right edge beam		0.500
Stiffener	1	0.075
	2	0.075
	3	0.075
	4	0.075
Plate Panel	1	0.050
	2	0.050
	3	0.050
	4	0.050

Vertical fillets 1/8" radius

No initial measurable imperfections in stiffeners.

Fig. 70 Stiffened Plate Number 4, Details, Dimensions and Loads.

Approved for Public Release

Contrails

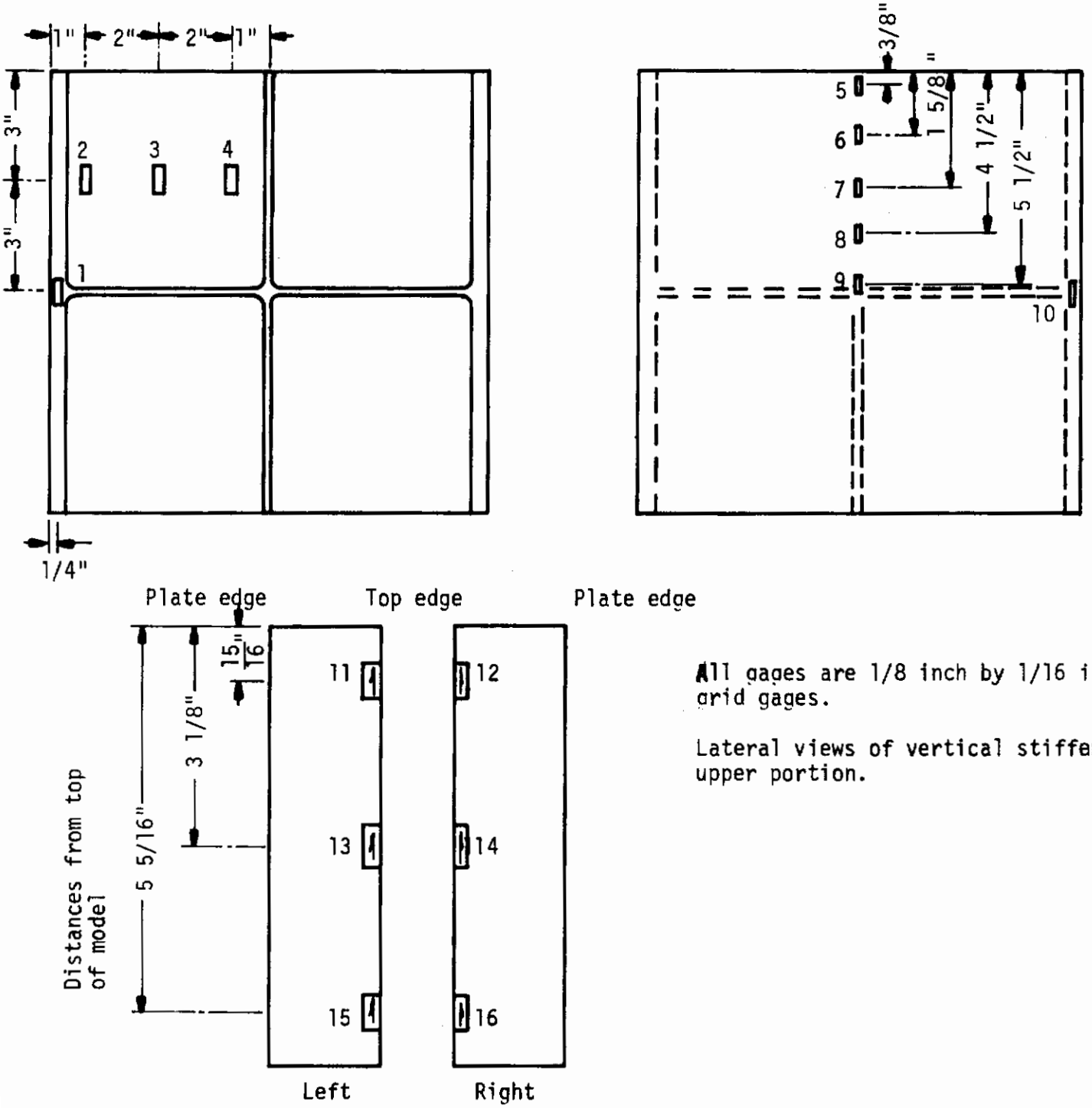

All gages are 1/8 inch by 1/16 inch grid gages.

Lateral views of vertical stiffener upper portion.

Fig. 71 Strain Gage Orientation, Stiffened Plate No. 4

Approved for Public Release

Contrails

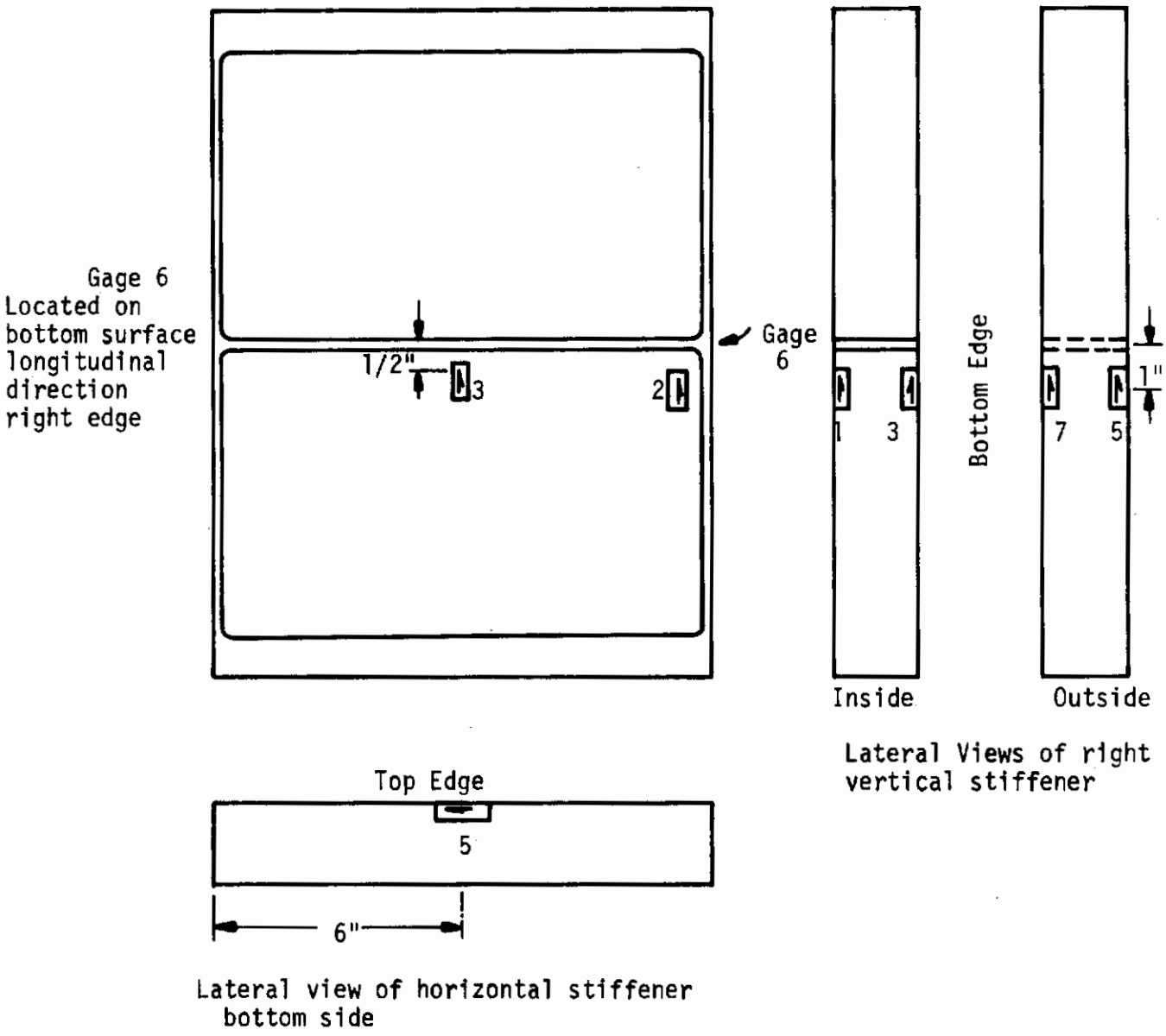

Fig. 72 Strain Gage Orientation, Stiffened Plate No. 2.

Approved for Public Release

Contrails

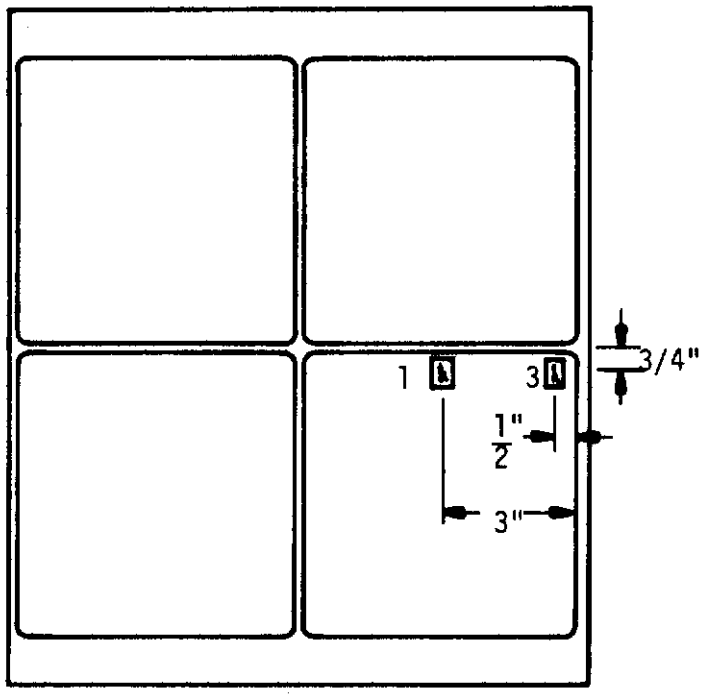

Right side of model

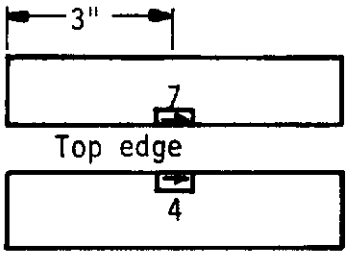

Lateral view of right horizontal stiffener

all gages are 1/8 inch by 1/16 grid gages.

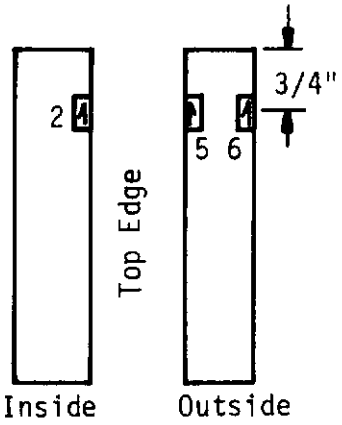

Lateral views of right vertical stiffener, lower half

Fig. 73 Strain Gage Orientation, Stiffened Plate No. 3.

Approved for Public Release

Contrails

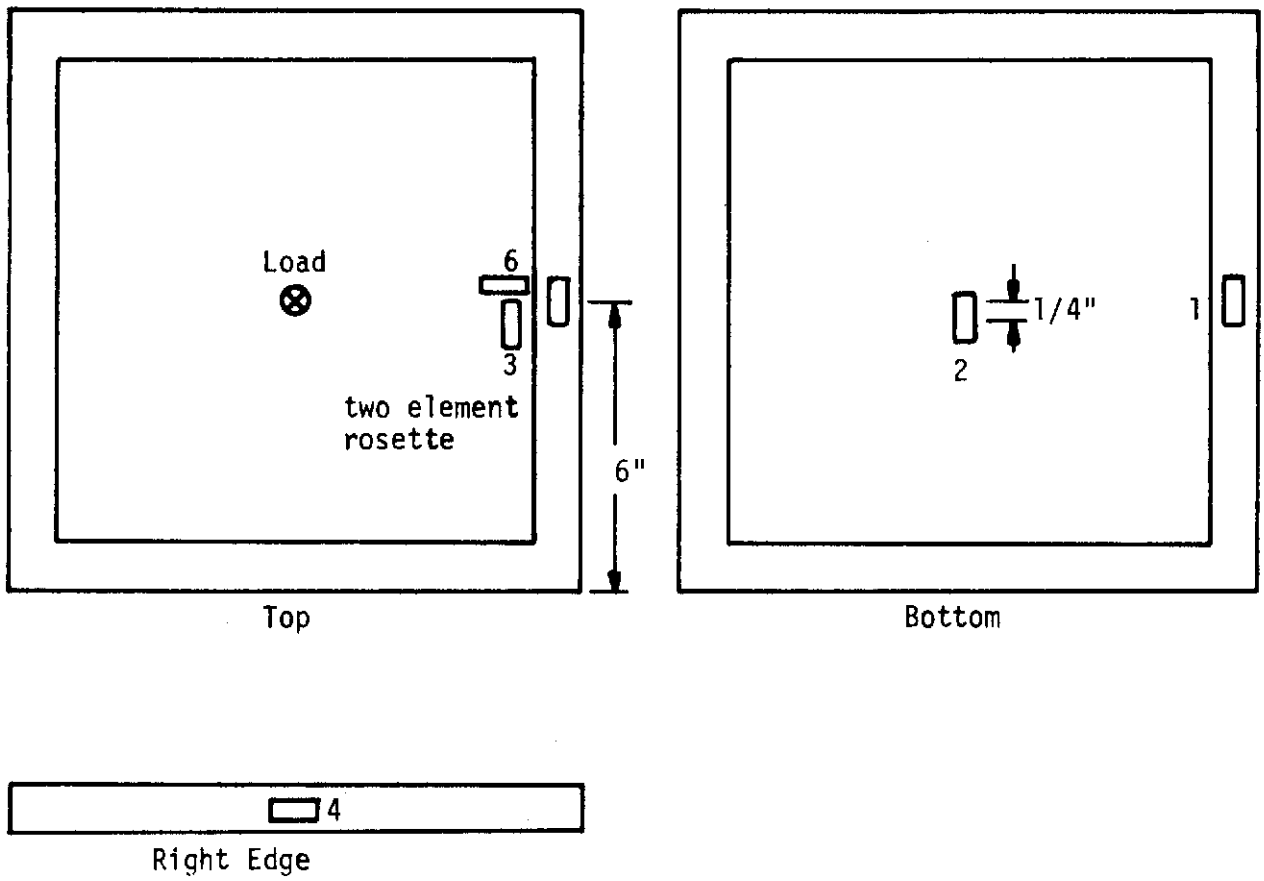

All strain gages on this model were 1/4 inch square grid.

Fig. 74 Strain Gage Orientation, Rectangular Plate

Approved for Public Release

Contrails

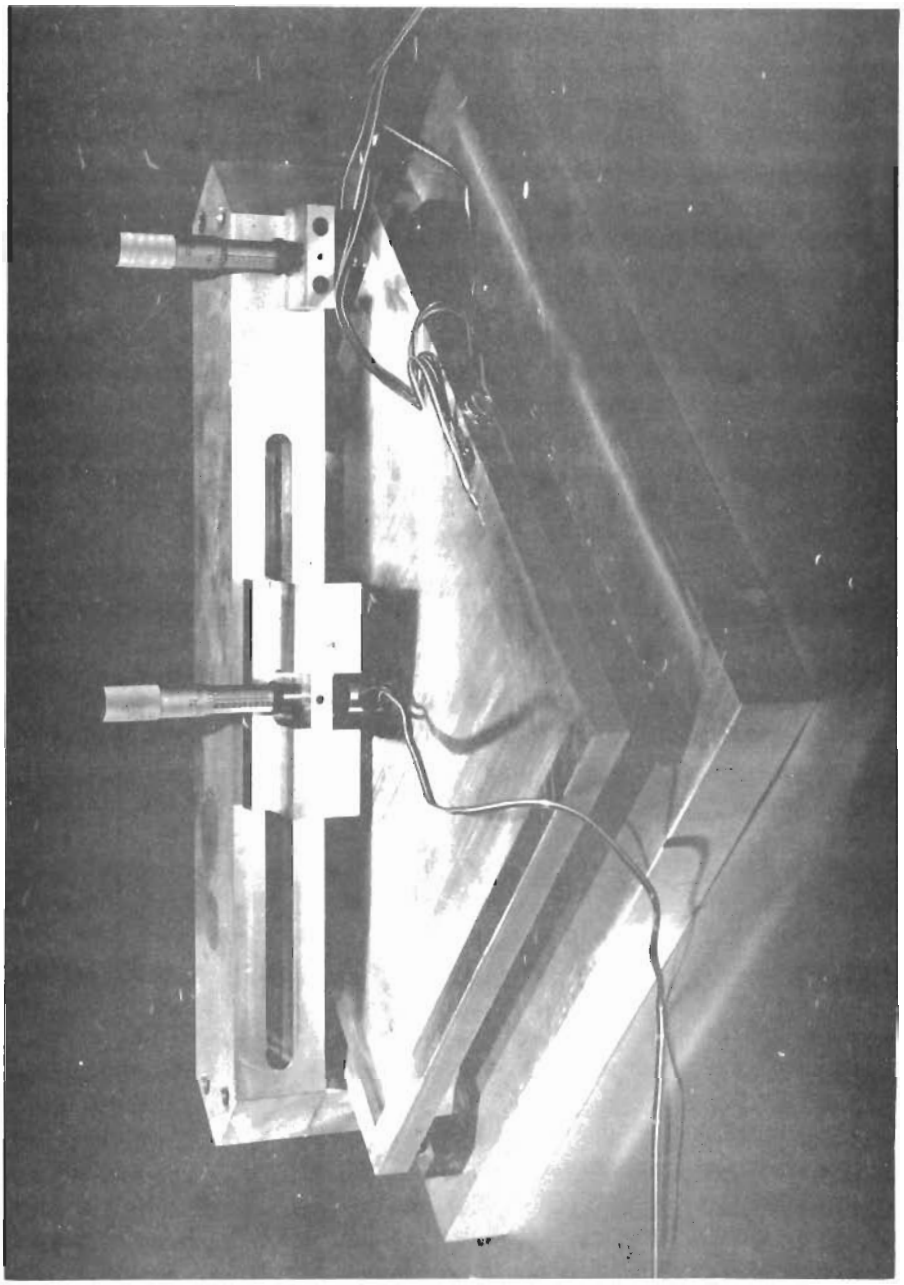

Fig. 75 Rectangular Plate in Test Fixture.

Approved for Public Release

Contrails

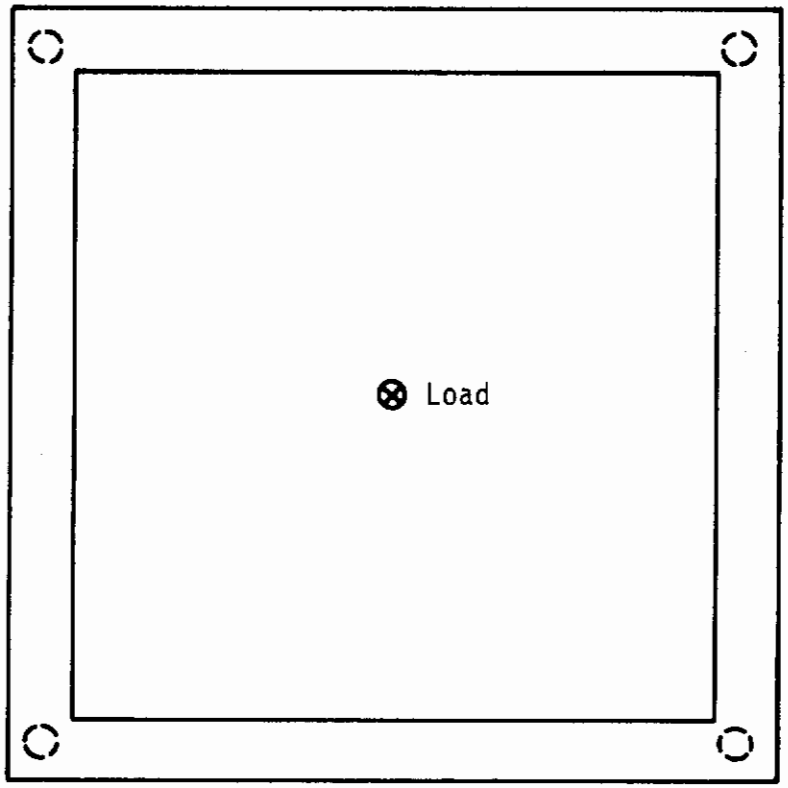

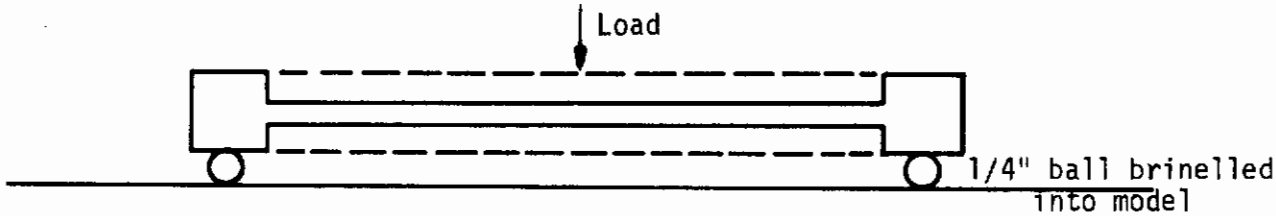

Deflection measured at load point with micrometer screw, other points with dial indicator.

Lateral contraction measured with vernier caliper.

Fig. 76 Test Orientation and Loads, Rectangular Plate

Approved for Public Release

Contrails

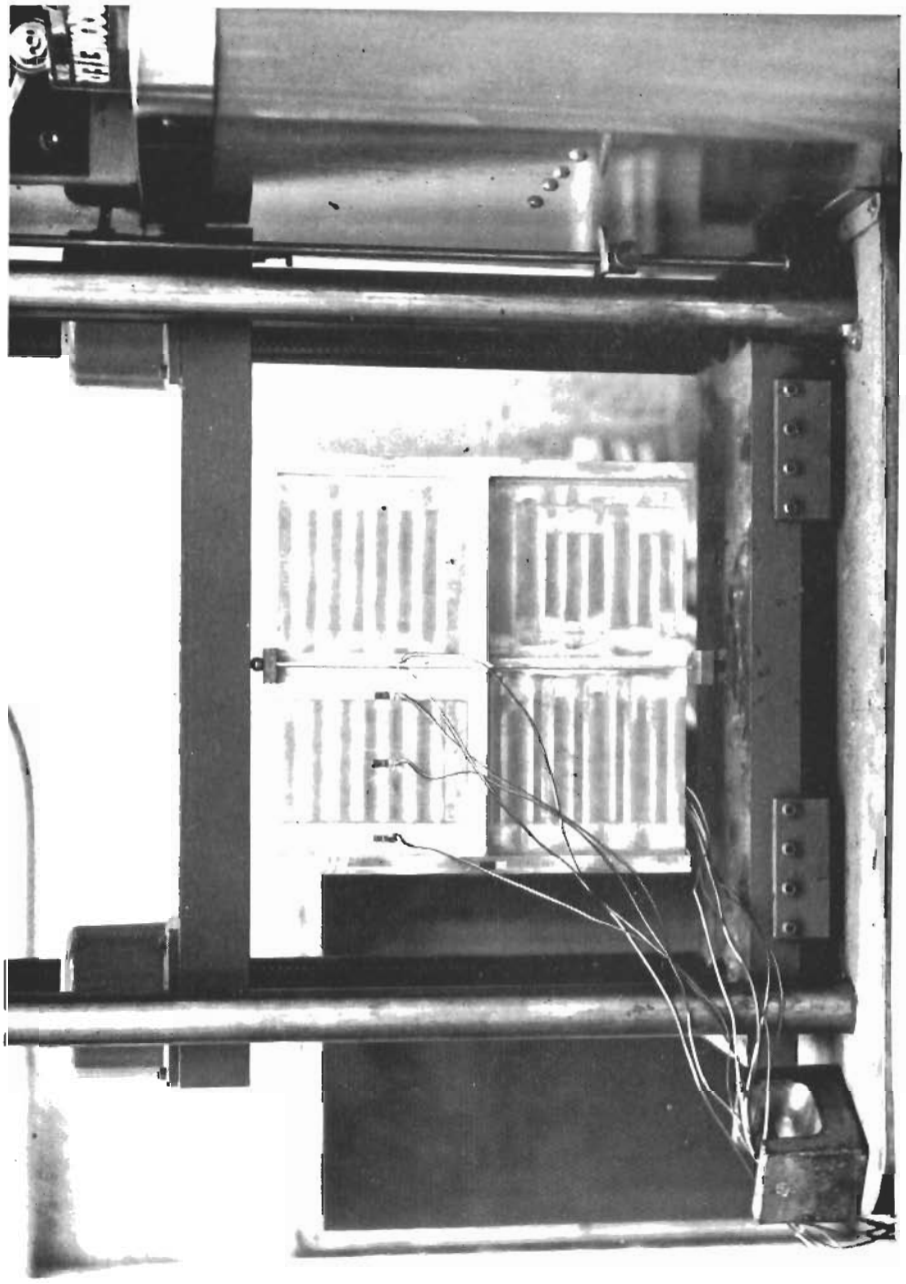

Fig. 77 Stiffened Plate No. 4, Inplane Load Test.

Approved for Public Release

Contrails

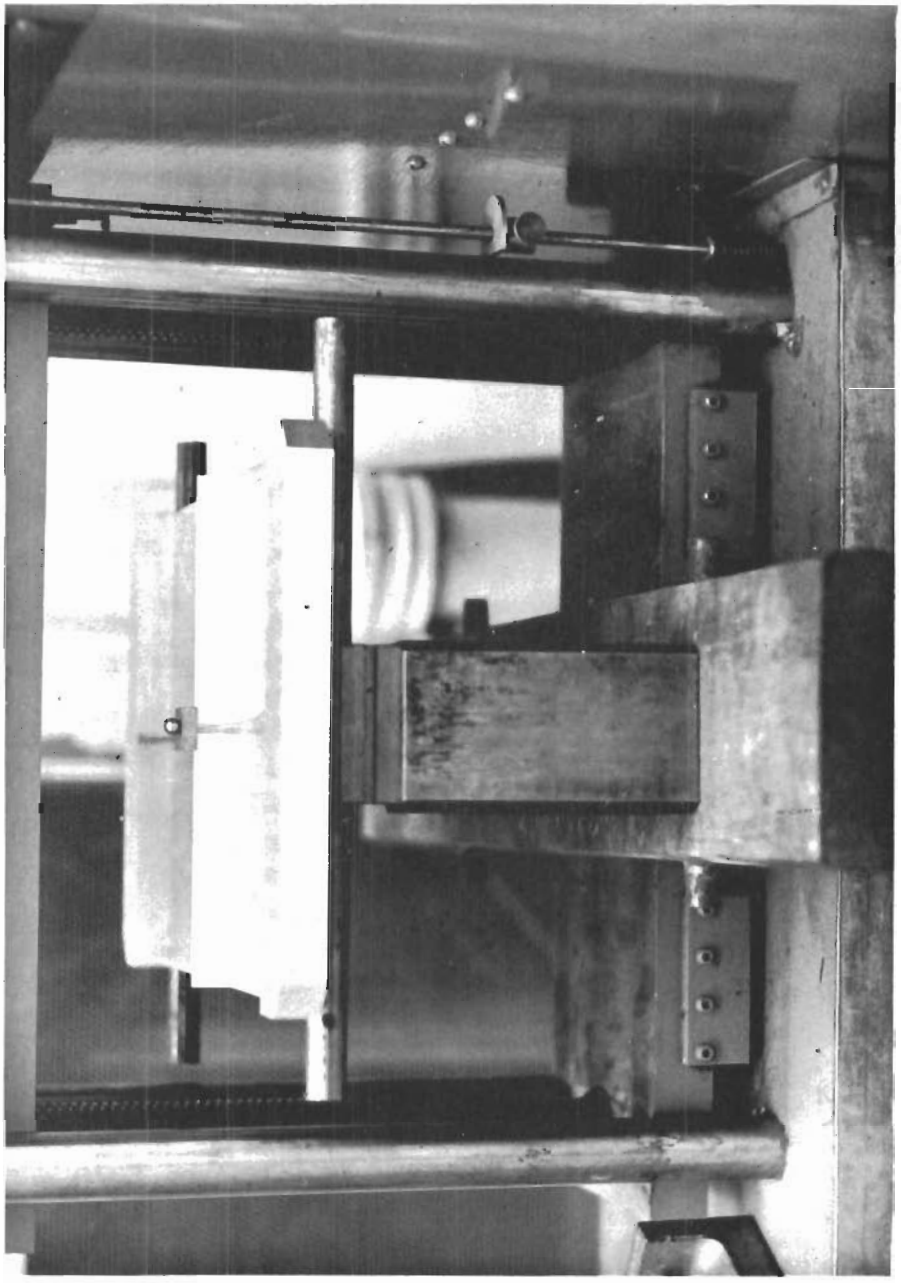

Fig. 78 Stiffened Plate No. 1, Transverse Load Test.

Approved for Public Release

Contrails

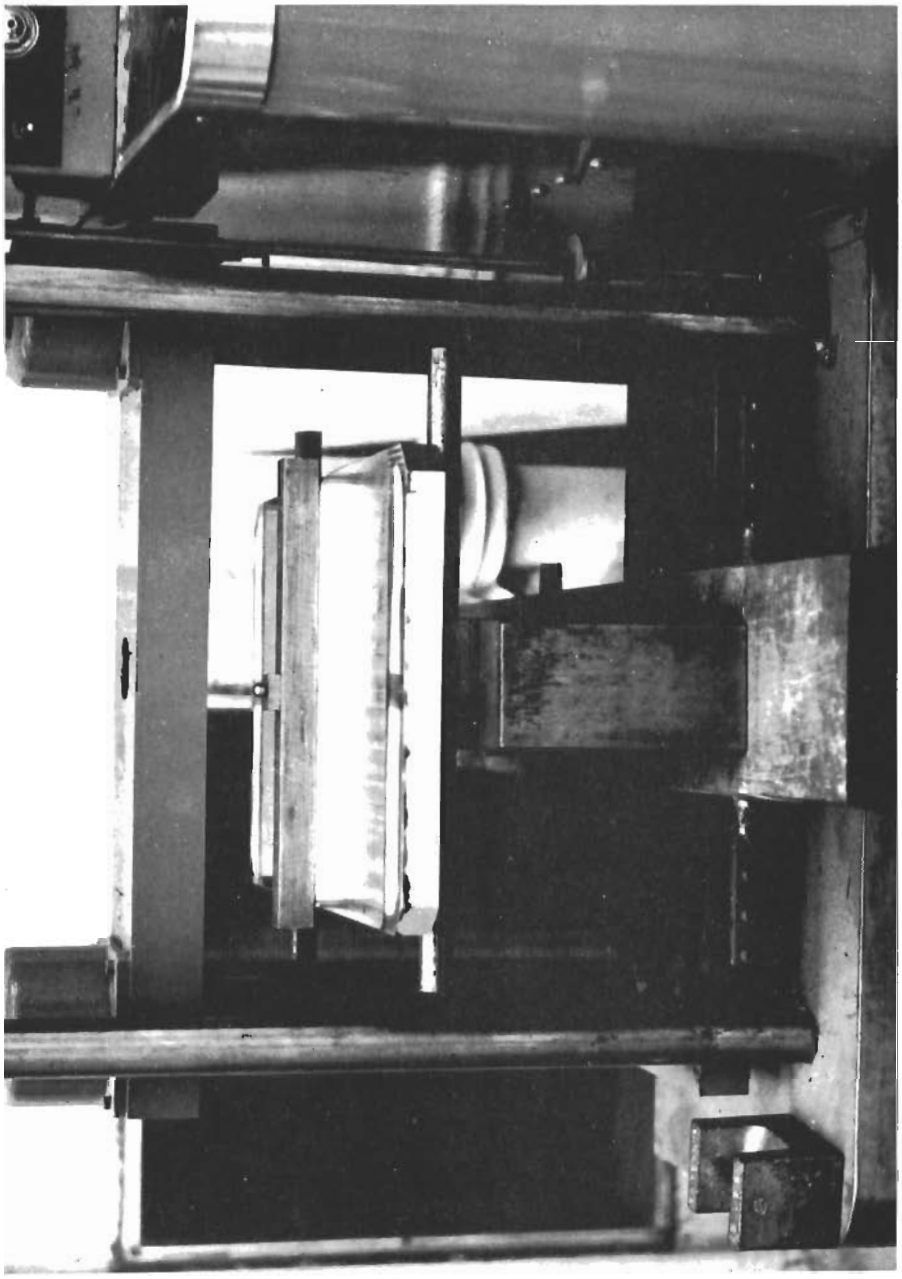

Fig. 79 Stiffened Plate No. 2, Transverse Load Test.

Approved for Public Release

Contrails

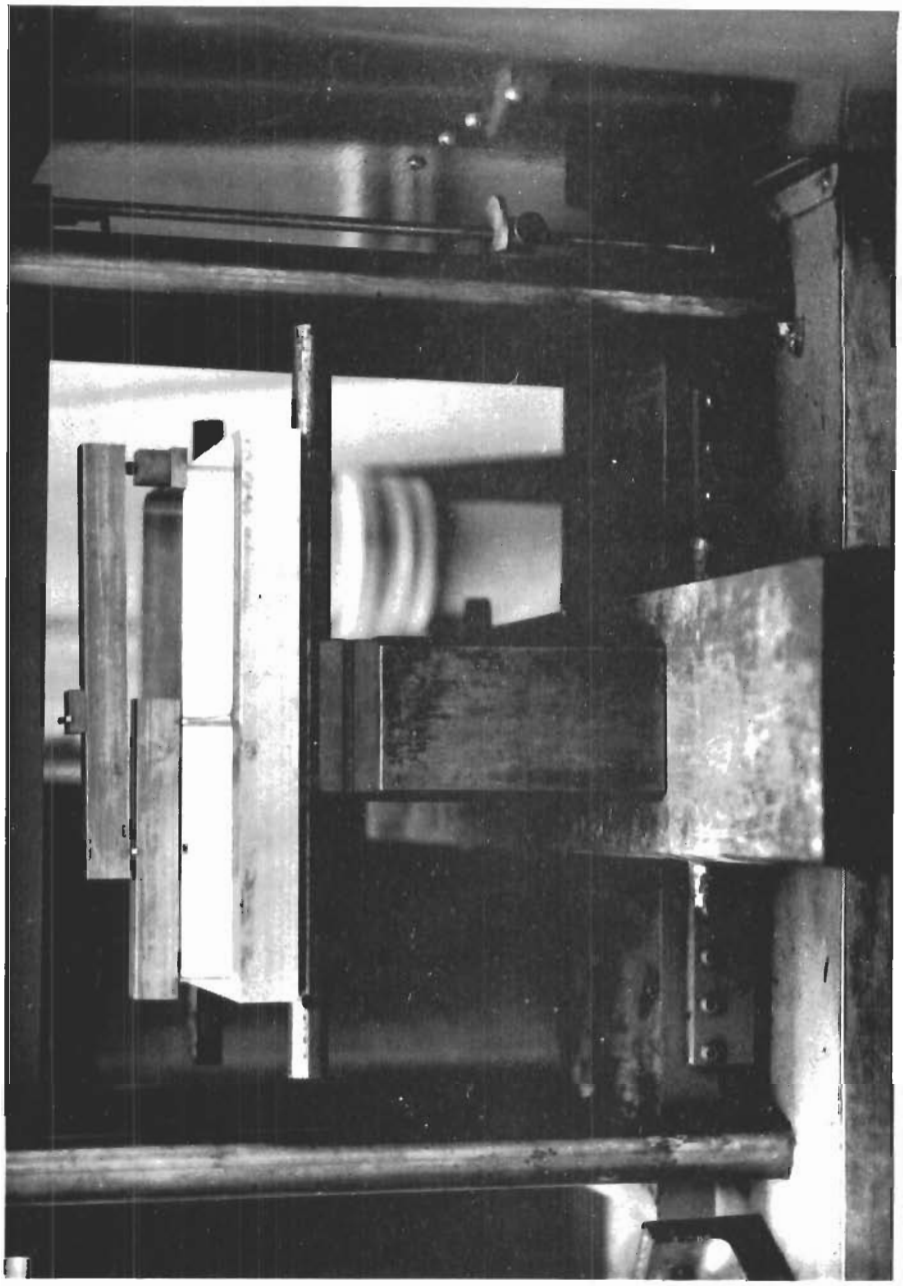

Fig. 80 Stiffened Plate No. 3, Transverse Load Test.

Approved for Public Release

Contrails

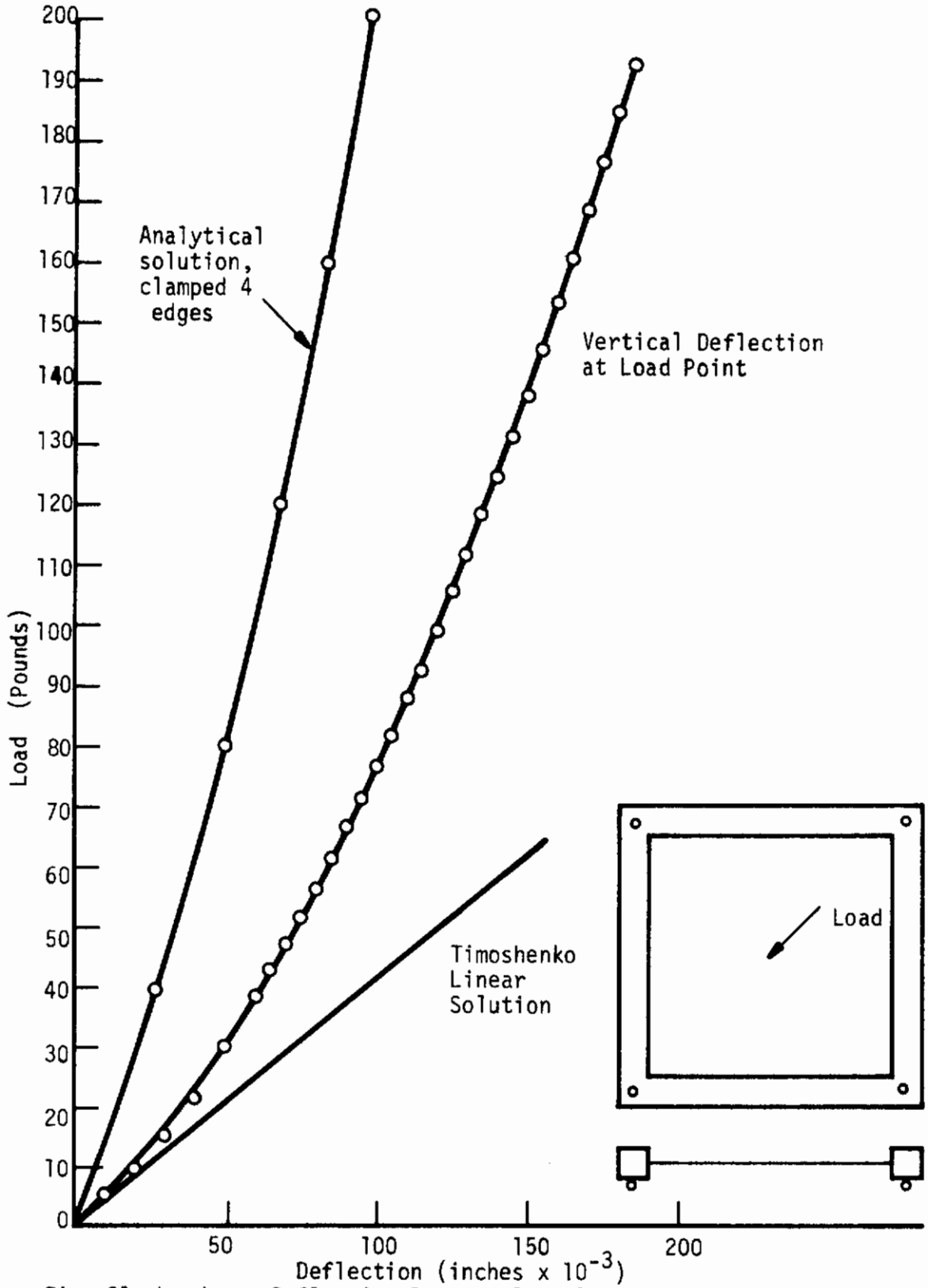

Fig. 81 Load vs. Deflection Rectangular Plate, Corner Supports, Elastic Edge Supports, Transverse Load at Center

Approved for Public Release

Contrails

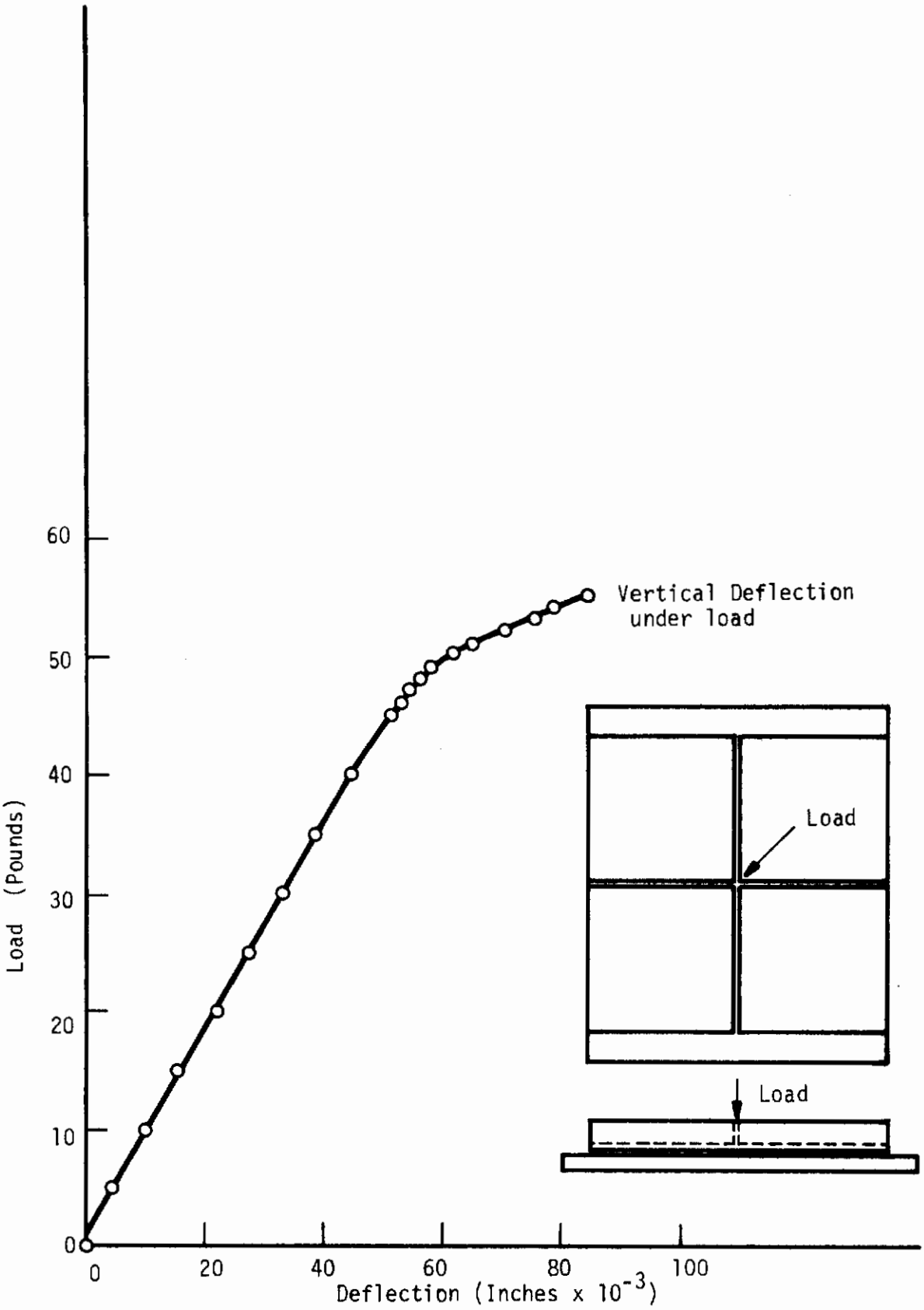

Fig. 82 Load vs. Deflection Transverse Loaded Stiffened Plate No. 1, Simply Supported

Approved for Public Release

Contrails

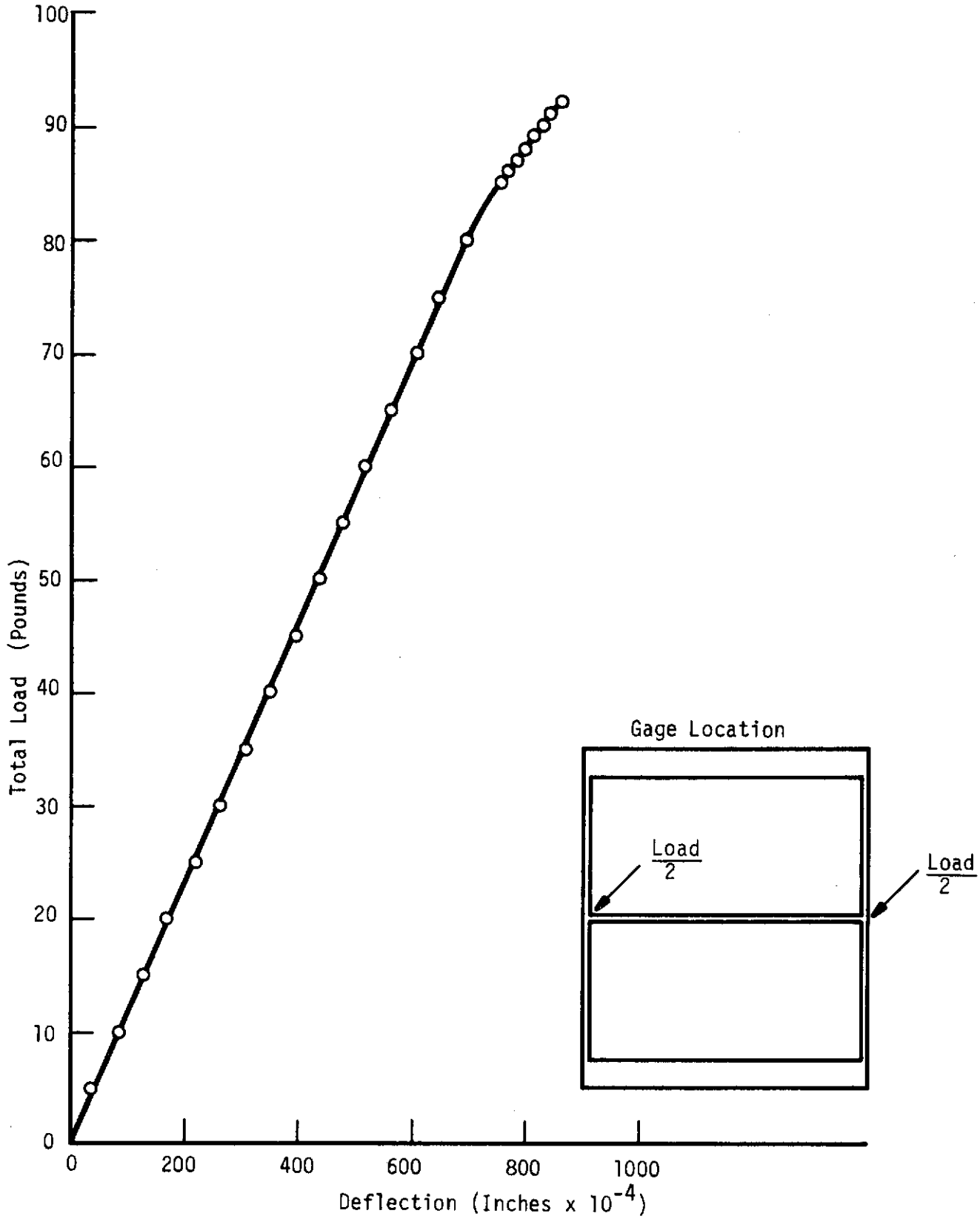

Fig. 83 Load vs. Deflection Transverse Loaded Stiffened Plate No. 2, Simply Supported.

Approved for Public Release

Contrails

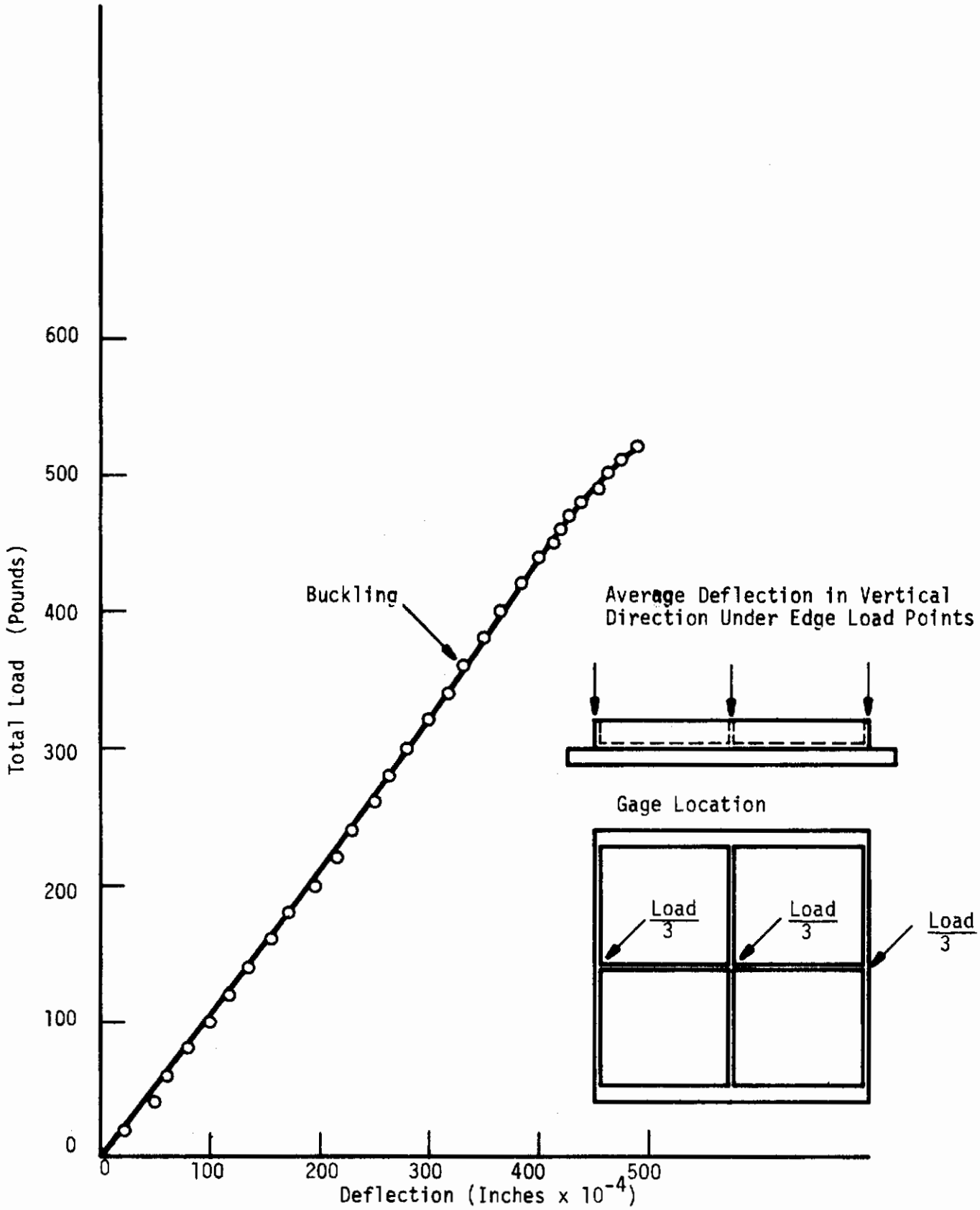

Fig. 84 Load vs. Deflection Transverse Loaded Stiffened Plate No. 3, Simply Supported.

Approved for Public Release

Contrails

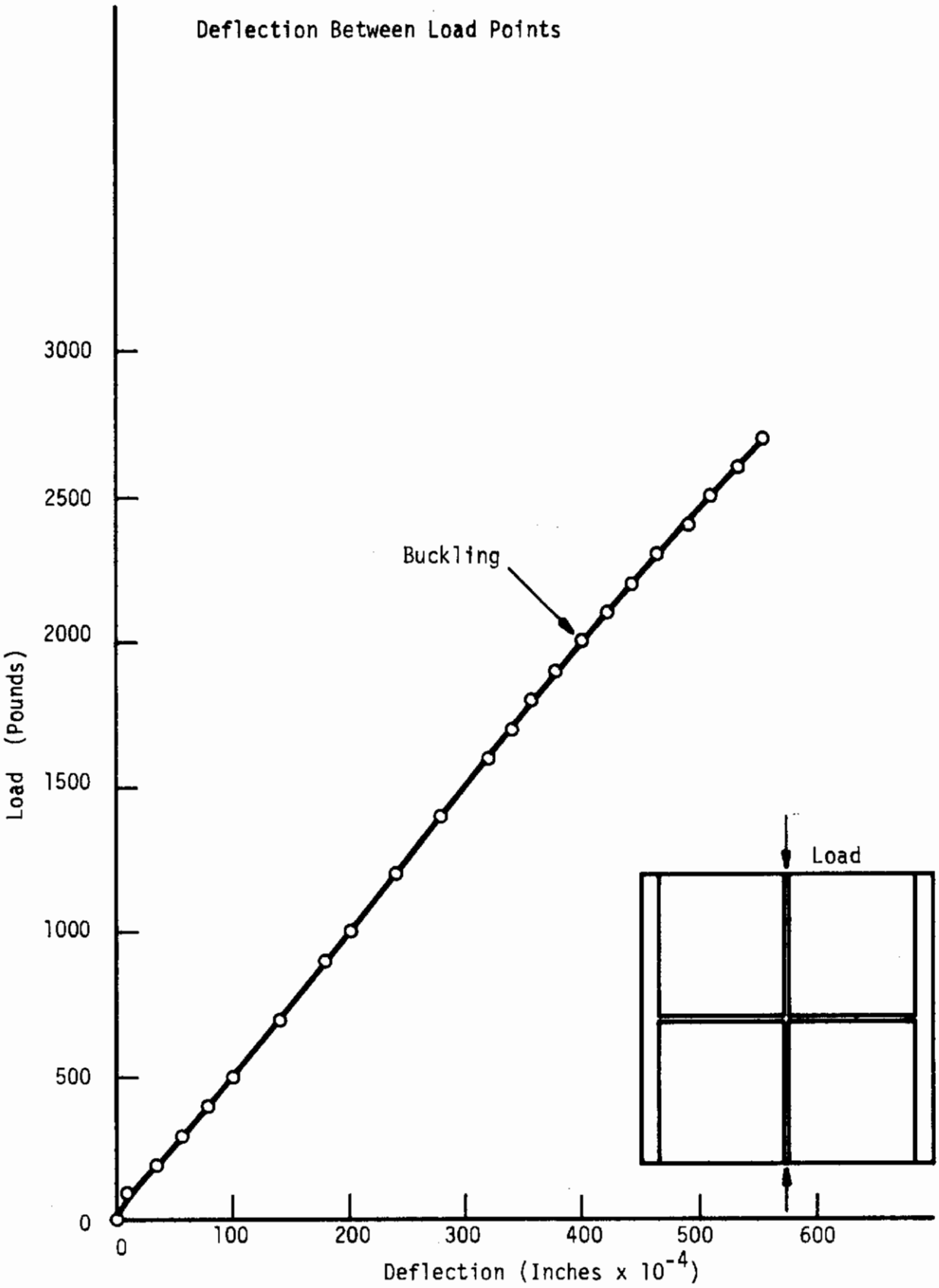

Fig. 85 Load vs. Deflection Inplane Loaded Stiffened Plate No. 4.

Approved for Public Release

Contrails

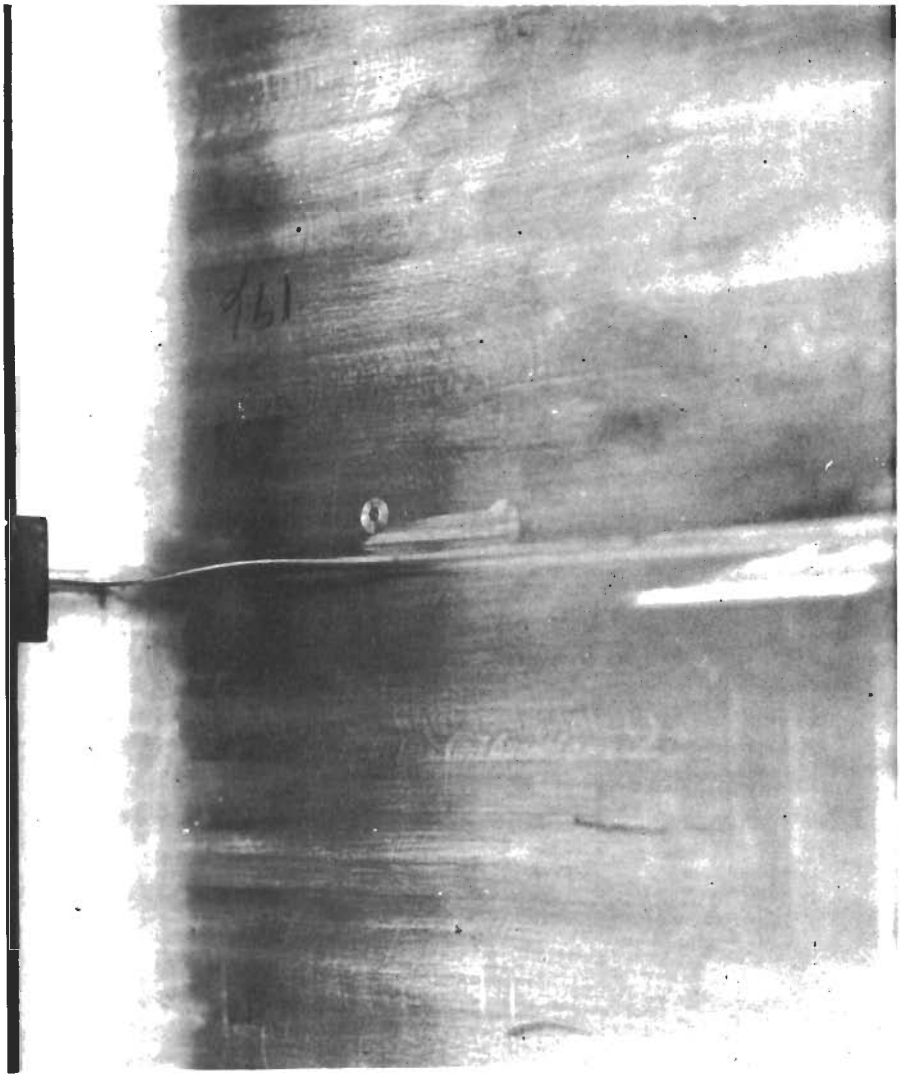

Fig. 86 Buckling of Longitudinal Stiffener in Model No. 1, Transverse Loading.

Approved for Public Release

Contrails

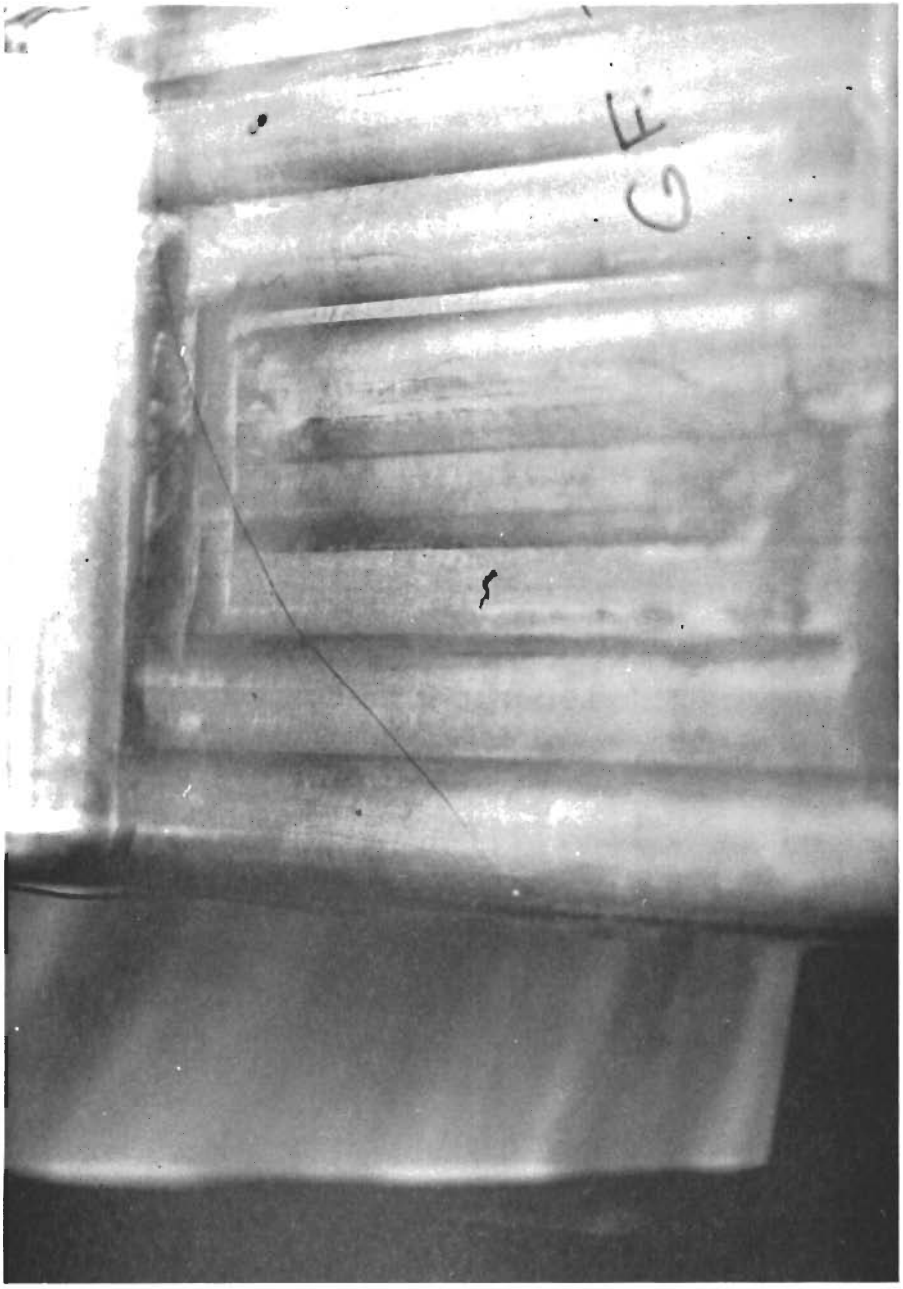

Fig. 87. Buckling of Longitudinal Stiffener in Model No. 2, Transverse Loading.

Approved for Public Release

Contrails

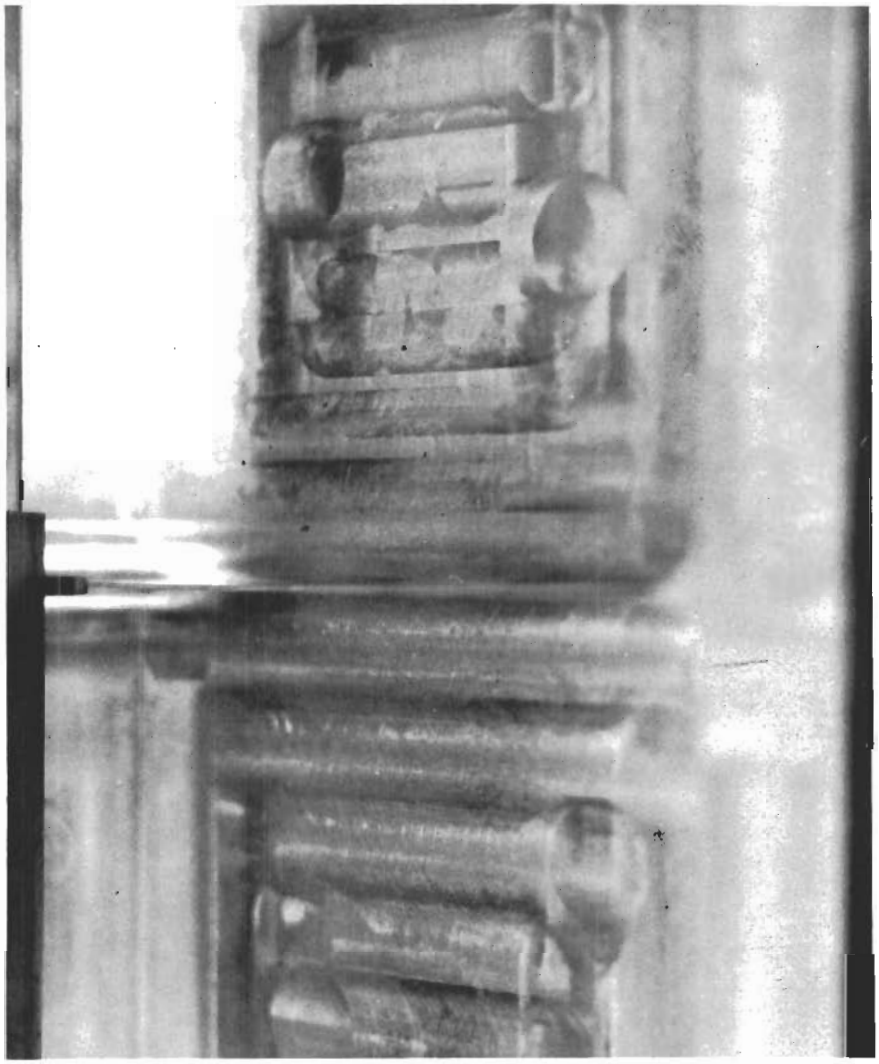

Fig. 88 Buckling of Longitudinal Stiffener in Model No. 3, Transverse Loading.

Approved for Public Release

Contrails

Table 1

Summary of Nonlinear Clamped Plate Results

(Section 2.5.1)

Load (psi) p_z	w_c (in.) Present	w_c (in.) Ref. 20 -P.421
0.2	.03760	.037
0.4	.06554	.065
0.6	.08607	.086
0.8	.10213	.103
1.0	.11535	.115
1.2	.12664	.126
1.4	.13650	.136
1.6	.14535	.145
1.8	.15327	.153
2.0	.16056	.160

Approved for Public Release

Contrails

Table 2

Summary of Pinched Cylindrical Shell Results

(Section 2.5.3)

Modeling	Degrees of Freedom	w under load poly (see sec. 2.3.1) inches	w under load circular (see sec. 2.3.3) inches
A	18	-0.00261	-0.00415
B	36	-0.0802	-0.0890
C	60	-0.0808	-0.0898
D	54	-0.1026	-0.1054
E	90	-0.1035	-0.1064
F	72	-0.1086	-0.1094
G	120	-0.1097(-0.115)*	-0.1105
H	210		-0.1129

* including geometrically nonlinear behavior (see Ref. 7, p. 150).

Approved for Public Release

Table 3

Linear Membrane Comparison-Π_R (Section 3.4.1)

Node	u microinches		v microinches		N_x lbs/inch		N_y lbs/inch		N_{xy} lbs/inch	
	Ref. 26 Exact	Π_R Approx.	Ref. 26 Exact	Π_R Approx.	Ref. 26 Exact	Π_R Approx.	Ref. 26 Exact	Π_R Approx.	Ref. 26 Exact	Π_R Approx.
1	0	0	- 2	- 2	56.3	57.5	0	0.015	0	0
2	0	0	- 0.6	- 0.4	28.1	29.4	-0.075	-0.071	0	0
3	0	0	0	0	0	0	-0.240	-0.244	0	0
4	0	0	- 0.5	- 0.3	-28.1	-29.2	-0.405	-0.409	0	0
5	0	0	- 2	- 2	-56.3	-57.2	-0.480	-0.491	0	0
6	86.1	96.6	-286	-292	42.3	44.2	0	0.017	0	-0.02
7	42.9	49.4	-285	-291	21.1	23.4	-0.075	-0.062	-1.65	-1.91
8	.1	- 6.9	-284	-291	0	0	-0.240	-0.236	-2.25	-2.36
9	-42.7	-43.6	-285	-291	-21.1	-23.5	-0.405	-0.416	-1.69	-1.74
10	-85.9	-90.5	-286	-292	-42.3	-44.3	-0.480	-0.490	0	-0.14
11	125.3	124.3	-991	-1020	0.1	0.9	0	0.009	0	-0.13
12	62.4	61.4	-991	-1020	0.1	0.9	-0.075	-0.075	-3.38	-3.48
13	.2	3.5	-991	-1020	0	0.4	-0.240	-0.242	-4.50	-4.70
14	- 62.0	- 63.4	-991	-1020	-0.1	-1.2	-0.405	-0.407	-3.38	-3.64
15	-124.8	-126.8	-991	-1020	-0.1	-1.2	-0.480	-0.490	0	-0.04

Approved for Public Release

Contrails

Table 4

Linear Bending Example-Π_R (Section 3.4.2)

	Π_R clamped boundary conditions imposed	Π_R clamped boundary conditions natural	Timoshenko Ref. 20 p. 197
w(a,0) in.	+0.203	+0.203	+0.202
M_x(0,0) in-lb/in	-16.7	-20.6	-20.5
M_x(a,0) in-lb/in	+0.42	+9.14	+9.24
Number of Variables	86	110	-----

Approved for Public Release

Contrails

Table 5

Nonlinear Plate Bending Example
(Section 3.4.3)

	Π_R	Timoshenko (Ref. 3.6)	Π_p
w(a,0) in.	0.117	0.117	0.117
$M_x(0,0)$ in-lb/in	-15.0	-----	-13.8
Max Stress lb/in^2	10,125	10,300	9,480
Number of Variables	144	-----	177

Approved for Public Release

Table 6

Stiffness Matrix Conditioning for Different Grid Geometries
(Section 4.3.2)

	Unscaled				Scaled			
$(a/b)_{max}$	R_m	λ_{max}	λ_{min}	C_N	$\tilde{R}_m$ [b]	λ_{max}	λ_{min}	C_N
≃1	2.58×10^{8}	1.765×10^{8}	2.608	6.766×10^{7}	3.24	1.911	491.0×10^{-5}	3.892×10^{2}
3	4.25×10^{8}	2.980×10^{8}	1.944	15.32×10^{7}	5.18	3.351	91.34×10^{-5}	36.68×10^{2}
5	6.64×10^{8}	4.492×10^{8}	1.604	28.00×10^{7}	5.80	4.325	28.80×10^{-5}	150.5×10^{2}
10	13.6×10^{8}	8.932×10^{8}	1.524	58.63×10^{7}	7.30	4.875	3.853×10^{-5}	$1265.\times10^{2}$

$(a/b)_{max}$ = Max element (a/b) $\quad R_m = \max_i (R_i) \equiv \max_i \left(\sum_{j\neq 1} |k_{ij}| \right) \quad C_N = \lambda_{max}/\lambda_{min}$,

Approved for Public Release

Confidential

Contrails

Table 7

Displacements and Stresses for the Thick Cylinder Subject to Internal Pressure (Section 5.3)

Displacement u in microinches at $r = r_1$:

Case	r_1	r_2	1 element	2 elements	5 elements	Ref. 26
1	1.0	1.2	194.85	194.86	194.86	194.85
2	1.0	2.0	65.53	65.55	65.55	65.56
3	1.0	10.0	37.22	41.78	43.80	44.00

Stress σ_θ in lbs/in^2 at $r = r_1$:

Case	r_1	r_2	1 element	2 elements	5 elements	Ref. 26
1	1.0	1.2	5547	5546	5547	5545
2	1.0	2.0	1693	1674	1667	1667
3	1.0	10.0	1075	1126	1076	1020

Note: Modulus of elasticity is 30,000,000 lbs/in^2.
Poisson's ratio is 0.3.
Pressure is 1,000 lbs/in^2.

Approved for Public Release

Contrails

Table 8

Maximum Displacements for the Laterally Loaded Annular Plate

(Section 5.3)

Case	Support Conditions at $r=r_1$, $r=r_2$	Load	Maximum Displacement in microinches Ref. 20	2 Elements
1	free, simple	line at $r=r_1$	341.	341.38
2	simple, free	pressure	20.2	20.317
3	clamped,free	pressure	2.31	2.3250
4	no slope, simple	pressure	3.43	3.4608
5	no slope, clamped	pressure	0.77	0.77189
6	no slope, clamped	line at $r=r_1$	1.29	1.2869
7	free, simple	pressure	184.	183.79
8	clamped, free	line at $r=r_2$	5.10	5.1044
9	free, clamped	line at $r-r_1$	5.04	5.0390
10	free, clamped	pressure	1.99	1.9921

Note: Modulus of elasticity is 10,000,000 lbs/in.^{2}
Thickness if 0.1 in.
Pressure loads are 10.0 lbs/in^2.
Line loads are 10.0 lbs/in.
r_1 = 0.8 in., r_2 = 1.0 in.

Approved for Public Release

Contrails

Table 9

Pinched Cylinder Gage Locations

(Section 7.3.1)

No.	Coordinates		
1	90°	5 1/4"	outer surface circumferential direction
2	90°	2 1/2"	outer surface longitudinal direction
3	90°	2 1/2"	outer surface circumferential direction
4	90°	1 1/4"	outer surface longitudinal direction
5	90°	1 1/4"	outer surface circumferential direction
6	45°	CL	outer surface circumferential direction
7	45°	CL	outer surface longitudinal direction
8	67 1/2°	CL	outer surface longitudinal direction
9	67 1/2°	CL	outer surface circumferential direction
10	0°	CL	outer surface circumferential direction
11	90°	5 1/4"	inner surface circumferential direction
12	90°	2 1/2"	inner surface longitudinal direction
13	90°	2 1/2"	inner surface circumferential direction
14	90°	1 1/4"	inner surface longitudinal direction
15	90°	1 1/4"	inner surface circumferential direction
16	45°	CL	inner surface circumferential direction
17	45°	CL	inner surface longitudinal direction
18	67 1/2°	CL	inner surface longitudinal direction
19	67 1/2°	CL	inner surface circumferential direction
20	0°	CL	inner surface longitudinal direction
21	0°	CL	inner surface circumferential direction
22	90°	CL	outer surface longitudinal direction

Approved for Public Release

Contrails

APPENDIX A

BOUNDARY CONDITION CONTRIBUTIONS TO REISSNER ENERGY

This appendix contains expressions for the boundary condition contributions to a rectangular element Reissner energy. These expressions are essentially the same as those given by Reissner in Ref. 23. The force boundary condition contribution is given by

$$S_1 = \int_{s_1} [\bar{N}_{x_\lambda} u + \bar{N}_{y_\lambda} v + Q_\lambda w - \bar{M}_{x_\lambda} \frac{\partial w}{\partial x} - \bar{M}_{y_\lambda} \frac{\partial w}{\partial y}] ds \quad (A1)$$

where

$$\bar{N}_{x_\lambda} = \cos(\lambda,x) \bar{N}_x + \cos(\lambda,y) \bar{N}_{xy} \quad (A2)$$

$$\bar{N}_{y_\lambda} = \cos(\lambda,x) \bar{N}_{xy} + \cos(\lambda,y) \bar{N}_y \quad (A3)$$

$$\bar{M}_{x_\lambda} = \cos(\lambda,x) \bar{M}_x + \cos(\lambda,y) \bar{M}_{xy} \quad (A4)$$

$$\bar{M}_{y_\lambda} = \cos(\lambda,x) \bar{M}_{xy} + \cos(\lambda,y) \bar{M}_y \quad (A5)$$

$$\bar{Q}_\lambda = \cos(\lambda,x) [\bar{V}_x + \bar{N}_x \frac{\partial w}{\partial x} + \bar{N}_{xy} \frac{\partial w}{\partial y}] + \cos(\lambda,y) [\bar{V}_y + \bar{N}_y \frac{\partial w}{\partial y} + \bar{N}_{xy} \frac{\partial w}{\partial x}] \quad (A6)$$

and it is understood that λ is the direction in the plane of the undeflected middle surface normal to the boundary. The quantities $\bar{N}_x$, $\bar{N}_y$, and $\bar{N}_{xy}$ represent prescribed membrane forces and the $\bar{M}_x$, $\bar{M}_y$ and $\bar{M}_{xy}$ represent prescribed moments acting on the boundary. The quantities $\bar{V}_x$ and $\bar{V}_y$ represent prescribed transverse shear forces acting on the boundary in the direction of

Approved for Public Release

Contrails

the normal to the deformed middle surface. Note that because the strain-displacement relations assume that normals to the undeformed middle surface remain normal to the middle surface after deformation, the following prescribed forces on the boundary are not entirely independent but rather they must satisfy the following equality constraints

$$\bar{V}_x = \frac{\partial \bar{M}_x}{\partial x} + \frac{\partial \bar{M}_{xy}}{\partial y} \tag{A7}$$

$$\bar{V}_y = \frac{\partial \bar{M}_y}{\partial y} + \frac{\partial \bar{M}_{xy}}{\partial x} \tag{A8}$$

The displacement boundary condition contribution is given by

$$S_2 = \int_{s_2} [(u-\bar{u})\, N_{x_\lambda} + (v-\bar{v})\, N_{y_\lambda} + (w-\bar{w})\, Q_\lambda - (\frac{\partial w}{\partial x} - \frac{\partial \bar{w}}{\partial x})\, M_{x_\lambda} - (\frac{\partial w}{\partial y} - \frac{\partial \bar{w}}{\partial y})\, M_{y_\lambda}]\, ds \tag{A9}$$

where

$$N_{x_\lambda} = \cos(\lambda,x)\, N_x + \cos(\lambda,y)\, N_{xy} \tag{A10}$$

$$N_{y_\lambda} = \cos(\lambda,x)\, N_{xy} + \cos(\lambda,y)\, N_y \tag{A11}$$

$$M_{x_\lambda} = \cos(\lambda,x)\, M_x + \cos(\lambda,y)\, M_{xy} \tag{A12}$$

$$M_{y_\lambda} = \cos(\lambda,x)\, M_{xy} + \cos(\lambda,y)\, M_y \tag{A13}$$

$$Q_\lambda = \cos(\lambda,x)\, [V_x + N_x \frac{\partial w}{\partial x} + N_{xy} \frac{\partial w}{\partial y}] + \cos(\lambda,y)\, [V_y + N_y \frac{\partial w}{\partial y} + N_{xy} \frac{\partial w}{\partial x}] \tag{A14}$$

Approved for Public Release

Contrails

and the transverse shear force resultants (V_x and V_y) in the direction of the normal to the deformed middle surface are given by

$$V_x = \frac{\partial M_x}{\partial x} + \frac{\partial M_{xy}}{\partial y} \tag{A15}$$

$$V_y = \frac{\partial M_y}{\partial y} + \frac{\partial M_{xy}}{\partial x} \tag{A16}$$

Note that in Eq. A9 the quantities $\bar{u}$, $\bar{v}$, and $\bar{w}$ represent prescribed boundary displacements. A discretized form of the boundary condition contributions to the Reissner energy is developed in Appendix D of Ref. 12.

Approved for Public Release

Contrails

APPENDIX B

PREPARATION OF DATA CARDS AND INTERPRETATION OF OUTPUT

THIS APPENDIX PROVIDES DETAILED RULES FOR PUNCHING DATA CARDS FOR THE COMPUTER PROGRAM DESCRIBED IN SECTION 6 OF THIS REPORT, AND SOME COMMENTS ON THE OUTPUT WHICH IT PRODUCES. FIGURE B1 ILLUSTRATES A SAMPLE STRUCTURE FOR WHICH DATA HAS BEEN PREPARED AND LISTED IN TABLE B1. THERE IS A COMMENTARY AT THE END OF THIS APPENDIX WHICH GUIDES THE READER THROUGH THIS DATA LISTING. THERE IS ALSO A REPRODUCTION OF THE OUTPUT GENERATED BY THE PROGRAM FOR THE SAMPLE STRUCTURE.

B.1. PREPARATION OF DATA CARDS.

INPUT DATA FORMATS HAVE BEEN SET UP TO ACCEPT A GREAT DEAL OF INFORMATION IN ALPHANUMERIC FORM, WHICH MAKES THE INPUT FORMATS EASIER TO REMEMBER AND THE DATA CARDS MORE READABLE. IN THE TEXT BELOW, WORDS OR PHRASES ENCLOSED IN CORNER BRACKETS <> CONSTITUTE ALPHANUMERIC DATA TO BE INTERPRETED LITERALLY. THE CHARACTER Δ IN THIS CONTEXT STANDS FOR A BLANK SPACE. A SINGLE INTEGER ENCLOSED IN SQUARE BRACKETS [ ] FOLLOWING AN ALPHANUMERIC SPECIFICATION INDICATES THE CARD COLUMN NUMBER OF THE LEFT-MOST CHARACTER OF THE ALPHANUMERIC DATA. TWO INTEGERS ENCLOSED IN SQUARE BRACKETS INDICATE THE LIMITS OF A FIELD WHERE A NUMBER IS TO BE PUNCHED. FIVE-CHARACTER FIELDS ARE TO BE FILLED WITH RIGHT-JUSTIFIED INTEGER CONSTANTS (FORTRAN I5 FORMAT

Approved for Public Release

Contrails

PHRASE), AND FIFTEEN-CHARACTER FIELDS ARE FOR FLOATING-POINT NUMBERS (FORTRAN E15.8 FORMAT PHRASE), WITH A DECIMAL MANTISSA AND, OPTIONALLY, A RIGHT-JUSTIFIED POWER OF TEN PRECEDED BY THE CHARACTER E. BLANK FIELDS ARE ASSUMED TO REPRESENT ZERO. OFTEN A 'DISPLACEMENT SPECIFIER' IS CALLED FOR IN THE TEXT BELOW, TO INDICATE WHICH ELEMENT DEGREE-OF-FREEDOM IS REFERENCED. THESE ARE TO BE CHOSEN FROM AMONG THE FOLLOWING: <U>, <UX>, <UY>, <UXY>, <V>, <VX>, <VY>, <VXY>, <W>, <WX>, <WY>, <WXY>, <WXX>, <WYY>, <WXXY>, <WXYY>, OR <WXXYY>.

DATA CARDS ARE DIVIDED INTO THREE GROUPS: SPECIFICATION CARDS, WHICH DESCRIBE THE STRUCTURE AND PRESCRIBE CERTAIN PROGRAM OPTIONS, LOAD CARDS WHICH DEFINE A SET OF FORCES AND IMPOSED DISPLACEMENTS TO BE ANALYZED, AND SEPARATOR CARDS.

B.1.1. SEPARATOR CARDS. THESE CARDS ACT SOMEWHAT LIKE CONTROL CARDS, IN THAT THEY INDICATE WHICH SUBROUTINE WILL GAIN CONTROL NEXT. THERE ARE FIVE KINDS OF SEPARATOR CARDS:

B.1.1.1. THE TITLE CARD IDENTIFIES THE CURRENT PROBLEM. ANY TITLE MAY BE PUNCHED IN COLUMNS 1-78 OF THIS CARD. CONTROL IS PASSED TO THE SETUP PHASE, WHICH READS EITHER A SPECIFICATION GROUP OR A RESTART CARD (SEE B.1.1.2 BELOW). UPON EXIT FROM THE SETUP PHASE, INDEPENDENT DEGREES-OF-FREEDOM WILL HAVE BEEN ASSIGNED AND STIFFNESS MATRICES WILL HAVE BEEN GENERATED AND WRITTEN ON DRUM (DISK).

B.1.1.2. THE RESTART CARD MAY TAKE THE PLACE OF THE

Approved for Public Release

Contrails

SPECIFICATION GROUP, AND INDICATES THAT THE RESULT OF THE SETUP PHASE OF A PREVIOUS RUN IS TO BE READ FROM TAPE. THIS CARD HAS <READ␣SETUP␣FROM␣TAPE> PUNCHED IN [1], AND THE LOGICAL TAPE UNIT NUMBER (1 OR 2) PUNCHED IN [21-25].

B.1.1.3. THE LOADS CARD PASSES CONTROL TO THE INPUT/OUTPUT PHASE OF THE PROGRAM WHICH WILL READ A GROUP OF LOAD CARDS AND GENERATE A WORK-EQUIVALENT LOAD VECTOR, AFTER WHICH THE ANALYSIS PHASE WILL TAKE CONTROL. THIS CARD HAS <LOADS> PUNCHED IN [1].

B.1.1.4. A NEW PROBLEM CARD INDICATES THAT AN ENTIRELY NEW PROBLEM IS TO BE RUN NEXT. THIS CARD HAS <NEW␣PROBLEM> PUNCHED IN [1], AND IS FOLLOWED IMMEDIATELY BY A TITLE CARD.

B.1.1.5. THE STOP CARD MUST BE THE LAST CARD OF THE DECK. PUNCH <STOP> IN [1].

THE FLOW CHART IN FIG. 34 ILLUSTRATES THE USE OF SEPERATOR CARDS, AND HOW THEY CONTROL FLOW AMONG PROGRAM PHASES. NOTE THAT A SPECIFICATION GROUP MAY BE FOLLOWED IMMEDIATELY BY A STOP CARD OR NEW PROBLEM CARD, IN WHICH CASE NO ANALYSIS WILL BE PERFORMED. THIS CAN BE USEFUL: THE USER CAN EXAMINE THE OUTPUT FROM THE SETUP PHASE, AND IF IT SEEMS SATISFACTORY, RUN THE PROBLEM WITH THE RESTART OPTION, WITH VERY LITTLE LOST TIME.

B.1.2. SPECIFICATION CARDS. THESE CARDS ARE ORGANIZED INTO SETS OF ONE OR MORE CARDS EACH. THE FIRST (AND SOMETIMES ONLY) CARD OF EACH SET HAS ALPHANUMERIC DATA

Approved for Public Release

Contrails

PUNCHED BEGINNING IN COLUMN ONE. MOST DATA SETS ARE OPTIONAL, AS INDICATED IN THE DESCRIPTIONS BELOW. THE SETS THAT ARE INCLUDED MUST APPEAR IN THE ORDER IN WHICH THEY APPEAR BELOW.

SET S1. ELEMENT CONNECTION SPECIFICATION. THE FIRST CARD OF THIS SET HAS <ELEMENT△CONNECTIONS> IN [1] AND THE NUMBER OF RELATIONSHIPS BETWEEN ELEMENTS PUNCHED IN [21-25]. FOLLOWING THIS PUNCH ONE CARD FOR EACH RELATIONSHIP. OF THE TWO ELEMENTS INVOLVED, CALL THE ONE WITH THE LOWER ELEMENT NUMBER THE PRIMARY ELEMENT, AND THE OTHER THE SECONDARY ELEMENT. IN [1-5] PUNCH THE PRIMARY ELEMENT NUMBER. IN [6-10] AND [11-15] PUNCH THE TWO CORNER NUMBERS OF THE PRIMARY ELEMENT WHICH BOUND THE EDGE IN QUESTION. IN [16-20] PUNCH THE SECONDARY ELEMENT NUMBER, AND IN [21-25] AND [26-30] THE TWO CORNER NUMBERS OF THE SECONDARY ELEMENT WHICH COINCIDE RESPECTIVELY WITH THE PRIMARY CORNER NUMBERS INDICATED IN [6-10] AND [11-15]. NOW OBSERVE THE RELATIONSHIP BETWEEN THE AXIS SYSTEMS OF THE TWO ELEMENTS. SLIDE THEM OVER THE SURFACES OF THE ELEMENTS TO THE EDGE IN QUESTION, IF NECESSARY. DETERMINE WHICH SECONDARY AXIS LINES UP WITH THE PRIMARY X-AXIS, AND PUNCH EITHER <X>, <Y>, OR <Z> IN [35] TO INDICATE THIS. IF THESE TWO AXES POINT IN OPPOSITE DIRECTIONS, PUNCH <-> IN [34], OTHERWISE <+>. SIMILARLY, DETERMINE WHICH SECONDARY AXIS LINES UP WITH THE PRIMARY Y-AXIS AND PUNCH <X>, <Y>, OR <Z> IN [40] AND <+> OR <-> IN [39]. TO SUPPRESS NORMAL STRAIN

Approved for Public Release

Contrails

CONTINUITY BETWEEN COPLANAR ELEMENTS, PUNCH <NORMAL> IN [46], OTHERWISE LEAVE THIS FIELD BLANK. TO SUPPRESS SHEAR STRAIN CONTINUITY PUNCH <SHEAR> IN [56] (BLANK OTHERWISE). FINALLY, IF THIS CONNECTION IS A HINGE, PUNCH <HINGED> IN [66] (OTHERWISE BLANK).

IN THE CASE OF A ONE-ELEMENT STRUCTURE SET S1 IS OMITTED. NO STRUCTURE MAY HAVE MORE THAN 50 ELEMENTS.

SET S2. SPECIFICATION OF ELEMENT PROPERTIES. MORE THAN ONE OF THESE SETS MAY BE INCLUDED. EACH SET SPECIFIES A NUMBER OF PROPERTIES WHICH APPLY TO ONE OR MORE ELEMENTS. IF ALL ELEMENTS IN THE STRUCTURE HAVE THE SAME PROPERTIES THEN ONLY ONE OF THESE SETS NEED BE PUNCHED. IN ANY CASE, ENOUGH SETS MUST BE INCLUDED TO ACCOUNT FOR ALL ELEMENTS. THE FIRST CARD HAS <ELEMENTS> IN [1], AND FROM ONE TO TWELVE ELEMENT NUMBERS PUNCHED IN [21-25], [26-30], [31-35], ETC. IF A GROUP OF PROPERTIES APPLIES TO MORE THAN TWELVE ELEMENTS, THEN MORE THAN ONE DATA SET MUST BE PUNCHED FOR SUCH A GROUP, SINCE THE FIRST CARD HAS ROOM FOR ONLY TWELVE ELEMENT NUMBERS.

THE SECOND CARD OF THIS SET MUST BE PUNCHED WITH EITHER <RECTANGULAR>, <CYLINDRICAL>, OR <ANNULAR> IN [6] TO INDICATE THE ELEMENT TYPE.

THE THIRD CARD INDICATES THE TYPE OF INTERPOLATION TO BE USED FOR MEMBRANE VARIABLES. PUNCH <MEMBRANE> IN [6], AND EITHER <POLYNOMIAL>, <TRIGONOMETRIC>, OR, IF MEMBRANE DEGREES-OF-FREEDOM ARE TO BE SUPPRESSED IN THESE ELEMENTS,

Approved for Public Release

Contrails

<NONE> IN [16]. LEAVE THE FIELD [31-35] BLANK IF <NONE> WAS SPECIFIED. PUNCH 0 IN THIS FIELD IF THESE ARE RECTANGULAR FLAT PLATE ELEMENTS AND ZEROTH-ORDER (LAGRANGE) INTERPOLATION IS DESIRED. OTHERWISE, PUNCH A 1, INDICATING FIRST-ORDER (OSCULATORY) MEMBRANE INTERPOLATION.

THE FOURTH CARD IS SIMILAR TO THE THIRD. PUNCH <BENDING> IN [6] AND EITHER <POLYNOMIAL>, <TRIGONOMETRIC>, OR <NONE> IN [16]. AGAIN, LEAVE [31-35] BLANK IF <NONE> WAS SPECIFIED. PUNCH A 2 THERE IF SECOND-ORDER (HYPEROSCULATORY) INTERPOLATION IS DESIRED, OTHERWISE PUNCH A 1.

THE NEXT CARD IS OPTIONAL AND IS USED TO INDICATE THAT THE ELEMENTS IN QUESTION ARE STIFFENER ELEMENTS. PUNCH <STIFFENER> IN [6].

THE NEXT CARD IS ALSO OPTIONAL AND MAY BE USED ONLY WITH CYLINDRICAL OR ANNULAR ELEMENTS. IT INDICATES THAT THE ELEMENTS IN QUESTION REPRESENT A CLOSED CYLINDER OR ANNULUS WHICH IS IN EVERY WAY AXIALLY SYMMETRIC, AND IS SUBJECT ONLY TO AXIALLY SYMMETRIC LOADINGS. PUNCH <AXISYMMETRIC> IN [6].

THE NEXT CARD IS MANDATORY AND INDICATES WHAT SET OF STRAIN-DISPLACEMENT RELATIONS IS TO BE USED. PUNCH <NONLINEAR> IN [6] IF HIGHER-ORDER TERMS ARE TO BE INCLUDED. OTHERWISE PUNCH <LINEAR> IN [6].

THE NEXT CARD HAS A MODULUS OF ELASTICITY PUNCHED IN [6-20], POISSON'S RATIO IN [21-35], AND SHELL THICKNESS IN

Approved for Public Release

Contrails

[36-50].

THE LAST CARD HAS DIFFERENT INFORMATION FOR DIFFERENT ELEMENT TYPES:

FOR RECTANGULAR ELEMENTS PUNCH THE PLANFORM DIMENSIONS IN THE X AND Y DIRECTIONS IN [6-20] AND [21-35], RESPECTIVELY.

FOR CYLINDRICAL ELEMENTS, PUNCH THE AXIAL LENGTH IN [6-20], THE RADIUS IN [21-35], AND EITHER THE ARC LENGTH, ARC IN RADIANS, OR ARC IN DEGREES IN [36-50]. PUNCH <ARC␣LENGTH>, <RADIANS>, OR <DEGREES> IN [56], WHICHEVER APPLIES TO THE NUMBER IN [36-50].

FOR ANNULAR PLATE ELEMENTS, PUNCH THE INNER RADIUS IN [6-20], THE OUTER RADIUS IN [21-35], EITHER THE INNER ARC LENGTH, ARC IN RADIANS, OR ARC IN DEGREES IN [36-50], AND EITHER <ARC␣LENGTH>, <RADIANS>, OR <DEGREES> IN [56].

SET S3 (OPTIONAL). BENDING EDGE BOUNDARY CONDITIONS. THE FIRST CARD OF THIS SET HAS <BENDING␣B.C.> IN [1] AND THE TOTAL NUMBER OF ELEMENT EDGES WHERE BENDING RESTRAINTS ARE PRESCRIBED IN [21-25]. FOR EACH SUCH EDGE, PUNCH A CARD WITH AN ELEMENT NUMBER IN [1-5], AN EDGE NUMBER IN [6-10], AND AN ALPHANUMERIC PHRASE TO INDICATE THE TYPE OF RESTRAINT IN [16]. THE CHOICES ARE:

<CLAMPED>, INDICATING THAT THE DISPLACEMENT W AND ITS SLOPE NORMAL TO THE EDGE ARE ZERO ALL ALONG THE EDGE;

<SIMPLY␣SUPPORTED>, SAME AS CLAMPED EXCEPT NORMAL SLOPE ALLOWED;

Approved for Public Release

Contrails

<SYMMETRY>, W ALLOWED BUT NO NORMAL SLOPE;

<ANTI-SYMMETRY>, W KEPT ZERO BUT NORMAL SLOPE ALLOWED;

<EDGE△STRAIGHT>, SAME AS SIMPLY SUPPORTED EXCEPT W IS ALLOWED TO TAKE ON A VALUE CONSTANT ALONG THE EDGE; OR

<EDGE△STRAIGHT,△NO△NORMAL△SLOPE>, SAME AS CLAMPED EXCEPT W IS ALLOWED TO TAKE ON A VALUE CONSTANT ALONG THE EDGE.

ANY EDGE FOR WHICH NO BOUNDARY CONDITIONS ARE PRESCRIBED IS ASSUMED TO BE FREE.

SET S4 (OPTIONAL). SPECIFICATION OF POINT SUPPORT AT CORNERS OF ELEMENTS. PUNCH <CORNER△RESTRAINTS> IN [1] AND THE NUMBER OF SUCH RESTRAINTS IN [21-25]. FOR EACH SUCH RESTRAINT PUNCH A CARD WITH AN ELEMENT NUMBER IN [1-5], A CORNER NUMBER IN [6-10], AND A DISPLACEMENT SPECIFIER IN [16].

SET S5 (OPTIONAL). OPTION TO DUMP CERTAIN ARRAYS FOR DEBUGGING PURPOSES. PUNCH <DEBUG> IN [1].

SET S6 (OPTIONAL). TWO DISPLACEMENTS MAY BE FORCED TO KEEP THE SAME VALUE. THIS OPTION MIGHT BE USED TO REDUCE THE NUMBER OF DEGREES-OF-FREEDOM IN A PROBLEM WHERE SYMMETRY EXISTS ABOUT A DIAGONAL LINE, FOR EXAMPLE. PUNCH <EQUALITY△CONSTRAINTS> IN [1] AND THE NUMBER OF SUCH CONSTRAINTS IN [21-25]. FOR EACH SUCH CONSTRAINT, PUNCH TWO CARDS, ONE FOR EACH OF THE TWO DISPLACEMENTS INVOLVED, EACH WITH THE FOLLOWING INFORMATION: ELEMENT NUMBER IN [1-5], CORNER NUMBER IN [6-10], AND DISPLACEMENT SPECIFIER IN

Approved for Public Release

Contrails

[16]. IF THE TWO DISPLACEMENTS ARE TO BE OPPOSITE IN SIGN, INDICATE THIS WITH A <-> PUNCHED IN [15] OF THE SECOND CARD OF THE PAIR.

SET S7 (OPTIONAL). THIS OPTION INDICATES THAT ENERGY SEARCH IS TO BE USED. ENERGY SEARCH MUST BE USED FOR NONLINEAR PROBLEMS OR PROBLEMS WITH IMPOSED DISPLACEMENTS; IT IS OPTIONAL FOR LINEAR PROBLEMS. PUNCH <FLETCHER-POWELL> OR <FLETCHER-REEVES> IN [1]. IF A LINEAR SOLUTION IS TO BE OBTAINED BY ENERGY SEARCH AS A STARTING POINT FOR NONLINEAR ENERGY SEARCH, INDICATE THIS BY PUNCHING A 1 IN [21-25]. IF NO SUCH LINEAR SOLUTION IS DESIRED, OR IF IT IS TO BE OBTAINED BY MATRIX INVERSION, LEAVE THIS FIELD BLANK.

SET S8 (OPTIONAL). IMPOSED DISPLACEMENTS. PUNCH <IMPOSED␣DISPL.> IN [1] AND THE NUMBER OF DISPLACEMENTS TO BE IMPOSED IN [21-25]. FOR EACH IMPOSED DISPLACEMENT PUNCH A CARD WITH AN ELEMENT NUMBER IN [1-5], A CORNER NUMBER IN [6-10], AND A DISPLACEMENT SPECIFIER IN [16]. THE VALUES TO BE IMPOSED WILL BE READ IN LATER.

SET S9 (OPTIONAL). MATRIX INVERSION. FOR LINEAR PROBLEMS, THIS INDICATES THAT DISPLACEMENTS WILL BE CALCULATED BY INVERTING A MASTER STIFFNESS MATRIX. FOR NON-LINEAR PROBLEMS (FLETCHER-POWELL OR FLETCHER-REEVES MUST ALSO BE SPECIFIED) A LINEAR SOLUTION WILL BE OBTAINED FIRST, THEN ENERGY SEARCH WILL BE INITIATED, WITH THE LINEAR SOLUTION AS A STARTING POINT. MATRIX INVERSION IS NOT ALLOWED WHEN IMPOSED DISPLACEMENTS HAVE BEEN SPECIFIED.

Approved for Public Release

Contrails

PUNCH <INVERT> IN [1].

SET S10 (OPTIONAL). MEMBRANE EDGE BOUNDARY CONDITIONS. PUNCH <MEMBRANE B.C.> IN [1] AND THE TOTAL NUMBER OF ELEMENT EDGES WHERE MEMBRANE BOUNDARY CONDITIONS ARE PRESCRIBED IN [21-25]. FOR EACH SUCH EDGE PROVIDE A CARD WITH AN ELEMENT NUMBER IN [1-5], AN EDGE NUMBER IN [6-10], AND AN ALPHANUMERIC PHRASE IN [16]. THE CHOICES AVAILABLE ARE:

<U PREVENTED>;

<V PREVENTED>;

<U AND V PREVENTED>;

<EDGE STRAIGHT>, INDICATING THAT A UNIFORM DISPLACEMENT NORMAL TO THE EDGE IS ALLOWED;

<EDGE STRAIGHT, U PREVENTED> (APPLIES ONLY TO CONSTANT Y EDGES);

<EDGE STRAIGHT, V PREVENTED> (APPLIES ONLY TO CONSTANT X EDGES);

<SYMMETRY>; OR

<ANTI-SYMMETRY>.

ANY EDGE FOR WHICH NO BOUNDARY CONDITIONS ARE PRESCRIBED IS ASSUMED TO BE FREE.

SET S11 (OPTIONAL). PRINT THE MATRICES GENERATED FOR USE IN CALCULATING ELEMENT STRAIN ENERGIES AND/OR THE MASTER STIFFNESS MATRIX. PUNCH <PRINT Q'S> IN [1].

SET S12 (OPTIONAL). PUNCH THE SOLUTION VECTOR AT THE END OF EACH LOAD CONDITION ONTO CARDS FOR POSSIBLE INPUT TO

Approved for Public Release

Contrails

FUTURE JOBS. PUNCH <PUNCH△SOLUTION> IN [1].

SET S13 (OPTIONAL). AN INITIAL SOLUTION VECTOR AND FLETCHER-POWELL H MATRIX, WRITTEN ON TAPE IN A PREVIOUS RUN (SEE SET S18), ARE TO BE READ IN. PUNCH <READ△X,H△FROM△TAPE> IN [1] AND THE LOGICAL TAPE UNIT NUMBER (1 OR 2) IN [21-25].

SET S14 (OPTIONAL). REDUCE PRINTING. UNLESS OTHERWISE SPECIFIED, THE FLETCHER-POWELL AND FLETCHER-REEVES ROUTINES WILL PRINT A SUMMARY OF EACH ITERATION CONSISTING OF 8 TO 10 LINES. IN ADDITION, THE SOLUTION VECTOR AND GRADIENT VECTOR ARE PRINTED AFTER EACH ITERATION, CONSUMING ABOUT N/2 LINES, WHERE N IS THE NUMBER OF DEGREES-OF-FREEDOM. THIS MAY BE ALTERED SO THAT THESE TWO VECTORS ARE PRINTED ONLY AFTER EVERY MTH ITERATION. PUNCH <REDUCE△PRINTING> IN [1] AND THE APPROPRIATE INTEGER M IN [21-25]. TO SUPPRESS ALL INTERMEDIATE OUTPUT FROM FLETCHER-POWELL OR FLETCHER-REEVES, PUNCH ZERO IN [21-25].

SET S15 (OPTIONAL). INFORMATION GENERATED DURING THE SETUP PHASE OF THE PROGRAM MAY BE SAVED ON TAPE, SO THAT IF THE SAME PROBLEM IS RUN LATER, THE SETUP PHASE CAN BE BYPASSED. PUNCH <SAVE△SETUP△ON△TAPE> IN [1].

SET S16 (OPTIONAL). THIS OPTION SPECIFIES THAT AT THE END OF EVERY MTH ITERATION OF THE MINIMIZATION ROUTINE THE CURRENT SOLUTION VECTOR (AND H MATRIX, IN THE CASE OF FLETCHER-POWELL MINIMIZATION) ARE TO BE WRITTEN ON AN OUTPUT TAPE, AND THE TAPE BACKSPACED. PUNCH <SAVE△X,H△ON△TAPE> IN

Approved for Public Release

Contrails

[1] AND THE DESIRED INTEGER M IN [21-25].

SET S17 (OPTIONAL). SUBDIVISION OF ELEMENTS. NORMALLY THE PROGRAM PRINTS DISPLACEMENTS, STRAINS, AND STRESSES ONLY AT ELEMENT CORNERS. THIS MAY BE ALTERED SO THAT ELEMENTS ARE SUBDIVIDED BY UNIFORM GRIDS, AND THESE QUANTITIES ARE CALCULATED AT THE NODE POINTS DEFINED BY THESE GRIDS. GRID SIZES ARE SPECIFIED BY A PAIR OF INTEGERS INDICATING THE NUMBER OF SUBDIVISIONS IN THE X AND Y DIRECTIONS, RESPECTIVELY. THUS A 2 BY 3 GRID WOULD RESULT IN OUTPUT FOR THE FOUR CORNERS, FOR SIX POINTS ON THE ELEMENT BOUNDARIES, AND FOR TWO INTERIOR POINTS. THE FIRST CARD OF THIS SET HAS <SUBDIVIDE> IN [1], AND THE NUMBER OF SUBDIVIDED ELEMENTS IN [21-25]. FOR EACH SUCH ELEMENT, PUNCH A CARD WITH AN ELEMENT NUMBER IN [1-5] AND THE GRID SIZE IN [6-10] AND [11-15].

B.1.3. LOAD CARDS. LOAD CARDS ARE ALSO ORGANIZED INTO SETS, ALL OF WHICH ARE OPTIONAL. THOSE THAT ARE INCLUDED MUST APPEAR IN THE ORDER SPECIFIED BELOW.

SET L1. POINT LOADS. PUNCH <POINTΔLOADS> IN [1] AND THE NUMBER OF POINT LOADS TO BE APPLIED IN [21-25]. FOR EACH SUCH LOAD PUNCH A CARD WITH AN ELEMENT NUMBER IN [1-5], A CORNER NUMBER IN [6-10], A DISPLACEMENT SPECIFIER IN [16], AND THE MAGNITUDE OF THE LOAD IN [21-35].

SET L2. LINE LOADS. LOADINGS DISTRIBUTED ALONG AN EDGE MAY BE SPECIFIED, ORIENTED IN THE U, V, OR W DIRECTIONS, DISTRIBUTED EITHER UNIFORMLY OR IN THE FOLLOWING

Approved for Public Release

Contrails

WAYS: ALONG EDGES Y=CONSTANT OF RECTANGULAR OR CYLINDRICAL ELEMENTS, LOADINGS MAY VARY WITH X OR X. ALONG EDGES X=CONSTANT OF RECTANGULAR OR CYLINDRICAL ELEMENTS (PROVIDED POLYNOMIAL INTERPOLATION IS USED), LOADINGS MAY VARY WITH Y OR Y. ALONG EDGES Y=CONSTANT OF ANNULAR ELEMENTS, LOADINGS MAY VARY WITH R OR R, WHERE R STANDS FOR THE RADIAL CO-ORDINATE MEASURED FROM THE POLE OF THE ELEMENT (SEE FIG. 30). FINALLY, WHEN TRIGONOMETRIC INTERPOLATION IS USED, LOADINGS ON CURVED EDGES MAY VARY WITH SINO, COSO, SIN(2O), OR COS(2O), WHERE O IS THE ANGULAR CO-ORDINATE. CORRESPONDING TO EACH OF THESE OPTIONS IS A 'VARIATION SPECIFIER' USED ON DATA CARDS. THESE ARE <X>, <X**2>, <Y>, <Y**2>, <R>, <R**2>, <SIN(T)>, <COS(T)>, <SIN(2T)>, OR <COS(2T)>. TO SPECIFY LINE LOADS, PUNCH A CARD WITH <LINE␣LOADS> IN [1] AND THE NUMBER OF SUCH LOADS IN [21-25]. FOR EACH SUCH LOAD, PUNCH A CARD WITH AN ELEMENT NUMBER IN [1-5], AN EDGE NUMBER IN [6-10], EITHER <U>, <V>, OR <W> TO INDICATE THE DIRECTION OF THE LOAD IN [16], AND THE MAGNITUDE OF THE LOAD IN [21-35]. FOR UNIFORMLY DISTRIBUTED LOADS, LEAVE THE REST OF THE CARD BLANK. OTHERWISE PUNCH <*> IN [36] (SYMBOLIZING MULTIPLICATION), AND A VARIATION SPECIFIER IN [37]. SPECIFICATIONS ARE CUMULATIVE, SO THAT A LOADING OF THE FORM 1-X+X , FOR EXAMPLE, MAY BE INPUT AS THREE SEPARATE LOADINGS.

SET L3. SURFACE LOADS. LOADINGS DISTRIBUTED OVER THE SURFACES OF ELEMENT MAY BE SPECIFIED, ORIENTED IN THE U, V,

Approved for Public Release

Contrails

OR W DIRECTIONS, DISTRIBUTED EITHER UNIFORMLY OR NON-UNIFORMLY AS INDICATED IN SET L2. THE FIRST CARD OF THIS SET HAS <SURFACE∆LOADS> IN [1] AND THE NUMBER OF SUCH LOADS IN [21-25]. FOR EACH LOAD, PUNCH A CARD WITH AN ELEMENT NUMBER IN [1-5], EITHER <U>, V>, OR <W> IN [16] TO INDICATE THE DIRECTION OF THE LOAD, AND ITS MAGNITUDE IN [21-35]. IF THE LOAD DOES NOT VARY IN X, LEAVE THE FIELD [36-42] BLANK, OTHERWISE PUNCH <*> IN [36] AND A VARIATION SPECIFIER (CHOOSE FROM AMONG <X>, <X**2>, <R>, OR <R**2>) IN [37]. (SEE SET L2 FOR AN EXPLANATION OF VARIATION SPECIFIERS). IF THE LOAD DOES NOT VARY WITH Y, LEAVE THE REST OF THE CARD BLANK; OTHERWISE PUNCH <*> IN [43] AND A VARIATION SPECIFIER IN [44] (CHOOSE <Y>, <Y**2>, <SIN(T)>, <SIN(2T)>, <COS(T)>, OR <COS(2T)>).

SET L4. IMPOSED DISPLACEMENTS. PUNCH <IMPOSED∆DISPL.> IN [1] AND THE NUMBER OF IMPOSED DISPLACEMENTS IN [21-25]. PROVIDE ONE CARD FOR EACH IMPOSED DISPLACEMENT WITH AN ELEMENT NUMBER IN [1-5], CORNER NUMBER IN [6-10], DISPLACEMENT SPECIFIER IN [16], AND THE MAGNITUDE OF THE DISPLACEMENT TO BE IMPOSED IN [21-35]. THE PURPOSE OF DATA SET S8 IS TO PROVIDE PROPER VARIABLE NUMBERING. THE PURPOSE OF THIS SET IS TO PRESCRIBE THE MAGNITUDE OF THE IMPOSED DISPLACEMENTS WHICH MAY CHANGE FROM ONE LOAD CONDITION TO THE NEXT.

SET L5. AUTOMATIC LOAD INCREMENTATION. IF THE APPLIED LOADS ARE TO BE INCREASED LINEARLY FOR A NUMBER OF LOAD

Approved for Public Release

Contrails

CONDITIONS, IT IS NOT NECESSARY TO PROVIDE A NEW GROUP OF LOAD CARDS FOR EACH INCREMENT OF LOAD. INSTEAD, THIS OPTION ALLOWS THE USER TO SPECIFY THAT FOR A CERTAIN NUMBER OF LOAD CONDITIONS, A CERTAIN INCREMENT OF LOAD WILL BE ADDED EACH TIME. THIS INCREMENT IS SPECIFIED AS SOME FRACTION OF THE LOAD VECTOR WHICH HAS JUST BEEN FORMED. THIS SAME FRACTION WILL ALSO BE APPLIED TO ANY IMPOSED DISPLACEMENTS WHICH HAVE BEEN SPECIFIED. IT IS ALSO POSSIBLE UNDER THIS OPTION TO EXTRAPOLATE LINEARLY THE SOLUTION FOR ONE LOAD CONDITION AS A STARTING POINT FOR THE NEXT LOAD CONDITION. THIS IS ACCOMPLISHED BY SPECIFYING A FRACTION OF THE SOLUTION FOR THE LOAD CONDITION CURRENTLY BEING SPECIFIED WHICH WILL BE ADDED AT EVERY INCREMENTATION STEP. PUNCH <INCREMENTATION> IN [1] AND THE NUMBER OF SUCCEEDING LOAD CONDITIONS FOR WHICH THIS INCREMENTATION IS TO APPLY IN [21-25]. ON A SECOND CARD PUNCH THE FRACTION TO BE APPLIED TO THE LOADS AND IMPOSED DISPLACEMENTS IN [1-15], AND THE FRACTION TO BE APPLIED TO THE SOLUTION IN [16-30]. NOTE THAT FOR EACH LOAD CONDITION DURING WHICH INCREMENTATION IS IN FORCE, NO DATA CARDS WILL BE READ.

SET L6. THIS SET SPECIFIES A STARTING SOLUTION FOR THIS LOAD CONDITION, PRESUMABLY OBTAINED AS OUTPUT FROM A PREVIOUS JOB. THE FIRST CARD HAS <STARTING&SOLUTION> IN [1] AND THE SOLUTION VECTOR FOLLOWS IN A (5E16.8) FORMAT.

8.2. INTERPRETATION OF OUTPUT.

A DESCRIPTION OF THE STRUCTURE IS PRINTED, FOLLOWING

Approved for Public Release

Contrails

THE DATA THAT WAS SUPPLIED. THIS SHOULD BE CHECKED FOR CORRECTNESS. A TABLE SHOWING HOW INDEPENDENT DEGREES-OF-FREEDOM WERE ASSIGNED IS PRINTED NEXT. A TABLE OF STORAGE REQUIREMENTS IS PRINTED, AND IF ANY OF THE ITEMS LISTED EXCEEDS THE MAXIMUM ALLOWED, THE RUN IS TERMINATED. THE INPUT/OUTPUT PHASE PRINTS A DESCRIPTION OF THE LOADS THAT WERE SPECIFIED, AND THE WORK-EQUIVALENT LOAD VECTOR WHICH WAS GENERATED. THE MATRIX INVERSION PORTION OF THE ANALYSIS PHASE PRINTS THE FINAL SOLUTION VECTOR. THE MINIMIZATION ROUTINES PRINT VARIOUS INFORMATION, AS DESCRIBED IN SPECIFICATION SET S14. FOLLOWING THE ANALYSIS PHASE, THE INPUT/OUTPUT PHASE TAKES OVER AND PRINTS DISPLACEMENTS, STRAINS, AND STRESSES AT EACH CORNER OF EACH ELEMENT, AND AT OTHER POINTS SPECIFIED BY DATA SET S17. STRAINS AND STRESSES ARE CALCULATED AT THE MIDDLE SURFACE AND BOTH FACES.

A WORD OF CAUTION ABOUT STRAINS AND STRESSES IS IN ORDER. AS STATED ABOVE, OSCULATORY INTERPOLATION IS THE LOWEST ORDER OF INTERPOLATION POSSIBLE FOR INTERPOLATION OF BENDING DISPLACEMENTS, WHILE FOR MEMBRANE DISPLACEMENTS LAGRANGE INTERPOLATION IS POSSIBLE. A RESULT OF THIS IS THAT WHEN OSCULATORY INTERPOLATION IS USED TO INTERPOLATE BOTH MEMBRANE AND BENDING DISPLACEMENTS, THE MEMBRANE STRAINS, OR MIDDLE SURFACE STRAINS, WHICH COME FROM FIRST PARTIAL DERIVATIVES OF U AND V, WILL BE MORE ACCURATE THAN SURFACE STRESSES, WHICH DEPEND ON SECOND DERIVATIVES OF W.

Approved for Public Release

Contrails

MEMBRANE STRAINS IN THIS CASE WILL VARY QUADRATICALLY IN X AND IN Y, AND WILL BE CONTINUOUS BETWEEN CO-PLANAR ELEMENTS (UNLESS THIS CONTINUITY HAS BEEN SUPPRESSED), WHILE BENDING MOMENTS WILL VARY LINEARLY IN X AND IN Y, AND ARE DISCONTINUOUS BETWEEN ELEMENTS. HOWEVER, WHEN HYPEROSCULATORY INTERPOLATION IS USED FOR BENDING VARIABLES, THE BENDING MOMENTS WILL VARY CUBICALLY, WILL BE CONTINUOUS BETWEEN ELEMENTS, AND WILL THEREFORE BE MORE ACCURATE. WHEN LAGRANGE INTERPOLATION IS USED FOR MEMBRANE VARIABLES, THE STATE OF MIDDLE-SURFACE STRESS WILL BE CONSTANT IN EACH ELEMENT, AND THUS WILL GENERALLY BE ONLY A ROUGH APPROXIMATION TO THE ACTUAL STRESS STATE.

B.3. A SAMPLE STRUCTURE.

TABLE B1 SHOWS THE DATA CARDS CORRESPONDING TO THE SAMPLE STRUCTURE SHOWN IN FIG. B1. THIS MODEL WAS CHOSEN TO ILLUSTRATE A WIDE VARIETY OF ELEMENT TYPES AND CONNECTIONS, AND DOES NOT REPRESENT ANY REALISTIC STRUCTURE. THE FOLLOWING COMMENTARY REFERS TO CARD NUMBERS ALONG THE LEFT-HAND MARGIN OF TABLE B1. THESE SERIAL NUMBERS ARE NOT ACTUALLY PUNCHED ON THE DATA CARDS.

CARD 1 IS THE TITLE CARD.

CARDS 2-16 CONSTITUTE SET S1. THE NUMBER 14 ON CARD 2 INDICATES THAT THERE ARE 14 CONNECTIONS BETWEEN ELEMENTS. CARD 3 INDICATES THAT ELEMENT 1, CORNERS 3 AND 4, JOINS ELEMENT 2, CORNERS 2 AND 1, AND THAT THE X AND Y AXES OF ELEMENT 1 LINE UP WITH THE X AND Y AXES OF ELEMENT 2.

Approved for Public Release

Contrails

NORMAL AND SHEAR STRAIN CONTINUITY BETWEEN THESE TWO ELEMENTS ARE SUPPRESSED BECAUSE OF THE STIFFENER BETWEEN THEM. CARD 4 INDICATES THAT ELEMENT 1 JOINS ELEMENT 8, AND THAT THE X AND Y AXES OF ELEMENT 1 LINE UP WITH THE -Z AND +Y AXES OF 8. NOTE THAT SINCE ELEMENT 1 IS JOINED TO 2, AND 1 IS JOINED TO 8, IT WOULD BE REDUNDANT TO SPECIFY EXPLICITLY THAT 2 IS JOINED TO 8. CONSIDER THE VERTICAL LINE WHERE ELEMENTS 5, 6, 7, AND 8 MEET. THREE RELATIONSHIPS AMONG THESE ELEMENTS ARE REQUIRED TO MAKE THESE ELEMENTS REMAIN MUTUALLY PERPENDICULAR. ELEMENT 5 IS JOINED TO 6, 7 TO 8, AND 5 TO 8. IT WOULD HAVE BEEN EQUALLY VALID TO CONNECT 5 TO 7, 6 TO 7, AND 6 TO 8.

CARDS 17 THROUGH 23 CONSTITUTE THE FIRST OF FIVE OCCURRENCES OF SET S2. THESE FIVE SETS COULD HAVE APPEARED IN ANY ORDER. CARD 18 INDICATES THAT ELEMENTS 1 AND 2 ARE RECTANGULAR. CARDS 19 AND 20 INDICATE THAT OSCULATORY (FIRST-ORDER) POLYNOMIALS WILL BE USED TO INTERPOLATE BOTH MEMBRANE AND BENDING DISPLACEMENTS. CARD 21 SPECIFIES NONLINEAR STRAIN-DISPLACEMENT RELATIONS FOR THESE ELEMENTS. CARD 22 HAS THE MODULUS OF ELASTICITY, POISSON'S RATIO, AND THICKNESS FOR THESE ELEMENTS, AND CARD 23 HAS THE PLANFORM DIMENSIONS OF THE ELEMENTS. THE SET 24-30 IS SIMILAR, EXCEPT THAT CARD 30 HAS THE AXIAL LENGTH, RADIUS, AND ARC IN DEGREES FOR THESE ELEMENTS, WHICH ARE CYLINDRICAL. CARD 46 INDICATES THE INNER RADIUS, OUTER RADIUS, AND ARC IN DEGREES FOR ELEMENT 7.

Approved for Public Release

Contrails

CARD 55 INDICATES THAT BENDING BOUNDARY CONDITIONS ARE TO BE APPLIED TO FOUR ELEMENT EDGES. CARD 56 INDICATES THAT EDGE 2 OF ELEMENT 1 IS CLAMPED, AND THE NEXT THREE CARDS ARE SIMILAR.

CARD 60 CALLS FOR FLETCHER-REEVES NONLINEAR ENERGY SEARCH. CARD 61 INDICATES THAT A LINEAR SOLUTION WILL BE SOUGHT FIRST, USING MATRIX INVERSION.

CARD 62 SPECIFIES THAT THERE ARE FOUR MEMBRANE BOUNDARY CONDITIONS, WHICH FOLLOW ON CARDS 63-66.

CARD 67 SPECIFIES PUNCHED OUTPUT OF THE SOLUTION VECTOR AT THE END OF EACH LOAD CONDITION.

CARD 68 CUTS DOWN THE OUTPUT FROM FLETCHER-REEVES. THE SOLUTION VECTOR AND GRADIENT VECTOR WILL BE PRINTED ONLY AFTER EVERY 69 ITERATIONS.

CARD 69 IS THE LOADS CARD, WHICH INDICATES THAT THE SPECIFICATION SECTION IS COMPLETE, AND A SET OF LOAD CARDS IS TO FOLLOW.

CARD 70 INDICATES THAT THERE ARE SIX LINE LOADS DISTRIBUTED ALONG ELEMENT EDGES. FIGURE B1 SHOWS A VERTICAL LINE LOAD ACTING ON THE EDGES OF ELEMENTS 1 AND 3. THIS LOAD MUST BE RESOLVED INTO RADIAL AND TANGENTIAL COMPONENTS FOR ELEMENT 3. ASSUME THE MAGNITUDE OF THE LOAD IS 5.0 (FORCE PER UNIT LENGTH). THEN, APPLYING THE TRANSFORMATION FOR A STATE OF PLANE STRESS AND NOTING THAT THE FREE EDGE OF THE CYLINDRICAL ELEMENT IS THE 0=0 EDGE, THE RADIAL COMPONENT OF THIS LOAD IS

Approved for Public Release

Contrails

2.5*[1+0.93969*COS(20)+0.34202*SIN(20)],

AND THE TANGENTIAL (SHEAR) COMPONENT IS

2.5*[0.34202*COS(20)-0.93969*SIN(20)].

CARD 71 SPECIFIES THE LINE LOAD FOR ELEMENT 1 (ELEMENT NUMBER, EDGE NUMBER, DIRECTION SPECIFIER, AND MAGNITUDE). SINCE THE RADIAL COMPONENT OF THE LOAD ON ELEMENT 3 CONSISTS OF THREE TERMS, IT IS ENTERED ON THREE CARDS: 72, 73, AND 74. FINALLY, THE TANGENTIAL COMPONENT IS ENTERED ON CARDS 75 AND 76.

CARD 77 INDICATES THAT TWO ELEMENTS ARE SUBJECTED TO SURFACE LOADS, WHICH ARE SPECIFIED ON CARDS 78 AND 79.

CARD 80 CALLS FOR THREE MORE LOAD CONDITIONS, EACH OBTAINED FROM THE PREVIOUS LOADS BY SUBTRACTING 25 PERCENT OF THE FIRST LOAD. THIS COULD HAVE BEEN DONE BY SPECIFYING THREE MORE LOAD SETS, EACH SIMILAR TO THE SET 70-79, WITH THE LINE LOAD TAKING ON THE VALUES 3.75, 2.5, AND 1.25, AND THE SURFACE LOAD TAKING THE VALUES -0.75, -0.5, AND -0.25.

CARD 82 MUST BE THE LAST CARD OF THE DECK.

TABLE B2 SHOWS OUTPUT WHICH WAS OBTAINED FROM THE UNIVAC 1108 COMPUTER FOR THE SAMPLE STRUCTURE. THIS OUTPUT IS SELF-EXPLANATORY. THE LAST PAGE, SHOWING DISPLACEMENT, STRAIN, AND STRESS RESULTS, DOES NOT CORRESPOND TO THE SAMPLE STRUCTURE, SINCE IT WAS FELT THAT RUNNING THIS UNREALISTIC PROBLEM TO COMPLETION WOULD BE A WASTE OF COMPUTER TIME. THIS PAGE WAS TAKEN FROM ANOTHER RUN, AND IS TYPICAL OF THE OUTPUT WHICH IS PRODUCED.

Approved for Public Release

Contrails

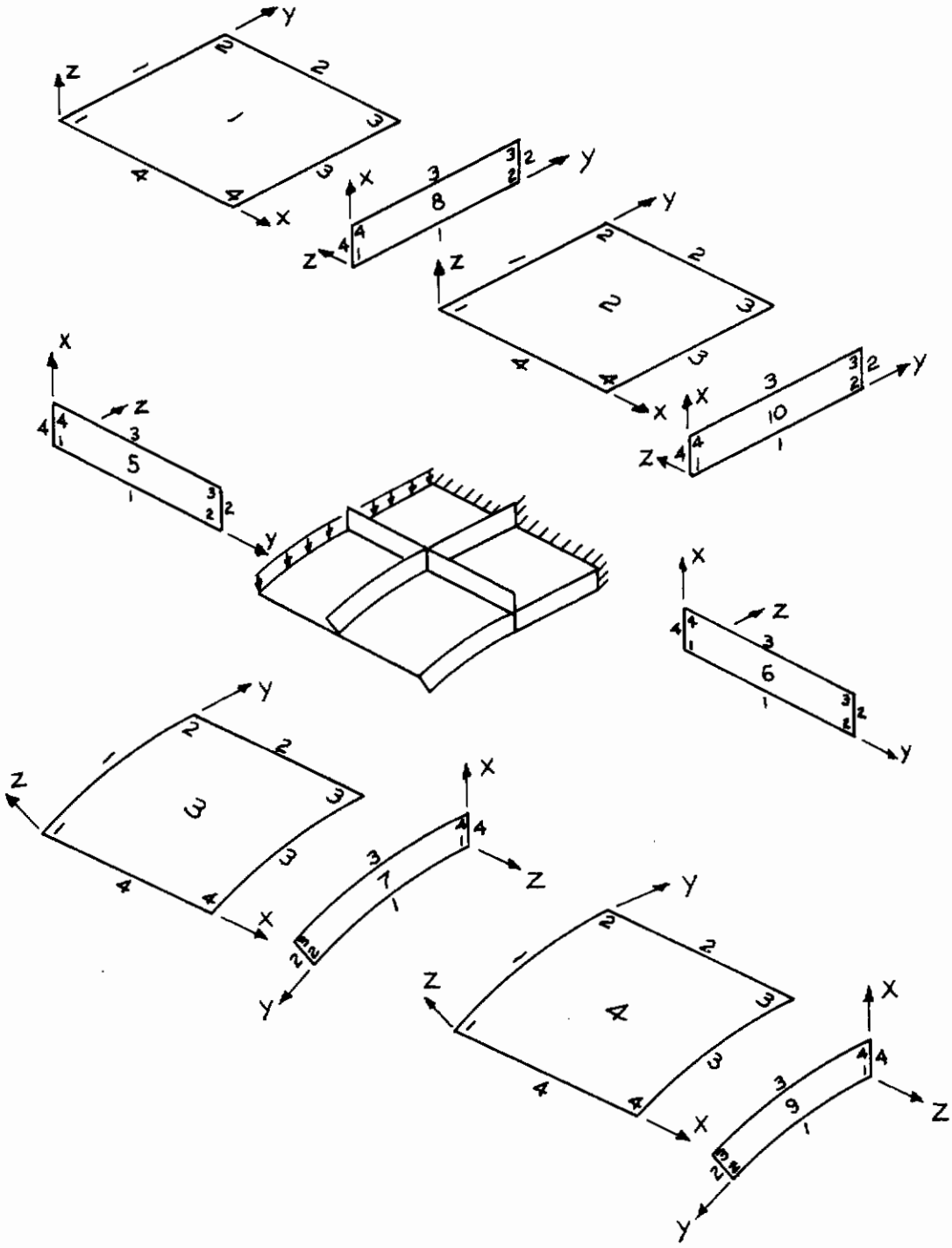

Fig. B1 Sample Structure

Approved for Public Release

Table B1 Sample Input Data

```
1.  STRUCTURE ILLUSTRATING DATA CARD PREPARATION
2.  ELEMENT CONNECTIONS    14
3.       1    3    4    2    2    1   +X   +Y      NORMAL     SHEAR
4.       1    3    4    8    2    1   -Z   +Y
5.       2    3    4   10    3    4   -Z   +Y
6.       1    1    4    3    2    3   +X   +Y      NORMAL     SHEAR
7.       7    1    4    8    1    4   +X   -Y      NORMAL     SHEAR
8.       2    1    4    4    2    3   +X   +Y      NORMAL     SHEAR
9.       9    1    4   10    1    4   +X   -Y
10.      1    1    4    5    1    2   +Y   +Z
11.      2    1    4    6    1    2   +Y   +Z
12.      5    2    3    6    1    4   +X   +Y      NORMAL     SHEAR
13.      5    2    3    8    1    4   +X   -Z
14.      3    3    4    4    2    1   +X   +Y      NORMAL     SHEAR
15.      3    3    4    7    1    2   +Z   -Y
16.      4    3    4    9    4    3   +Z   -Y
17. ELEMENTS                  1    2
18.       RECTANGULAR
19.       MEMBRANE  POLYNOMIALS          1
20.       BENDING   POLYNOMIALS          1
21.       NONLINEAR
22.       10000000.        .3                .01
23.       1.0              1.0
24. ELEMENTS                  3    4
25.       CYLINDRICAL
26.       MEMBRANE  TRIGONOMETRIC         1
27.       BENDING   TRIGONOMETRIC         1
28.       LINEAR
29.       10000000.        .3                .01
30.       1.0              10.0              10.0                    DEGREES
31. ELEMENTS                  5    6    8   10
32.       RECTANGULAR
33.       MEMBRANE  POLYNOMIALS          1
34.       BENDING   POLYNOMIALS          1
35.       STIFFENER
36.       LINEAR
37.       10000000.        .3                .01
38.       0.1              1.0
39. ELEMENTS                  7
40.       ANNULAR
41.       MEMBRANE  TRIGONOMETRIC         1
42.       BENDING   TRIGONOMETRIC         1
43.       STIFFENER
44.       LINEAR
45.       10000000.        .3                .01
46.       10.0             10.1              10.0                    DEGREES
47. ELEMENTS                  9
48.       ANNULAR
49.       MEMBRANE  TRIGONOMETRIC         1
50.       BENDING   TRIGONOMETRIC         1
51.       STIFFENER
52.       LINEAR
53.       10000000.        .3                .01
```


Approved for Public Release

Table B1 Sample Input Data (Continued)

```
      9.9                  10.0                 10.0                 DEGREES
BENDING B.C.                    4
    1     2      CLAMPED
    8     2      CLAMPED
    2     2      CLAMPED
   10     2      CLAMPED
FLETCHER-REEVES
INVERT
MEMBRANE B.C.                   4
    1     2      U AND V PREVENTED
    8     2      U AND V PREVENTED
    2     2      U AND V PREVENTED
   10     2      U AND V PREVENTED
PUNCH SOLUTION
REDUCE PRINTING                69
LOADS
LINE LOADS                      6
    1     1      W    5.0
    3     1      W    2.5
    3     1      W    2.349225          *COS(2T)
    3     1      W    0.855050          *SIN(2T)
    3     1      V   -0.855050          *COS(2T)
    3     1      V    2.349225          *SIN(2T)
SURFACE LOADS                   2
    1            W   -1.0
    2            W   -1.0
INCREMENTATION                  3
     -0.25               -0.25
STOP
```


Approved for Public Release

Table B2 Output for Sample Structure

STRUCTURE ILLUSTRATING DATA CARD PREPARATION 22 JUL 68 PAGE 1

ELEMENT CONNECTIONS

	ELEMENT	EDGE	CORNERS		AXIS ALIGNMENT	
PRIMARY	1	3	3	4	+X	+Y
SECONDARY	2	1	2	1	+X	+Y
PRIMARY	1	3	3	4	+X	+Y
SECONDARY	8	1	2	1	-Z	+Y
PRIMARY	2	3	3	4	+X	+Y
SECONDARY	10	3	3	4	-Z	+Y
PRIMARY	1	4	1	4	+X	+Y
SECONDARY	3	2	2	3	+X	+Y
PRIMARY	7	4	1	4	+X	+Y
SECONDARY	8	4	1	4	+X	-Y
PRIMARY	2	4	1	4	+X	+Y
SECONDARY	4	2	2	3	+X	+Y
PRIMARY	9	4	1	4	+X	+Y
SECONDARY	10	4	1	4	+X	-Y
PRIMARY	1	4	1	4	+X	+Y
SECONDARY	5	1	1	2	+Y	+Z
PRIMARY	2	4	1	4	+X	+Y
SECONDARY	6	1	1	2	+Y	+Z
PRIMARY	5	2	2	3	+X	+Y
SECONDARY	6	4	1	4	+X	+Y
PRIMARY	5	2	2	3	+X	+Y
SECONDARY	6	4	1	4	+X	-Z
PRIMARY	3	3	3	4	+X	+Y
SECONDARY	4	1	2	1	+X	+Y
PRIMARY	3	3	3	4	+X	+Y
SECONDARY	7	1	1	2	+Z	-Y
PRIMARY	4	3	3	4	+X	+Y
SECONDARY	9	3	4	3	+Z	-Y

ELEMENT PROPERTIES

GROUP 1

Approved for Public Release

Table B2 Output for Sample Structure
(continued)

STRUCTURE ILLUSTRATING DATA CARD PREPARATION 22 JUL 68 PAGE 2

ELEMENT NUMBER(S)	1
	2
TYPE	RECTANGULAR PLATE
MEMBRANE INTERPOLATION	OSCULATORY POLYNOMIALS
BENDING INTERPOLATION	OSCULATORY POLYNOMIALS
GEOMETRY	NONLINEAR
X LENGTH	.10000000+01
Y LENGTH	.10000000+01
ELASTIC MODULUS	.10000000+08
POISSON'S RATIO	.30000000-00
THICKNESS	.99999999-02
GROUP 2	
ELEMENT NUMBER(S)	3
	4
TYPE	CYLINDRICAL SHELL
MEMBRANE INTERPOLATION	OSCULATORY POLYNOMIALS AND OSCULATORY TRIGONOMETRICS
BENDING INTERPOLATION	OSCULATORY POLYNOMIALS AND OSCULATORY TRIGONOMETRICS
GEOMETRY	LINEAR
AXIAL LENGTH	.10000000+01
ARC IN DEGREES	.10000000+02
RADIUS	.10000000+02
ELASTIC MODULUS	.10000000+08
POISSON'S RATIO	.30000000-00
THICKNESS	.99999999-02
GROUP 3	
ELEMENT NUMBER(S)	5
	6
	8
	10
TYPE	RECTANGULAR PLATE STIFFENER
MEMBRANE INTERPOLATION	OSCULATORY POLYNOMIALS
BENDING INTERPOLATION	OSCULATORY POLYNOMIALS
GEOMETRY	LINEAR
X LENGTH	.99999999-01
Y LENGTH	.10000000+01
ELASTIC MODULUS	.10000000+08
POISSON'S RATIO	.30000000-00
THICKNESS	.99999999-02
GROUP 4	
ELEMENT NUMBER(S)	7
TYPE	ANNULAR PLATE STIFFENER
MEMBRANE INTERPOLATION	OSCULATORY POLYNOMIALS AND OSCULATORY TRIGONOMETRICS
BENDING INTERPOLATION	OSCULATORY POLYNOMIALS AND OSCULATORY TRIGONOMETRICS
GEOMETRY	LINEAR
INNER RADIUS	.10000000+02

Approved for Public Release

Table B2 Output for Sample Structure
(Continued)

STRUCTURE ILLUSTRATING DATA CARD PREPARATION 22 JUL 68 PAGE 3

OUTER RADIUS	.10100000+02
ARC IN DEGREES	.10000000+02
ELASTIC MODULUS	.10000000+08
POISSON'S RATIO	.30000000-00
THICKNESS	.99999999-02

GROUP 5

ELEMENT NUMBER(S)	9
TYPE	ANNULAR PLATE STIFFENER
MEMBRANE INTERPOLATION	OSCULATORY POLYNOMIALS AND OSCULATORY TRIGONOMETRICS
BENDING INTERPOLATION	OSCULATORY POLYNOMIALS AND OSCULATORY TRIGONOMETRICS
GEOMETRY	LINEAR
INNER RADIUS	.99000000+01
OUTER RADIUS	.10000000+02
ARC IN DEGREES	.10000000+02
ELASTIC MODULUS	.10000000+08
POISSON'S RATIO	.30000000-00
THICKNESS	.99999999-02

EDGE RESTRAINTS (BENDING)

ELEMENT	EDGE	RESTRAINT
1	2	CLAMPED
8	2	CLAMPED
2	2	CLAMPED
10	2	CLAMPED

EDGE RESTRAINTS (MEMBRANE)

ELEMENT	EDGE	RESTRAINT
1	2	U AND V PREVENTED
8	2	U AND V PREVENTED
2	2	U AND V PREVENTED
10	2	U AND V PREVENTED

CORRELATION OF ELEMENT DISPLACEMENT VARIABLES TO INDEPENDENT DEGREES-OF-FREEDOM
INTEGERS INDICATE COMPONENTS OF THE SOLUTION VECTOR
(-) MEANS THE NEGATIVE OF THE INDICATED COMPONENT
0 MEANS ZERO DISPLACEMENT MAINTAINED
(I) INDICATES A COMPONENT OF THE IMPOSED DISPLACEMENT VECTOR
(I-) MEANS THE NEGATIVE OF THE INDICATED IMPOSED DISPLACEMENT VECTOR COMPONENT

ELEMENT 1

CORNER	U	UX	UY	UXY	V	VX	VY	VXY	W	WX	WY	WXY
1	1	2	3	4	12	13	14	15	23	24	25	26
2	0	0	5	6	0	0	16	17	0	0	0	0
3	0	0	0	7	0	0	18	19	0	0	0	0

Approved for Public Release

Table B2 Output for Sample Structure (Continued)

STRUCTURE ILLUSTRATING DATA CARD PREPARATION — 22 JUL 68 — PAGE 4

4 8 9 10(-) 11 20 10 21 22 27 28(-) 29 0

ELEMENT 2

CORNER	U	UX	UY	UXY	V	VX	VY	VXY	W	WX	WY	WXY
1	8	30	10(-)	31	20	10	21	22	27	28(-)	29	0
2	0	0	0	32	0	0	18	19	0	0	0	0
3	0	0	0	33	0	0	38	39	0	0	0	0
4	34(-)	35	36(-)	37	40	41	42	43	44	45	46	47

ELEMENT 3

CORNER	U	UX	UY	UXY	V	VX	VY	VXY	W	WX	WY	WXY
1	48	49	50	51	56	57	58	59	68	69	70	71
2	1	2	3	4	12	13	60	61	23	24	25	26
3	8	9	10(-)	11	20	10	62	63	27	28(-)	29	0
4	52	53	54	55	64	65	66	67	72	73	74	75

ELEMENT 4

CORNER	U	UX	UY	UXY	V	VX	VY	VXY	W	WX	WY	WXY
1	52	76	54	77	64	65	66	67	72	73	74	75
2	8	30	10(-)	31	20	10	62	63	27	28(-)	29	0
3	34(-)	35	36(-)	37	40	41	42	82	44	45	46	47
4	78	79	80(-)	81	83(-)	84	85	86	87	88(-)	89(-)	90

ELEMENT 5

CORNER	U	UX	UY	UXY	V	VX	VY	VXY	W	WX	WY	WXY
1	23	0	24	0	1	91	2	92	12	25(-)	13	26(-)
2	27	0	28(-)	0	8	28	9	93	20	29(-)	10	0
3	27	0	28(-)	0	94	95	96	97	102	103	104	105
4	23	0	24	0	98	99	100	101	106	107	108	109

ELEMENT 6

CORNER	U	UX	UY	UXY	V	VX	VY	VXY	W	WX	WY	WXY
1	27	0	28(-)	0	8	28	30	110	20	29(-)	10	0
2	44	0	45	0	34(-)	111	35	112	40	46(-)	41	47(-)
3	44	0	45	0	113	114	115	116	119	120	121	122
4	27	0	28(-)	0	94	95	117	118	102	103	104	105

ELEMENT 7

CORNER	U	UX	UY	UXY	V	VX	VY	VXY	W	WX	WY	WXY
1	27	0	29(-)	0	20(-)	29	62	123	8	28	10	0
2	72	0	74(-)	0	64(-)	124	66	125	52	73(-)	54(-)	75
3	72	0	74(-)	0	126	127	128	129	132	133	134	135
4	27	0	29(-)	0	102(-)	103(-)	130	131	94	95	104	105

ELEMENT 8

CORNER	U	UX	UY	UXY	V	VX	VY	VXY	W	WX	WY	WXY
1	27	0	29	0	20	29(-)	21	136	8(-)	28(-)	10	0
2	0	0	0	0	0	0	18	137	0	0	0	0
3	0	0	0	0	0	0	138	139	0	0	0	0
4	27	0	29	0	102	103	140	141	94(-)	95(-)	104	105

ELEMENT 9

CORNER	U	UX	UY	UXY	V	VX	VY	VXY	W	WX	WY	WXY
1	44	0	46(-)	0	142(-)	143(-)	144	145	154(-)	155(-)	156	157

Approved for Public Release

Table B2 Output for Sample Structure
(Continued)

STRUCTURE ILLUSTRATING DATA CARD PREPARATION 22 JUL 68 PAGE 5

2	87	0	89	0	146	147	148	149	158	159	160	161
3	87	0	89	0	83	150	85	151	78	88	80	90
4	44	0	46(-)	0	40(-)	152(-)	42	153	34(-)	45(-)	36	47

ELEMENT 10

CORNER	U	UX	UY	UXY	V	VX	VY	VXY	W	WX	WY	WXY
1	44	0	46	0	142	143	144	145	154	155	156	157
2	0	0	0	0	0	0	162	163	0	0	0	0
3	0	0	0	0	0	0	38	164	0	0	0	0
4	44	0	46	0	40	152	42	153	34	45	36	47

STORAGE INFORMATION

	CALLED FOR	MAX ALLOWED
ELEMENTS	10	50
DEGREES OF FREEDOM	164	250
IMPOSED DISPLACEMENTS	0	30
EQUALITY GROUPS	102	500
CORE STORAGE FOR FP, FSUB	8093	40000

SETUP TIME 30.88 SECONDS

Approved for Public Release

Table B2 Output for Sample Structure
(Continued)

STRUCTURE ILLUSTRATING DATA CARD PREPARATION LOAD 1 22 JUL 68 PAGE 6

PRESCRIBED LOADS FOR CONDITION 1

LINE LOADS

ELEMENT	EDGE	DIRECTION	MAGNITUDE
1	1	W	.50000000+01
3	1	W	.25000000+01
3	1	W	.23492250+01*COS(2T)
3	1	W	.85505000-00*SIN(2T)
3	1	V	-.85505000-00*COS(2T)
3	1	V	.23492250+01*SIN(2T)

SURFACE LOADS

ELEMENT	DIRECTION	MAGNITUDE
1	W	-.10000000+01
2	W	-.10000000+01

	INITIAL SOLUTION VECTOR				WORK-EQUIVALENT LOAD VECTOR			
1	.00000000	83	.00000000		1	.00000000	83	.00000000
2	.00000000	84	.00000000		2	.00000000	84	.00000000
3	.00000000	85	.00000000		3	.00000000	85	.00000000
4	.00000000	86	.00000000		4	.00000000	86	.00000000
5	.00000000	87	.00000000		5	.00000000	87	.00000000
6	.00000000	88	.00000000		6	.00000000	88	.00000000
7	.00000000	89	.00000000		7	.00000000	89	.00000000
8	.00000000	90	.00000000		8	.00000000	90	.00000000
9	.00000000	91	.00000000		9	.00000000	91	.00000000
10	.00000000	92	.00000000		10	.00000000	92	.00000000
11	.00000000	93	.00000000		11	.00000000	93	.00000000
12	.00000000	94	.00000000		12	.13041984+01	94	.00000000
13	.00000000	95	.00000000		13	.00000000	95	.00000000
14	.00000000	96	.00000000		14	.00000000	96	.00000000
15	.00000000	97	.00000000		15	.00000000	97	.00000000
16	.00000000	98	.00000000		16	.00000000	98	.00000000
17	.00000000	99	.00000000		17	.00000000	99	.00000000
18	.00000000	100	.00000000		18	.00000000	100	.00000000
19	.00000000	101	.00000000		19	.00000000	101	.00000000
20	.00000000	102	.00000000		20	.00000000	102	.00000000
21	.00000000	103	.00000000		21	.00000000	103	.00000000
22	.00000000	104	.00000000		22	.00000000	104	.00000000
23	.00000000	105	.00000000		23	.72290059+01	105	.00000000
24	.00000000	106	.00000000		24	-.91666668-01	106	.00000000
25	.00000000	107	.00000000		25	-.10747314+01	107	.00000000
26	.00000000	108	.00000000		26	-.67944448-02	108	.00000000
27	.00000000	109	.00000000		27	-.50000000-00	109	.00000000
28	.00000000	110	.00000000		28	.10626451-08	110	.00000000
29	.00000000	111	.00000000		29	-.83333336-01	111	.00000000
30	.00000000	112	.00000000		30	.00000000	112	.00000000
31	.00000000	113	.00000000		31	.00000000	113	.00000000
32	.00000000	114	.00000000		32	.00000000	114	.00000000
33	.00000000	115	.00000000		33	.00000000	115	.00000000
34	.00000000	116	.00000000		34	.00000000	116	.00000000

Approved for Public Release

Table B2 Output for Sample Structure (Continued)

STRUCTURE ILLUSTRATING DATA CARD PREPARATION LOAD 1 22 JUL 68 PAGE 7

35	.00000000	117	.00000000	35	.00000000	117	.00000000
36	.00000000	118	.00000000	36	.00000000	118	.00000000
37	.00000000	119	.00000000	37	.00000000	119	.00000000
38	.00000000	120	.00000000	38	.00000000	120	.00000000
39	.00000000	121	.00000000	39	.00000000	121	.00000000
40	.00000000	122	.00000000	40	.00000000	122	.00000000
41	.00000000	123	.00000000	41	.00000000	123	.00000000
42	.00000000	124	.00000000	42	.00000000	124	.00000000
43	.00000000	125	.00000000	43	.00000000	125	.00000000
44	.00000000	126	.00000000	44	-.25000000-00	126	.00000000
45	.00000000	127	.00000000	45	.41666666-01	127	.00000000
46	.00000000	128	.00000000	46	-.41666668-01	128	.00000000
47	.00000000	129	.00000000	47	.69444445-02	129	.00000000
48	.00000000	130	.00000000	48	.00000000	130	.00000000
49	.00000000	131	.00000000	49	.00000000	131	.00000000
50	.00000000	132	.00000000	50	.00000000	132	.00000000
51	.00000000	133	.00000000	51	.00000000	133	.00000000
52	.00000000	134	.00000000	52	.00000000	134	.00000000
53	.00000000	135	.00000000	53	.00000000	135	.00000000
54	.00000000	136	.00000000	54	.00000000	136	.00000000
55	.00000000	137	.00000000	55	.00000000	137	.00000000
56	.00000000	138	.00000000	56	.13034284+01	138	.00000000
57	.00000000	139	.00000000	57	.00000000	139	.00000000
58	.00000000	140	.00000000	58	.37924321-00	140	.00000000
59	.00000000	141	.00000000	59	.00000000	141	.00000000
60	.00000000	142	.00000000	60	-.37974198-00	142	.00000000
61	.00000000	143	.00000000	61	.00000000	143	.00000000
62	.00000000	144	.00000000	62	.00000000	144	.00000000
63	.00000000	145	.00000000	63	.00000000	145	.00000000
64	.00000000	146	.00000000	64	.00000000	146	.00000000
65	.00000000	147	.00000000	65	.00000000	147	.00000000
66	.00000000	148	.00000000	66	.00000000	148	.00000000
67	.00000000	149	.00000000	67	.00000000	149	.00000000
68	.00000000	150	.00000000	68	.49768308+01	150	.00000000
69	.00000000	151	.00000000	69	.00000000	151	.00000000
70	.00000000	152	.00000000	70	.14478274+01	152	.00000000
71	.00000000	153	.00000000	71	.00000000	153	.00000000
72	.00000000	154	.00000000	72	.00000000	154	.00000000
73	.00000000	155	.00000000	73	.00000000	155	.00000000
74	.00000000	156	.00000000	74	.00000000	156	.00000000
75	.00000000	157	.00000000	75	.00000000	157	.00000000
76	.00000000	158	.00000000	76	.00000000	158	.00000000
77	.00000000	159	.00000000	77	.00000000	159	.00000000
78	.00000000	160	.00000000	78	.00000000	160	.00000000
79	.00000000	161	.00000000	79	.00000000	161	.00000000
80	.00000000	162	.00000000	80	.00000000	162	.00000000
81	.00000000	163	.00000000	81	.00000000	163	.00000000
82	.00000000	164	.00000000	82	.00000000	164	.00000000

Approved for Public Release

Table B2 Output for Sample Structure (Continued)

PINCHED CYLINDER MODEL 6 LINEAR POLYNOMIALS LOAD 1 18 MAR 68 PAGE 15

DISPLACEMENTS, STRAINS, AND STRESSES IN ELEMENT 8

CORNER	U	UX	UY	UXY
1	-.14658550-04	-.11402526-04	.00000000	.00000000
2	-.71237683-05	-.64462703-05	.13278152-04	.64922139-05
3	-.78453140-05	-.15164656-04	.26650326-07	-.24784351-04
4	-.20537116-04	-.20400627-04	.00000000	.00000000

CORNER	V	VX	VY	VXY
1	.00000000	.00000000	-.19890969-01	-.42804177-05
2	-.35080367-01	-.21701133-04	-.14487696-01	-.24468860-04
3	-.35152446-01	-.32491545-04	-.14557713-01	-.44257669-04
4	.00000000	.00000000	-.19903605-01	-.18947650-04

CORNER	W	WX	WY	WXY
1	.98393346-01	.15851048-03	.00000000	.00000000
2	.71648242-01	.21815344-03	-.26638548-01	-.83755359-05
3	.72261584-01	.11600729-02	-.26688365-01	-.29498336-03
4	.98863593-01	.13246261-02	.00000000	.00000000

TOP SURFACE

CORNER	EX	EY	EXY	SX	SY	SXY
1	.28429238-04	.49189094-03	.00000000	.21195072+04	.58272008+04	.00000000
2	.25713711-04	.42163767-03	-.80475338-05	.18324419+04	.49998336+04	-.32190134+02
3	-.81543180-04	.49027159-03	-.53530966-05	.83939699+03	.50845794+04	-.21412346+02
4	-.10259562-03	.56100228-03	.00000000	.84616829+03	.61549515+04	.00000000

MIDDLE SURFACE

CORNER	EX	EY	EXY	SX	SY	SXY
1	-.11402526-04	-.25564805-04	-.00000000	-.72564687+03	-.33894509+03	-.00000000
2	-.64462703-05	-.22070831-04	-.84229814-05	-.15526871+03	-.28026520+03	-.33691926+02
3	-.15164656-04	.31745759-04	-.32464895-04	-.61022329+02	.31426100+03	-.12985957+03
4	-.20400627-04	.56740595-04	-.00000000	-.31059679+02	.58607009+03	-.00000000

BOTTOM SURFACE

CORNER	EX	EY	EXY	SX	SY	SXY
1	-.51234286-04	-.54302055-03	-.00000000	-.25708009+04	-.65050909+04	-.00000000
2	-.38606251-04	-.46577933-03	-.87984290-05	-.21429794+04	-.55603640+04	-.35193715+02
3	.51213867-04	-.42678007-03	-.59576694-04	-.95598435+03	-.47799359+04	-.23830678+03
4	.61794370-04	-.44752108-03	-.00000000	-.90828764+03	-.49828113+04	-.00000000

Approved for Public Release

Contrails

APPENDIX C

EXPERIMENTAL DATA

Approved for Public Release

Contrails

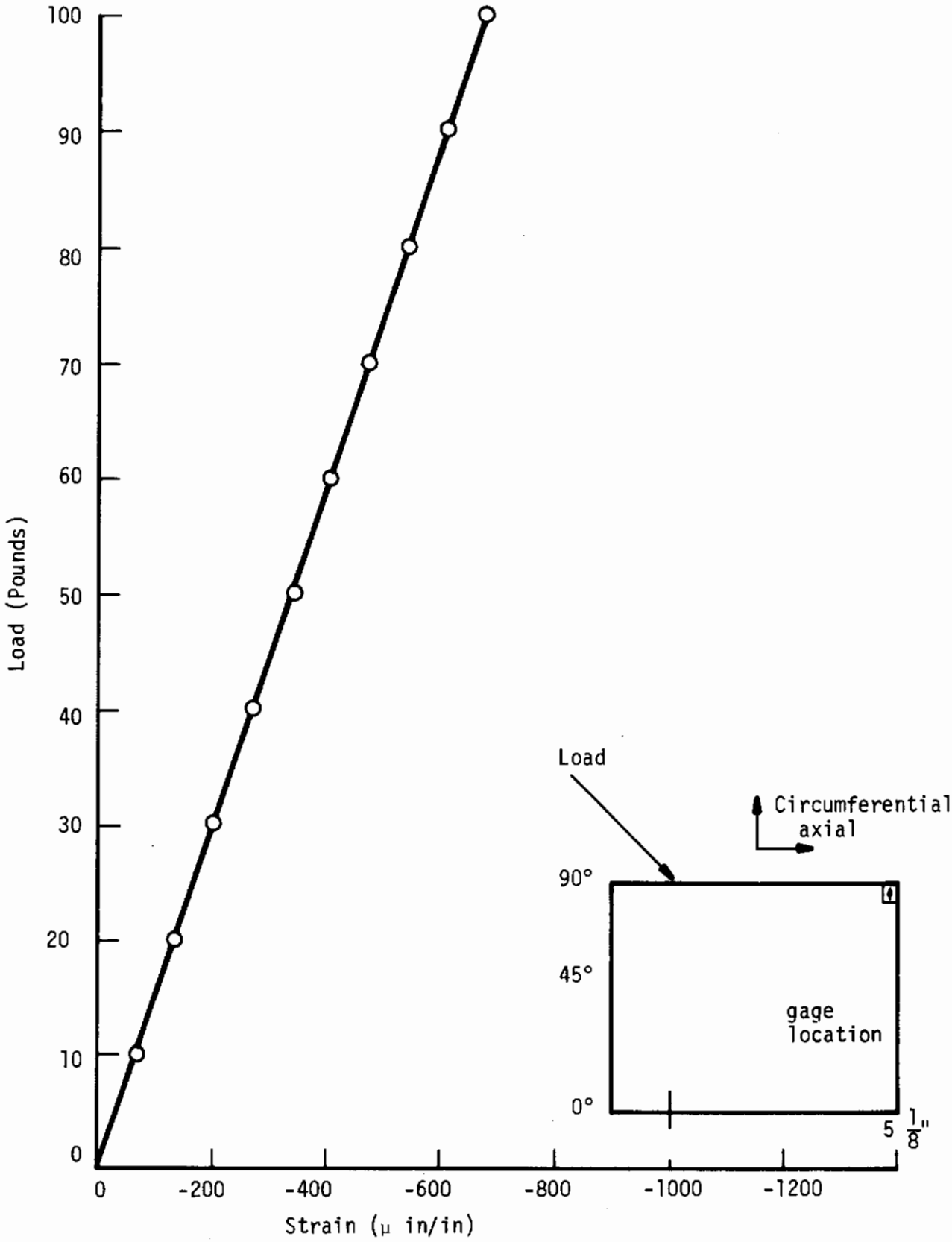

Figure C.1 Load vs. Strain Pinched Cylinder , Gage No. 1

Approved for Public Release

Contrails

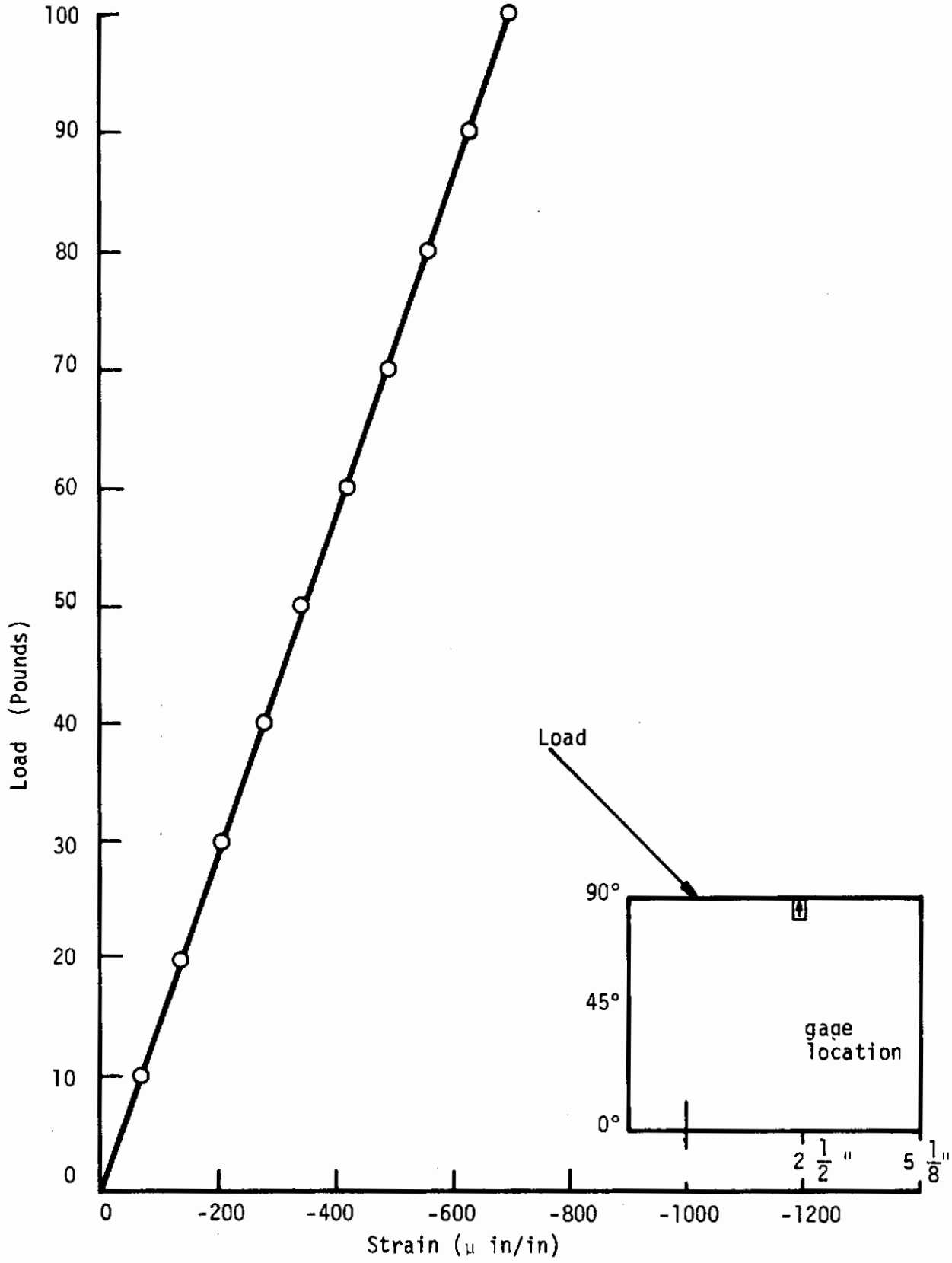

Figure C.2 Load vs. Strain Pinched Cylinder, Gage No. 3

Approved for Public Release

Contrails

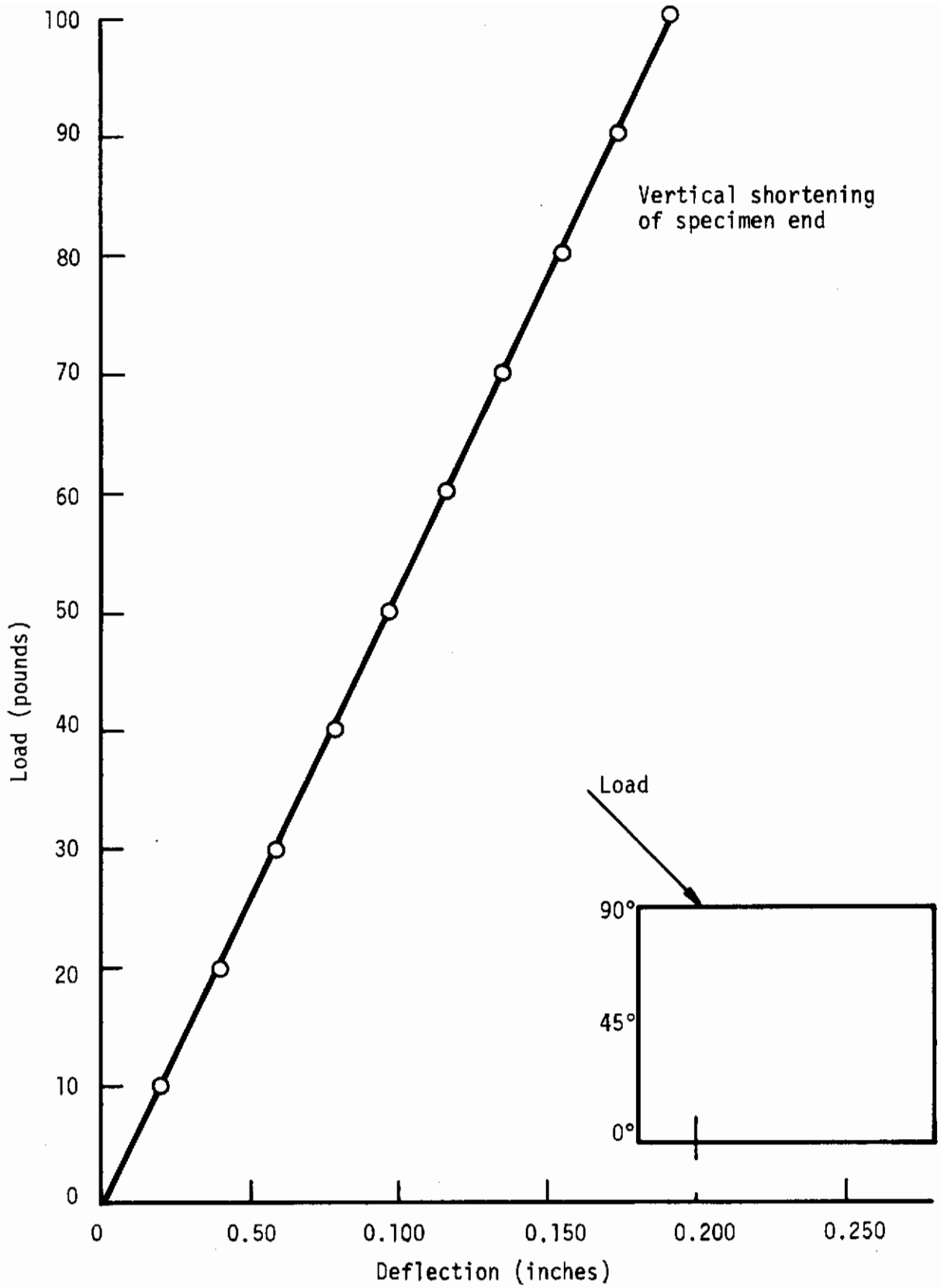

Figure C.3 Load vs. Deflection Pinched Cylinder

Approved for Public Release

Contrails

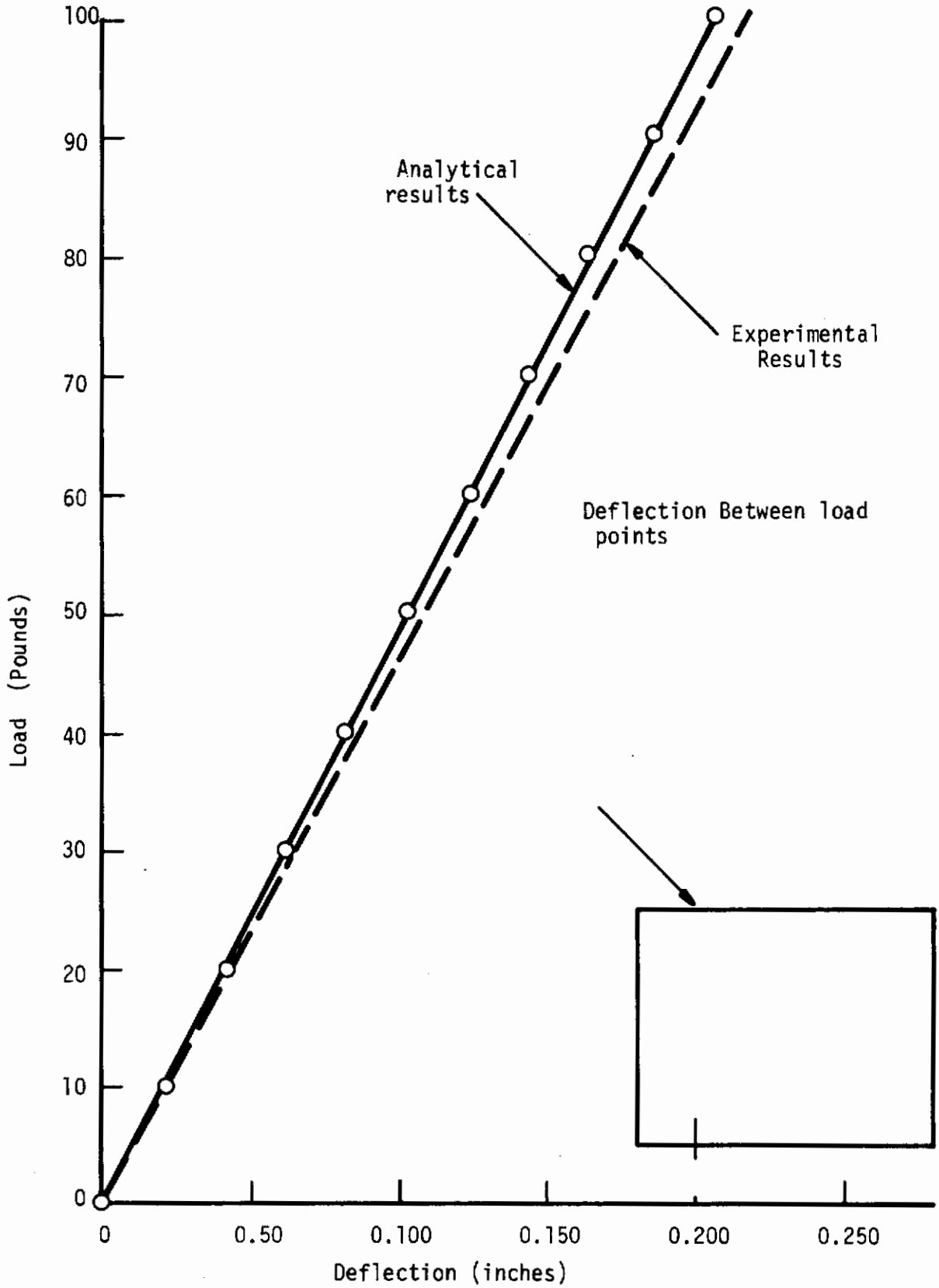

Figure C.4 Load vs. Deflection Pinched Cylinder

Approved for Public Release

Contrails

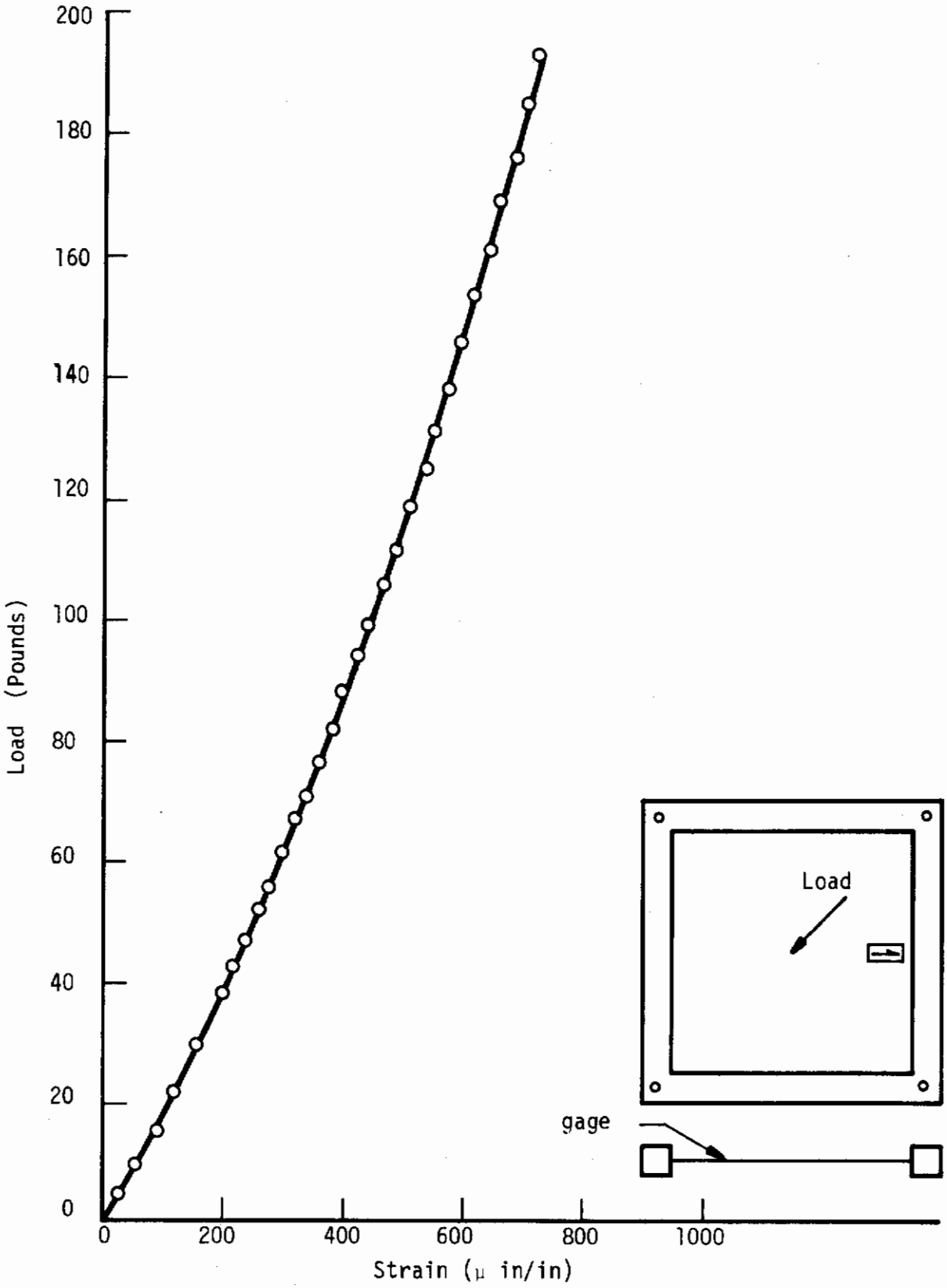

Figure C.5 Load vs. Strain, Rectangular Plate, Corner Supports, Elastic Edge Supports, Transverse Load at Center. Gage No. 6

Approved for Public Release

Contrails

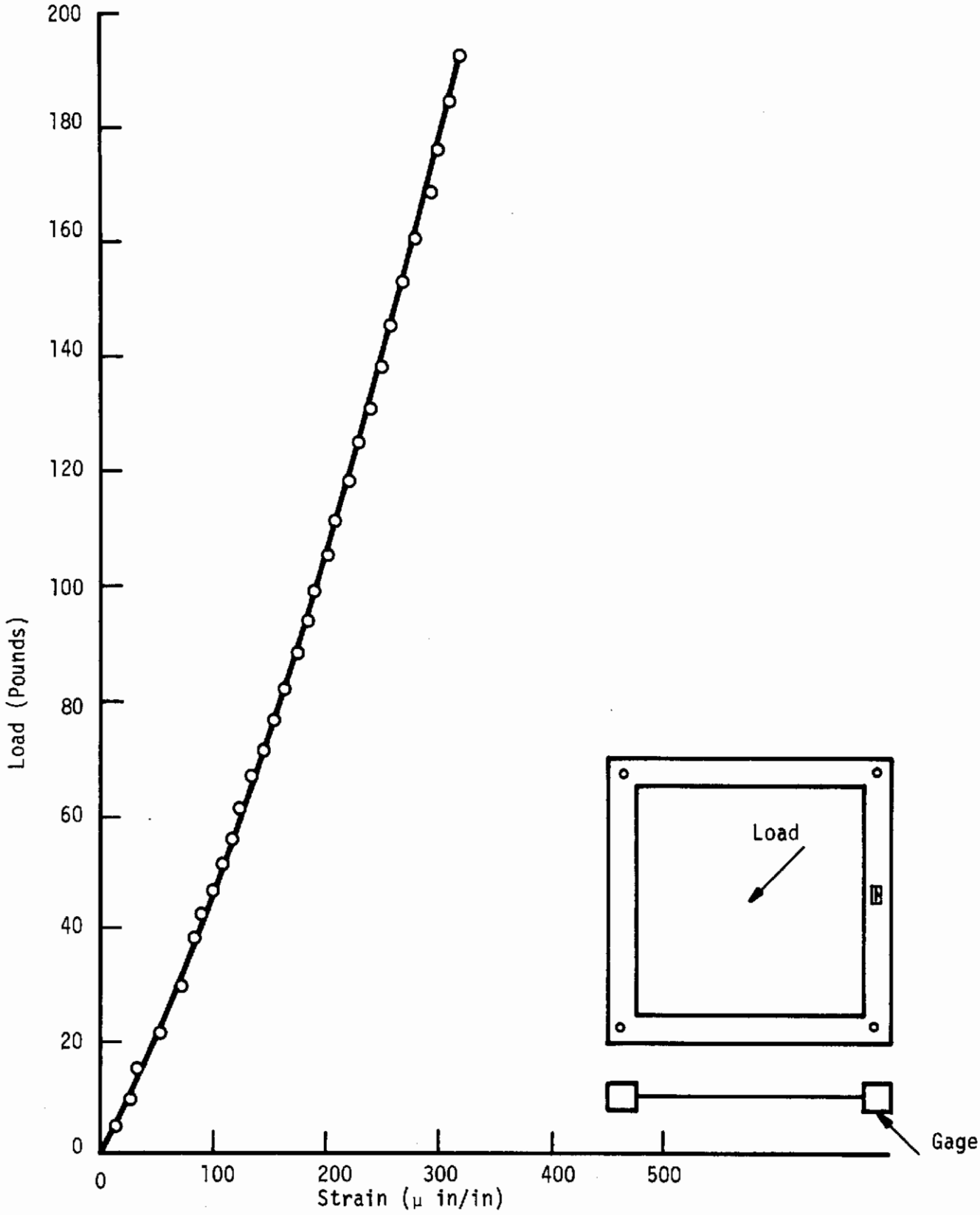

Figure C.6 Load vs. Strain, Rectangular Plate, Corner Supports, Elastic Edge Supports, Transverse Load at Center, Gage No. 1

Approved for Public Release

Contrails

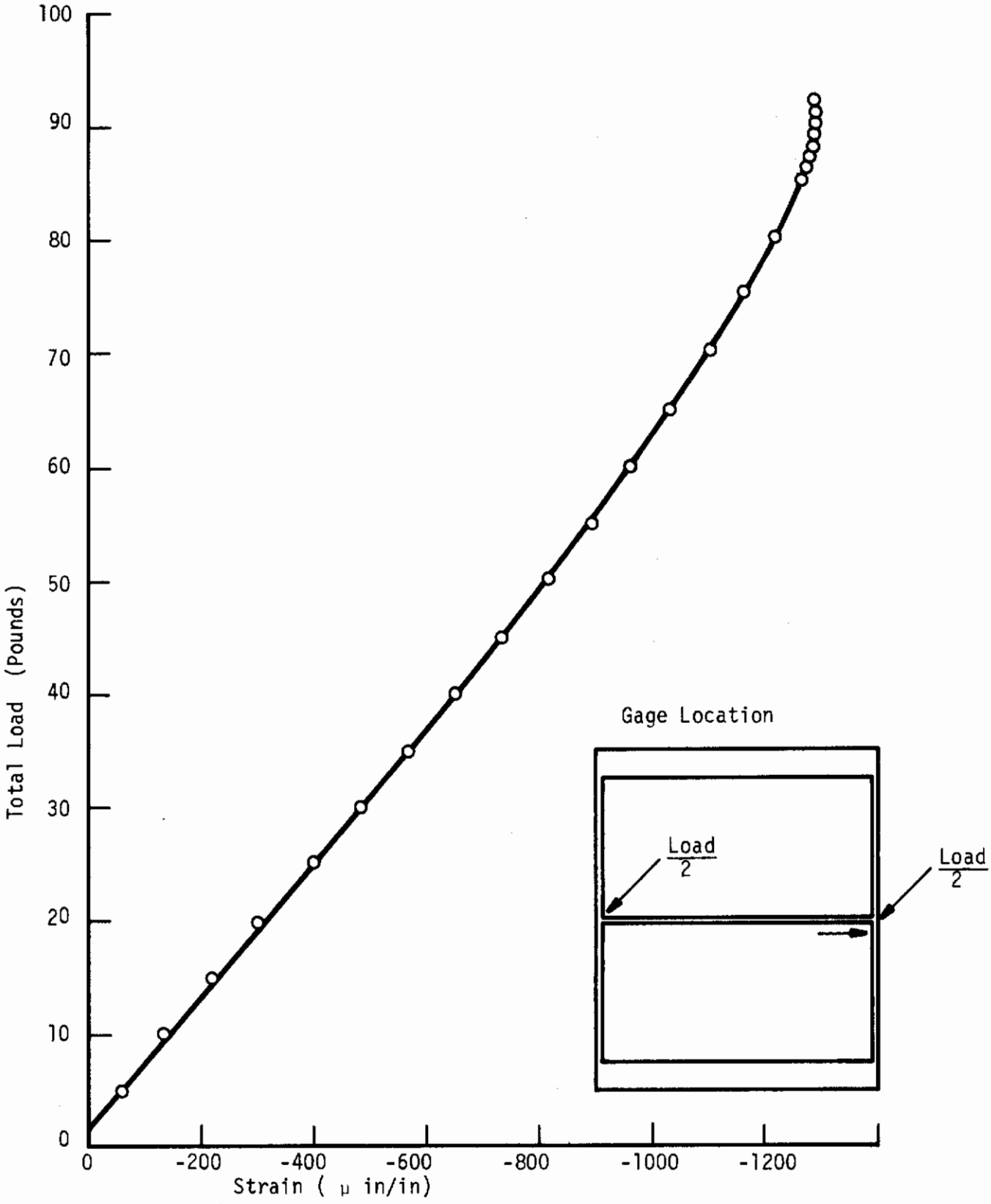

Figure C.7 Load vs. Strain, Transverse Loaded Stiffened Plate No. 2, Simply Supported.

Approved for Public Release

Contrails

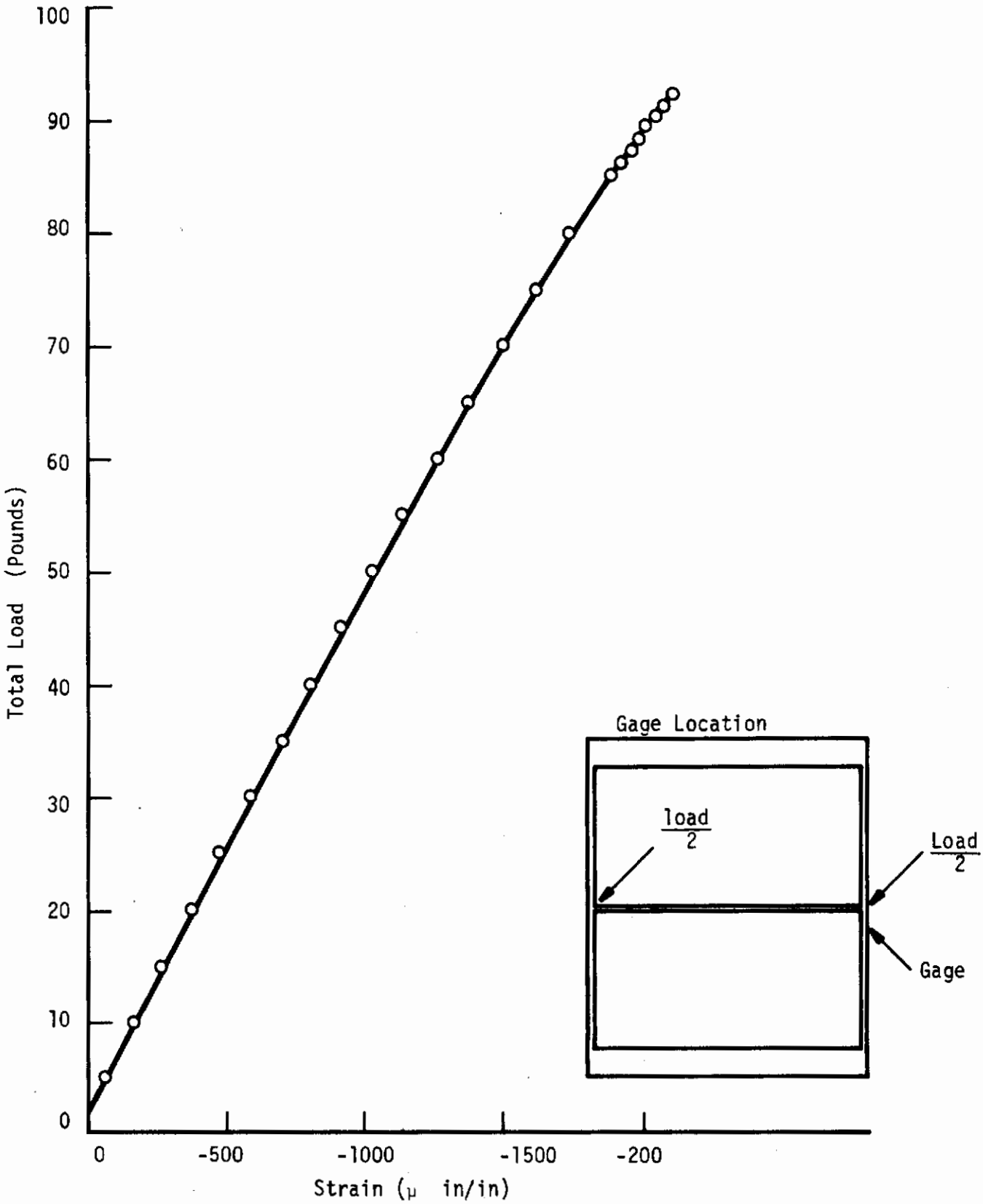

Figure C.8 Load vs. Strain, Transverse Loaded Stiffened Plate No. 2, Simply Supported

Approved for Public Release

Contrails

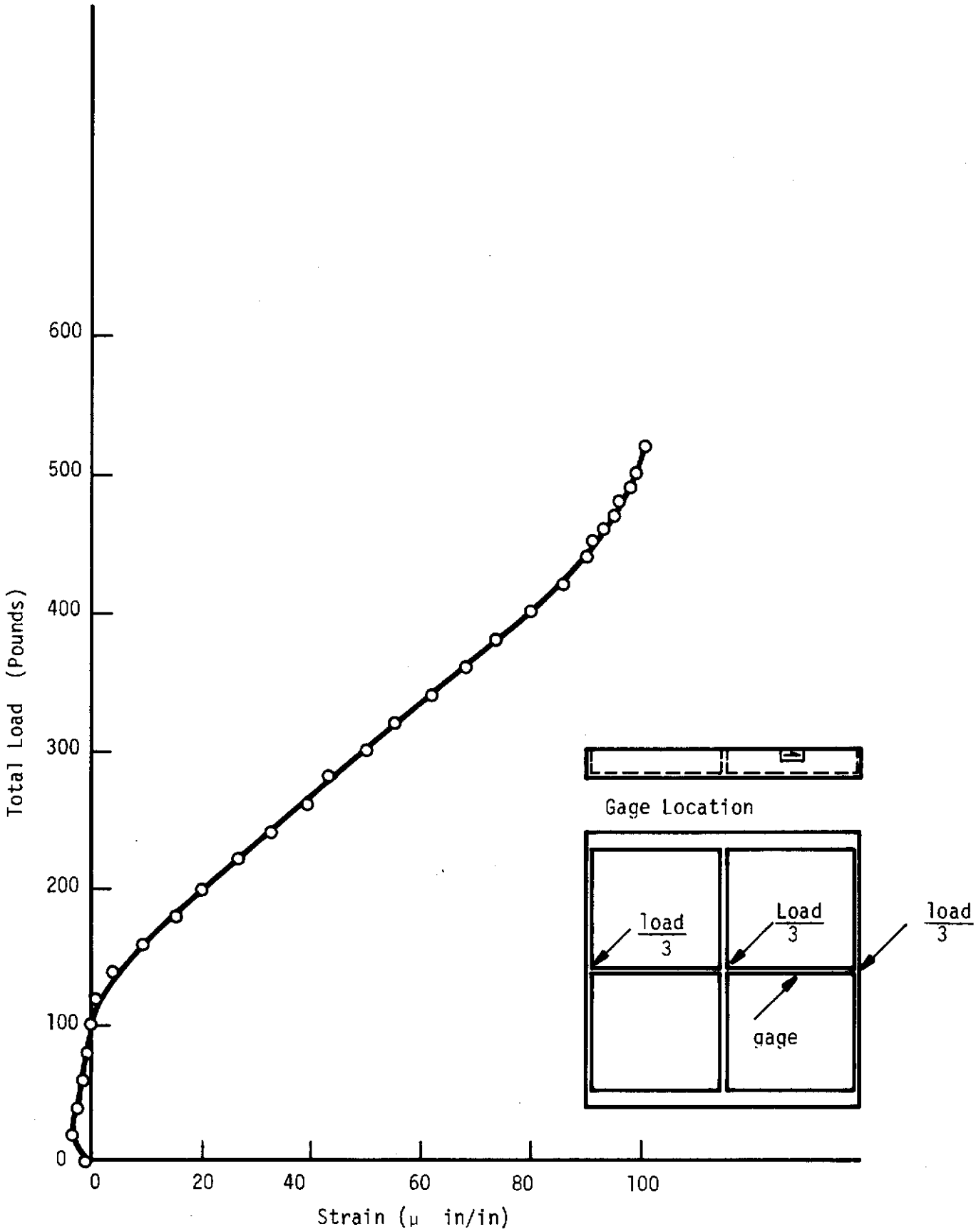

Figure C.9 Load vs. Strain, Transverse Loaded Stiffened Plate No. 3, Simply Supported

Approved for Public Release

Contrails

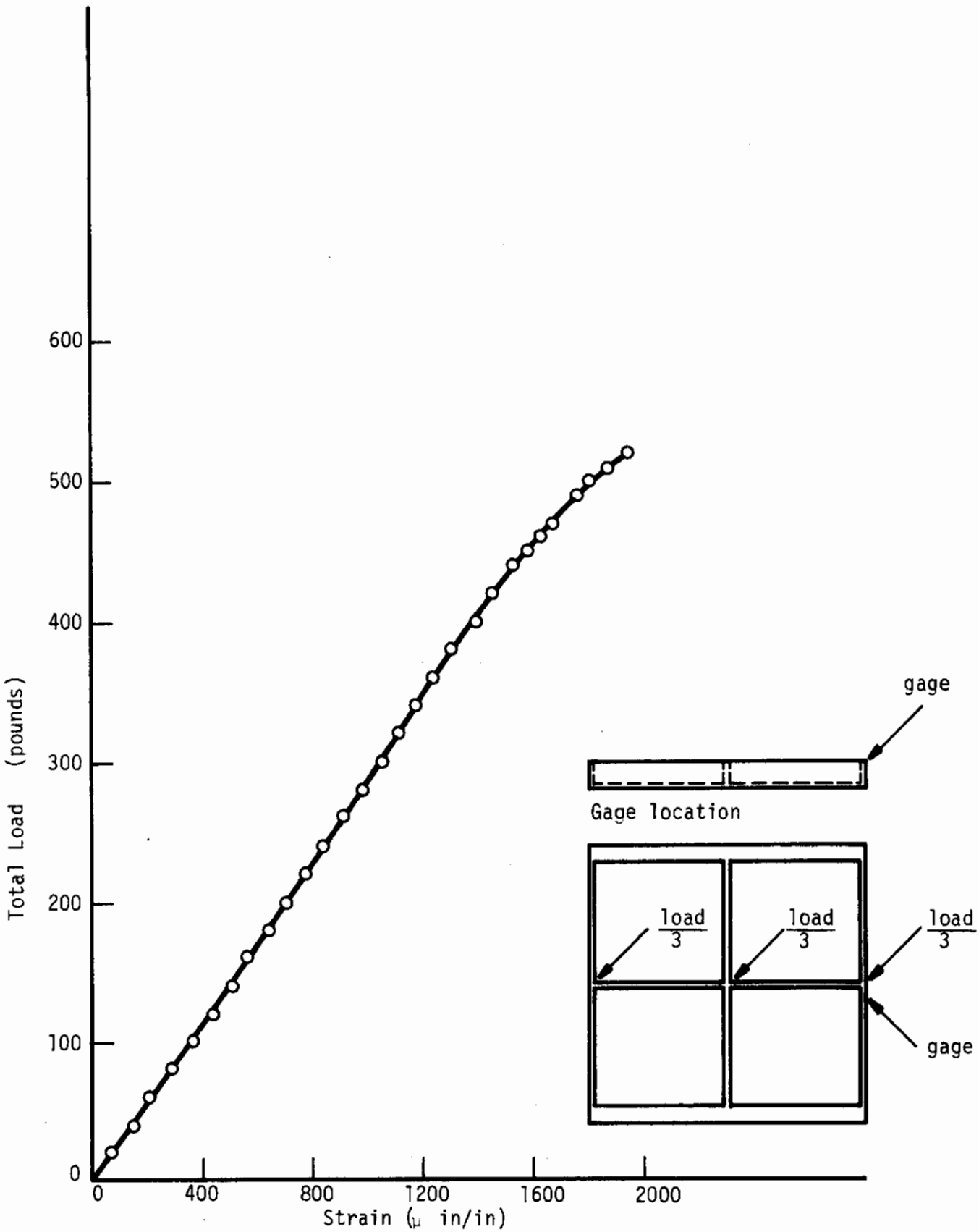

Fig. C.10 Load vs. Strain, Transverse Loaded Stiffened Plate No. 3 Simply Supported

Approved for Public Release

Contrails

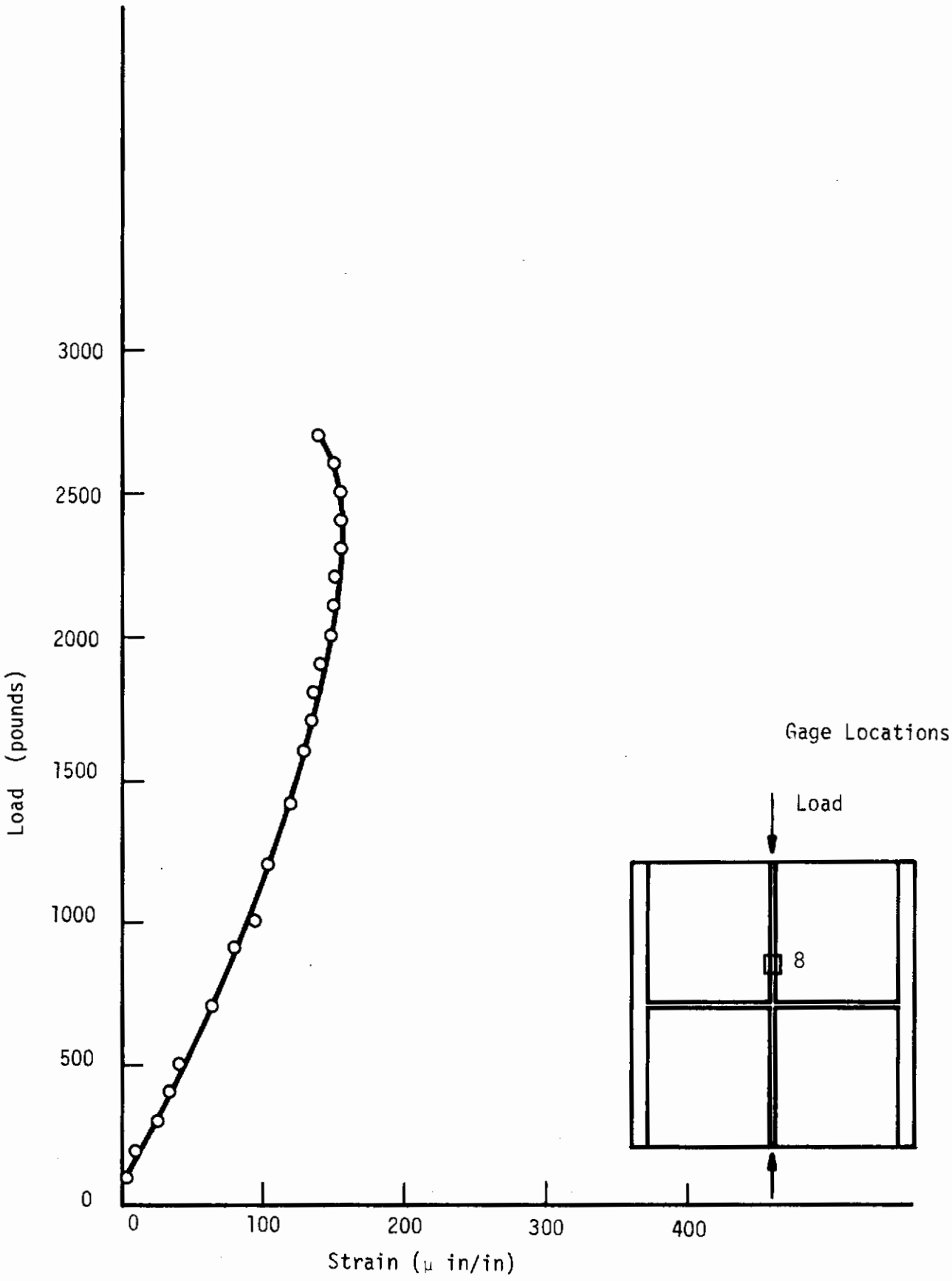

Fig. C.11 Load vs. Strain Inplane Loaded Stiffened Plate No. 4.

Approved for Public Release

Contrails

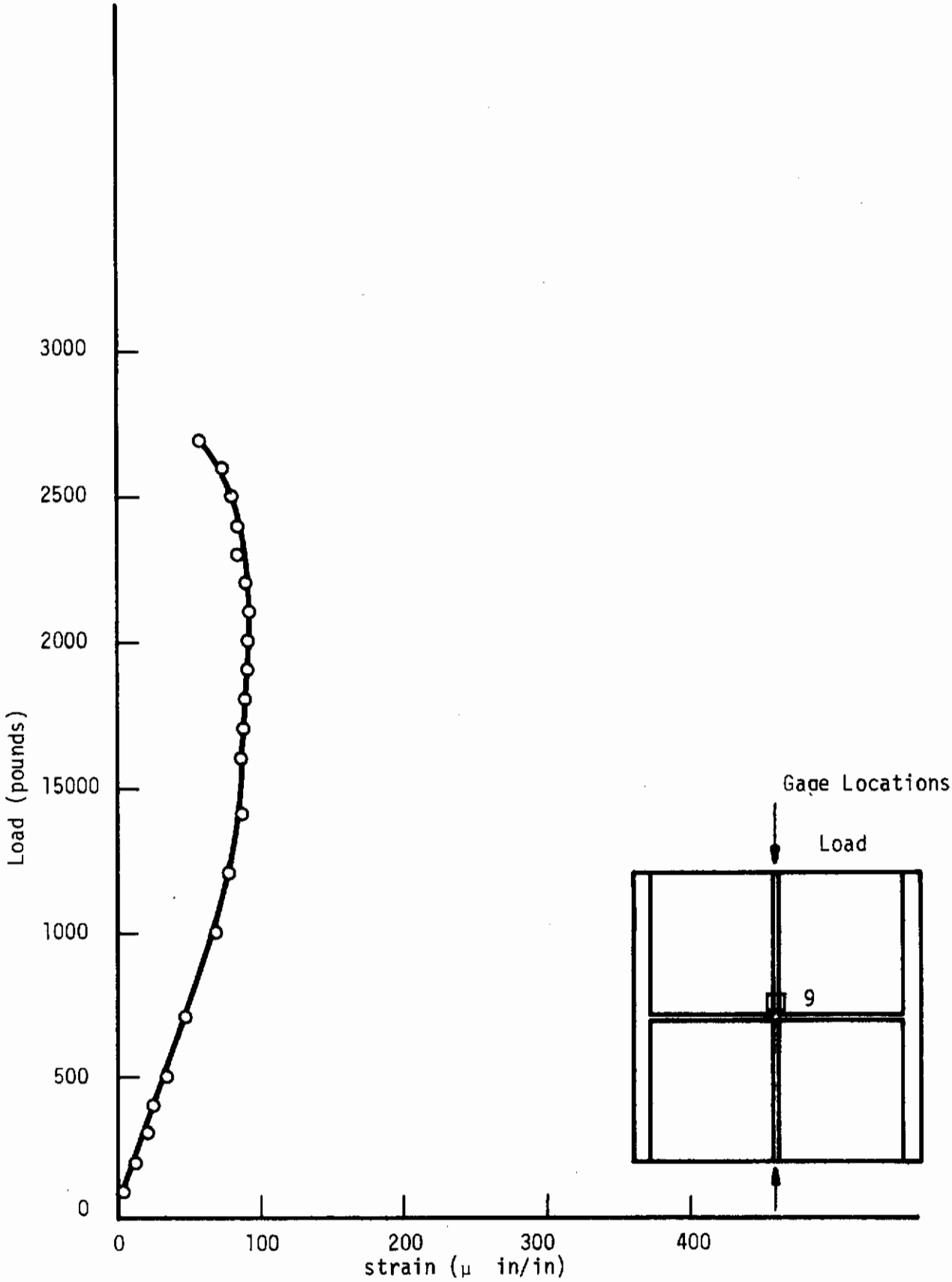

Fig. C.12 Load vs. Strain Inplane Loaded Stiffened Plate No. 4

Approved for Public Release

Contrails

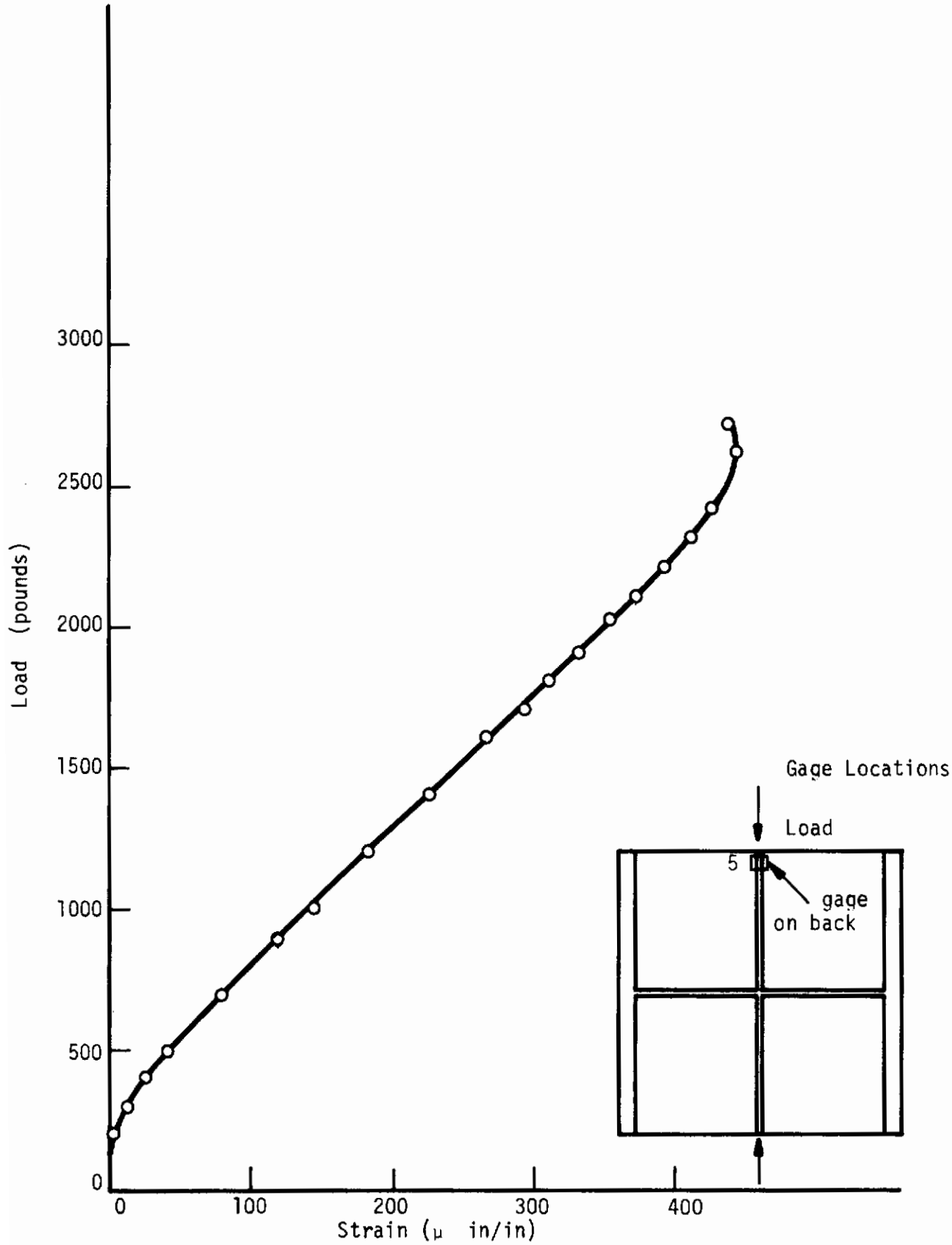

Fig. C.13 Load vs. Strain Inplane Loaded Stiffened Plate No. 4.

Approved for Public Release

Table C1

Test Data for Pinched Cylinder

Load	Deflections (in)		Strain Readings (μ in/in)						
Lbs.	(Between Load Pts.)	(End Pts.)	1	2	3	4	5	6	7
10	0	0	2	-3	+4	1	-2	1	5
20	0.0212	0.020	-68	-4	-70	2	-80	14	7
30	0.0435	0.040	-136	-6	-139	5	-164	29	9
40	0.0620	0.059	-205	-8	-209	6	-247	42	12
50	0.0820	0.079	-272	-9	-280	7	-330	57	14
60	0.1032	0.098	-344	-10	-343	8	-411	72	15
70	0.1241	0.118	-408	-11	-422	10	-504	80	18
80	0.1440	0.139	-477	-12	-496	12	-582	94	21
90	0.1642	0.158	-548	-14	-569	16	-670	105	24
100	0.1860	0.178	-615	-15	-640	18	-751	120	26
110	0.2073	0.197	-677	-16	-709	22	-839	134	28

Approved for Public Release

Table C1

Test Data for Pinched Cylinder
(Continued)

Load	Strain Readings												
Lbs	8	9	10	11	12	13	14	15	16	18	19	20	21
10	-3	-2	-1	-12	4	2	0	3	-1	0	0	-2	+2
20	4	-26	48	58	4	74	13	87	-12	0	22	-3	-51
30	11	-53	97	116	4	149	25	175	-25	-1	42	-5	-102
40	17	-80	144	172	4	222	38	262	-38	-1	63	-7	-151
50	25	-105	195	230	4	295	52	350	-49	-2	83	-9	-204
60	34	-132	242	290	4	372	68	437	-62	0	105	-10	-251
70	41	-154	300	352	3	441	79	524	-73	0	125	-12	-305
80	48	-180	352	414	2	518	92	612	-85	1	148	-13	-360
90	55	-206	404	472	1	593	105	708	-96	2	167	-15	-407
100	60	-231	454	531	0	666	120	796	-109	4	188	-17	-460
110	68	-257	500	593	0	741	132	885	-122	6	209	-18	-510

Approved for Public Release

Table C2

Test Data for Unstiffened Plate

Deflections	Load at Center (Lbs)	Strain Gage Readings (μ in/in)					
		1	2	3	4	5	6
0.000"	0	0	0	0	0	0	0
0.010	5.74	17	58	- 5	- 2	- 18	+28
0.020	9.79	26	92	- 6	- 2	- 27	+58
0.030	15.53	34	135	-11	- 4	- 40	+92
0.040	22.06	54	187	-14	- 4	- 59	120
0.050	30.02	69	246	-19	- 6	- 78	158
0.060	38.59	83	305	-25	-10	- 97	203
0.065	43.01	89	337	-28	-13	-108	222
0.070	47.19	100	368	-30	-15	-122	237
0.075	51.76	109	398	-32	-15	-131	260
0.080	56.26	117	433	-38	-16	-143	278
0.085	61.68	126	465	-41	-20	-158	302
0.090	66.84	137	502	-46	-23	-165	324
0.095	71.15	145	533	-50	-25	-183	344
0.100	76.70	153	571	-53	-27	-195	366
0.105	81.85	163	599	-55	-29	-201	382
0.110	87.99	172	640	-60	-34	-223	402
0.115	93.93	184	679	-64	-36	-237	428
0.120	98.95	190	710	-70	-40	-251	446
0.125	105.48	203	750	-77	-46	-273	469

Approved for Public Release

Table C2

Test Data for Unstiffened Plate
(Continued)

Deflections	Load at Center (Lbs)	Strain Gage Readings (μ in/in)					
		1	2	3	4	5	6
0.130	111.55	208	785	-80	-49	-285	490
0.135	118.53	220	825	-87	-55	-300	516
0.140	124.80	229	861	-90	-58	-318	538
0.145	131.07	244	890	-96	-61	-334	556
0.150	138.12	250	928	-101	-68	-350	577
0.155	145.63	258	963	-106	-73	-368	597
0.160	153.32	269	1003	-112	-75	-385	621
0.165	160.57	281	1040	-118	-80	-403	646
0.170	168.47	294	1078	-124	-86	-421	661
0.175	176.25	301	1113	-128	-90	-439	687
0.180	184.46	311	1150	-134	-95	-456	707
0.185	192.29	321	1184	-140	-99	-474	727
0.000	0	-2	3	-3	-3	-1	+4

Approved for Public Release

Contrails

Table C3

Test Data for Stiffened Plate No. 1

Load (lbs)	Deflection (under load) (inches)	
0	0	
5	0.0045	
10	0.0100	
15	0.0155	
20	0.0220	
25	0.0278	
30	0.0334	
35	0.0386	Buckling, longitudintal stiffener
40	0.0451	
45	0.0518	
46	0.0532	
47	0.0552	
48	0.0565	
49	0.0582	
50	0.0622	
51	0.0656	
52	0.0710	
53	0.0760	
54	0.0790	
55	0.0850	

Approved for Public Release

Table C4

Test Data for Stiffened Plate No. 2

Load (lbs)	Deflection (in)	Strain Readings (μ in/in)						
		1	2	3	4	5	6	7
2	0	10	0	0	0	0	0	0
5	0.0037	-60	5	0	0	-56	6	2
10	0.0079	-161	8	1	-6	-134	14	4
15	0.0128	-268	13	1	-8	-220	24	6
20	0.0168	-376	19	1	-9	-303	33	10
25	0.0218	-482	25		-8	-396	12	14
30	0.0262	-593	31		-6	-483	49	16
35	0.0367	698	36		-3	-572	58	20
40	0.0350	-806	42	-4	3	-650	66	24
45	0.0393	-918	47		6	-734	75	27
50	0.0436	-1034	54	-9	9	-807	83	30
55	0.0476	-1144	61		12	-892	91	34
60	0.0519	-1257	67	-12	15	-965	99	38
65	0.0564	-1379	74		18	1035	108	42
70	0.0607	-1496	83	-17	22	1106	117	46
75	0.0648	-1620	91		25	1164		50
80	0.0698	-1742	99	-22	29	1223	133	55
85	0.0758	-1890	111		32	1268	141	61

Approved for Public Release

Table C4

Test Data for Stiffened Plate No. 2
(Continued)

Load (lbs)	Deflection (in)	Strain Readings (μ in/in) 1	2	3	4	5	6	7
86	0.0768	-1925	114			1276	144	
87	0.0783	-1957	118			1280	146	
88	0.0798	-1989	122		35	1286	148	
89	0.0816	-2024	127		35	1290	149	
90	0.0828	-2054	130	-32	36	1293	150	67
91	0.0843	-2086	135		39	1292	151	69
92	0.0858	-2113	140	-35	39	1289	152	70

Approved for Public Release

Confidential

Table C5

Test Data for Stiffened Plate No. 3

Load (lbs)	Deflection under load (in)	Strains (μ in/in)						
		1	2	3	4	5	6	7
0	0	-1	0	0	0	0	0	0
20	0.0021	-3	-90	1	-4	-74	2	0
40	0.0050	-5	-178	4	-3	-148	8	1
60	0.0060	-7	-269	6	-2	-214	17	2
80	0.0080	-10	-357	9	-1	-292	22	2
100	0.0100	-11	-444	11	0	-369	30	3
120	0.0115	-13	-534	13	1	-440	37	4
140	0.0135	-15	-616	16	4	-507	43	4
160	0.0155	-17	-700	18	9	-578	49	5
180	0.0172	-19	-783	21	15	-643	56	6
200	0.0195	-21	-867	24	20	-708	62	8
220	0.0215	-23	-958	25	27	-774	70	10
240	0.0230	-24	-1041	28	33	-843	76	12
260	0.0250	-25	-1124	32	39	-915	84	14
280	0.0264	-27	-1209	35	43	-983	91	16
300	0.0280	-29	-1297	37	50	-1049	97	18
320	0.0300	-31	-1387	40	55	-1113	105	20
340	0.0317	-33	-1475	44	62	-1176	112	21
360	0.0330	-35	-1561	47	68	-1242	120	23
380	0.0350	-37	-1650	49	73	-1310	127	25

Approved for Public Release

Table C5

Test Data for Stiffened Plate No. 3
(Continued)

Load (lbs)	Deflection under load (in)	Strains (μ in/in) 1	2	3	4	5	6	7
400	0.0365	-40	-1729	52	80	-1388	134	27
420	0.0383	-42	-1820	56	86	-1453	142	28
440	0.0400	-43	-1903	59	90	-1531	150	28
450	0.0415	-44	-1950	60	91	-1570	---	29
460	0.0420	-44	-1970	62	93	-1628	159	30
470	0.0428	-45	-2033	64	95	-1677	162	31
480	0.0438	-47	-2069	66	95		166	32
490	0.0455	-47	-2101	68	96	-1760	170	35
500	0.0465	-49	-2128	69	98	-1802	174	35
510	0.0475	-51	-2145	70	99	-1875	178	35
520	0.0490	-53	-2151	71	101	-1942	181	35

Approved for Public Release

CONFIDENTIAL

Table C6

Test Data for Stiffened Plate No. 4

Load (lbs)	Deflection (in)	Strain Readings (μ in/in) 4	3	13	14	5	6	7	8	9
50	0	1	8	- 24	- 22	2	- 3	- 4	2	0
100	0.0010	-13	8	- 84	- 86	1	-13	-11	-3	-3
200	0.0034	-28	-2	-199	-210	-4	-40	-23	-13	-13
300	0.0057	-44	-5	-287	-328	-13	-64	-40	-25	-22
400	0.0078	-61	-10	-415	-456	-26	-88	-52	-36	-28
500	0.0100	-78	-15	-566	-579	-42	-105	-60	-43	-35
700	0.0141	-107	-28	-820	-834	-81	-153	-91	-64	-47
900	0.0181	-141	-39	-1046	-1080	-120	-190	-114	-81	-56
1000	0.0200	-154	-46	-1196	-1215	-144	-217	-127	-94	-70
1200	0.0239	-193	-62	-1477	-1483	-183	-257	-150	-105	-78
1400	0.0279	-224	-73	-1768	-1766	-232	-294	-171	-120	-86
1600	0.0320	-255	-90	-2056	-2045	-267	-335	-190	-132	-88
1700	0.0340	-270	-94	-2194	-2192	-294	-357	-198	-137	-91
1800	0.0357	-284	-104	-2350	-2334	-311	-373	-203	-138	-89
1900	0.0377	-302	-110	-2464	-2471	-333	-392	-212	-143	-92
2000	0.0400	-316	-116	-2655	-2624	-357	-409	-218	-149	-92
2100	0.0420	-332	-124	-2819	-2774	-374	-426	-224	-152	-92
2200	0.0442	-346	-131	-2946	-2927	-397	-443	-230	-152	-90
2300	0.0464	-363	-142	-3120	-3081	-412	-458	-233	-155	-85
2400	0.0491	-380	-154	-3304	-3224	-426	-473	-237	-155	-84
2500	0.0510	-398	-158	-3503	-3368	-437	-487	-241	-155	-80
2600	0.0533	-417	-169	-3685	-3511	-445	-499	-242	-153	-74
2700	0.0555	-435	-182	-3980	-3656	-438	-506	-237	-140	-56

Approved for Public Release

Confidential

Contrails

REFERENCES

1. Bogner, F.K., Mallett, R.H., Minich, M.D. and Schmit, L.A., Development and Evaluation of Energy Search Methods of Nonlinear Structural Analysis, AFFDL TR-65-113, Air Force Flight Dynamics Laboratory, Wright-Patterson Air Force Base, Ohio, October 1965.

2. Bogner, F.K., Fox, R.L. and Schmit, L.A., The Generation of Inter-element-compatible Stiffness and Mass Matrices by Use of Interpolation Formulas, Proceedings of the Conference on Matrix Methods in Structural Mechanics, AFFDL TR-66-80, Air Force Flight Dynamics Laboratory, Wright-Patterson Air Force Base, Ohio (1966), pp. 397-443.

3. Mallett, R.H. and Schmit, L.A., "Nonlinear Structural Analysis by Energy Search", J. of the Struct. Div., ASCE, Vol. 93, No. ST3, June 1967, pp. 221-234.

4. Mallett, R.H., "A Mathematical Programming Approach to Nonlinear Structural Analysis", EDC Report No. 2-65-10, Case Institute of Technology, Cleveland, Ohio, November 1965.

5. Mallett, R.H. and Berke, L., Automated Method for Large Deflection and Instability Analysis of Three-Dimensional Truss and Frame Assemblies, AFFDL TR-66-102, Air Force Flight Dynamics Laboratory, Wright-Patterson Air Force Base, Ohio, December 1966.

6. Rybicki, E.F., "An Incremental Complementary Energy Method of Nonlinear Stress Analysis", Division of Solid Mechanics, Structures and Mechanical Design, Report No. 17, School of Engineering, Case Western Reserve University, Cleveland, Ohio, June 1968.

7. Bogner, F.K., Finite Deflection Discrete Element Analysis of Shells, AFFDL TR-67-185, Air Force Flight Dynamics Laboratory, Wright-Patterson Air Force Base, Ohio, June 1968.

8. Bogner, F.K., Fox, R.L. and Schmit, L.A., "A Cylindrical Shell Discrete Element", AIAA Journal, Vol. 5, No. 4, April 1967.

9. Schmit, L.A., Bogner, F.K. and Fox, R.L., "Finite Deflection Structural Analysis Using Plate and Shell Discrete Elements", AIAA Journal, Vol. 6, No. 5, May 1968, pp. 781-791.

10. Monforton, G.R. and Schmit, L.A., "Finite Element Analysis of Skew Plates in Bending", AIAA Journal, Vol. 6, No. 6, June 1968, pp. 1150-1152.

11. Monforton, G.R., "Finite Element, Displacement and Vibration Analysis of Skew Plates", Division of Solid Mechanics, Structures and Mechanical Design, Report No. 18, School of Engineering, Case Western Reserve University, Cleveland, Ohio, March 1968.

Approved for Public Release

Contrails

REFERENCES (Continued)

12. Minich, M.D., "Discrete Element Analysis by Combined Method Formulation", Division of Solid Mechanics, Structures and Mechanical Design, Report No. 10, School of Engineering, Case Western Reserve University, Cleveland, Ohio, October 1967.

13. Fox, R. L. and Stanton, E., "Developments in Structural Analysis by Direct Energy Minimization", AIAA Journal, Vol. 6, No. 6, June 1968, pp. 1036-1042.

14. Key, S.W., "A Convergence Investigation of the Direct Stiffness Method", Ph.D. Thesis, Dept. of Aeronautics and Astronautics, Univ. of Washington, Seattle, Wash., 1966.

15. Isakson, G., Armen, H., Jr., and Pifko, A., "Discrete Element Methods for for Plastic Analysis of Structures", NASA CR-803, October 1967.

16. Fulton, R.E., Eppink, R.T. and Walz, J.E., "The Accuracy of Finite Element Methods in Continuum Problems," Fifth U.S. National Congress of Applied Mechanics, June 1966, University of Minnesota, Minneapolis, Minn.

17. Gallagher, R.H., "The Development and Evaluation of Matrix Methods for Thin Shell Structural Analysis", Ph.D. Thesis, 1966, State University of New York, Buffalo, New York.

18. Cantin, G., and Clough, R.W., "A Curved, Cylindrical Shell, Finite Element", AIAA Journal, Vol. 6, No. 6, June 1968, pp. 1057-1062.

19. Stricklin, J.A., Tidwell, D.R., Haisler, W.E., and Samson, C.H., Jr., "Consistent Stiffness Matrices in the Analysis of Shells", AIAA/ASME 8th Structures, Structural Dynamics, and Materials Conference, AIAA, New York, 1967, pp. 162-174.

20. Timoshenko, S.P., and S. Woinowsky-Krieger, Theory of Plates and Shells, Second Edition, McGraw-Hill Book Company, New York, 1959.

21. Timoshenko, S.P. and Gere, J.M., Theory of Elastic Stability, Second Edition, McGraw-Hill Book Company, New York, 1961.

22. Guyan, R.J., "A Study of the Effectiveness of the Stiffness Methods of Structural Analysis in Selected Applications," Ph.D. Thesis, Case Institute of Technology, Cleveland, Ohio, 1964.

23. Reissner, E., "On the Variation Theorem for Finite Elastic Deformations", Journal of Mathematics and Physics, Vol. 32, pp. 129-135, 1953.

24. Powell, M.J.D., "An Iterative Method for Finding Stationary Values of a Function of Several Variables", The Computer Journal, Vol. 5, pp. 147-151, 1962.

Approved for Public Release

Contrails

REFERENCES (Continued)

25. Woodrow, P.J., "Methods for Locating the Extreme of Multivariate Functions", Control Systems Laboratory, Dept. of Electrical Engr., Princeton University, Princeton, N.J., TR No. 4, November, 1962.

26. Timoshenko, S.P. and Goodier, J.N., Theory of Elasticity , Second Edition, McGraw-Hill Book Company, New York, 1951.

27. Fletcher, R. and Reeves, C.M., "Function Minimization by Conjugate Gradients", Computer Journal, Vol. 7, 1964, pp. 163-168.

28. Fletcher, R. and Powell, M.J.D., "A Rapidly Convergent Descent Method for Minimization", Computer Journal, Vol. 6, 1963, pp. 163-168.

29. Hestenes, M.R. and Stiefel, E., "Method of Conjugate Gradients for Solving Linear Systems", Journal Res. Natl. Bur. of Standards, Sec. B, Vol. 49, 1952, pp. 409-436.

30. Kowalik, J., "Iterative Methods for Linear Equations in Matrix Structural Analysis", International Shipbuilding Progress, Vol. 13, 1966, pp. 59-68.

31. Isaacson, E. and Keller, H.B., Analysis of Numerical Methods , John Wiley and Sons, Inc. 1966, Chapter 3.

32. Rutishauser, H., "Algorithm 150", Comm. of A.C.M., Vol. 6, No. 2, Feb. 1963, pp. 67-68.

33. Britvec, S.J. and Chilver, A.H., "Elastic Buckling of Rigidly-Jointed Braced Frames", J. of the Engr. Mech., Div., Proc. ASCE, Vol. 89, No. EM6, Dec. 1963, pp. 217-255.

34. Godley, M.H.R. and Chilver, A.H., "The Elastic Post-Buckling Behavior of Unbraced Plane Frames", Int. J. Mech. Sci., Vol. 9, 1967, pp. 323-333.

35. Thompson, J.M.T., "Stability of Elastic Structures and Their Loading Devices", J. of Mech. Engr. Sciences, Vol. 3, No. 2, 1961, pp. 153-162.

Approved for Public Release

UNCLASSIFIED
Security Classification

Contrails

DOCUMENT CONTROL DATA - R & D

(Security classification of title, body of abstract and indexing annotation must be entered when the overall report is classified)

1. ORIGINATING ACTIVITY *(Corporate author)*
CASE WESTERN RESERVE UNIVERSITY
Cleveland, Ohio

2a. REPORT SECURITY CLASSIFICATION
UNCLASSIFIED

2b. GROUP
NA

3. REPORT TITLE
(U) DEVELOPMENTS IN DISCRETE ELEMENT FINITE DEFLECTION STRUCTURAL ANALYSIS BY FUNCTION MINIMIZATION

4. DESCRIPTIVE NOTES *(Type of report and inclusive dates)*
Final Report on Research Conducted from December 1965 to May 1968.

5. AUTHOR(S) *(First name, middle initial, last name)*
LUCIEN A. SCHMIT, JR., Principal Investigator
(see FOREWORD for complete list of contributors)

6. REPORT DATE
September 1968

7a. TOTAL NO. OF PAGES
295

7b. NO. OF REFS
35

8a. CONTRACT OR GRANT NO.
AF 33(615)-3432

b. PROJECT NO.
1467

c. Task No. 146701

d.

9a. ORIGINATOR'S REPORT NUMBER(S)
NA

9b. OTHER REPORT NO(S) *(Any other numbers that may be assigned this report)*
AFFDL-TR-68-126

10. DISTRIBUTION STATEMENT
This document has been approved for public release and sale. Its distribution is unlimited.

11. SUPPLEMENTARY NOTES

12. SPONSORING MILITARY ACTIVITY
Air Force Flight Dynamics Laboratory
Research and Technology Division
Wright-Patterson Air Force Base, Ohio 45433

13. ABSTRACT
The discrete element energy search method of structural analysis is extended to predicting the geometrically nonlinear behavior of plate and shell type structures. Numerical results for example problems exhibiting nonlinear bending-membrane coupling and stable post-buckling behavior are presented. The results of a laboratory type experimental program, designed to provide data for comparison with analytical behavior predictions, are reported. It is shown that displacement patterns formed from products of one-dimensional interpolation functions can be used to generate a useful class of shell discrete elements, including geometric nonlinearity. These conforming elements can be joined together at arbitrary angles, although the current computer program is limited to tangential and right angle joining. While the major portion of this research program was based upon the principle of minimum potential energy, a rectangular plate discrete element exhibiting bending membrane coupling is developed within the Reissner energy framework. Energy search methods of structural analysis based on potential energy formulations and gradient minimization algorithms are found to be computationally competitive with conventional solution procedures. A variable scaling technique that has a strong effect on the convergence of the gradient minimization algorithms is presented. Using this variable scaling-technique it is found that the conjugate gradient algorithm often converges in substantially less than n cycles for over-discretized linear problems, where n is the number of independent degrees-of-freedom. A computer program, that draws together most of the important separate contributions made within the potential energy framework during the course of this research program, is described. This computer program implements discrete element finite deflection analysis of a class of structures that can be modeled as assemblages of plate, cylindrical shell, and annular plate elements connected together tangentially or at right angles.

DD FORM 1 NOV 65 1473

UNCLASSIFIED
Security Classification

Approved for Public Release

Contrails

14. KEY WORDS	LINK A		LINK B		LINK C	
	ROLE	WT	ROLE	WT	ROLE	WT
Matrix Structural Analysis						
Discrete Element Analysis						
Finite Deflections						
Geometric Nonlinearity						
Potential Energy Principle						
Elastic Post-Buckling Behavior						
One-Dimensional Hermite Interpolation Polynomials						
Numerical Solutions						
Thin Elastic Plates and Shells						
Energy Search Structural Analysis						
Unconstrained Minimization						
Reissner Energy Principle						
Stiffened Plates and Shells						

Approved for Public Release